Final Report 2000-24

Research

Evaluation of Electrochemical Chloride Extraction (ECE) and Fiber Reinforced Polymer (FRP) Wrap Technology

Technical Report Documentation Page

1. Report No.	2.	3. Recipient's Accession No.
MN/RIC-2000-24		

4. Title and Subtitle	5. Report Date
EVALUATION OF ELECTROCHEMICAL CHLORIDE EXTRACTION (ECE) AND FIBER REINFORCED POLYMER (FRP) WRAP TECHNOLOGY	June 2000
	6.

7. Author(s)	8. Performing Organization Report No.
Mark Chauvin, Carol Shield, Catherine French, William Smyrl	

9. Performing Organization Name and Address	10. Project/Task/Work Unit No.
University of Minnesota Department of Civil Engineering 122 CivE Bldg., 500 Pillsbury Drive SE Minneapolis, MN 55455-0220	11. Contract (C) or Grant (G) No. (c) 74708 (wo) 57

12. Sponsoring Organization Name and Address	13. Type of Report and Period Covered
Minnesota Department of Transportation 395 John Ireland Boulevard Mail Stop 330 St. Paul, Minnesota 55155	Final Report1997-1999
	14. Sponsoring Agency Code

15. Supplementary Notes

16. Abstract (Limit: 200 words)

Methods for mitigating corrosion in reinforced concrete structures were investigated on the substructure of a bridge in Minneapolis, Minnesota. Several corrosion-damaged columns and pier caps were treated with electrochemical chloride extraction (ECE), and then selected ECE-treated and untreated structures were wrapped with FRP wraps or sealed with concrete sealers to prevent future chloride ingression. Embeddable corrosion monitoring instrumentation was installed in the field structures to evaluate the effectiveness of ECE treatment.

Although the ECE process reduced average chloride levels in the treated structures by approximately 50%, several locations still had chloride concentrations in excess of the established corrosion threshold following ECE treatment. Resistivity probe failures that occurred at some of these locations indicated corrosion within the treated structures could still occur, despite re-passivation of the reinforcing steel following ECE treatment. Continued monitoring of the installed instrumentation is required to evaluate the long-term effectiveness of ECE treatment and concrete wrapping/sealing as a corrosion mitigation technique.

17. Document Analysis/Descriptors	18. Availability Statement
corrosion, electrochemical chloride extraction, fiber reinforced polymer wraps	No restrictions. Document available from: National Technical Information Services, Springfield, Virginia 22161

19. Security Class (this report)	20. Security Class (this page)	21. No. of Pages	22. Price
Unclassified	Unclassified	248	

Evaluation of Electrochemical Chloride Extraction (ECE) and Fiber Reinforced Polymer (FRP) Wrap Technology

Final Report

Prepared by

Mark Chauvin
Carol K. Shield
Catherine E. French
Department of Civil Engineering

and

William Smyrl
Department of Chemical Engineering and Materials Science
University of Minnesota

June 2000

Published by

Minnesota Department of Transportation
Office of Research and Strategic Services
First Floor
395 John Ireland Boulevard
St. Paul, MN 55155

ACKNOWLEDGEMENTS

Funding for this research was provided by the Minnesota Department of Transportation and the University of Minnesota. I would like to thank both for the financial support given.

I would also like to thank many people for giving a helping hand or providing knowledge. These include: Paul Bergson, Pat James, Luis Garfias, Mike Parent, Bryan Pivovar, Shawn Kelly, Lon Shi, and Justin Ocel at the University of Minnesota as well as Rod Koehn, John Barke, and Mark Hagen at Mn/DOT. I would also like to thank Dave Whitmore, Mark Turley, and Sean Abbott at Vector Construction.

TABLE OF CONTENTS

LIST OF TABLES

LIST OF FIGURES

EXECUTIVE SUMMARY

Methods for mitigating corrosion in reinforced concrete structures were investigated on the substructure of a bridge in Minneapolis, Minnesota. The structures chosen for this investigation constituted a portion of the substructure of I-394, Bridge #27831, over Dunwoody Blvd. in Minneapolis, MN. The bridge had a history of corrosion related problems, especially in the substructure, related to leaky expansion joints in the bridge deck above. The study included a total of twelve columns and three full pier caps and a portion of two additional pier caps. Six of the structural elements (i.e. columns and associated pier caps) were wrapped with three types of FRP, three of the structural elements were sealed with conventional sealers, and three of the structural elements served as controls. Half of the wrapped structural elements and all of the sealed structural elements were subjected to electrochemical chloride extraction (ECE) prior to being wrapped or sealed.

Prior to the initiation of the ECE process, areas with corrosion-related concrete damage were located and repaired using a chipping and patching technique. Upon completion of the concrete surface repair, chloride concentration samples and half-cell potential readings were collected in October 1997 at several locations on every column and pier cap included in the investigation. Chloride concentrations from five different depth ranges (0-1.25 cm, 1.25-2.5 cm, 2.5-3.75 cm, 3.75-6.25 cm, and 6.25-8.75 cm) at each of 69 selected sample locations were determined in accordance with ASTM C1152-90. Chloride samples were typically collected at eight locations on each pier cap and three locations on each column. Half-cell potential readings were collected with a copper-copper sulfate electrode (CSE) according to ASTM C 876-91 at 30 cm intervals, vertically and horizontally from all surfaces except the tops of the pier caps due to access difficulty.

The results of the October 1997 (pre-ECE) site condition survey indicated that there were several locations for concern in the structures. In total, 35% of the collected chloride samples indicated a chloride concentration in excess of 2000 PPM by weight of cement, this correlated with 69% of the locations having at least one chloride sample (one depth) in excess of this established corrosion threshold. Areas indicating a 90% probability of ongoing corrosion, identified by half-cell potentials more negative than -0.35 V vs. CSE, were located on several columns and almost every pier cap included in the study.

Although the level of chloride contamination was significant in all of the structures of the study, Pier 34 North (structural elements 34A-C) had the most severe chloride ingression; 66% of all of the chloride samples collected from that pier exceeded 2000 PPM. In addition, 92% of the locations where chloride samples were collected from Pier 34 North had at least one chloride sample (one depth) in excess of 2000 PPM. The column portion of structural element 34A had average chloride concentrations of more than twice the established threshold for corrosion in the first 2.5 cm of concrete and continued to exceed the corrosion threshold up to 6.25 cm below the concrete surface, indicating significant and long standing chloride permeation. These results can most likely be attributed to the proximity of this pier, and specifically the column portion of 34A, to the intersection of Dunwoody Blvd. and W. Linden Ave. At that location, the potential for splashing of chloride-laden melted snow and ice onto the surfaces of the column portions of 34A-C was greatest. The other piers in the study were not likely to experience any chloride ingression from splashing water.

The ECE process was initiated on Pier 34 North and Pier 37 North in mid-April 1998. These two piers were chosen based on the visual observations of corrosion, and the ease of access for the contractor. The ECE system, installed and maintained by Vector Construction, was run continuously until at least one of the three requirements for terminating the process had been met: 60 days of extraction, 1400 A-hr/m^2 of current passed through the structures, or a reduction in chloride levels of 50% (from 4 samples). After 60 days, all three criteria were met, and the current had plateaued, so the extraction process was terminated.

During a two month drying period following the ECE treatment, a complete survey of chloride concentrations was conducted in the same manner as the site survey taken during the fall of 1997. All 69 originally sampled locations were tested again in early August 1998. The samples were collected approximately 5 cm away from the original sample location to avoid drilling through repair mortar. Half-cell mapping was not performed before concrete wrapping and sealing commenced because the rebar was assumed to be highly repassivated through the ECE process.

Effectiveness of the ECE process was determined by comparing the number of samples and locations with chloride levels over the threshold before and after the process. Exact comparisons of the chloride concentrations from before and after ECE cannot be made because the chloride samples obtained after ECE could not be taken from the exact same location as those

taken prior to ECE. Following ECE, the percentage of powder samples with a chloride concentration in excess of 2000 PPM was reduced from 66% to 23% on Pier 34 North and from 25% to 5% on Pier 37 North. This is in contrast to the structures not treated with ECE which showed a reduction from 29% to 27%. It can be assumed that this reduction is within the uncertainty of the chloride sampling process. However, the effectiveness of the treatment process varied greatly by location, sample depth, and original chloride content. In general, ECE reduced the average chloride concentrations the most near the concrete surface, and the effectiveness decreased slightly with depth into the structure. Certain locations also experienced greater chloride reductions than others, but this disparity might be associated with the proximity of each location to reinforcing steel. Chloride ions closer to reinforcing steel would be expected to be subject to a larger driving force, from the negatively charged rebar, towards the external anode and out of the structure, than chloride ions further from the rebar.

The concrete wrapping and sealing process was initiated in late-August 1998. To simplify the wrapping/sealing procedure and to acknowledge the continuity between the column and pier cap, each sealant system was applied to both the column and the corresponding overhead pier cap area. The application of all FRP wrap systems and concrete sealers was performed by Vector Construction. Each structural element was wrapped or sealed entirely except for the 30 cm of each column directly above grade, and the underside of the pier caps, aside from a 10 cm extension provided onto either side of the bottom face. The gaps in the wrapped surfaces were intended to avoid trapping moisture within completely FRP-encased columns and pier caps. The 10 cm FRP extensions around the bottom corners of the pier caps were intended to provide a "drip-strip" for chloride laden moisture to run from the face of the pier caps. Column and pier cap wrapping was completed during the first week of September 1998 after the application of a coat of UV protection paint over the entire surface of each cured wrap system.

Because the concrete surface was not visible or accessible in the columns and pier caps wrapped with FRP materials, surface measurement of half-cell potentials and visual inspection for corrosion damage were not viable monitoring options for those structural elements. To ensure that all of the columns and pier caps in the study were monitored in the same fashion, embeddable instruments were used to monitor corrosion in both the wrapped and unwrapped structures. Three types of embeddable instruments were used: ELGAARD Embeddable silver/silver-chloride half-cells, relative humidity sleeves (monitored with a Protimeter Concrete

Master II humidity sensing probe), and resistivity probes developed at the University of Minnesota were selected.

The resistivity probes used in this investigation were designed as "on/off" corrosion indicators. The probe consisted of a 2.5 cm loop of thin iron wire with ends soldered to lead wire. These soldered connections were coated with silicone caulk to ensure that only the iron wire loop was exposed to the environment. Two different wire diameters were used in the study, 0.5 mm or 0.25 mm, herein referred to as large and small probes, respectively. Because the wire loop was relatively short, initial resistance measurements were less than 2 Ohms. Once corrosion of the iron wire was severe enough to cause breakthrough of the cross section, either by completely corroding through the metal or creating a corrosion induced stress failure at some point along the loop, resistance was infinite due to the discontinuity in the wire.

The selected instruments were installed in the columns and pier caps in December 1998. The resistivity probes and Ag/AgCl half-cells were grouped (two resistivity probes and one half-cell) at some of the chloride sample locations to enable correlation of the instrumentation results with the chloride concentration data that was collected in the October 1997 and August 1998 sampling periods. The resistivity probes and embeddable half-cells were grouted into holes that were drilled to the depth of the reinforcing steel. Humidity sleeves were installed in the columns between instrument locations to avoid congestion at the chloride sample locations. Monitoring of these instruments is ongoing.

1. Introduction

Reinforced concrete is an economical, durable and widely used construction material in the world today. Concrete provides the ideal environment for reinforcing steel because the high alkalinity causes the development of a thin, protective oxide film on the surface of the steel, providing indefinite corrosion protection. However, in states where de-icing salts are used to clear roadways, reinforced concrete structures with exterior exposure can often become contaminated with chloride ions. Chloride-contaminated concrete can lead to a breakdown in the passivity of the reinforcing steel and the initiation of the corrosion processes. This is particularly common in bridge decks and bridge substructures where the exposure to high levels of de-icing salts can be severe. Unchecked corrosion will often lead to cracking, spalling, and delamination of the concrete cover resulting in either excessive maintenance costs or a reduced service life of the structure, due to a loss of structural integrity. Extensive corrosion, causing a reduction in the cross-sectional area of steel reinforcement and concrete spalling, can result in structural collapse. Traditional methods of corrosion repair consist of the removal of corrosion damaged concrete, or chipping and patching. This repair technique treats the symptoms, rather than the source, of corrosion problems, resulting in a temporary solution.

A promising technique has been developed to permanently remove chloride ions from reinforced concrete structures through a temporary electrochemical treatment process. Electrochemical chloride extraction, or ECE, can reduce the chloride concentrations of a contaminated structure, and re-passivate the reinforcing steel, through the application of an electric field between the reinforcing steel and a temporary external anode mesh embedded in a cellulose fiber electrolyte. During treatment, negatively charged chloride ions are driven away from the negatively charged rebar, and potentially out of the concrete. The electrochemical reactions that take place at the reinforcing steel during treatment increase the alkalinity of the surrounding concrete through the creation of hydroxyl ions, which act to re-passivate the rebar. Corrosion will not re-initiate unless either sufficient chloride ions remain within the structure after ECE treatment, and migrate back to the level of reinforcing steel, or new chloride ions re-contaminate the concrete.

To prevent the ingress of new chloride ions after completion of the treatment process, a traditional sealant, such as silane, or a fiber reinforced polymer wrap (FRP), can be used to seal the concrete. The combination of chloride removal and concrete wrapping/sealing can potentially

halt corrosion in reinforced concrete structures, and significantly extend their remaining service life. While the technique is promising, questions remain about the long-term effectiveness of the ECE treatment process, and the use of concrete sealers or FRP wraps in corrosion mitigation systems. While ECE can significantly reduce chloride concentrations, sufficient chloride ions may remain that can migrate back to the level of reinforcement, reducing the passivity of the rebar and re-initiating corrosion. Although new chloride ions may be prevented from entering an impermeably sealed/wrapped structure, existing chloride, oxygen, and water within the concrete may be prevented from naturally exiting the structure. Additional water that could potentially contain chloride ions, from melted snow and ice treated with de-icing salts, may also enter the structures through the ground or from the pier cap above and accumulate inside the structure, behind the sealant system. Therefore, the potential for a contained corrosive environment exists within a wrapped/sealed structure, even if it is treated with ECE.

1.1 Research Objectives

To investigate the effectiveness of ECE as a potential corrosion rehabilitation technique, in conjunction with fiber reinforced polymer wraps and concrete sealers, the Minnesota Department of Transportation (Mn/DOT) commissioned a five year study in association with the University of Minnesota. Three different types of FRP wrap and three different concrete sealers were used in combination with ECE treatment to rehabilitate corrosion damaged concrete columns and pier caps. The retrofits were demonstrated on portions of the substructure on T.H. I-394, Bridge #27831, over Dunwoody Boulevard in Minneapolis, MN. The study included twelve columns and three pier caps, and a portion of two additional pier caps. The selected treatment schedule for each structure is discussed in Chapter 3. The main objective of the research was to assess the benefits of electrochemical chloride extraction and fiber reinforced polymer wrapping of corrosion damaged concrete structures, and evaluate the ability of the repair technique to stop the corrosion process from occurring in existing bridge structures. More specifically, the objectives of the research were to evaluate the effect of ECE on corrosion rates and determine which combination of ECE and wrapping/sealing was most effective.

The corrosion mitigation benefits provided by column wrapping are dependent upon the ability of the FRP wraps to prevent future chloride ingression while remaining sufficiently

adhered to the concrete surface. Therefore, additional objectives of the research were to evaluate the diffusion properties of the FRP wraps, and examine the durability of bond between the composites and the concrete when subjected to environmental effects. If proven durable and cost efficient, this rehabilitation method may provide an alternative to traditional corrosion repair methods of chipping and patching damaged concrete.

In typical reinforced concrete structures, corrosion can be monitored through visual inspection of the concrete (cracks, rust stains, and delaminations of the concrete cover) and half-cell potential mapping. However, in structures that are wrapped with FRP composites, contact with the concrete surface is obscured, and corrosion damage cannot be seen. Therefore, traditional monitoring techniques cannot be used when long-term corrosion monitoring of a wrapped structure is necessary. In order to evaluate the corrosion conditions within wrapped structures, embeddable corrosion monitoring instrumentation is required. For this investigation, three different types of embeddable sensors were selected to instrument the field structures. Data collected from these instruments was used in conjunction with data collected before and immediately after the ECE treatment period, to assess the effectiveness of ECE and wrapping/sealing mitigation technique.

1.2 Organization

Chapter 2 presents background information on the process and electrochemical nature of corrosion, and more specifically metallic corrosion, before focusing on the corrosion of reinforcing steel within concrete structures. Previous research completed in the fields of corrosion in concrete, electrochemical chloride extraction, fiber reinforced polymer wraps, concrete sealers, and embeddable corrosion monitoring instrumentation are then summarized.

Chapter 3 presents a detailed description of the project site and the portions of the bridge substructure that were included in the investigation, as well as a synopsis of the field work undertaken in this study. Initial site conditions are illustrated and discussed, and the evaluation methods used in the pre- and post-ECE corrosion condition surveys are summarized. The ECE process and the application procedure of the FRP wraps to the columns and pier caps are presented. Procedures used to prepare test specimens for laboratory evaluations of bond strength and diffusion properties of the FRP wrap systems are also included.

Chapter 4 presents the results of the chloride concentration samples and half-cell potentials collected from the structures included in the investigation, before and after the ECE treatment period, and average site conditions are examined. The initial effectiveness of the ECE process is determined through comparison and evaluation of the pre- and post-treatment results.

Chapter 5 summarizes the three different types of embeddable corrosion monitoring instruments that were selected for installation. The locations selected for instrumentation in the field structures are illustrated, and the installation procedure is discussed.

Chapter 6 summarizes the laboratory work completed in this investigation. Experiments conducted to calibrate and evaluate each type of corrosion monitoring instrument, and the results of the testing are discussed. The remaining sections of Chapter 6 address two of the objectives of this research. The first concerned the deterioration of bond strength between the FRP wraps and the concrete, due to environmental exposure. The testing methods used to evaluate bond strength, and the results from the initial series of peel tests are discussed, and the quality of the initial bond exhibited by each of three systems is analyzed. The second objective was to determine the permeability of each of the FRP wraps with respect to the diffusion of water. The testing methods used to evaluate the diffusion properties of the three FRP wrap systems are summarized, and the results are discussed.

Chapter 7 presents and analyzes the initial data collected from the embedded corrosion monitoring instrumentation. Results of chloride samples and half-cell potentials collected before and after the ECE treatment procedure are used in conjunction with the results of laboratory experimentation to analyze the initial sensor readings.

Chapter 8 begins to address the primary objectives of this investigation. This objective was to evaluate the long-term effectiveness of the ECE process on corrosion rates, in conjunction with various concrete sealant systems. An analysis of the preliminary effectiveness of the corrosion mitigation technique is presented and recommendations for future research projects applying or investigating ECE are discussed.

One appendix has also been included in this report. Appendix A presents the detailed results of the pre- and post-ECE chloride concentration sampling periods, and indicates the change from initial values at each sample depth.

2. Corrosion Background and Literature Review

This investigation utilizes and combines knowledge from multiple areas of previous research. These areas include corrosion, especially with regards to concrete structures, electrochemical chloride extraction, fiber reinforced polymer wrapping of concrete, and embeddable corrosion monitoring instrumentation. These topics will be discussed in this chapter starting with a general overview of corrosion and then focusing on corrosion within concrete structures. Information on ECE including the principles of the treatment process and observed results from other treated structures will be summarized. A discussion of the use of FRP wraps for rehabilitation and strengthening of concrete structures will then be presented. Included in this discussion will be a summary of previous laboratory testing done on similar composite wrap systems in the area of bond strength to a concrete substrate, including studies that evaluated the effects of environmental exposure. The final portion of this chapter will focus on research conducted on and with various types of embeddable corrosion monitoring instrumentation for reinforced concrete structures.

2.1 Principles of Corrosion

The deterioration or destruction of a metal or metal alloy as a result of exposure to its environment can be classified as corrosion [1]. Metallic corrosion can be likened to extractive metallurgy in reverse because the chemical reactions that produce corrosion emit the same amount of energy that was input to refine the metals from their natural states in minerals or chemical compounds.

2.1.1 Electrochemistry of Corrosion

Any chemical reaction that can be divided into partial reactions of oxidation and reduction can be classified as electrochemical [2]. To fully comprehend the fundamentals of metallic corrosion, it is first necessary to discuss the electrochemical nature of the process. This can be accomplished through analysis of an example of metallic corrosion.

The placement of an iron plate in sulfuric acid can be represented by the chemical reaction:

$$Fe + H_2SO_4 \Downarrow \; FeSO_4 + H_2 \qquad (1)$$

Upon reaction with the acid, iron is converted to soluble iron sulfate and hydrogen bubbles form on the surface of the iron plate. This equation can also be represented in ionic form as follows:

$$Fe + 2H^{+} + (SO_4)^{-2} \Downarrow \; Fe^{+2} + (SO_4)^{-2} + H_2 \qquad (2)$$

With sulfate ions present in the reaction as reactants and products, they can be eliminated from both sides of the equation leaving:

$$Fe + 2H^{+} \Downarrow \; Fe^{+2} + H_2 \qquad (3)$$

This equation can then be separated into two partial reactions or half-cell reactions:

$$Fe \Downarrow \; Fe^{+2} + 2e^{-} \qquad \text{anodic reaction} \qquad (4)$$

$$2H^{+} + 2e^{-} \Downarrow \; H_2 \qquad \text{cathodic reaction} \qquad (5)$$

As iron is oxidized in the anodic reaction, and becomes an electron donor, hydrogen ions are reduced in the cathodic reaction as electrons are accepted. An illustration of these reactions is shown in Figure 2.1 [1]. In this example, the sulfuric acid solution is called the electrolyte, and the iron plate is an electrode.

2.1.2 Metallic Corrosion

A fundamental law of metallic corrosion is that the oxidation rate must be equivalent to the rate of reduction and the anodic and cathodic reactions must occur simultaneously [2]. An anodic reaction will always result in the production of electrons. In metallic corrosion this is typically through the oxidation of a metal to its ion. A cathodic reaction will always consume electrons, although the exact form of the reaction is variable. During metallic corrosion the cathodic reaction is commonly either hydrogen evolution, metal ion reduction, or the reduction of dissolved oxygen [3].

A requirement for the electrochemical process of corrosion to initiate is the presence of both an anode and a cathode located in the same electrolyte. Electron transfer occurs through the electrolyte, which by definition must contain some degree of moisture. Therefore, corrosion can only occur with some degree of water present, either in the liquid or condensed vapor phases.

As each half-cell reaction proceeds, vast amounts of energy are released. The changes in energy provide the driving force and spontaneous direction for the corrosion reaction [1]. Therefore, the theories of thermodynamics are an integral tool for understanding both corrosion and corrosion potential.

The change in free energy that can be associated with an electrochemical reaction is given by the equation:

$$\div G = -nFE \tag{6}$$

where n represents the number of electrons exchanged in the reaction and F is Faraday's constant of 96,500 coulombs per equivalent [1]. The electrode potential of the reaction, E, is computed from the sum of the potentials of the oxidation and reduction half-cell reactions, or anodic and cathodic reactions, as

$$E = e_a + e_c \tag{7}$$

Some standard electrochemical potentials for common half-cell reactions that are relevant to this investigation, against a standard hydrogen electrode (SHE) at 25 ∀C, have been listed in Table 2.1 [4]. Considering the example presented earlier of an iron plate in sulfuric acid, the total potential involved can be calculated as the sum of the partial reaction potentials, as determined in Table 2.1. That is,

$$E = 0.440 + 0.000 \tag{8}$$

where the electrode potential for the half-cell reaction involving iron is positive because it is an oxidation, or the reverse of the reduction potential listed in Table 2.1. A positive overall cell potential indicates a negative free energy change, $\div G$. Therefore, the products are more stable than the reactants, and both half-cell reactions proceed in the directions indicated in equations (4) and (5).

The values listed in Table 2.2 correspond to standard half-cell potentials. The Nernst equation provides a more accurate computation of the total electrochemical potential of an oxidation-reduction reaction, based on the concentrations of the oxidizing and reducing species. The Nernst equation is:

$$E \mid E^{o} 2 \left(\frac{0.059}{n} \right\} * \log \left(\frac{\mid OX \mid}{\mid REDOX \mid} \right\} \tag{9}$$

where the standard half-cell potentials listed in Table 2.1 are indicated by $E\forall$, n represents the number of electrons transferred during the reaction, and $|OX|$ or $|REDOX|$ indicate the concentration of oxidizing and reducing species, respectively. As the concentrations of the oxidizing and reducing species change through corrosion processes, the potential of the corrosion cell also changes, in accordance with the Nernst equation.

To determine the driving force in an electrochemical reaction, the Nernst equation can be used to calculate cell potential. When the potential of one of the half-cell reactions is known, it can be treated as a reference electrode. The use of a reference electrode enables the potential of the other reaction to be determined directly. Different types of reference electrodes are available and commonly used for laboratory experimentation. The standard potentials for common reference electrodes, against a standard hydrogen electrode, are listed in Table 2.2 [1]. Of the listed electrodes, the saturated calomel electrode is the most convenient for corrosion evaluation because chloride ion activity can be regulated by sustaining saturation in a solution of KCl [1]. Comparing potentials obtained with one type of reference electrode to a different reference electrode requires an adjustment of the potential according to the difference between reference values listed in Table 2.2. For example, a potential of –0.096 V against a copper-copper sulfate electrode is equivalent to a potential of 0.00 V with respect to a silver-silver chloride electrode.

For a given metal and electrolyte system, Pourbaix diagrams developed by Marcel Pourbaix establish equilibrium conditions as a function of both pH and electrochemical potential. Based on the theories of thermodynamics, these diagrams are a useful tool for evaluating the spontaneous direction of a reaction, estimating the composition of corrosion products, and determining the environment to prevent corrosive activity [2]. However, these diagrams cannot be used to obtain corrosion rates, and are inaccurate for contaminated systems. An example of a Pourbaix diagram for iron and water is given in Figure 2.2, where the potential of the iron with respect to a standard hydrogen electrode (SHE) is plotted against electrolyte pH [1]. As shown in Figure 2.2, pH and electrode potential can be adjusted so that the corrosion of iron can be thermodynamically prevented. Corrosion immunity occurs, for the iron and water example, when electrode potential is highly cathodic, regardless of the solution pH.

For many metals, the corrosion rate decreases significantly above a critical electrochemical potential, E_p, as shown in Figure 2.3 [1]. Corrosion rates steadily increase up to E_p, where the passive film becomes stable, and the corrosion rates fall dramatically. This phenomenon is defined by Fontana as passivity, and it can be defined as “a loss of chemical reactivity under certain environmental conditions” [3]. The decrease in corrosion rate is caused by the formation of a thin, protective, hydrated oxide film on the surface of the metal under an oxidizing condition with high anodic polarization, which acts to protect the metal from the surrounding corrosion conditions [1]. Although the existence of the thin film has been

established, the exact characteristics and properties of the thin film remain unknown [3]. As shown in Figure 2.3, the corrosion rate increases again at higher anodic potentials in the transpassive state, due to a breakdown in the passive layer on the metal. However, only very strong oxidizers, rarely seen in practice, produce potentials in the transpassive region [1]. Low corrosion rates are also witnessed at low levels of anodic potential, and this is the basis of cathodic protection, which will be discussed in Section 2.3. Pourbaix diagrams can also assist in determining the conditions in which passivity may occur. As shown in Figure 2.2, solutions of high pH generally retard the corrosion of iron, even in regions of high anodic polarization. At high cathodic potential, iron is immune to corrosion, or is cathodically protected. The issue of passivity will be discussed further, with respect to reinforcing steel in concrete structures, in the next section.

The various types of metallic corrosion, relevant to reinforced concrete structures, can be identified by their general characteristics as follows:

1) Uniform corrosion is the uniform, regular removal of metal from the surface when the corrosive environment has the same access to all areas of the metal surface. This is the expected form of corrosion when the metal is compositionally and metallurgically uniform [1].
2) Galvanic corrosion occurs when two dissimilar alloys are placed in the same corrosive electrolyte. The alloy with a more positive corrosion potential will be protected while corroding the less noble alloy. Therefore, the coupling of different metals can create and prevent corrosion. For example, in zinc-coated reinforcing steel, the steel is more noble than zinc and thus it is galvanically protected while the sacrificial zinc layer is corroded [5].
3) Pitting corrosion is a localized corrosive attack in an otherwise resistant surface. Local breakdowns of the passive layer at isolated sites on stainless steels and nickel alloys with chromium, can result in pitting corrosion [1].
4) Environmentally induced cracking is defined as the brittle fracture of a normally ductile material in an environment that initiates minimal uniform corrosion. Three types of failure are stress corrosion cracking (SCC), corrosion fatigue cracking (CFC), and hydrogen-induced cracking (HIC). SCC is the brittle failure of an alloy, exposed to a corrosive environment, at a relatively

low static tensile stress. Three conditions must be simultaneously present for SCC to occur: a susceptible material, a corrosive environment, and some degree of tensile stress. CFC is the brittle failure of an alloy caused by fluctuating stress in a corrosive environment. Finally, HIC is the brittle mechanical fracture after the penetration and diffusion of atomic hydrogen into the crystal structure of an alloy [1].

Uniform corrosion is the most common form of corrosion in concrete structures, but localized forms of corrosion can be more difficult to predict and control. Epoxy-coated rebar, and reinforcing steel located at cracks in the concrete cover, tend to exhibit pitting corrosion. Although, localized corrosion, such as pitting, may not consume as much metal as uniform corrosion, failure may occur more rapidly due to localized penetration that causes a reduction in cross-sectional area, and consequent increased stresses [1].

2.2 Corrosion in Reinforced Concrete Structures

A passive film, created by the alkaline environment of the surrounding concrete, initially protects the reinforcing steel within a new concrete structure from corrosion. The initial concrete alkalinity (pH 12 to 13) is the result of the concentrations of potassium and sodium hydroxides in the pore solution, and not the calcium hydroxides released during curing, as was initially believed [6]. If the concrete is exposed to air, oxygen is generally present at the level of reinforcing steel due to the porosity of the concrete matrix. This combination can result in an insoluble oxide film, of gamma ferric oxide νFe_2O_3, on the rebar surface [3]. The corrosion resistance of the reinforcing steel created by this passive layer will remain indefinitely, unless a mechanical or chemical concrete intrusion changes the environment surrounding the rebar.

Certain environmental exposure conditions of concrete structures can lead to intrusions that act to breakdown the passive film on the reinforcing steel. The porous nature of concrete can allow intrusions to percolate deep into the structures, eventually reaching the level of the reinforcing steel. The penetration of carbon dioxide into moist concrete can lead to carbonation. This occurs after the carbon dioxide combines with available lime in the concrete, and carbonates are formed. As carbonation progresses and the concrete pH falls below the critical value, of approximately 9.5, the passive film on the reinforcing steel is destroyed. The removal

of the passive layer, and the lowering of the concrete pH, can lead to spontaneous corrosion of the steel [7].

A more common concrete intrusion is the chloride ion [8]. Chloride ions in concrete typically originate from either admixtures, used as early setting additives, or de-icing salts used to clear roadways during the winter months. However, when chloride ions are introduced directly in the concrete mix through admixtures, some are immediately bound into the hydrated cement, and are not available to destroy the passivity of the reinforcing steel. Nonetheless, set accelerators containing chloride ions, such as calcium chloride, have been identified as corrosion accelerators, and their use has been limited by ACI committee 212 [9,10]. When contaminated mix materials, or admixtures containing chloride ions, are used to cast concrete, the de-passivation of the reinforcing steel can occur immediately, and corrosion is dependent on the levels of water and oxygen present within the concrete. Corrosion initiated by external sources of chloride contamination, typically from de-icing salts, is dependent on the rate of chloride ion diffusion through the concrete matrix, or the permeability of the cured concrete. The use of road salts in winter maintenance activities was intensified after the "bare roads policy" initiated in the 1960's, leading to a significant increase in the chloride contamination of concrete bridges and roadways [11]. Chloride ions reduce the pH of the surrounding concrete, destroying the passive layer on the reinforcing steel, and increasing the active corrosion rate of carbon steel in neutral and alkaline pore water solutions [1]. The removal of the passive layer on the rebar often leads to uniform corrosion as water and oxygen become available to the steel. The resultant ferrous corrosion products form an acid solution with the chloride, which neutralizes the alkaline concrete environment. Pitting corrosion may also result if chloride intrusion is localized, and only portions of the passive film are destroyed, as chloride ions replace hydroxyl ions.

The chemical reactions that occur within a concrete structure during the corrosion of reinforcing steel are complex and vary depending on the composition of the concrete matrix and the concentrations of intrusions, such as chloride ions. The types of corrosion cells can also vary, from macrocells to microcells. A macrocell refers to the forms of corrosion in which the anodic and cathodic elements of the cell are either separate, discrete elements, or large portions of one element. An example would be positively and negatively charged layers of reinforcing steel, electrically connected by stirrups, chairs, or ties. Exposing the two layers to different environmental conditions, such as oxygen availability or chloride ion concentration, could create

a difference in potential. Therefore, the anodic and cathodic elements of the corrosion cell would be the two distinct layers of steel reinforcement. Microcell corrosion refers to the forms of corrosion that occur over very localized areas. The anode and cathode of the microcell form alternately in close proximity to each other. An example is pitting corrosion initiated by an anode and a cathode located on the same reinforcing bar. Differences in oxygen levels, moisture contents, chloride concentrations, or concrete pH may create differences in electrochemical potential along the same bar, initiating microcell corrosion [3]. Variations in the metallurgical composition along a reinforcing steel bar may also lead to pitting corrosion. Examples of typical macrocells and microcells in reinforced concrete structures are shown in Figure 2.4 [5].

The typical corrosion cells within the structures included in this investigation are probably macrocells, although microcells are possible as well. Because the columns are reinforced with spiral and vertical reinforcement, a macrocell may form between adjacent vertical bars, electrically connected by the spiral reinforcement. Corrosion cells within the pier caps may form between the layers of horizontal reinforcement, connected by the vertical stirrups.

A more thorough illustration of macrocell corrosion in reinforced concrete is shown in Figure 2.5 [5]. The chemical reactions included in this figure represent a simplified model of the corrosion of iron in the presence of water and oxygen. These reactions are:

$$2Fe \Downarrow \; 2Fe^{++} + 4e^{-} \tag{10}$$

$$2Fe^{++} + 4OH^{-} \Downarrow \; 2Fe(OH)_2 \tag{11}$$

$$O_2 + 2H_2O + 4e^{-} \Downarrow \; 4OH^{-} \tag{12}$$

As iron is oxidized on the surface of the anode, electrons move to the cathode through electronic conductance where they are consumed by a reduction reaction. The hydroxyl ions produced at the cathode during the reduction reaction then move to the anode to react with the ferrous ions. The reaction at the anode results in the production of ferrous hydroxide. The volume of the corrosion products is greater than the volume of the original steel. This additional volume creates large stresses in the concrete that can lead to cracking, spalling, and delamination of concrete cover. As cracks form in the concrete, and oxygen becomes more readily available at the level of reinforcing steel, the ferric hydroxide undergoes an additional electrochemical reaction. Because ferrous hydroxide is relatively unstable in the presence of oxygen, if sufficient oxygen is present ferrous hydroxide will be converted to ferric salt, or red rust, through the reaction listed:

$$2Fe(OH)_2 + \tfrac{1}{2} O_2 + H_2O \Downarrow 2Fe(OH)_3 \quad (13)$$

These rust stains on the surface of a concrete structure can be considered a visual symptom for corrosion damage, in addition to cracking, spalling, and delaminations. In uncracked concrete, the corrosion products will generally remain in the ferrous state, or in the form of ferrous hydroxide [3]. However, the reactions presented for the corrosion of iron in the presence of water and oxygen are simplified somewhat, with respect to reinforced concrete structures. The actual corrosion products that are created can vary significantly and will depend on electrochemical cell potential, concrete pH, and the metallurgic composition of the reinforcing steel. Potential corrosion products may include magnetite (Fe_3O_4), hematite (Fe_2O_3), or goethite (FeOOH) [3].

An additional schematic of a type of microcell corrosion, in the form of pitting corrosion, is shown in Figure 2.6 [3]. Although no definitive theory on the initiation of pitting corrosion is agreed upon, the localized breakdown of the reinforcing steel passivity is a necessary factor [2,12]. As indicated in Figure 2.6, pitting corrosion is a self-perpetuating process. As metal is dissolved at the anodic portion of the steel bar, a pit develops. As conditions inside the pit become increasingly more acidic from the formation of corrosion products, additional metal is dissolved [3]. The portions of the steel bar adjacent to the pit sustain the oxygen reduction reaction while metal is continually oxidized. Because minimal oxygen exists within the pit, oxygen reduction does not occur. Therefore, the cathodic regions of the steel bar are protected from corrosion while metal in the anodic region is continually removed.

Multiple factors affect the initiation of an electrochemical corrosion cell in concrete, and the type of cell that is created. As previously discussed, an aggressive agent that deteriorates the passivity of the reinforcing steel is required. However, water, or moisture, is a necessary component of the corrosion process so that the pore water of the concrete acts as an electrolyte and facilitates the flow of ions between electrodes in the electrochemical corrosion cell, whether a microcell or a macrocell [13]. Oxygen is required to maintain the cathodic reaction, as shown earlier in Equation (12) and Figure 2.5. Each of the three components necessary to initiate a typical corrosion cell in reinforced concrete (water, oxygen, and an aggressive agent) must either diffuse through the concrete, or must be present when the concrete is cast, at the level of reinforcing steel. The absence of water or oxygen at the cathode will effectively stop the corrosion process because the rate of reduction at the anode must equal the oxidation rate of the

cathode. However, because water and oxygen can exist in the gaseous form, and the concrete is typically permeable to at least some degree, the cathodic reaction will generally not be controlled by these variables. In most above-ground exterior structures, water and oxygen are readily available from the atmosphere and external moisture, respectively. The availability of oxygen would likely limit corrosion rates in underwater structures, even though moisture and chloride ions, in the case of seawater, would be abundant.

The corrosion resistance of reinforcing steel is also dependent on several concrete mix design, and structured design, variables. The overall permeability of the concrete is a direct function of the water/cement (w/c) ratio of the cement paste, although it can also be greatly affected by concrete cracks, shrinkage cracks, and aggregate defects [13,14]. Higher w/c ratios have been identified by many researchers as increasing the probability and rate of corrosion, due to the increased permeability of the concrete matrix [15,16,17,18]. Research conducted by Pfeifer, Landgren and Zoob indicated that a reduction in w/c ratio from 0.51 to 0.4 resulted in an 80% reduction in chloride ion permeation, to a 2.54 cm depth in normal concrete [19]. The amount of concrete cover that is provided over the reinforcing steel will also affect corrosion rates [17,19]. Breakdown of the passive layer on the rebar depends on the diffusion of water, oxygen, and chloride ions to the reinforcing steel level. Therefore, the longer the travel distance for each of these species, or the more concrete cover that is provided, the longer the time to corrosion.

2.2.1 Relevant Studies of Corrosion in Reinforced Concrete

Although multiple studies in the past 30 years have effectively monitored the corrosion of reinforcing steel in concrete structures, this section will only describe some of the key references in this area that specifically relate to the objectives of this investigation. Key references were identified as studies of corrosion thresholds through research that evaluated relatively normal members, exposed to reasonably natural environments

The time-to-corrosion studies on concrete slabs completed by K.C. Clear, et al., for the Federal Highway Administration (FHWA) address a wide range of corrosion factors [16,17,18,20,21]. The five volumes of “Time-to-Corrosion of Reinforcing Steel in Concrete Slabs” that summarize their findings collected through nine years of research (1973-1982) are commonly referenced in papers discussing corrosion of reinforcing steel in concrete. Test

procedures used in this study were based on the assumption that the corrosion of reinforcing steel is primarily caused by macroscopic corrosion cells. The study conducted by Clear, et al., consisted of 124 concrete slabs (1.22 m by 1.52 m by 15 cm thick) that were subjected to daily salt applications over an extended period of time in outdoor conditions [16,17,20].

The results from the initial work completed by Clear, Hay, and Lewis indicated that a value of 2000 ppm Cl^- by weight of cement represented an average threshold concentration of chloride at which corrosion of the reinforcing steel initiated [16]. This value corresponds to 289 ppm by weight of concrete, assuming a concrete unit weight of 6589 kg/m^3. Testing of chloride content versus slab depth of over 1200 samples produced results that not only related chloride concentration with time-to-corrosion of reinforcing steel, but also assessed the effects of w/c ratio and depth of concrete cover. Both of these variables were determined to have a major influence on permeation of chloride ions into the concrete, as shown in Table 2.3, where concentrations are included as ppm by weight of concrete [17]. Chloride concentrations of less than 102 ppm by weight of concrete were considered baseline values, or concentrations originally present in the concrete, and are indicated in Table 2.3 as BL.

A chloride concentration study of three prestressed girders and the bridge deck of a twenty-year-old bridge removed from service over Interstate 694 in Minneapolis, Minnesota, was conducted by Coggins and French [22]. Chloride samples were collected from 20 different locations on two of the girders, seven on the third girder, and five on the bridge deck.

Their findings indicated that chloride concentrations in the girders at sample depths of less than 3.75 cm inch varied significantly, due to the degree of exposure associated with each sample location, from 40 to 1180 ppm by weight of concrete. Maximum chloride concentrations at depths greater than 3.75 cm were not significantly higher than 250 ppm by weight of concrete. Corrosion damage was not found on the prestressing strands in the bridge girders, except for the end faces where the epoxy coating had been chipped, and some corrosion staining was evident. Samples collected from the bridge deck reported much higher chloride concentrations but this result was expected due to the direct application and ponding of deicing salts on the surface of the deck. At a depth of 3.75 cm inch, where the top layer of steel was located, chloride ion concentrations ranged from 1110 to 1940 ppm by weight of concrete. Coggins and French estimated a 20% cement factor (cement contribution to concrete weight) translating the range of these concentrations to 5550 to 9700 ppm by weight of cement. Although the chloride

concentrations at the depth of the steel were over twice the corrosion threshold established by Clear et al., of 2000 ppm by weight of cement, significant corrosion related deterioration was not detected [16].

After 830 field saltings (approximated as roughly 23 service years in Minnesota), Clear et al. reported that the average chloride concentration at a depth of one inch was 2912 ppm by weight of cement, in the test slabs containing a w/c ratio of 0.5. Slabs containing a w/c ratio of 0.4 reported an average chloride concentration of 404 ppm by weight of cement at a depth of 2.54 cm [17]. The twenty-year-old bridge deck analyzed by Coggins and French contained an average chloride concentration of 1900 ppm by weight of concrete at a depth of 2.54 cm [22]. Estimating the w/c ratio of the bridge deck analyzed by Coggins and French to be between 0.4 and 0.5 indicates that these results correlated loosely with the results obtained from the study by Clear, et al. [17]. Although this comparison of results is fairly crude and inconclusive, it does indicate that the time-to-corrosion values used to relate the experimental method of the FHWA studies to actual field saltings of bridge structures in Minnesota were not impractical.

A corrosion study conducted in 1986 at Queen's University in Kingston, Ontario, Canada by Hope and Ip, monitored the microcell corrosion of concrete containing admixed chlorides and chloride bearing aggregates in concrete slabs (2.5 in x 12 in x 16 in) exposed to laboratory and outdoor conditions. Three electrically isolated steel rods, or two working electrodes and one reference electrode, measuring 13 mm in diameter were cast into the slabs to evaluate corrosion. Differential levels of calcium dihydrate, from 0 to 2 percent by mass of cement, were mixed into eight slab sets and chloride-bearing aggregates, 0.136 and 0.197 percent chloride-ion content, were mixed into the other two sets. Each set contained six slabs, of which three were stored in the laboratory and wet-dry cycled, and three were kept outdoors. Because the electrodes were not electrically connected within the concrete, and differential levels of chloride ions at the electrodes initiated corrosion, the form of corrosion that was monitored was microcell. Corrosion was monitored using the linear polarization technique, AC-impedence, visual inspection, and the gravimetric mass loss method. Through the results of this experimental program, Hope and Ip concluded that the chloride threshold limit to initiate reinforcing steel corrosion was between 2000 and 4000 ppm calcium dihydrate by mass of cement, depending on the test method [23].

These results correlated well with the research conducted by Clear, et al. that indicated an average chloride threshold of 2000 ppm Cl^- by weight of cement [17]. Although the research

conducted by Hope and Ip analyzed microcell corrosion using isolated steel electrodes that were not electrically connected (therefore, microcell corrosion and not pitting corrosion), and the research conducted by Clear et al. investigated macrocell corrosion, both cell types were analyzed as galvanic corrosion cells. Differential levels of chloride concentration at either the levels of reinforcement in the slabs, or at the electrodes, were the primary initiators of corrosive activity. Therefore, the comparison of corrosion thresholds is relevant.

Research conducted by Stratfull and others at Caltrans indicates that electrode potential measurements can be used to indicate areas of probable corrosive activity [9]. The measurements of potential, between the reinforcing steel under consideration and a standardized half-cell or reference electrode, can be obtained with a voltmeter. The most common reference electrodes for laboratory testing are copper-copper sulfate, saturated calomel, or silver-silver chloride but for field testing of structures, the copper-copper sulfate electrode is typically used because of its durability and reliability. Although this technique can determine areas of probable corrosive activity, it cannot determine a corrosion rate.

Based on their large amount of experience with the corrosion of steel in concrete, ASTM has established the probability of corrosive activity for a given system, based on differences in electrochemical potential, as shown in Table 2.4 [24]. ASTM C876 test specifications list that potential readings between –0.20 and –0.35 volts indicate "uncertain" corrosive probability, more negative than –0.35 volts indicate a 90% probability of corrosive activity, and more positive than –0.20 V indicate a 90% probability of no corrosive activity. The ranges of potential presented are with respect to a copper-copper sulfate electrode.

2.3 Corrosion Mitigation Techniques for Reinforced Concrete Structures

Although the corrosion process in reinforced concrete structures is extremely complex, and still not completely understood, advances have been made in corrosion protection and treatment through years of research. As discussed, the use of low w/c ratios and increased concrete cover can delay the onset of corrosion and increase the service life of an concrete structure with exterior exposure [17]. The addition of calcium nitrate to a concrete mix may help delay the onset of reinforcing steel corrosion, as determined through research conducted by Virmani, Clear, and Pasko [18]. Improved materials can also provide additional protection from corrosion. The use of epoxy-coated rebar has also been investigated by Virmani, et. al.

Their results indicated that if an uncoated reinforcing bar is assigned an arbitrary service life in chloride contaminated concrete of one year, an epoxy-coated bar would require 46 years of exposure in the same contaminated environment for corrosion to consume the same amount of iron [18]. However, constructability concerns have arisen with regards to the use of epoxy-coated rebar in concrete structures. Extensive care needs to be taken to ensure that defects in the epoxy coating are not created during manufacturing, handling, or placement of the bars, because a small defect in the coating may accelerate the corrosion process. The increase in corrosion rate is due to the unfavorable effect of having a large cathode and a very small anode, which would be the small area of steel exposed by the defect in the epoxy, when only the top layer of reinforcement is epoxy-coated.

While each of the aforementioned techniques may help reduce or delay the effects of corrosion, each is only applicable for new concrete structures. For existing structures with corrosion problems, few techniques are available to engineers to stop or reduce corrosion of the reinforcing steel in chloride-contaminated concrete. Electrochemical chloride extraction is a technique that can reduce chloride levels in contaminated concrete, which may stop corrosion, as discussed in the next section. The use of concrete sealers or composite wraps to seal the concrete surface, in order to prevent additional chloride ion intrusion into the concrete, may help mitigate corrosion and will be discussed further in Section 2.4. However, the FHWA concluded in the late 1970's that cathodic protection was the only technique that was capable of stopping the corrosion of reinforcing steel in chloride-contaminated concrete, regardless of the chloride concentration of the concrete [25].

Cathodic protection was first used in the United States in the 1920's and is now widely used to prevent the corrosion of buried steel pipelines, offshore drilling structures, ship hulls, water tanks, and various chemical equipment located in corrosive environments. In principle, cathodic protection can prevent corrosion of a metal or alloy exposed to an aqueous electrolyte indefinitely, if the system is properly maintained [1].

Cathodic protection reduces the corrosion rate of a corroding metal surface by cathodic polarization, and can be provided with either an impressed current or sacrificial anode. To describe each type of cathodic protection, the corrosion of iron is presented as an example.

The partial reactions for the corrosion of iron in the presence of water and oxygen were presented in Section 2.2 as Equations (10) and (12). When an excess of electrons is provided at

the level of the iron, the rate of the iron oxidation reaction is reduced, Equation (10), while the rate of oxygen reduction and OH^- production is increased, Equation (12). For cathodic protection with an impressed current anode, a DC rectifier is typically used to supply the current, and thus the excess of electrons. Electrically connecting the iron to a second metal with a more active corrosion potential than iron, or a sacrificial anode, can also cathodically protect the iron using a galvanic couple. This type of cathodic protection does not require an external power supply, because the source of the DC current is the anode itself. Electric current naturally flows from the anode to the cathode, through the system electrolyte. The sacrificial anode is preferentially consumed by anodic dissolution, while the more noble metal, or in this case iron, is cathodically protected [1]. However, to indefinitely protect the more noble metal, the sacrificial anode needs to be periodically replaced.

Cathodic protection was first applied on the Sly Park Bridge in 1973, by the California Department of Transportation [13]. The majority of cathodic protection systems currently in place on reinforced concrete structures are of the impressed current type. The systems are typically used on bridge decks, where chloride contamination from road salts is the most severe. An external anode, capable of sustaining an oxidation reaction without suffering significant physical damage, is attached to the structure. A titanium mesh is the most common anode used. An external power supply is used to force current from the anode, through the concrete, to the reinforcing steel. After connecting the positive terminal of a power supply to the anode, and the negative terminal to the reinforcing steel, the reinforcing steel cage becomes the system cathode and only reduction reactions, or electron consumption reactions, can occur. Therefore, the reinforcing steel is cathodically protected and corrosion reactions will not take place. The anodic reaction will depend on the type of anode used, and may be a mixture of oxygen evolution, chloride evolution, and carbon oxidation to carbon dioxide or carbonate [11]. The dominant cathodic reaction at the reinforcing steel level will be oxygen reduction. The possible cathodic reactions are as follows:

$$O_2 + 2H_2O + 4e^- \Downarrow 4OH^- \quad (14)$$

$$2H_2O + 2e^- \Downarrow \ H_2 + 2OH^- \quad (15)$$

The limited availability of oxygen in concrete will control the rate of the first reaction, Equation (14), and thus most of the current entering the reinforcing steel will result in the production of hydrogen and hydroxyl ions on the steel surface. Because the reinforcing steel is

negatively charged, the negatively charged chloride ions are driven away from the rebar, towards the positively charged anode mesh. While corroded steel cannot be returned to its original state, the corrosion process can be stopped and continued corrosion can be averted using cathodic protection [11]. The migration of chloride ions away from the rebar, and the production of hydroxyl ions at the reinforcing steel level, act to increase the alkalinity of the surrounding concrete, and recreate the passive layer on the reinforcing steel.

Cathodic protection of reinforced concrete structures with impressed current requires approximately 0.5-1.5 mA of current per square foot of concrete surface area [11]. The requirements for indefinite cathodic protection with impressed current, in terms of system installation, maintenance, and power supplied, can make this mitigation technique economically infeasible, especially on large reinforced concrete structures. In contrast, cathodic protection with a sacrificial anode does not require an external power supply, decreasing overall costs and maintenance costs, because of the created galvanic couple. Current is naturally forced from the more anodic metal, to the less active metal, through the concrete. Therefore, any metal more anodic than steel could be used as a sacrificial anode for a cathodic protection system on a reinforced concrete structure. However, studies conducted on the use of sacrificial zinc anodes has indicated that they are not active enough to provide enough system current for adequate cathodic protection of the reinforcing steel. Research conducted by the FHWA on the Bryant Patton Bridge in Eastpoint, Florida has indicated that an aluminum-zinc-indium alloy applied with a thermal spray (using a combination of flame and arc spraying), at a uniform thickness of approximately 400 σm over the surface of the structure, supplied sufficient system current to provide adequate cathodic protection. The external spray anode was electrically connected to the reinforcing steel, but current was not supplied to the system because cathodic protection was instead established through the creation of a galvanic cell between the anode and the reinforcing steel. This galvanic cell preferentially corroded the sacrificial anode, while the reinforcing steel was cathodically protected. This aluminum alloy anode was also determined to possess a reasonable service life of 10 to 15 years before replacement was required, although a suggested method of reapplication or replacement was not indicated [25].

2.3.1 Electrochemical Chloride Extraction

Cathodic protection of reinforced concrete structures with impressed current is an effective method to stop corrosion of the reinforcing steel in chloride-contaminated concrete. However, to maintain the effectiveness of the system, a continuous power supply and regular electrical maintenance are required. An alternative to cathodic protection is chloride removal, or electrochemical chloride extraction (ECE). While similar in principle to cathodic protection, ECE is a temporary treatment process that supplies 50 to 500 times the current, in amperes, that is continually supplied in a cathodic protection system [26]. The total amount of charge applied in a typical ECE treatment process of approximately eight weeks is equivalent to what ten years of cathodic protection would deliver. Therefore, ECE is a short-term corrosion treatment process that requires no additional maintenance after completion, whereas cathodic protection is normally intended to remain in operation throughout the service life of a structure.

Electrochemical chloride extraction has been studied as a permanent rehabilitation method for reinforced concrete structures since the mid-1970's. The Kansas Department of Transportation studied the use of a sacrificial copper anode to show that chloride ions could be driven from concrete by negatively charging the reinforcing steel with a considerably higher current than that used in cathodic protection [27,28]. A study conducted by Battelle Columbus Laboratories also indicated that a temporary chloride treatment, 12-24 hours with a current density of 23-28 A/m^2 at a constant system voltage of 100V, could effectively remove chloride from concrete [29]. However, the high levels of current used in each of these studies had some side effects such as increased concrete permeability, decreased concrete-steel bond, and cracking of the concrete [30]. Although the movement of anions and cations through the concrete, towards the positively and negatively charged electrodes respectively, did not appear to have a harmful effect on the concrete, changes at the reinforcing steel interface raised concerns about the process. As discussed previously, the cathodic reactions that occur at the reinforcing steel were given in Equations (14) and (15). Because oxygen is limited, most of the system current will produce hydrogen and hydroxyl ions on the steel surface through Equation (15). Similar to cathodic protection, the hydroxyl ions will act to increase the concrete alkalinity and re-passify the steel, potentially preventing the re-initiation of corrosion. However, the production of large quantities of hydrogen created concerns about the potential hydrogen embrittlement of the reinforcing steel or damage to the reinforcement bond with the surrounding concrete, after

softening of the cement paste [26]. Potential etching of the concrete surface in contact with the electrolyte, caused by the evolution of hypochlorous acid at the anode, was also a concern.

Developed in Norway in the mid-1980's, the NORCURE process for ECE consists of a temporary external anode, either steel or titanium mesh, and a cellulose fiber electrolyte applied to the concrete surface, with current passed between this anode and the reinforcing steel for approximately eight to eleven weeks [31]. Similar to cathodic protection, by connecting the positive terminal of a power supply to the anode, and the negative terminal to the reinforcing steel, the steel becomes the cathode in the electrochemical cell. The negatively charged chloride ions migrate toward the anode, away from the negatively charged reinforcing steel, and potentially out of the concrete into the external electrolyte, as shown in Figure 2.7 [30]. Once the chloride content has been reduced to acceptable levels and the concrete pH has become more alkaline, the temporary anode and electrolyte are removed and treatment is complete. The rate of chloride extraction is largely dependent on the magnitude of applied current [26].

Several criteria have been established for structures to be considered as candidates for ECE with the NORCURE process. The most significant is that the structure is undergoing chloride-induced corrosion, which can be verified by visual inspection, chloride sampling, and half-cell potential mapping. Because of the evolution of hydrogen at the reinforcing steel, prestressed concrete structures cannot be treated due to concerns of hydrogen embrittlement. Structures containing alkali-reactive aggregates cannot be treated because the chloride removal process may aggravate the expansive reaction, although the use of lithium ions in the electrolyte is being investigated as a potential control for this reaction [32]. Good continuity between the reinforcing steel of the structure, less than 1 mV between two pieces of steel, is required to distribute the system current throughout all portions of the structure. Finally, several additional criteria have been established as desirable to ease the installation and maintenance of the treatment process. These include, but are not limited to, simple geometry, minimum concrete damage and exposed steel, minimum disruption of traffic, and low concrete resistance [26].

Adverse side effects of elevated system current (such as increased concrete permeability, decreasing steel-concrete bond, and cracking in the concrete) witnessed in early studies conducted on ECE, prompted more thorough investigations [30]. Research on the NORCURE treatment process was conducted by Bennett, et al., on laboratory slabs and portions of some bridge elements, for the Strategic Highway Research Program in 1993, and each of these

concerns were addressed [31,33,34]. These studies concluded that if the electrolyte pH is controlled and kept basic, and the system current is kept below 5 A/m^2, the NORCURE process for chloride extraction is unlikely to adversely affect the concrete. The ECE treatments removed 20-50% of the chloride ions from the concrete, and relocated the remaining chloride ions away from the reinforcing steel. The results of this research also confirmed the increased passivation of the reinforcing steel through the production of hydroxyl ions at the rebar interface, because of the reduction of water at the cathode. The SHRP project also reached several conclusions about the effectiveness of chloride removal. The percentage of removal was dependent on the design of the reinforcement, with regards to spacing and placement of the bars, the degree of chloride ingression, and the distribution of chloride ions. Effective chloride removal is usually accomplished after a total charge passed of 60 to 150 $A\text{-}hr/m^2$. Treatment with less total charge will not remove sufficient chloride, nor noticeably increase the concrete alkalinity. A higher total charge is recommended for structures in which the chloride content is considered high, although a specific threshold was not cited. In general, sufficient chloride will remain in the structure following ECE to reinitiate corrosion, although these chloride ions are usually distributed away from the reinforcement. The increase in alkalinity and the travel distance back to the reinforcing steel level tend to delay the return to corrosive conditions [26].

Additional field studies of ECE have indicated similar results to those reported in the SHRP studies. A recent study conducted in 1995 evaluated the ECE treatment process on four reinforced concrete columns in the substructure of the Highway 2 & 642 Overpass in Alberta, Canada. The results of this study showed that ECE had reduced chloride levels near the reinforcing steel to levels below the threshold for corrosion. Potential measurements collected in 1996 indicated that 90% of the treated areas were in the passive range, and the remaining 10% reported uncertain corrosive potential [32]. However, initial site conditions were not reported. Similar results on concrete passivity were reported from ECE treatment during 1995 of 30 columns that comprise the substructure of the Highway 6 & 11 Overpass in Regina, Saskatchewan, Canada. The bridge was reported as being contaminated with chloride ions through salt-spray and the accumulation of salt-contaminated snow, although initial chloride levels and half-cell potentials were not reported. After treatment, corrosion potentials were passive in 99% of areas, with the remaining one percent reporting uncertain potential [32]. The Virginia DOT used ECE to treat a 28-year-old concrete bridge deck on the 34^{th} Street Bridge

over Interstate 395 in 1996. The bridge deck consisted of four half-spans, identified as 4N, 4S, 5N, and 5S. Prior to ECE, 100% of the chloride samples collected from the sample depth range of 1.9-3.2 cm exceeded the established threshold for corrosion in each half-span. The amount of chloride removed through ECE treatment varied from approximately 80% in the first 1.9 cm of concrete, to 75% between 1.9 and 3.2 cm of depth [30]. Although these removal percentages were very high, multiple chloride samples still exceeding the corrosion threshold were located following ECE. The percentage of samples exceeding the corrosion threshold following ECE varied from 20% on decks 4N and 5S, to 33% on deck 5N. The results of chloride samples collected in the sample depth range of 1.9-3.2 cm before and after ECE treatment are summarized in Table 2.5. The results from this study also indicated that the percentage of chloride ions removed was highest in the vicinity of reinforcing steel.

Many research projects have indicated that ECE can significantly reduce chloride concentrations in contaminated reinforced concrete structures and can re-passify the reinforcing steel. However, questions remain about the length of the protection period that ECE provides, with respect to corrosion mitigation. Only a few studies have evaluated the long-term effectiveness of the process. During 1989, a trial of electrochemical chloride extraction was completed on a section of the Burlington Skyway in Ontario, Canada. Chlorides had extensively contaminated the piers of this bridge, after leaking through faulty expansion joints located in the bridge deck above, and corrosion problems were evident [35]. Three of the pier faces were treated with ECE, and only the North face was left untreated. Half-cell potential results collected during the seven years following the extraction process are listed in Table 2.6, where the percentage of readings falling into each potential range are presented [32]. The potential ranges presented are in mV and are negative. The effectiveness of the process in re-passivating the concrete structure is clearly evident in this table, especially upon comparison with the untreated side of the pier. An active corrosion potential has not been measured on a treated pier face and only a few potentials have indicated uncertain corrosion potential, even seven years after completion of the treatment. Half-cell potentials have also remained very stable in the years following treatment. Additional piers in the bridge substructure were treated in the fall of 1997, based on the results of the trial project [32].

ECE treatment was also performed on 24 reinforced concrete columns that formed the substructure of the Highway 11 and 16 Overpass in Saskatoon, Saskatchewan, Canada in 1994.

Chloride ions had extensively contaminated the concrete from salt spray and contaminated snow that had been piled up against the columns during the winter months [32]. After ECE, the chloride content in each of the columns was significantly reduced, and between 62 and 89 percent of the free chloride ions were removed. The pre- and post-ECE corrosion potentials on this substructure are shown in Table 2.7 [32]. Prior to ECE, corrosion potential measurements were very high and multiple areas of probable corrosive activity were located on each column. As shown in Table 2.7, the percentage of potentials that indicated a 90% probability of active corrosion varied from 8% to 36%. Following ECE, almost all corrosion potentials were in the passive range, with only a few indicating uncertain potential, as shown in Table 2.7 [32]. Over 95% of the potential measurements collected following ECE from Column Line No. 4 indicated a 90% probability of corrosive inactivity, and the percentage of passive readings was even higher on the other column lines. As evident in Table 2.7, corrosion potentials have remained highly passive in the two years following the treatment.

Unpublished reports from a follow-up investigation of the concrete slabs and portions of field structures tested in the aforementioned SHRP studies have also indicated the same long-term passivation effects of the reinforcing steel [30]. Summarizing the results of the field studies mentioned provides general conclusions about the effectiveness of the NORCURE process for ECE. Large quantities of chloride ions were removed from the treated structures, especially in the vicinity of reinforcing steel and in the concrete cover, although not all of the chloride ions were removed and areas with chloride contents exceeding the corrosion threshold following ECE occurred. Chloride ions between bars or away from the reinforcing steel are removed much more slowly due to a decreased electromagnetic driving force [32]. The majority of corrosion potentials are reduced to passive levels, and this passivation can remain for several years following treatment.

A laboratory study, to evaluate the degree and nature of chloride extraction through the ECE process, was conducted by Castellote, Andrade, and Alonso in 1999 [36]. The study consisted of a number of concrete cylinders, 130 mm in height and 100 mm in diameter, in which the position of the cathode, and the length of treatment were varied, among other parameters. Treatment length varied form one to eight weeks, and the cathode was provided either internally or externally. The external cathode was placed at the base of an unreinforced concrete cylinder, and the internal cathode was placed within the concrete cylinder, transversely

to the axis, as shown in Figure 2.8. The concrete was seeded at an initial chloride concentration of 0.2% total chloride by weight of sample. The results of this laboratory study indicated that the total charge passed during ECE, and not the duration of the process, controlled the effectiveness of the treatment, as also concluded by SHRP [26]. However, Catellote, et al., also concluded that the position of the cathode, with respect to the anode, significantly affected the chloride extraction process. In the specimens containing the internal cathode, chloride concentrations were found to significantly decrease in the region between the cathode and the anode, located at the top of the specimen, by up to 60%. However, chloride concentrations increased by up to 40% in the region between the cathode and the base of the cylinder [36]. Experiments conducted with the external cathode indicated that chloride reduction was not as severe at mid-height of the cylinder, and chloride concentration remained around the initial percentage of 0.2%. Areas near the anode and external cathode experienced reductions of between 50-60%. In both the internal and external cathode configurations, an increase in hydroxyl ions was reported at the cathode. These results indicate that areas away from the anode and cathode are not treated as effectively. These results support those witnessed by Hansson and Hansson in 1993 [37]. Therefore, in field structures with high initial chloride concentrations in the vicinity of reinforcing steel, the potential for chloride ions to accumulate behind the bars as a result of ECE, as opposed to being extracted, is extremely plausible and needs to be considered. These relocated chloride ions would then be free to migrate back to the reinforcing steel level to re-initiate corrosion, once the treatment is complete.

2.4 Fiber Reinforced Polymer Concrete Wraps

The use of fiber reinforced polymer (FRP) concrete wraps to retrofit and rehabilitate concrete structures is rapidly becoming a popular new technology. The advantages of using composite materials for retrofitting, as opposed to steel plate bonding or jacketing, are that the FRP wraps are lightweight, have a high tensile strength (up to ten times that of steel), and possess a high resistance to acids and bases making them essentially non-corrosive.

The most common usage of FRP wraps in retrofitting and rehabilitation is for external strengthening of structures. Considerable research has shown that concrete columns wrapped with FRP sheets exhibit considerably higher strength and ductility in seismic events, due to increased confinement of the concrete, than similar unwrapped structures [38,39,40].

The use of FRP sheets for flexure and shear strengthening of reinforced concrete structures has also been investigated extensively. A recent laboratory study conducted by Chaallal et al., included three reinforced concrete beams, one designed at full strength for flexure and shear and two under-designed for flexure and shear but externally reinforced with unidirectional CFRP sheets [41]. Each of the beams was 3300 mm long, 200 mm wide and 400 mm in height, and was fabricated using identical materials, aside from the differences in quantities of steel reinforcement. The objective of the study was to strengthen the two under-designed beams using external CFRP reinforcement so that the combined ultimate strength in shear and flexure would be equivalent to the strength of the fully designed concrete beam from steel reinforcement alone. This was accomplished by epoxying two, 50 mm wide strips of CFRP composite, applied 50 mm apart, along the underside of the under-reinforced specimens for external flexural reinforcement, and 50 mm wide, 400 mm long composite strips at 250 mm intervals applied perpendicular to the longitudinal axis of the beam, for external shear reinforcement. The beams were tested in four-point flexural bending. The results of these experiments indicated that increased shear strength and stiffness could be achieved, in comparison with the beams designed at full capacity, through reduced shear cracking, by restoring or upgrading beam shear strength with FRP strips [41].

The shear strengthening effects of CFRP sheets were also investigated at the University of Manitoba, Canada, through a laboratory study of four externally reinforced, prestressed concrete girders [42]. Each of the girders was I-shaped (measuring 415 mm deep, with a bottom flange width of 150 mm, and a web width of 70 mm) and cast with a 480 mm wide, 60 mm deep, concrete slab. One girder was used as a control, and the other three were reinforced with three different types of CFRP wraps in six different combinations of wrap configuration (combinations of vertical, horizontal, and diagonal reinforcement). The vertical CFRP sheets were 250 mm wide and were separated by 100 mm gaps to allow for moisture drainage. The sheets were applied on each side of the cross section, from immediately below the slab to the underside of the beam where they were overlapped for a minimum of 100 mm. A 220 mm horizontal CFRP sheets was then applied over top of the vertical sheets. Diagonal CFRP sheets were applied at 45∀using the same technique as used to apply the vertical sheets, except a 20 mm gap was provided between adjacent sheet sections on the specimen with only diagonal wrap sections. A 100 mm gap between adjacent sections was provided on the specimen that also had a horizontal

CFRP sheet applied over top of the diagonal sections. All four girders were tested as simply supported, and subjected to two equivalent point loads. Results from this study indicated that external CFRP reinforcement increased the shear capacity of the girders from 10-36% depending on the configuration of the wrap sheets [42].

Additional research on the shear strengthening effects of CFRP reinforcement was conducted by Taljsten at the Lulea University of Technology [43]. Eight reinforced concrete beams measuring 4500 mm long, 500 mm deep, and 180 mm wide, were fabricated. Five were externally reinforced with CFRP sheets. Four different types of CFRP systems were investigated, two of which used a hand lay-up application procedure, one was applied with vacuum injection, and one was pre-preg. Although the type of external reinforcement varied on each of the five wrapped beams, each was wrapped with the CFRP sheets oriented at 45∀to the horizontal plane of the beams. The method used to anchor the CFRP sheets was not specified. Each of the eight beams were tested in four point bending. The results of this study indicated that shear capacity of the wrapped beams increased by up to 300% over similar unwrapped beams. Two of the control beams were tested to failure in shear, and then externally reinforced with diagonal CFRP sheets, and each exhibited almost a 100% increase in shear capacity from the reference values even after being completely fractured in shear [43].

Although the effects of external CFRP strengthening of reinforced concrete beams and columns on increasing shear and flexural capacity vary significantly, depending on the experiment referenced, all of the experiments report increases in capacity. The percentage increase depends on the type of specimen tested, and the orientation and type of CFRP reinforcement and specimen loading.

2.4.1 FRP Wraps for Corrosion Mitigation and Rehabilitation

While the use of external FRP reinforcement has been researched extensively in the areas of flexural, shear, and seismic strengthening of concrete, the retrofitting of reinforced concrete structures with FRP sheets to prevent or mitigate corrosion is a much less researched technique. By sealing the concrete, using either concrete sealers or FRP wraps, the diffusion of new chloride ions into the concrete structures may be either significantly reduced or prevented altogether, if either system is impermeable. In addition, an impervious surface coating may limit levels of oxygen and moisture in the concrete, reducing the rate of the cathodic reaction during

corrosion. Wrapping a reinforced concrete structure with FRP sheets may also restore or improve the strength of the concrete member that may have been lost due to a reduction in steel cross section from corrosion processes.

While the technology is promising, multiple researchers have raised concerns regarding the use of FRP wraps or concrete sealers to mitigate corrosion. A concrete sealant system may prevent the ingress of new chloride ions, but existing chloride concentrations within the structures will not be affected, and ongoing corrosion processes may even be accelerated. When analyzing the advantages of FRP plates for strengthening of concrete structures, Leming and Peshkam concluded that "it is necessary to remove all chloride contaminated concrete….to avoid further corrosion of the reinforcement which could lead to further delamination and spalling. With composite systems, it would be possible to encapsulate the beam in these materials so stifling any further corrosion. Composites in general are not affected by chlorides."[44]. Emmons, Vaysburd, and Thomas have expressed the opinion that strengthening concrete with FRP does not arrest corrosion, and will most likely accelerate the corrosion process, although no experimental work was cited to support this opinion [45]. They suggest that FRP strengthening only be applied after the current corrosion situation of the structure is properly determined and addressed. The FHWA has also officially stated that "concrete overlays, waterproof membranes, and sealers placed on salt contaminated concrete containing corroding reinforcing steel, do little to reduce the effects of corrosion" [11].

In light of these opinions, a field study of note has been undertaken at the Universite de Sherbrooke in Quebec, Canada where carbon and glass FRP wraps have been used to mitigate corrosion in field structures [46]. Multiple structures experiencing ongoing corrosion were retrofitted with composite wraps in 1995, and long-term corrosion monitoring was initiated in some of the structures. Existing chloride concentrations in the selected structures were not addressed, aside from the removal and repair of delaminated and spalled concrete, before the wrapping process was initiated. Chloride concentrations within the wrapped structures were not reported by the authors, and no indication was given as to the nature or procedures of any chloride sampling processes that were undertaken prior to wrapping [46].

In the fall of 1995, two exterior reinforced concrete columns in a location of high exposure to de-icing salts were wrapped with a glass fiber composite after the removal and repair of spalled and delaminated concrete. The wraps were intended to confine the concrete and thus

potentially restore or increase the structural capacity of the columns, while prohibiting the future ingress of chloride ions. A laboratory study of wrapped concrete columns with similar properties to the field structures, and subjected to accelerated corrosion, was also undertaken to evaluate the effectiveness of the retrofit. Further details on the laboratory study or field monitoring of the structure were not provided.

Additionally, twelve columns in the substructure of Highway 10 at Saint-Etienne-de-Bolton near Sherbrooke, Quebec, Canada, were also wrapped with FRP to protect the columns against an increase in corrosion, and to evaluate the FRP wraps in cold weather climates [46]. Corrosion processes in the columns were initiated by the splashing of de-icing salts. Five of the twelve columns were retrofitted with glass fiber wraps, four with carbon fiber wraps, and three with conventional methods (the exact methods selected were not described) after corrosion damage was removed and repaired. Each of the columns was instrumented with fiber optic sensors, although many of the sensors were broken during application of the wrap systems. The type and properties of the fiber optic sensors used were not disclosed. A concrete bridge pier of the Clement Bridge in Montreal, Quebec, Canada, that was experiencing corrosion, initiated by the leakage of de-icing salts through faulty expansion joints, was also retrofitted with nine layers of a glass FRP wrap to prevent future corrosion and restore the original member strength. This bridge was not instrumented with corrosion monitoring equipment. Results from both field studies are pending.

The final corrosion rehabilitation project included in this study was conducted on the concrete columns and beams of the Webster Parking Garage in Sherbrooke, Quebec, Canada, using FRP wraps. Repair of corrosion damage was completed before the structural members were wrapped with either glass or carbon fiber wraps, which were intended to increase the confinement and ductility of the columns and either the positive or negative flexural capacity of the concrete beams, where each was needed. The authors reported that flexural strength of the beams increased 15%, and shear capacity by 20%, following the retrofit, although the experiments conducted to ascertain these values were not described [46].

The effectiveness of an FRP wrap or concrete sealer in preventing future corrosion hinges on the ability of the sealant to prevent the ingress of new chloride ions. Several laboratory studies have been conducted by Zematjis and Weyers to evaluate the service lives of concrete surface coatings and their diffusion properties, with regards to chloride ions [7]. In one such

experiment, four surface coatings were selected: a water-based epoxy (WBE), a solvent-based epoxy (SBE), silane (SIL), and siloxane (SLX). Each sealant was applied using the manufacturers recommended application procedures. A total of 15 horizontal slabs (910 x 910 x 100 mm) and a wall surface (4.88 m long, 1.83 m high, and 300 mm thick) were cast with a concrete containing a water/cement ratio of 0.47. Three slabs were each sealed entirely with one of the four sealer types, and the remaining three slabs were left as controls. The wall was spilt into five equal sections, four of which each were sealed with a different sealant type and one was left as a control. The slabs were exposed to direct sunlight and subjected to cyclic ponding of a 3% NaCl solution, three days wet and four days dry. The wall was exposed to partial sunlight and cyclic running of the 3% NaCl solution from a pipe located on top of the wall which distributed the solution across the entire vertical surface evenly. The wall-wetting period lasted eight hours for three consecutive days, followed by four days of drying. The total exposure period lasted 30 weeks.

Chloride concentration samples were collected from three locations in each of the slabs, and five locations in each wall section, at three sample depths (13, 25, and 38 mm), in accordance with ASTM C 1152-90 for acid-soluble chloride content. The results of these samples are presented in Table 2.8 [7]. The corrosion threshold value for corrosion initiation of bare steel was identified by the authors as 0.71 kg/m^3. The authors then used the average laboratory chloride concentration increases, Fick's Second Law of Diffusion, sealer characteristic coefficients (determined through a regression analysis of increases in Cl^- concentration), and average chloride ingression rates in the field, to obtain service life estimates of each sealer on an equivalent field system in three selected states. The average chloride ingression rates were 8.68, 4.31, and 3.73 kg/m^3, obtained from New York, Virginia, and Pennsylvania, respectively, indicating New York experienced the worst chloride ingression rates. The estimates of sealer service life are listed in Table 2.9 by exposure condition, and estimates that exceeded 75 years have been listed as 75 years [7]. These results indicate that the two sealers, silane and siloxane, were much more effective in preventing chloride ingression than the two epoxies, although the effectiveness of each depended on the exposure condition. A similar study conducted by the same authors investigated the effectiveness of three different sealers (epoxy, urethane, and methyl methacrylate (MMA)) in preventing chloride ingression under four different exposure conditions. This study also indicated that the urethane and MMA sealed

concrete reported lower increases in chloride concentration than the epoxy sealed concrete, under the same exposure conditions [47].

Minimal research has been conducted on the diffusion of water or chloride ions through FRP wraps. Although the diffusion of water through pre-preg composites has been investigated by many in materials science, the dissimilarity of many of the test specimens, with regards to FRP concrete wraps, discourages any comparisons of diffusion properties. However, research on wet lay-up, epoxy composites has indicated that water penetration through the polymer composite occurs by permeation through the free volume of the matrix (or voids, pores and microcracks), and flow along the fiber-resin interface, and can be assumed to initially follow Fick's Second Law of Diffusion [48]. Therefore, permeation does not occur through the fibers themselves, but in the spaces not occupied by fibers. Once water enters the system, it migrates to the fiber-matrix interphase, where it accumulates around the reinforcement fibers and may cause de-bonding of the fibers and degradation of mechanical properties [49]. However, composite systems similar to those used in this study contain high fiber volumes, which will severely impede the diffusion process [48].

In addition to the rates of chloride diffusion through the wrap sheets, the use of FRP wraps for corrosion mitigation and rehabilitation raises several other concerns regarding the properties of the composite systems. Typically, the corrosion of reinforcing steel initiated by extensive chloride contamination of concrete can be linked to exposure of the structure to either de-icing salts or a marine environment. Contamination arising from the use of de-icing salts implies that the structure resides in a northern, or cold weather, environment. Therefore, the effectiveness of FRP wraps as a corrosion mitigation and rehabilitation technique, to externally strengthen and prevent chloride ingression in reinforced concrete, is dependent on the systems durability in cold weather, and freeze/thaw conditions.

A laboratory study into the freeze/thaw behavior of FRP wrapped concrete column and beam specimens was conducted by Green and Soudki [50]. The column specimens were standard concrete cylinders (150 mm x 300 mm), unwrapped or wrapped with either one or two layers of FRP wrap. Approximately half of the cylinders were reinforced with steel (1 or 2 %). Either one or two layers of CFRP wrap were applied continuously and overlapped for 80 mm. Some wrapped and unwrapped columns were not subjected to freeze/thaw cycling, to be used as controls. The beam specimens (100 mm x 150 mm x 1200 mm) were strengthened with internal

shear and flexural reinforcement, and by one layer of glass or carbon FRP placed along the underside of the beam. Some beams were left unwrapped to be used as controls. The concrete used for both types of specimens had an average compressive strength of 34 MPa and an air content of 5%. The freeze/thaw tests were conducted by placing each of the specimens in a cold room overnight (-18 ∀C) for 16 hours and then thawed the next day for eight hours in a water bath (at 18 ∀C). The cylinders were subjected to 200 cycles and the beams to 50 cycles. Upon completion of freeze/thaw cycling, the cylinders were subjected to axial compression tests, and the beams were loaded to failure in four-point bending.

The results of these experiments indicated that the unwrapped cylinders exposed to freeze/thaw cycling experienced a large reduction in strength in comparison with the unwrapped cylinders left at room temperature. Much smaller strength reductions were observed between wrapped cylinders that were exposed to freeze/thaw cycling and similarly wrapped cylinders that were left at room temperature. For the plain concrete cylinders at room temperature, one layer of reinforcement increased the axial capacity by 15% and two layers increased it by 28%. The plain concrete cylinders that were subjected to freeze/thaw cycling experienced a 195% increase in axial capacity with one layer of reinforcement, and by 255% for two layers. The wraps were also effective in the cylinders containing reinforcing steel, although the percent increases in axial strength were much less. Failures in the freeze-thaw cycled cylinders were catastrophic and the wraps “suddenly bounced off in the form of a series of broken loops” because the strength was governed by the confining effects of the FRP wraps [50]. The freeze/thaw beams that were strengthened with FRP sheets all failed at slightly higher loads than the wrapped beams kept at room temperature, although the load that initiated the first crack was relatively similar for all specimens. The predominant mode of failure was peeling of the FRP sheet off of the bottom of the beam. The authors concluded that because the beams exposed to freeze/thaw action did not fail earlier than those kept at room temperature, the peeling mode of failure, and thus the bond of the sheets to the underside of the beam, was not affected by freeze/thaw cycling [51].

A similar study of the effects of freeze/thaw cycling on the ultimate strength of twelve concrete beams (104 x 104 x 1320 mm), six of which were externally reinforced with MBrace CFRP wrap on the underside of the beam, indicated similar performance of the test specimens [52]. Six of the beams were prepared with no flaws in the external reinforcement, and six contained individual flaws, or unbonded areas, equivalent to 30% of the total external

reinforcement area. Three beams from each of the two sets were subjected to a total of fifty freeze/thaw cycles that varied from –10 ∀to 27∀C over a 24 hour period, and then were tested in third-point loading. The load that caused the first crack in each specimen was very similar for each of the FRP cases, in terms of freeze/thaw cycles and void content, and all beams performed similarly in terms of overall stiffness and ultimate failure mode. The mode of failure in each case was delamination of the CFRP sheet initiated by transverse shear deflections in the extreme combined flexure and shear crack [52]. Data also indicated that the beams with 30% unbonded areas and subjected to freeze/thaw cycling exhibited a similar ultimate strength to the beams with no voids in the composite lay-up. The authors concluded that the adhesive bond between the CFRP and the concrete performed well, and the ultimate strength was not significantly affected by freeze/thaw conditions. Results from additional tests of similar beams subjected to a 100 freeze/thaw cycles are pending [52].

In contrast with the aforementioned studies, the results of research completed by Karbhari and Engineer indicate that the type of environment in which the composite reinforced concrete is subjected, and the type of composite used, may significantly affect the load at failure, and the flexural stiffness of the system [54]. To evaluate the change in relative performance as a result of environmental exposure, the authors tested plain concrete beams (330 mm long x 50.8 mm wide x 25.4 mm thick), prepared with a water/cement ratio of 0.45, and reinforced with one of four different types of composite. Each type of composite reinforcement consisted of a unidirectional tow sheet, either glass fibers or carbon fibers, and one of two different types of epoxy, applied on the underside of each beam using a wet lay-up procedure. The total length of composite reinforcement was 152.4 mm centered over each specimen, and three total layers of reinforcement were applied. However, this length of composite reinforcement was less than the development length required for the external reinforcement. Four different environmental exposure conditions were selected in addition to control beams kept at room temperature: submerged in water at ambient temperature, submerged in synthetic seawater, frozen at –15.5 ∀C, and freeze/thaw cycled between –15.5 ∀C for 24 hours and 20 ∀C for 24 hours. Various combinations of the composite type and subsequent environmental exposure were selected to encompass all possibilities and analyze the durability of all retrofit systems. The beams were tested in four-point bending after 60 days of continuous exposure to their selected environments, and the results were compared with similar beams kept at ambient conditions.

The results of these tests indicated that the most significant deterioration of capacity and flexural stiffness was observed in the specimens submerged in water and sea water, while the frozen specimens exhibited the lowest overall change from ambient conditions [53]. Failure load and stiffness in the carbon fiber systems, submerged in water and sea water, decreased by an average of 20% and 10% respectively, although the exact performance was dependent on the selected resin system. The performance of the glass systems was much more dependent on the type of resin used, and the decreases in failure load and flexural stiffness for specimens submerged in salt water varied from 25% and 20%, respectively, for one system, to 45% and 30%, respectively, for the other. The authors concluded that water absorption into the epoxy matrix, through microcracks and voids along imperfect interfaces, caused a reduction in mechanical properties and a weight gain of the composite, affecting the overall system performance. Resin swelling and osmotic pressure have been noted to cause de-bonding stresses along the fiber-resin interface, reducing overall performance in composites subjected to high moisture levels [54,55]. On average, the beams frozen at –15.5 ∀C, and freeze/thaw cycled experienced only minimal change in failure load, and slight increases in flexural stiffness. However, one of the carbon fiber systems experienced a reduction in failure load of 15% and 10%, for the frozen and freeze/thaw cycling conditions, respectively, but freeze/thaw conditions increased the flexural stiffness of the same system by 5%. The glass fiber composite with the same epoxy type had decreases in failure load of 35% and 15%, while flexural stiffness increased 2% and 30%, for the frozen and freeze/thaw conditions, respectively. The authors concluded that the glass fiber systems generally experienced higher degradations in performance than the carbon fiber systems, and that significant attention should be paid to the type of environmental exposure to which the structure is subjected, when selecting the type of composite system for retrofitting.

Additional studies have demonstrated that the material properties of the composite itself can also be affected when subjected to extreme freeze/thaw cycling. In one study, two different groups of composite materials (graphite/epoxy and glass/epoxy) were exposed to freeze/thaw cycling, and then tested in axial tension. The results of this study indicated that tensile strength of the graphite/epoxy and glass/epoxy composites were reduced by 25% and 10%, respectively, through 100 freeze/thaw cycles. However, the temperature extremes used for cycling in the study were unrealistic for concrete field systems (-60 to 60 ∀C) [56].

2.4.2 Bond Testing of FRP Wraps

While the use of FRP wraps for the external strengthening of a reinforced concrete structure may be advantageous, all of the benefits that this type of system provides are dependent on the bond of the composite to the concrete substrate. Because the FRP wraps are typically applied to reinforced concrete structures using a wet lay-up technique, the epoxy/resin layer serves as both the matrix for the composite and as the interlayer between the concrete and the composite, or as the system adhesive. Any deterioration of this layer, potentially due to weathering or environmental exposure, automatically results in a bond deterioration between the concrete and the composite, causing degradation of the rehabilitation system and its strengthening or sealing benefits.

Karbhari and Engineer continued their research discussed in the previous section, of four different composite systems exposed to various environmental conditions, and include an evaluation of bond strength, through the use of a peel test [57]. The same composite systems were evaluated in the bond strength experiments, carbon and glass fiber composites with two different epoxy/resin systems (noted as systems A and B), as in the previously discussed testing program. Five composite strips were applied side by side, using a wet lay-up procedure, on the upper surface of plain concrete blocks (22.86 cm long x 13.54 cm wide x 2.54 cm thick). The strips were each 30.48 cm long, and 2.54 cm wide, and consisted of two plies of unidirectional fiber reinforcement. The strips were applied to the blocks with the fibers oriented parallel to the length of the blocks, and were separated from each other using a putty knife. After curing the applied peel strips for one week, the test specimens were subjected to one of five different environmental exposure conditions, creating a test matrix that enabled evaluation of each type of composite in each exposure condition. The five conditions were the same as the previous experiment: ambient, immersion in fresh water, immersion in sea water, frozen at –15.5 ∀C, or freeze/thaw cycled by alternating 24 hour periods at –15.5 ∀C and 20 ∀C. After 60 days of continuous exposure, controlled peel testing of the composite strips was performed to evaluate the bond strength of each system.

The peel testing apparatus used by Karbhari and Engineer is of special significance because a similar fixture was used to evaluate the bond strength of FRP wrap systems in this investigation, as will be discussed in Chapter 6. A modified peel test was selected by Karbhari and Engineer to evaluate the bond strength. As opposed to a pure shear or blister test, the

modified peel test allows bond failure to proceed at a controlled rate, the peel force is a direct measure of the work of detachment, and critical interfacial fracture energies can be evaluated [58]. A schematic of the mechanics of the test set-up is included in Figure 2.9, and a schematic of the testing apparatus is shown in Figure 2.10 [57]. When a force, P, is applied to the peel strip at an angle of ζ to the concrete substrate, and the actuator moves up, the composite peels from the substrate, and the apparatus slides forward keeping the line of applied load vertical. The state of stress at the peel front can be considered to be independent of the amount of peeling prior to that instant [58]. Peel force was directly measured by a load cell and was adjusted for frictional resistance of the slider, after determining the load required to move only the testing apparatus forward. The interfacial fracture energy, *G*, was computed from an energy balance and is equal to

$$G = \frac{P(1 - \kappa)(1 + \cos\zeta)}{w} + U t \tag{16}$$

where *P* is the peel force, κ is the strain, ζ is the peel angle, *w* is the width of the strip, *t* is the thickness of the strip, and *U* is the strain energy [59]. Strain was computed as follows:

$$\kappa = \frac{P}{w t}\left(\frac{1}{E}\right) \tag{17}$$

where *E* was the modulus of elasticity of the strip. The strain energy, *U*, was taken as one half of the strain presented in Equation (17), or

$$U = \frac{1}{2}\left(\frac{P}{w t}\right)\left(\frac{1}{E}\right) \tag{18}$$

All peel tests were conducted at a constant actuator speed of 5.08 mm/min and peel angles were varied for each combination of environmental exposure and composite type [57].

The results of the peel tests indicated that the interfacial fracture energy was highly dependent on the type of resin system used, and resin A performed significantly better than resin B for all types of environmental exposure and both types of fibers [57].

The peel tests were conducted at room temperature at the completion of the environmental exposure periods. The specimens that were exposed to freezing or freeze/thaw environments reported an increase in peel force and interfacial fracture energy over those kept at ambient conditions. The authors postulated that because of exposure to low, or freezing,

temperatures, stable brittle crack growth is achieved resulting in an increase in toughness due to a brittle/ductile transition [57].

Bond failures in the frozen and freeze/thaw specimens were of a mixed-mode variety, alternating between the concrete and composite interfaces. Specimens submerged in water and seawater generally exhibited a decreased interfacial fracture energy, of approximately 10%, for resin system B with glass fibers these changes were significant (50%). However, the authors concluded that this decrease was caused by the degradation of the bulk resin, plastification of the resin itself, and resulting plasticity at the crack tip, and not from damage that occurred at the interface due to submergence [58]. Overall, the carbon fiber system experienced the smallest changes in system performance, regardless of resin system or exposure condition. In all cases, the peel force, *P*, was found to decrease with increasing peel angle, reaching an asymptotic limit between angles of 85-100∀. The interfacial fracture energy increased with peel angle. The decrease in peel force with increasing peel angle was anticipated, because a peel angle of 0∀ corresponds to a direct tension test of the composite, and thus maximum peel force. A peel angle of 180∀would produce a minimum peel force as the strip is peeled back over itself.

2.5 Embeddable Corrosion Monitoring Instrumentation

Multiple techniques are currently available for engineers to assess the corrosion rates and conditions within reinforced concrete structures. For structures or situations in which typical external methods of corrosion evaluation, such as half-cell potentials and visual inspection of the concrete, are not applicable, embeddable corrosion monitoring instruments are required to determine if the reinforcing steel is actively corroding. Embeddable instruments are also used when continuous or remote monitoring of structures is desired, depending on the type of instrument installed. A structure wrapped with FRP composites meets this criteria because the wrap obscures the concrete surface, preventing the collection of half-cell potentials and the inspection of the structure for spalls, delaminations, and rust stains.

Only a few types of embeddable corrosion monitoring instruments that would be applicable for wrapped concrete structures have been cited in recent literature. The “three linear polarization” technique is a common method of monitoring the corrosion conditions and obtaining corrosion rates within field structures [60]. However, this technique was not an option for this investigation because changes in potential measured with an external reference electrode

could not be obtained, for the same reasons that standard half-cell potentials could not be collected. Variations of the common "3LP" monitoring technique have been researched by Schiessl and Raupach, and would be applicable for wrapped structures. The monitoring system consisted of a corrosion resistant cathode (i.e. stainless steel), and series of steel anodes, embedded in close proximity to each other in new concrete structures, forming a galvanic corrosion cell [61]. The electron flow between the two electrodes was monitored with a low resistance amperemeter. Any measurement of current between the electrodes indicated the onset of corrosion at the anode, and increases in current over time could be used to evaluate the corrosion conditions within the monitored structure, and obtain corrosion rates [61]. A relatively similar system was installed for corrosion monitoring in the bridge deck and parapets of a new reinforced concrete bridge by Hansson and Marcotte [62]. However, installation of either monitoring system would be complicated in existing structures. Because these types of galvanic cell systems, or variations of this concept, were not used for corrosion monitoring in this investigation, they will not be discussed further.

An embeddable Ag/AgCl electrode for in-situ monitoring of chloride contents in concrete has been investigated by Climent-Llorca et al. [63]. Silver wires (99.99% purity), 0.5 mm in diameter and 4 cm in length were used to fabricate the electrodes. A 3 cm portion of each silver wire was immersed in 0.1 M HCl to create an anodized zone. The non-anodized zone of the wire, 1 cm in length, was then protected with Teflon tape. The silver-silver chloride wires were each calibrated against a saturated Hg_2SO_4 electrode before the 3 cm active portions of the electrodes were embedded in mortar specimens (4 x 4 x 16). Chloride ions were seeded into the concrete, and the concentration of chlorides varied from 100 to 4000 ppm by weight of cement. The potential measurements of the electrodes were measured periodically over a period of approximately 4.5 months. Readings were obtained against a saturated Hg_2SO_4 electrode that was placed in contact with the mortar surface, through a piece of filter paper impregnated with 1M KNO_3, on the face nearest the embedded Ag/AgCl electrode. Potentials were recorded after two to three minutes of contact with the mortar surface to stabilize the readings.

The results of this study indicated that readings from the embedded electrodes were stable for the 4.5 month testing period when chloride concentrations were higher than 1000 ppm, while potential readings in specimens with lower chloride concentrations show a progressive decrease [63]. The authors suggested that the developed Ag/AgCl electrodes could be used as in-

situ sensors for the monitoring of total chloride concentration in short-term tests, or less than three months, unless high sensitivity was not required at low chloride concentrations. The potentials collected with these sensors at low chloride concentrations were extremely variable. The authors also indicated that in tests of longer duration, the potential readings collected with these sensors may lead to ambiguous results, because potential readings declined, at each chloride concentration, throughout the duration of the experiment. The authors noted that the chloride concentration played an important role in the stability of the potentiometric response of the electrodes, although the origin of this influence was not known [64]. A more robust and field worthy Ag/AgCl electrode, specifically designed for reinforced concrete structures, was used in this investigation for corrosion monitoring.

Electrical resistance probes can also be used in an embeddable corrosion monitoring system. The electrical resistance of any conductor is given by:

$$R = \frac{\psi L}{A} \tag{19}$$

Where ψ is the resistivity, L is the length of the conductive element, and A is the cross-sectional area [1]. As corrosion reduces the cross section of the element over time, the resultant increase in R can be used to evaluate corrosion rates. Therefore, uniform loss in cross-sectional area is used to evaluate corrosion, and not weight loss, as in other types of probes [1]. A typical design of a commercial resistance probe is included in Figure 2.11 [64]. Temperature sensors are typically included within the probes to compensate for resistance changes due to fluctuations in temperature. Only uniform corrosion rates are measurable with these probes, because pitting or localized corrosion does not have the same proportionate effect on cross-sectional area and probe resistance [1]. A variation of this concept was also used in this investigation for corrosion monitoring.

3. Initial Site Conditions, ECE and FRP Treatment Procedures, and Laboratory Specimen Fabrication

This chapter provides a detailed description of the project site and the portions of the bridge substructure that were included in the investigation, as well as a synopsis of the field work undertaken in this study. Initial site conditions are discussed briefly along with concrete surface rehabilitation work completed prior to electrochemical chloride extraction (ECE). Specifics on the installation and duration of the ECE process are presented along with an overview of the post ECE site condition survey. The column wrapping and sealing process, including the development of test specimens for laboratory evaluations of the FRP systems, are then discussed. The final portion of this chapter briefly introduces, and establishes the need for, embeddable corrosion monitoring instrumentation.

3.1 Site Location and History

The structures chosen for this investigation constituted a portion of the substructure of I-394, Bridge #27831, over Dunwoody Blvd. in Minneapolis, MN. This bridge was constructed in 1970 and was widened in 1989. A bridge rehabilitation project, to replace many of the strip seals, immediately followed the deck widening in 1989. The location of the site is shown on the map in Figure 3.1. A photograph of the site, facing Pier 34 North, is shown in Figure 3.2. The bridge consisted of prestressed concrete girders and reinforced concrete pier caps and columns. The bridge had a history of corrosion related problems, especially in the substructure, initiated primarily by leaking expansion joints located in the bridge deck above. These faulty joints allowed significant amounts of melted snow and ice, often containing chlorides from road salt applications, to flow through the bridge deck and onto the pier caps and columns below. This phenomenon accelerated the corrosion process in these structures. Although the expansion joints were since replaced, corrosion problems persisted due to previous chloride ingression in both the bridge columns and pier caps. The study included a total of twelve columns and three pier caps and a portion of two additional pier caps. The specific columns and pier caps investigated in the study are shown highlighted in gray in Figures 3.3 and 3.4.

3.2 Pre-ECE Rehabilitation and Site Survey

To initiate the investigation, the site was mapped to indicate areas of previous patching and drainage damage. Corrosion-related concrete damage to almost every column and to a number of the pier caps was observed. The damage included staining, cracking, and occasional large expanses of delaminated concrete that required repair. Delaminated concrete was located using a hammer to sound the concrete, in accordance with ATSM D 4580-86 [65]. All initial concrete repair was performed by Mn/DOT personnel. Pier 34 North, after the removal of damaged concrete, is shown in Figure 3.5. Figure 3.6 shows column 34C immediately before patching [66]. All patching was completed with a cement based repair mortar.

A determination was then made regarding which columns and pier caps were to undergo which treatments, bearing in mind the following criteria:

1) Sections on each pier to be subjected to ECE must all be subjected to ECE because of the inter-conductivity.
2) Piers to be subjected to ECE should be relatively near each other to facilitate the contractor's setup.
3) Variations in types of retrofits to be investigated, including control columns, should be investigated together on each pier.

The pier caps and columns selected to receive ECE treatment are highlighted in dark gray in Figure 3.4.

A total of six different concrete sealing systems were selected for this investigation, three of which were fiber reinforced polymer wraps and three of which were concrete sealers. The three wraps applied to the bridge were an AMOCO CFRP sheet (Carbon Fiber) applied with Tyfo S epoxy, a Tonen Forca Tow sheet (Carbon Fiber) with MBrace epoxy, and a fiberglass composite with MBrace epoxy. These wraps will hereafter be referred to as AMOCO CFRP, MBrace CFRP, and GFRP respectively. The three chosen concrete sealers were Hydrozol Enviroseal and Hydrozol Silane 40, both silane sealers, and Nicotote Forsoc, a siloxane/silane sealer. Mn/DOT selected these particular sealer brands for evaluation in order to assess their potential applications for future bridge sealing projects. The chosen retrofitting schedule is presented in Section 3.5.

Upon completion of the concrete surface repair, a pre-ECE site condition survey was conducted. This survey documented all locations of concrete repair on all of the columns and

pier caps included in the study. Diagrams indicating the locations of all patches, painted areas, and surface cracks located on the structures have been included as Figures 3.7 through 3.12, with a legend. The legend for these figures, indicating the chosen method of column and pier cap representation and the symbols selected to identify areas of concrete repair, is included as Figure 3.7. These illustrations represent the pier cap and column surfaces as if unfolded. The dashed line down the center of each column sketch indicates the northwest side of the column, the side facing Linden Avenue. Position markers have also been included identifying the distance in feet from the top of the column to grade level, and from the north end of the pier cap to the south end.

After documenting areas of surface repair, chloride concentration samples and half-cell potential readings were collected at several locations on every column and pier cap included in the investigation. The locations where the chloride samples were taken were determined during the initial site investigation. In general, chloride samples were either collected from areas immediately adjacent to patched or repaired areas, in order to correlate chloride levels with the visual evidence of corrosion, or away from patched and repaired areas, to assess chloride ingression in areas where corrosion was not outwardly visible. The locations where Mn/DOT collected chloride samples are indicated in Figures 3.8-3.12 by solid black circles. Each of these chloride sample locations was designated with a unique identification tag as shown in the drawings. The location identifier assigned to each chloride sample will be discussed in more detail in Chapter 5.

To determine the acid-soluble chloride content, a total of 370 powder samples were collected in accordance with ASTM C1152-90 by drilling at five different depths (0-1.25 cm, 1.25-2.5 cm, 2.5-3.75 cm, 3.75-6.25 cm, and 6.25-8.75 cm), at each of the 72 selected sample locations [67]. Once powder samples were collected from all five depths, the holes were patched with a repair mortar by Vector Construction. In general, each pier cap had chloride samples collected at eight locations, four on each vertical face, while each column was sampled at three different locations. All chloride samples were collected and analyzed by Mn/DOT personnel.

Half-cell potential readings were collected with a copper-copper sulfate electrode at 30 cm intervals, vertically and horizontally, on every column and pier cap, enabling contour plots of potential to be generated. Similar to a topographic map, a contour plot indicates areas of the structure with equal potential and can be used to determine areas of probable corrosive activity. This corrosion potential survey was completed according to ASTM C 876-91, by Mn/DOT

personnel [24]. Half-cell potentials were not collected on the tops of the pier caps due to access difficulty. All pre-ECE chloride concentration and half-cell potential results are documented and discussed in Chapter 4.

To prepare the selected structures for ECE treatment, additional chipping and patching of spalled and delaminated concrete along with grouting of surface cracks was completed by Vector Construction. Delaminated concrete was located using a hammer to sound the concrete, in accordance with ATSM D 4580-86 [65]. In addition, areas of concrete cover less than 10 mm were located with a pachometer and subsequently patched with a cement based repair mortar until the cover exceeded 10 mm. This process took place during the fall of 1997 immediately preceding installation of the NORCURE system to begin ECE.

3.3 Electrochemical Chloride Extraction

With the necessary concrete surface repair and preliminary site surveys completed, the ECE phase was initiated. Installation of the NORCURE system for chloride extraction commenced in the fall of 1997. As discussed in Chapter 2, the NORCURE system is a chloride extraction process which requires an external anode mesh, in a cellulose fiber electrolyte, applied to the concrete surface. An electrical connection between the anode mesh and the reinforcing steel, which acts as the cathode, is then made. Similar to cathodic protection, once current is passed through the system, chloride ions are driven away from the negatively charged reinforcing steel towards the external anode, and potentially out of the concrete. This system was installed and maintained by Vector Construction.

The structural components selected to receive ECE treatment were Pier 34 North and Pier 37 North. The extraction treatment included the entire pier cap and the three columns beneath (columns A-C) on each pier. After establishing multiple connections to the reinforcing steel cages in each of the selected piers and columns, the continuity between the cages was evaluated by Vector Construction. A resistance of less than 5 Ohms, between all of the connections on each pier, was required to maximize the effectiveness of the ECE process by providing the maximum possible current to each column and pier sub-zone. The results of the reinforcing steel continuity checks are included in Tables 3.1 and 3.2 [66]. After determining that there was sufficient continuity in each of the structures, wooden battens were applied to the concrete surface to support the steel mesh anode. With the anode mesh in place, all necessary electrical connections

between the surface sub-zones and the DC rectifiers, providing the overall system power, were made. Four, 40V DC rectifiers were provided to supply the system power. Each of the pier caps, Piers 34 North and 37 North were powered with individual rectifiers. The remaining two units each powered a column set, 34A-C and 37A-C, respectively. This format was selected by Vector based on desired levels of current per square meter of surface area to be treated. In addition, a system of drip hoses running along the tops of the pier caps was installed in order to maintain a steady flow of water down the faces of the pier caps and columns. Although installation of the system was virtually complete in the fall of 1997, imminent cold weather conditions delayed the electrolyte application and extraction process until the following spring of 1998.

Due to concerns over potential chloride level changes through the winter, nine of the 72 locations where chloride powder samples were collected in the fall of 1997 were selected randomly for additional chloride concentration testing in March 1998. Additional chloride concentration data was collected at two new, randomly selected, locations. The new locations were close to, and generally between, previously sampled locations. The powder samples were collected by American Engineering Testing (AET) and chloride analysis was performed by Mn/DOT personnel. Only three sample depths (0-2.5 cm, 2.5-5 cm, 5-7.5 cm) were used for this round of testing at each of the eleven sample locations. The locations where AET collected chloride samples are indicated in Figures 3.8-3.12 by solid, gray circles. The locations sampled by AET were not designated with a unique identification tag and will be referenced by the nearest Mn/DOT sample location. This form of identification was chosen because post-ECE chloride samples were not collected, and corrosion monitoring instrumentation was not installed, at the locations sampled only by AET. Results from this sampling period have been included in Chapter 4.

Installation of the NORCURE system recommenced during the second week of April 1998 and application of the cellulose fiber was completed within days. Figure 3.13 provides an example of this process as performed on another corrosion treatment project in Regina, SK, Canada, by Vector Construction. To ensure that the fiber stayed damp, the rate of flow through the system of drip hoses was adjusted to create a slight flow of water over and down the pier caps. The pier caps and columns were also wrapped in thick plastic sheets to minimize the amount of water evaporation from the electrolyte. On April 16, 1998 the system was energized at Pier 34 North, and the following day at Pier 37 North. Overall treatment was required to last

either a minimum of 60 days, approximately 1000 Amps/hrs, or until the levels of chloride found in samples taken in the vicinity of reinforcing steel had decreased by 50%. The ECE system in place on Piers 34 and 37 North can be seen in Figures 3.14 and 3.15, respectively.

During the treatment period, daily voltage and amperage readings were collected to ensure that the system was operational, the rectifiers were not operating any higher than 40 V, and most importantly to monitor chloride extraction. Although exact measurements of chloride removal or extraction were not made, decreasing current through the columns and pier caps at a steady system voltage of 40V indicated an increase in concrete resistivity. Current flow through concrete is a function of multiple variables including concrete cover, spacing of reinforcing steel, and chloride content. Therefore, an increase in resistivity (or decrease in current flow) could indicate a decrease in chloride content of the concrete, because the other major variables remain unchanged. As shown in Figure 3.16, current decreased rapidly after a week of treatment, at which time a brief power outage occurred due to a melted cable. A relatively steady decline rate followed for approximately six weeks. Current readings then began to plateau, indicating that the system was no longer removing chlorides efficiently. The reduction in efficiency is related to the declining levels of chloride within the treated structures. As the level of chlorides in the concrete, especially near the reinforcing steel, declines, the driving force for removal also decreases. Therefore, a situation of diminishing returns develops where the energy used to draw out the remaining chloride ions in the concrete, outweighs the amount of chloride removed. As evident in Figure 3.16, the current through the structures began to plateau during the first few weeks of June 1998 indicating the extraction process was essentially complete, and it was no longer worthwhile to continue the extraction treatment.

On June 11, 1998 several concrete powder samples were collected from Pier 34 North and Pier 37 North by Vector Construction. These samples were collected to determine whether or not the ECE treatment process should be continued, by evaluating the reduction in chloride content from pre-ECE levels. The chloride concentration results of these samples are listed in Tables 3.3 and 3.4, alongside chloride content results reported by Vector prior to initiation of the ECE process [66]. As evident in these tables, the overall decrease in chloride content between pre and post-ECE values was approximately 50%, and varied from over 90% on Column 37C to around 40% on the east face of Pier 37 North. On average, 57.6% of the chlorides were removed

from the first 2.5 cm of concrete, and 38% was removed from the deepest sample depth, 5-7.5 cm

Because average chloride concentration had decreased by approximately 50% in both Pier 34 North and Pier 37 North, and current through each of the structures had begun to plateau, a decision was made to terminate the ECE process on June 16, 1998. The system was shut down after a total treatment time of almost exactly 60 days, a total charge passed of over 1400 A-hr/m^2, and a decrease in average chloride concentration of approximately 50%. Therefore, all of the specified treatment duration criteria had been met, even though only one of the three was required. Once turned off, the steel mesh anode and wooden battens were removed and disposed of along with the cellulose fiber electrolyte.

Before concrete wrapping and sealing could commence, the columns and piers subjected to ECE were given two months to dry out. After two months with a continuously moist electrolyte applied to the concrete surface, water likely permeated the concrete cover. There was significant concern that if the columns were not given sufficient time to dry, excessive retained water in the concrete from the ECE process could be sealed into the columns which could potentially accelerate the corrosion rate.

3.4 Post-ECE Site Survey

During the two month drying period following the ECE treatment, a complete survey of chloride concentrations was conducted in the same manner as the site survey taken during the fall of 1997. All 72 originally sampled locations were tested again in early August 1998, with samples collected approximately 5 cm away from the original sample location to avoid drilling through repair mortar. The chloride powder samples were collected by Braun Intertec and analysis was performed by Mn/DOT personnel. Samples were again obtained at five different depths at each location (0-1.25 cm, 1.25-2.5 cm, 2.5–3.75 cm, 3.75-6.25 cm, and 6.25-8.75 cm). Results from this sampling period are discussed in Chapter 4.

In light of the increased polarization of the reinforcing steel in the concrete that was treated with ECE, half-cell potentials were not collected before concrete wrapping and sealing because the results obtained would have been essentially meaningless for the treated structures, due to the re-passivation of the rebar by the ECE process.

3.5 Concrete Wrapping and Sealing

In order to determine the most effective corrosion mitigation technique, six different concrete sealants were applied in a manner that would allow comparisons to be made between columns and pier caps that had been treated with ECE and those that had not. This was accomplished by applying each of the three FRP wrap types to areas that had been treated with ECE as well as to similar areas that had not. In order to simplify the wrapping/sealing procedure and to acknowledge the continuity between the column and pier cap, each sealant was applied to both the column and the corresponding overhead pier cap area. The overhead pier cap area was bound by either the ends of the pier cap or by the midpoint of the pier cap between columns. The AMOCO CFRP was applied to the northern most column of Pier 34 North and the southern most column of Pier 34 South, Columns 34A (ECE) and 34F (Non-ECE), both located alongside Dunwoody Blvd. and at the edges of the bridge deck of I-394. The two interior columns, Columns 34B (ECE) and 34D (Non-ECE), also along Dunwoody Blvd. were both sealed with the GFRP wrap. The northern most columns on Pier 37 North and Pier 40 North were both sealed with the MBrace CFRP, Columns 37A (ECE) and 40A (Non-ECE). The three remaining columns that were not treated with ECE were left as control columns, Columns 34D, 37D, and 40C, each located on a separate pier within the interior of the substructure. The three remaining columns that had received ECE, Columns 34C, 37B, and 37C, were sealed with the three selected concrete sealers. This treatment schedule is illustrated in Figure 3.17. The application of all FRP wrap systems and concrete sealers was performed by Vector Construction.

Surface preparation for concrete wrapping and sealing commenced on August 24, 1998. In order to apply the fiber reinforced polymer wraps and the concrete sealers correctly, the concrete surface to be covered had to be completely clean and free of moisture or contaminants that could inhibit bond. The nature of the ECE process however, drawing chlorides away from the negatively charged reinforcing steel towards the external steel anode mesh, left considerable amounts of by-products and debris on the concrete surfaces that were treated. There was extensive staining of the concrete from the corrosion products of the external anode, and large clusters of the cellulose fiber electrolyte that had adhered to the concrete surface. In order to remove the debris and clean the concrete, all columns and pier caps in the study were grit blasted prior to wrap and sealer application. Sand blasting all columns and pier caps ensured that all concrete surfaces were prepared in the same fashion, whether they were subjected to ECE or not.

The first wrap system to be installed was the MBrace CFRP applied to Columns 37A and 40A. To smooth the column surface and fill air voids or holes, a primer was first brushed onto the concrete. This primer was also intended to increase the bond strength of the applied system. To further repair any column defects and increase bond, a thin layer of putty was then spread over the primed concrete surface. The FRP wrap system was then applied in three separate steps. An initial layer of the MBrace epoxy was applied with a paint roller, followed by the application of a section of CFRP wrap pressed firmly into the epoxy by hand with the fibers oriented in the hoop direction on the columns, and vertically on the pier cap faces. Each wrap section applied to a column was approximately 60 cm wide (the manufactured width), and long enough to wrap entirely around the column with approximately a 30 cm circumferential overlap. Sections applied on the pier caps were also 60 cm wide, and long enough to continuously wrap the top, both vertical faces, and approximately 10 cm on both sides of the bottom face of the pier cap. In areas where the prestressed bridge girders were bearing on the top of the pier cap, the FRP wrap sheets were cut so the wrap did not cover the bearing plate and only a minimal area was exposed between the edge of the wrap and the bearing plate. The exposed area was then sealed with the appropriate epoxy or resin. Once the CFRP sheet was in place, air pockets were removed with a roller before the epoxy set, and then a final coat of epoxy was applied on the outside of the CFRP sheet. This process began at the base of each column and proceeded up the column height and then onto the pier cap. Each column and overhead pier area were wrapped entirely except for the 30 cm of each column directly above grade, and the underside of the pier area, aside from the 10 cm extension provided onto either side of the bottom face. The undersides of the pier caps were not wrapped because of corrosion problems that have developed in entirely wrapped pier caps in California [68]. The decision to leave the bases of the columns unwrapped was made by Vector Construction. Adjacent FRP wrap sections were butted up against each other, vertically on the columns and horizontally on the pier caps, so that concrete was not visible through the seam, rather than overlapping. The MBrace system in place on Column A of Pier 40 North is shown in Figure 3.18. The 10 cm wrap extensions around the corners of the bottom pier face are also visible in Figure 3.18.

The GFRP system was applied to Columns 34B and 34D using the same procedure as the MBrace system because the two used the same MBrace putty/epoxy application method. The only difference between the two application procedures was that the GFRP wrap contained

braided fibers oriented in two perpendicular directions. Therefore, while the dimensions of each wrap section and the application procedure were the same as used with the MBrace CFRP, the orientation of the GFRP fibers were both parallel and perpendicular to the vertical axes of the columns and pier caps.

The AMOCO CFRP wrap was applied to Columns 34A and 34F in a somewhat different manner than the previous two wrap systems. A primer was again applied to increase bond and smooth over minor surface defects, but the AMOCO system did not include a putty layer. The CFRP sheets were instead first saturated in a Tyfo epoxy/resin as they were pressed through a series of rollers to ensure permeation of the resin into the fiber matrix, prior to application on the structure. The saturated fiber sheets were then hand-pressed onto the concrete with the fibers oriented in the hoop direction on the columns, and vertically on the pier caps. A roller was then used to roll over the applied wrap sections to ensure there were no air voids trapped behind the wrap. This process began approximately 30 cm above grade level on each column, and proceeded up the column height and onto the overhead pier area. The unwrapped area at the base of each column can be seen in Figure 3.19. Adjacent sections of wrap were butted up against each other so that concrete was not visible through the seam, rather than overlapping. Application of the AMOCO CFRP to Column 34F and the overhead pier area is shown in Figure 3.19.

While each of the three types of FRP systems were being applied to the field structures, laboratory test specimens for each FRP system were prepared. The preparation of these specimens and the types of testing to be conducted are discussed in more detail in Section 3.7.

After all FRP wrap systems were in place, a drip ledge was installed along the edge of each wrap extension onto the bottom pier cap faces. The ledge was created by beading silicone caulk along the edge of the wrap. This was a precaution to inhibit possible water accumulation and subsequent permeation at or past the wrap edge. Silicone caulk was also applied at the joint between the top of each column and the pier cap to prevent water from leaking in behind the column wrap as shown in Figure 3.20. Column and pier wrapping was completed with the application of a coat of UV protection paint over the entire surface of each cured wrap system.

To ensure that the wrap systems sufficiently adhered to the concrete surface, pull off tests between the fiber reinforced wrap and the concrete substrate were performed in the field. These tests were required to demonstrate that the bond stress exceeded 1.4 MPa for each of the wrap

types in both a column and a pier cap. As shown in Table 3.5, each composite system exhibited bond strength in excess of 1.4 MPa indicating acceptable system installation on each structure of the study [66]. In each case, failure was either observed in the concrete or in the dolly paste of the testing apparatus. This indicates that each system had attained its maximum possible bond strength because failure was governed by either the strength of the paste used in the testing apparatus or the tensile strength of the concrete substrate, and not the composite-concrete bond. All damaged wrap areas from these tests were removed and then repaired with sections of FRP wrap cut to the dimensions of the damaged section, and applied using the same procedures previously discussed.

Each of the three sealers was sprayed onto the specified concrete surfaces without any surface preparation, aside from sand blasting. Similar to the wrap systems, the sealers were not applied on the underside of the pier caps, aside from a 10 cm overlap sprayed on both sides of the bottom face, or in the 30 cm directly above grade on each of the columns. Silicone caulk was not applied to the edge of the sealer overlap sprayed onto the bottom of the pier caps. Column wrapping and sealing were completed during the first week of September 1998.

3.6 Corrosion Monitoring Instrumentation

After the wrapping and sealing process was completed, embeddable corrosion monitoring instruments were installed to determine if corrosion was occurring within the columns and pier caps included in the study.

Many techniques are available for engineers to assess corrosion damage or potential for corrosion in typical concrete structures. These techniques include, but are not limited to, chloride concentration samples, half-cell potentials, concrete resistance measurements, visual inspection, and sounding. Visual inspection surveys are the most common and reliable methods because cracking, rust staining, and spalling or delaminations of concrete cover are typically obvious. Many of these techniques were used in the two site surveys, before and after ECE. However, because half of the columns and pier caps in the investigation were wrapped with FRP materials, the concrete surface was not visible or accessible in the case of the wrapped columns. Consequently, surface measurement of half-cell potentials was not an option because contact with the concrete surface was not possible. Without embeddable instrumentation, corrosion of the steel reinforcement could go undetected behind the FRP materials. Therefore, instruments

that could be embedded within the structure itself were required. These instruments were placed in all the columns and piers in the study to ensure that all were monitored in the same fashion and with the same type of instruments, even though the control columns could still be monitored using conventional techniques, if desired.

Embeddable silver/silver-chloride half-cells, humidity sleeves, and resistivity probes developed at the University of Minnesota were selected to instrument the structures in the study. These instruments were installed in December 1998 and monitoring was ongoing at the time of writing this document. A complete discussion of the corrosion monitoring instrumentation is presented in Chapter 5. This discussion includes a description of instrument locations and installation procedure. The laboratory testing conducted to evaluate and calibrate each type of instrument, and the results from those tests, are presented in Chapter 6. Collected field data from the sensors are included and discussed in Chapter 7.

3.7 Laboratory Testing of FRP wraps

As discussed in Chapter 2, the flexural and shear strengthening benefits of FRP column wraps have been established and documented by many researchers [38,39,40,41,42,43]. Applications of these wraps with regards to mitigating corrosion are much more uncertain, particularly when considering the discussed problems FRP wraps present to corrosion monitoring and the obstruction of visual corrosion symptoms.

Retrofitting the columns and pier caps with an impenetrable surface sealant would likely inhibit additional chloride ions from entering the sealed structures. However, the potential exists for chloride ions and water already within the columns and pier caps to be trapped inside. If the ECE treatment did not remove enough of the chloride ions from the concrete or if chlorides migrate back to the reinforcing steel level, corrosion could conceivably reinitiate if sufficient water and oxygen were present. In addition to the existing water retained in the structures, more water may find a way into the concrete, potentially coming down from the pier caps above or drawing up the columns from the ground through capillary action. While excess water in an unsealed structure could simply exit the concrete radially, in an impermeably sealed structure, the water would become trapped. Therefore, an impermeable concrete sealant could create a contained corrosive environment, especially on structures containing high chloride concentrations that were not treated with ECE but were wrapped or sealed. However, this type of

seal might also keep air or oxygen out of the concrete hindering the ability of the concrete to breathe, but limiting the levels of available oxygen, which may impede corrosion. A permeable surface sealant would allow the concrete to breathe and water could move in and out of the structures, but unfortunately so could chloride ions. Therefore, wrapping or sealing a structure after ECE treatment might only provide temporary corrosion mitigation as chloride ions slowly migrate back into the concrete. It was not immediately obvious which alternative was more desirable.

These concerns necessitated a laboratory investigation into the permeation characteristics and diffusion rates through each of the wrap systems. In order to conduct laboratory tests of the FRP wrap systems, samples were collected while application of the wraps to the field structures took place. The procedure used to collect test specimens has been included in Section 3.7.1. A discussion of the selected diffusion testing procedure, and the results obtained for each FRP system, is presented in Chapter 6.

Deterioration of bond strength between the FRP wraps and the concrete surface was also an issue for investigation. While the three wrap systems exhibited high initial bond strength between the composite and the concrete surface in the field, it was not certain that this strength would be maintained throughout the duration of the study, especially when exposed to winter weather conditions or freeze/thaw cycling. To evaluate the bond strength between each of the FRP wrap systems and the concrete substrate, a peel test apparatus was constructed and bond tests were performed on concrete specimens with strips of FRP samples applied in the field. The laboratory specimens are discussed in more detail in Section 3.7.2. A complete discussion of the peel test apparatus, testing procedure, and results obtained for each FRP system is presented in Chapter 6.

3.7.1 FRP Diffusion Test Specimens

Test specimens of each of the three FRP systems were made in the field while each particular composite system was being applied to the columns and pier caps. The test specimens were created using similar methods as used to wrap the structures in the field to ensure that all diffusion rate results were indicative of the actual systems in place on the bridge. However, due to the nature of the composite systems and the strength of bond developed when applied to a concrete surface, all laboratory specimens were applied to a Plexiglas substrate pre-treated with

mold release. This technique allowed the hardened wrap sheets to be removed without damaging either the fibers or the epoxy. This also ensured that all diffusion results would be indicative of the cured composite wrap sheets alone, as desired. To provide enough material to run multiple tests on each FRP wrap if desired, two samples of each wrap (GFRP, AMOCO CFRP, and MBrace CFRP) were obtained with each sample measuring 60 cm long and 30 cm wide. All of the test specimens were prepared by University of Minnesota personnel.

The GFRP and MBrace CFRP test specimens were prepared by first spreading a thick layer of epoxy on the Plexiglas with a paint roller, then pressing the cut section of the wrap into the epoxy by hand. A final thick coat of epoxy was then applied over top of the wrap sheets again with a paint roller. The finished wrap was then rolled to remove air voids. The completed laboratory specimens of the MBrace CFRP are shown Figure 3.21. Two samples of the MBrace epoxy alone were also obtained by rolling a thick layer of the epoxy onto a treated piece of Plexiglas, and letting it sit for approximately five minutes before applying a final thick coat. The AMOCO CFRP specimens were created by first cutting a 60 cm long by 30 cm wide specimen, from the principal CFRP sheet, after the fiber mat had been saturated with the Tyfo epoxy/resin and pressed through the AMOCO roller apparatus. This saturated wrap section was then pressed onto the Plexiglas and subsequently rolled to ensure the air voids were removed. Each test specimen was cured for 72 hours in the field before being removed from the Plexiglas substrates. Visual inspection of the specimens after removal revealed multiple voids in the resin layer located on the underside of each AMOCO CFRP specimen. Although the source of these voids cannot be determined specifically, the use of mold release to pre-treat the Plexiglas may have caused the resin to accumulate or puddle beneath the FRP section, as opposed to the concrete substrate of the field systems which would have absorbed the epoxy instead. Therefore, rolling of the specimens to remove air voids might not have been as effective on the treated Plexiglas as on the field structures. All of the diffusion test specimens were then transported to the laboratory where they were stored until testing began.

Each system applied on the wrapped field structures included the epoxy and FRP sheet, but also included the surface primer applied to the concrete before wrap application, and the UV paint coat applied over top of each of the cured wrap systems. The MBrace CFRP and GFRP systems also included a putty layer to smooth over the surface defects. While it is not clear how each of these additional components would affect the diffusion rates of the field FRP systems, it

can be assumed that each would likely increase the time of permeation through the system. Therefore, testing only the cured FRP wrap and epoxy layers provided a conservative estimate of diffusion rates through each of the three composite systems. Actual diffusion rates in the field would be expected to be lower than the values determined in the lab.

3.7.2 FRP Peel Test Specimens

Prior to FRP wrap application in the field, concrete blocks measuring 17.75 cm wide by 27.5 cm long, by 3.75 cm thick were fabricated in the laboratory to be used as the concrete substrates for the peel test specimens. As determined using standard cylinder tests at 28 days, the concrete used in the blocks had an average compressive strength of 32 MPa and an average split tensile strength of 2.8 MPa. The blocks were not reinforced. A total of nine blocks were made with each block designed to hold three strips of the same type of composite wrap, creating 27 total peel specimens or nine for each type of FRP system.

The peel test specimens were created by applying narrow strips of each of the three composite wraps to concrete substrates using the same FRP application techniques as used on the field structures. Each test specimen block was sandblasted on the side that was to have FRP application before having a concrete surface primer applied to the same side with a paint roller. This primer was allowed to cure on each of the specimens for at least 3 hours, in accordance with FRP application on the field structures. The MBrace CFRP and GFRP sample blocks were coated with a thin MBrace putty layer to smooth over any surface defects. After allowing the putty to dry for about 30 minutes, a coat of the MBrace epoxy was applied uniformly with a paint roller. Three separate 2.5 cm wide strips of either the GFRP or MBrace FRP sheets were then cut from the manufactured FRP roll, and pressed into the epoxy on the concrete blocks, each strip spaced approximately 1.25 cm apart. The cut FRP strips were approximately 38 cm long and were applied so that a 10 cm overhang was present at one end of the block. Once the strips were in place, a final coat of epoxy was rolled over the top of the block and all air voids underneath the strips were removed with a hand roller. Epoxy was also rolled on the top of the overhang to minimize the possibility of sample failure at the lip of the block during laboratory testing, and to enhance the rigidity of the entire peel strip sample. Completed peel test samples for the MBrace CFRP system are shown in Figure 3.22.

Peel test samples for the AMOCO CFRP were also 2.5 cm wide strips, approximately 38 cm long, but because of the nature of the AMOCO CFRP mat, obtaining 2.5 cm wide samples was much more difficult than with the MBrace CFRP and GFRP sheets. Cutting through the AMOCO CFRP mat lengthwise, or in the fiber direction, resulted in some edge fibers being frayed, although care was taken to minimize the strip edge damage. Both the MBrace CFRP and GFRP sheets were much easier to cut through because of the reduced mat thickness, resulting in more precisely cut edges. The AMOCO CFRP strips were also applied to the blocks differently. After the appropriate size strips were cut from the AMOCO CFRP sheet roll, they were soaked in the epoxy/resin for approximately five minutes. Because of the small size, excess resin on the FRP strips was strained out manually between two putty knives, taking care to avoid damage to the fiber mat, until the strips were no longer dripping but still fully saturated. The strips were then pressed into the primed surface of the concrete block providing a 10 cm overhang at one end. All of the AMOCO CFRP and MBrace CFRP wrap samples were placed with the fibers oriented in the lengthwise direction of the strip. Once all samples were prepared, and after a 24 hour curing period, they were moved to the top of the pier cap of Pier 37 North, where they remained until laboratory testing. Field storage exposed each test specimen to the same environmental conditions as the FRP wraps on the columns and pier caps. To conduct laboratory testing, three test specimens, each containing three strips of one type of FRP wrap, were brought back to the lab a day before testing to ensure that the specimens were aged in the same fashion as the field structures.

4. Chloride Concentration and Half-Cell Potential Results

Results from the pre- and post-ECE site condition surveys are included in this chapter. Chloride concentrations and half-cell potentials collected prior to ECE treatment are presented and discussed first. These results are used to assess the average initial site conditions, and locate specific areas of concern with respect to established corrosion thresholds, before ECE treatment. Results from the chloride samples collected following completion of the ECE process are then presented, and the changes in chloride content and corrosion conditions are discussed. The final portion of this chapter summarizes and discusses the initial effectiveness of the ECE process.

4.1 Data Presentation Format

Chloride concentration samples and half-cell potentials were collected from all of the structures included in this investigation by Mn/DOT personnel in October 1997, as discussed in Section 3.2. Additional chloride samples were collected prior to the ECE process in March 1998, by American Engineering Testing, as discussed in Section 3.3. During the two month drying period following ECE treatment, a complete sampling of chloride concentrations was performed in the same manner as the site survey conducted during October 1997, as discussed in Section 3.4. Chloride concentration results of the collected powder samples from each of these sampling periods are illustrated in Figures 4.1-4.6, with a legend, and contour plots of pre-ECE half-cell potential are included as Figures 4.7-4.11. The legend for both sets of figures is included in Figure 4.1.

To graphically depict the measured chloride concentration as a function of sample depth, two stacks of five data boxes are placed at each chloride sample location in Figures 4.2-4.6. The data box stack corresponding to post-ECE chloride concentration results is located to the right of the pre-ECE stack, and each pair of stacks is centered over the location of the chloride sample. As shown in Figure 4.1, each individual data box represents a particular sample depth, increasing in depth from top to bottom of the stack, and illustrates the severity of the sample obtained using a color scale. Data boxes with solid outlines correspond to the chloride samples collected by Mn/DOT personnel, and the AET samples from March 1998 are indicated by data boxes with thick, dashed outlines. These figures are replicates of the column and pier illustrations presented

and discussed in Chapter 3, which identified and labeled the locations where Mn/DOT collected chloride samples, and indicated all areas of concrete repair.

Only the severity of each chloride concentration has been indicated on the chloride concentration figures, using a color scale to shade each data box based on the range of chloride contents in which the sample falls. The selected color scale, as a function of chloride concentration in ppm by weight of cement, is illustrated in Figure 4.1. As discussed in Chapter 2, the established threshold for corrosion is 2000 ppm by weight of cement [16]. Chloride concentrations higher than 2000 ppm are highlighted dark gray. Data boxes for pre-ECE Mn/DOT chloride samples that have been cross-hatched indicate depths where samples were either not collected, because of difficulties with the concrete drill, or misplaced. Because AET chloride samples were collected from only three depth ranges, as opposed to five during Mn/DOT sampling, the second and fourth data boxes (representing the depth ranges 1.25 cm-2.5 cm and 3.75-6.25 cm) are cross-hatched indicating an inapplicable sample range. This particular data presentation format facilitates visual evaluations of the pre and post-ECE corrosion potential at each location, as well as the change in chloride concentration severity between sampling periods. The exact concentrations of each collected chloride sample collected by Mn/DOT, from both the pre and post-ECE sampling periods, are tabulated in Appendix A.

All of the pre-ECE half-cell potentials collected in October 1997 were obtained with respect to a copper-copper sulfate electrode. Each collected reading was then adjusted with respect to a silver-silver chloride electrode by adding +0.096 V [1]. This adjustment was made to ease data comparisons between the initial site conditions and results collected from the Ag/AgCl electrodes installed in the field structures. The collected half-cell potential results, with respect to an Ag/AgCl electrode, were used to generate contour plots for each column and pier cap included in the study using a color scale to indicate the severity of pre-ECE corrosion potential. The selected color scale is indicated in Figure 4.1, and the contour plots are included as Figures 4.7-4.11. As discussed in Chapter 2, a half-cell potential reading more negative than –0.35V, with respect to a copper-copper sulfate electrode, indicates a greater than 90% chance of corrosive activity [24]. This value correlates to –0.254V with respect to a silver-silver chloride electrode. Areas of half-cell potential exceeding this value have been highlighted on the contour plots using a dark gray.

4.2 Comparison of AET and Mn/DOT Pre-ECE Chloride Concentrations

As discussed in Chapter 3, the chloride samples drilled by AET during March 1998 were collected to determine if large changes in chloride content had occurred in the structures of the investigation, through the winter months. Because all of the AET chloride samples were collected at least a few feet away from the location of the nearest Mn/DOT sample, only general conclusions on changes in chloride content could be drawn through comparison of results.

As shown in Figure 4.2, the AET chloride sample collected on Pier 34 North, near location PIER 34N-W4, reported chloride content levels very similar to the Mn/DOT sample collected during October 1997. This observation is reinforced through comparison of the chloride concentration values at that location, listed in Appendix A, which indicate similar results were obtained at all sample depths. On Pier 34 South, four AET samples were collected for comparison with the pre-ECE Mn/DOT samples, as shown in Figure 4.3. At location 34D-3, the severity of chloride concentrations reported during both the Mn/DOT and AET sampling periods were very similar at all sample depths. Although the AET sample collected near location 34F-3 was drilled on the opposite side of the concrete repair patch at the top of the column, the severity of the reported chloride concentrations was similar. The exact concentration values were fairly different however, and this can probably be attributed to the distance between sample locations. Similarly, both of the AET samples collected on the pier cap of Pier 34 South, near location PIER 34S-E1 and between locations PIER 34S-W1 and PIER 34S-W2, correlated well with respect to the chloride concentration severity witnessed in October 1997, but not as closely with respect to exact concentrations. Results of the two AET samples collected from Pier 37 North, near location PIER 37N-E1 and in-between locations PIER 37N-W2 and PIER 37N-W4, are indicated in Figure 4.4. Both AET samples indicated differing chloride content severity and concentrations, in comparison with the Mn/DOT results. This difference is very noticeable when comparing the results of the AET sample collected between PIER 37N-W2 and PIER 37N-W4, and the Mn/DOT chloride content results at those two locations. Although the chloride concentrations within the deeper sample depths are similar, in the first 1.25 cm of concrete the AET sample reported a concentration of less than 500 ppm, while each Mn/DOT sample reported a concentration exceeding the corrosion threshold. This can probably be attributed more to the distance between the compared samples, approximately five feet in each direction, than changes in chloride content through the winter. Finally, the AET results from location PIER 37S-

W2, on the pier cap of Pier 37 South, correlated very closely with the Mn/DOT results in the first sample depth, as shown in Figure 4.5, although differences were reported at subsequent depths. In conclusion, pre-ECE chloride concentrations measured during March 1998 compared well with the results collected in the October 1997 sampling period, indicating only minimal changes in chloride concentration had occurred through the winter months.

4.3 Pre-ECE Corrosion Conditions

A total of 77 different sample locations were selected for chloride concentration analysis prior to installation of the ECE system, of which 34 were on columns or pier caps that were scheduled to receive ECE. The 34 sampled locations on the ECE structures, Piers 34 and 37 North, provided a total of 168 powder samples. Of the 168 samples, 42.9% contained chloride contents in excess of the established threshold for corrosion of 2000 ppm by weight of cement. On Pier 34 North, this value was even higher, 63.6% of all collected chloride samples exceeded 2000 ppm. This can most likely be attributed to the proximity of this pier to the intersection of Dunwoody Blvd. and W. Linden Ave. Here, the potential for splashing of melted snow and ice, containing chlorides from road salt applications, onto the column surfaces was greatest. This method of chloride intrusion likely combined with chlorides entering the structure from run-off through the faulty expansion joint in the bridge deck above, increasing the chloride concentrations in the concrete with respect to the structures on the interior of the project site that were not exposed to roadway splashing. This would explain why the percentage of samples exceeding the corrosion threshold was so much higher in Pier 34 North than in the other piers included in the study. The percentage of samples exceeding the corrosion threshold was lower on the structures that were not scheduled to receive ECE at 30.6%, or 60 of 196 samples. Combining the percentages on both the ECE and non-ECE structures, out of a total of 364 collected powder samples, 132 indicated the potential for corrosive activity by reporting chloride concentrations higher than 2000 ppm by weight of cement. This correlated to 36.3% of all collected pre-ECE chloride samples. These overall percentages, as well as the number of samples in excess of 2000 ppm on each structure of the study, have been included in Table 4.1.

General conclusions regarding the pre-ECE chloride concentration results can be obtained after averaging all of the samples from a specific sample depth, in each structure. This data presentation format permits general conclusions to be drawn about chloride concentration as

a function of depth for each column or pier cap in the study, based on the few locations sampled from each structure. The results of this averaging process have been included in Table 4.2. In this table it can again be seen that Pier 34 North clearly had the most severe chloride concentrations of any structure included in the investigation. Column 34A reported average chloride concentrations of more than twice the established threshold for corrosion in the first 2.5 cm of concrete and continued to exceed the corrosion threshold up to 6.25 cm below the concrete surface, indicating significant and long standing chloride permeation. These results further support the theory of road salt splashing significantly increasing the chloride concentrations in the concrete, because the base of column 34A was only approximately 2 m away from the intersection of Dunwoody Blvd and W. Linden Avenue. However, average chloride concentrations were higher in Column 34C than in Column 34B. In fact, in the sample depth range of 1.25-2.5 cm the average chloride concentration in Column 34C was the highest average witnessed in the pre-ECE chloride sampling period (4371 ppm by weight of cement) of all of the structures included in the investigation, as shown in Table 4.2. Columns 34B and 34C were approximately equidistant from Dunwoody Blvd. Average chloride levels in the columns of Pier 37 North were significantly lower than all of the other structures included in the study. These results are interesting in light of the average chloride concentrations in the pier cap above, which were very comparable to the other pier caps in the study. This would indicate that the expansion joint located above Pier 37 North was not significantly better than the other expansion joints. Surface splashing was not possible on Columns 37A-C, because of the pier location in the interior of the project site, but this was no different than Columns 37D, 40A and 40C also located on the site interior. Those three columns exhibited higher initial chloride concentrations than Columns 37A-C and similar concentrations to the pier cap of Pier 37 North in each of their respective pier caps. A potential explanation for these results is that run-off through the expansion joint in the bridge deck above Pier 37 North was somehow either inhibited from flowing from the pier cap to the column surfaces, or was removed from the column surface more rapidly than on other piers.

In Table 4.3, the average pre-ECE chloride concentration as a function of sample depth has been presented. Pre-ECE chloride concentrations are averaged for the ECE structures, the non-ECE structures, and the study as a whole. As evident in this table, chloride concentrations were highest closest to the concrete surface and decreased with depth into the structures. The

average chloride concentration prior to ECE treatment, for the site as a whole, was in excess of the established threshold for corrosion in the first 2.5 cm below the concrete surface. In addition, chloride concentrations with respect to sample depth, were found to be higher in the structures scheduled to receive ECE than in the untreated structures, with the exception of the first sample depth where average concentrations were nearly equal. However, this can be attributed to the very high chloride concentrations observed in Pier 34 North which weighted the sample depth averages, especially when considering the low percentage of samples in excess of 2000 ppm that were collected from the columns of Pier 37 North. This conclusion can be verified when comparing Figures 4.2 and 4.4 in terms of pre-ECE chloride severity, or the number of boxes highlighted dark gray. In general, chloride concentrations exceeded the corrosion threshold in the first 2.5 cm and gradually decreased with depth from the concrete surface to levels below 2000 ppm by weight of cement.

Specific areas of concern prior to ECE treatment were determined through analysis and comparison of the chloride concentration illustrations and tables, with the half-cell potential contour plots. While areas reporting half-cell potentials more negative than –0.254V indicate a greater than 90% probability of active corrosion, areas meeting this criteria and reporting chloride concentrations in excess of 2000 ppm by weight of cement can almost certainly be identified as areas of ongoing corrosion.

From a total of 77 chloride sample locations, 47 reported a chloride concentration higher than 2000 ppm for at least one sample depth range in the pre-ECE chloride sampling period (or 61%). Eight of the locations with at least one chloride concentration in excess of 2000 ppm also reported a half-cell potential lower than –0.254V. This corresponds to 10.4% of the total sample locations. Two locations matching this criterion were located on each pier included in the investigation with the exception of Pier 34 South, which did not have a sample location that exceeded both criteria at the same location. The two locations exceeding both the chloride concentration and half-cell potential corrosion thresholds on Pier 34 North were located on the pier cap, at locations PIER 34N-W3 and PIER 34N-W4(AET). On Pier 37 North, both locations meeting this criteria were also on the pier cap, at locations PIER 37N-W2 and PIER 37N-E1. Of the two locations meeting this criteria on Pier 37 South, one was located on a column, at 37D-3, while the other location was on the pier cap, at PIER 37S-E1. Similarly, on Pier 40 North, one location was on a column, 40A-3, and the other was located on the pier cap, at location PIER

40N-W3. All eight of these sample locations exceeding both of the established corrosion thresholds were identified as areas of probable corrosive activity.

Four of the eight sample locations that reported chloride concentrations and half-cell potentials that exceeded the established corrosion thresholds were found on the structures scheduled to receive ECE. This correlated to 11.7% of the 34 chloride sample locations on the ECE structures, Pier 34 North and Pier 37 North. Likewise, the other four areas exceeding both corrosion thresholds were on the non-ECE structures, corresponding to 9.3% of 43 sampled locations on the non-ECE structures. The similarity of both the number and percentage of total samples that meet this criteria, regardless of location within the project site, indicates that the majority of corrosive activity occurring within the columns and pier caps could be attributed to the faulty expansion joints located in the bridge deck above. The joints were probably very similar in terms of drainage performance, so it would be expected that both the amount of road salt within the run-off and the amount of run-off that flowed through the joint, and onto the pier cap, were similar at each pier location. The only exceptions to this conclusion were Columns 34A and 37A-C, which exhibited unusually high and low chloride concentrations, respectively.

Analyzing only the pre-ECE chloride concentration results, Pier 34 North reported at least one powder sample containing a chloride concentration higher than the corrosion threshold of 2000 ppm by weight of cement at every sample location except 34B-1, as shown in Figure 4.2. At most sample locations on Pier 34 North, chloride concentrations exceeded the corrosion threshold at multiple sample depths. Most of the sample locations on Pier 34 South, except for Column 34E, also possessed multiple locations where chloride concentrations exceeded 2000 ppm, as evident in Figure 4.3. Although only one sample location reported high chloride concentrations on the columns of Pier 37 North, multiple locations with multiple sample depths in excess of the corrosion threshold were located on the pier cap. This can be seen in Figure 4.4. Samples collected from Pier 37 South and Pier 40 North also indicated many areas of chloride concentrations in excess of 2000 ppm.

Considering only the pre-ECE half-cell potential contour plots, areas indicating a 90% probability of corrosive activity existed on almost every column and pier cap included in the study. In some cases, especially on the pier caps, these areas were extensive. Column 34A showed the largest area, with respect to the other columns included in the study, which had half-cell potential more negative than -0.254V. Pier 34 North also reported an area of probable

corrosive activity above Column 34C on the pier cap. These areas can be seen in Figure 4.7. The most extensive area of probable corrosive activity on Pier 37 North was observed between Columns 37B and 37C, as shown in Figure 4.9. It is also interesting to compare the areas of concrete repair indicated in Figures 4.2-4.6 and the darkly shaded areas on the contour plots (indicating a 90% probability of corrosive activity) in Figures 4.7-4.11. In every case but one, on Column 37C, these areas matched almost exactly in terms of size and location. Therefore, the pre-ECE corrosion potentials supported the visual evidence of damage or deterioration that was observed and repaired prior to initiation of the ECE process.

4.4 Post-ECE Corrosion Conditions

4.4.1 ECE-Treated Structures

From April 16,1999 to June 16, 1999, ECE was conducted on Pier 34 North and Pier 37 North. Following ECE, Pier 34 North experienced reductions in chloride concentration at almost all chloride sample locations, as evident in Figure 4.2. Prior to ECE, fourteen of fifteen chloride sample locations reported a chloride concentration in excess of 2000 ppm by weight of cement from at least one of the five sample depths. This correlated to 93.3% of the pre-ECE sample locations. After ECE treatment, only eight locations reported a chloride concentration in excess of 2000 ppm in at least one drill depth. This correlated to 47% of the 17 post-ECE sample locations. Therefore, locations reporting at least one chloride concentration exceeding the corrosion threshold were reduced by 50% on Pier 34 North as a result of ECE. The effectiveness of the treatment process varied somewhat, as evident in the chloride concentration tables in Appendix A, and certain locations experienced greater chloride reductions than others. For example, sample locations 34A-1 and 34A-2 had pre-ECE chloride contents that exceeded the established corrosion threshold at multiple sample depths, but all post-ECE samples were found to have chloride contents below 2000 ppm. In contrast, location 34A-2 had chloride concentrations almost as severe as 34A-3 prior to ECE, and yet the percentages of chloride reduction were much less at 34A-3, even though the two locations were on the same column and less than a meter away. Location 34A-C also had similar initial chloride concentrations to locations 34A-1 and 34A-2 but experienced much lower reductions in chloride content and still reported four sample depths in excess of 2000 ppm, even after ECE treatment. This disparity, in

terms of treatment effectiveness, can probably be attributed to the proximity of each sample location to reinforcing steel. Chloride ions close to reinforcing steel would have been subjected to a larger driving force, from the negatively charged rebar, towards the external anode and out of the structure. Therefore, percentages of chloride removal would be much greater for sample locations near reinforcing steel.

The effectiveness of the treatment process was similar on Pier 37 North, with respect to locations reporting at least one powder sample exceeding 2000 ppm, as evident in Figure 4.4. From a total of 19 pre-ECE sample locations, nine reported at least one drill depth where chloride concentrations exceeded the corrosion threshold, or 47.4% of sample locations. All but one of these locations was found on the pier cap. Following ECE, only three of 17 sample locations (or 17.6%) produced at least one chloride concentration above 2000 ppm. Therefore, locations reporting at least one chloride concentration in excess of 2000 ppm were reduced by 63% in Pier 37 North as a result of ECE. Multiple locations with high initial chloride concentrations, such as location PIER 37N-W1, PIER 37N-W4, PIER 37N-E1 and PIER 37N-E4, were treated very efficiently and chloride content was reduced by over 50% at most sample depths. However, other locations with relatively high initial chloride concentrations, such as PIER 37N-W2 and PIER 37N-E2, were not treated as effectively. The average reduction in chloride content was closer to 20% at location PIER 37N-W2, and the first two sample depth ranges still reported concentrations in excess of 2000 ppm by weight of cement, following ECE treatment. At location PIER 37N-E2, where pre-ECE chloride concentrations were not as high as PIER 37N-W2, the chloride concentration in the first sample depth range increased by 50%, and was unchanged in the range of 1.25-2.5 cm

More specifically, location PIER 37N-E1 reported a pre-ECE chloride concentration of 5500 ppm by weight of cement in the first sample depth range. This concentration was reduced to 1175 ppm through ECE treatment. The location on the opposite face of the pier cap at approximately the same position, PIER 37N-W2, also reported a high initial chloride concentration of 2657 ppm by weight of cement in the first sample depth range. However, following ECE this location reported an increase in chloride concentration to 2750 ppm in the first sample depth range, and was thus apparently unaffected by the ECE process. The disparity can probably be attributed to the proximity of each location to reinforcing steel, as previously discussed. Chloride reductions were also not as severe in the columns of Pier 37 North, but this

can be attributed to the low chloride levels reported in each column prior to ECE, which would have provided a much lower driving force for the extraction process. The complete results from all locations are included in Appendix A.

Combining the treatment results for both Pier 34 North and Pier 37 North, the ECE process reduced the percentage of locations indicating a potential for corrosive activity from 67.6% to 32.3%. This correlated to a reduction of slightly over 50%. Locations identified as exhibiting corrosive potential were those with at least one pre-ECE chloride sample in excess of 2000 ppm. While the total number of locations with chloride concentrations exceeding the corrosion threshold was reduced significantly, multiple locations on Pier 34 North and Pier 37 North still exhibited corrosive potential following treatment.

4.4.2 Untreated Structures

In terms of the structures that were not treated with ECE, it was anticipated that chloride levels measured during August 1998 should correlate fairly well with samples collected during October 1997. This expectation was based on both the lack of any form of chloride treatment performed on these structures and the good correlation of chloride levels between the October 1997 samples and the AET samples, as discussed in Section 4.2.

The results collected from Pier 34 South, shown in Figure 4.3, indicate that most sample locations produced powder samples containing similar chloride ion intensities in both sampling periods. Some examples of this similarity can be seen at 34D-1, 34E-1, 34E-2, 34F-2, and 34F-3, where the colored data boxes are identical for the pre and post-ECE sampling periods. Although some variability existed, at location 34D-2 for example, and some chloride ion movement between sample depth ranges was apparent, at multiple locations on both faces of the pier cap, the results from both sampling periods correlated fairly well. This correlation was less evident on Pier 37 South, shown in Figure 4.5, where chloride intensities do not match up as well graphically, especially on the pier cap. This can be seen at both PIER 37S-W1 and PIER 37S-W2 where chloride levels dropped significantly. Pre- and post-ECE chloride concentrations on Pier 40 North are illustrated in Figure 4.6. The results from the two sampling periods correlated the best on this pier, in comparison with the other untreated structures. The correlation between the pre- and post-ECE sampling periods on Pier 40 North is especially noticeable on the pier cap, as shown in Figure 4.6, where chloride concentration intensities remained the same within most

sample depth ranges, at most sample locations. However, chloride movement between depths was apparent at a few of the chloride sample locations, and the level of chloride contamination within the entire pier appeared to increase somewhat, between the pre- and post-ECE sampling periods. In general, chloride concentration analysis of the structures not treated with ECE indicated that many locations of corrosive potential still existed on the untreated structures after ten months.

Aside from a few questionable results and some apparent migration of chloride ions between sampling depths within the structures, chloride contents correlated satisfactorily between pre- and post-ECE sampling periods. Any of the inconsistencies that were observed between chloride concentrations collected in the pre- and post-ECE sampling periods on the untreated structures, where chloride concentrations should have remained essentially the same between the two sampling periods, can probably be attributed to the sampling process. Concrete is an inhomogeneous material, and the ingression of chloride ions, whether from leaking expansion joints or road splashing, is very non-uniform. Therefore, samples collected even short distances apart, from the same drill depth, can report dissimilar chloride concentrations. Much of the variability witnessed between the values collected in the pre- and post-ECE sampling periods can probably be attributed to these factors.

4.4.3 General Analysis Following the ECE Treatment Period

To analyze the results of the post-ECE sampling period more generally, chloride concentration results were averaged based on location and depth of sample. In Table 4.1, the number of chloride samples in excess of the corrosion threshold, collected from each structure, has been documented. In comparison with values obtained in the pre-ECE sampling periods, the number of collected samples exceeding 2000 ppm was reduced significantly on both of the ECE-treated structures, by approximately 75% on both Pier 34 North and Pier 37 North. In terms of the untreated structures, the total number of chloride samples above the corrosion threshold increased on Pier 40 North, but decreased on the other two untreated structures, Pier 34 South and Pier 37 South, which was unexpected.

An additional method used to draw general conclusions of the effectiveness of the ECE treatment was to average the chloride concentrations collected in the post-ECE sampling period in each structure, at each sample depth, as shown in Table 4.4, with the percent change from pre-

ECE averages included in Table 4.5. Average chloride concentrations were reduced by approximately 58% in the columns of Pier 34 North, but increased by approximately 11% in Columns 37A-C while remaining comparatively low (to the values of Pier 34 North). However, the increase in average chloride concentration in Columns 37A-C can be attributed to the low initial chloride levels in these columns, which provided a lower driving force for removal during the ECE process and weighted the reduction average in areas of higher initial concentrations. This conclusion is supported when comparing the effectiveness of removal in the pier caps of Pier 34 North and Pier 37 North. Average chloride concentrations on the pier cap of Pier 37 North, where initial chloride levels were much higher, were reduced by an average of 48%, which is closer to the average removal percentage witnessed on the pier cap of Pier 34 North, or 44%. These two pier caps reported relatively similar pre-ECE average chloride concentrations, as shown in Table 4.2. In general, average chloride concentrations were reduced the most near the concrete surface by ECE treatment, and the effectiveness decreased slightly with depth into the structure, on both Pier 34 North and Pier 37 North. As shown in Table 4.5, the average chloride concentration in the pier cap of Pier 37 South decreased by 54%, even though this structure was not treated with ECE. However, differences between the average values, as determined in the pre- and post-ECE sampling periods, can probably be attributed to the sampling process.

The average chloride concentration at each sample depth, as determined in the pre- and post-ECE sampling periods, is included in Table 4.6. The percent change within each depth range from pre-ECE values is indicated in parentheses, with bolded font. As evident in this table, average chloride concentrations within each depth range decreased by approximately 43% in the treated structures and 16% in the untreated structures.

Prior to ECE, a total of eight sample locations exhibited a high corrosive potential by reporting at least one powder sample with a chloride concentration over 2000 ppm by weight of cement, and a half-cell potential more negative than –0.254V. Of the four identified locations meeting this criteria on the ECE structures, three still reported at least one sample depth with a chloride content in excess of 2000 ppm following ECE. These locations were PIER 34N-W4(AET sample), PIER 37N-W2, and PIER 37N-E1. Half-cell potentials were not collected following ECE treatment because both structures were assumed to be very passive due to the increased polarization of the concrete, as discussed in the next section. Because of the increased passivity, or polarization, of the reinforcing steel, it is unlikely that these three locations were

actively corroding following ECE. However, each location still exhibited elevated chloride concentrations and thus the potential for future corrosive activity.

4.5 Vector Construction Half-Cell Potential Results

At the request of Mn/DOT personnel, half-cell potentials were also collected by Vector Construction, on only the structures that received ECE. These potentials were obtained approximately 2.5 months after installation of the FRP wrap systems, or 5 months after termination of the ECE treatment process. Because contact with the concrete surface could not be achieved on the wrapped portions of Pier 34 North and Pier 37 North, only the unwrapped components of each were mapped. These portions of both structures had been sealed with concrete sealers however, so the exact values may have been influenced by the presence of the sealer, in-between the surface electrode and the concrete surface. Half-cell potentials were collected with a copper-copper sulfate electrode and the readings were then adjusted by adding +0.096V so that each potential was with respect to a silver-silver chloride electrode [1]. This was done to ease future data comparisons with the embeddable Ag/AgCl electrodes. Results from this mapping period have been illustrated in Figures 4.12 and 4.13 [66]. The results have been presented in these figures in millivolts and are negative, unless otherwise indicated.

As evident in Figures 4.12 and 4.13, almost every single half-cell potential collected was in the passive range, or more positive than –104 mV, indicating a greater than 90% probability of no corrosive activity. Only three readings, one on the east face of Pier 34 North and two from the west face of Pier 37 North, fell into the range of uncertain corrosion potential between –104 mV and –254 mV, and there were no readings that indicated areas of active corrosion. In comparison with the pre-ECE half-cell potential contour plots for Pier 34 North and Pier 37 North, presented in Figures 4.7 and 4.9, respectively, ECE significantly lowered the corrosion potential of both structures. The extensive region of highly negative potential between Column 37B and 37 C on the pier cap of Pier 37 North was eliminated and half-cell potentials on Column 37C were reduced extensively. Even though only portions of each structure were mapped, it can be assumed from these results that Pier 34 North and Pier 37 North became very passive as a result of the ECE treatment. As discussed in Chapter 2, the ECE process generates hydroxyl ions at the reinforcing steel interface which act to increase the pH of the surrounding concrete, while re-

establishing the passivity of the steel [26,30,32,36]. This increase in passivity can be clearly seen upon comparison of the pre and post ECE half-cell potentials on the treated structures.

4.6 Summary of the Initial Effectiveness of the ECE Process

The half-cell potentials collected by Vector Construction on Pier 34 North and Pier 37 North indicated that both structures had become very passive as a result of the ECE treatment. However, these results were expected based on the increased polarization of the concrete during, and following, the ECE process. As discussed in Chapter 2, this period of increased polarization and passivation generally lasts anywhere from six months to a year following removal of the ECE system. Therefore, the period of interest with respect to the half-cell potentials is in the years following ECE treatment. The half-cell potentials collected by Vector were obtained only five months after the treatment was completed. If the chloride content of the concrete is reduced significantly, and chloride ions are prevented from re-entering the structures, the ratio of hydroxyl ions to chloride ions should remain about the same. Therefore, the structure would remain passive, and would exhibit a 90% probability of no corrosive activity. If only some of the chloride ions were removed, or if new chloride ions penetrated the structure, the corrosion process could potentially re-initiate as the structure de-polarized.

The preliminary field results indicated that while ECE considerably reduced the overall chloride concentration of a contaminated structure, while re-passifying the reinforcing steel, it probably should not be considered a complete and lifelong cure. This determination was based on the effectiveness of chloride removal in the treated structures, especially with respect to sample locations and depths containing chloride concentrations exceeding the corrosion threshold, following ECE treatment. Although ECE reduced the chloride levels in Pier 34 North and Pier 37 North significantly, sample locations reporting chloride concentrations still in excess of 2000 ppm were located on each structure. At some locations, multiple sample depths reported concentrations in excess of 2000 ppm, following treatment. The specific sample locations of concern on the treated structures following ECE treatment (identified as locations reporting at least one chloride concentration in excess of 2000 ppm) are as follows:

Columns 34A-C:	Locations 34A-3, 34C-1, and 34C-3
Pier 34 North:	Locations PIER 34N-W1, 34N-W2, 34N-W4, 34N-E1, and 34N-W4

Columns 37A-C: Location 37C-1

Pier 37 North: Locations PIER 37N-W2, and 37N-E1

Therefore, because areas of high chloride concentration still existed within the treated structures, it can be assumed that the increased passivation of Pier 34 North and Pier 37 North was only temporary. The pH of the concrete can be expected to slowly return to pre-ECE levels as chloride ions migrate back to the reinforcing steel, and the concrete surrounding the steel becomes less alkaline. Provided that sufficient oxygen and water are present at the reinforcing steel levels, corrosion could conceivably re-initiate. This phenomenon will be discussed further in Chapter 7.

5. Corrosion Monitoring Instrumentation

The need for embeddable corrosion monitoring instrumentation is established in this chapter and the three different types of instruments that were selected for installation are discussed. The locations selected for instrumentation in the field structures are explained and illustrated. Finally, the installation procedure is presented along with a discussion of the surface repair work used to reseal the concrete following installation of the instrumentation.

5.1 Embeddable Instrumentation

To ensure that all columns and pier caps were evaluated in the same manner, corrosion monitoring techniques and instruments applicable for both the sealed and unsealed concrete were needed. Because 75% of the structures included in the study were either wrapped with FRP or sealed with concrete sealers, corrosion evaluation was more complicated than with standard reinforced concrete structures.

Because contact could not be made with the concrete surface on any of the wrapped or sealed areas, collecting half-cell potentials using standard methods was not an option. Although chloride samples could be obtained by drilling into the concrete through the wraps, this evaluation method would have compromised the integrity and continuity of the wrap systems, and is planned only on a limited basis. Visual inspection of the concrete was also eliminated, because the wrap obscured the concrete surface. Therefore, in order to determine whether corrosion was taking place within the columns and pier caps of the bridge substructure, embeddable corrosion monitoring instrumentation was required. To effectively evaluate the corrosion conditions within the columns and pier caps, three embeddable instruments (embeddable Ag/AgCl half-cells, corrosion monitoring probes, and humidity sleeves for use with a relative humidity probe) were selected to monitor site conditions. The three different types of instruments were grouped at each instrumentation location so that results from a particular type of instrument could be correlated with the others. The following sections describe each of these instruments in detail, including the reasons for selection. Laboratory testing and calibration of the sensors is discussed in Chapter 6.

5.2 Ag/AgCl Half-Cells

Embeddable half-cells were used to instrument the columns and pier caps to enable corrosion evaluation of the structures as the reinforcing steel within the treated concrete becomes de-polarized, and chloride ions migrate back to the reinforcing steel level. These potentials, in correlation with the chloride samples collected in the post-ECE sampling period, and any additional data, were used to monitor the conditions within the structures following ECE and concrete wrapping. The silver/silver-chloride reference electrode that was selected to instrument the columns and pier caps of this study was manufactured by ELGARD Corporation. This particular half-cell is a permanent, embeddable reference electrode for reinforced concrete structures. Potential measurements were made by closing the circuit between each installed half-cell and a connection to the reinforcing steel cage within the concrete structure. Voltage measurements were collected with a standard voltmeter.

Advantages of this half-cell included its durability, applicability to existing structures, and reproducible readings to within millivolts. The disadvantages of this instrument were that the readings were only reliable when the concrete temperature was above freezing and the readings could only be obtained at the specific location of installation.

As shown in Figure 5.1, the half-cell consisted of an outer PVC housing with a porous frit placed at the end of the electrode. The membrane allowed for ionic transfer between the reference solution in the half-cell, 3.5M KCl in methyl-cellulose-based gel, and the concrete. The silver wire, coated with molten silver chloride and situated in the reference gel (in essence the electrode) was epoxied into the cell body for stability and soldered to a No. 10 AWG lead wire for electrical connections. The actual body of the reference cell was approximately 10.5 cm in length and 1.875 cm in diameter. A picture of the silver/silver-chloride reference electrode is shown in Figure 5.2.

To ensure that valid results are obtained from Ag/AgCl electrodes installed in reinforced concrete structures, each needed to be grouted into the concrete at the depth of the reinforcing steel. This was necessary so that resistance between the two electrodes, the Ag/AgCl reference and the reinforcing steel, would be minimized. A connection to the reinforcing steel cage, within the structure in which the half-cells were embedded, was then necessary to collect data with the half-cells. Although installation instructions specified that a connection to the reinforcing steel should be provided for each reference cell, discussions with the manufacturer indicated that one

connection to the reinforcing steel cage was sufficient for all installed half-cells on an entire pier provided sufficient continuity between the pier cap and column steel cages existed. A resistance of less than 5 Ohms, between any two reinforcing steel connections, was the established threshold for acceptable continuity. Multiple connections were already present on the columns and pier caps of Pier 34 North and Pier 37 North, because they were needed for the ECE procedure. At least two connections to the reinforcing steel were provided on the three other piers by Vector Construction, prior to concrete wrapping and sealing. Continuity checks were performed between all of the provided reinforcing steel connections, on each of the five piers, by University of Minnesota personnel. As shown in Table 5.1, sufficient continuity was found in all five pier caps, between all tested connections. Therefore, only one reinforcing steel connection was used on each pier to obtain half-cell potential readings with the Ag/AgCl electrodes. The specific reinforcing steel connection used on each pier is indicated in Table 5.1 with bolded font.

Continuity measurements collected by Vector were obtained through direct connections between the reinforcing steel and an ohmmeter. Measurements collected by University of Minnesota personnel required approximately 20 feet of lead wire attached to one of the reinforcing steel connections to be tested. This was necessary to establish the connections with the terminals of the ohmmeter used. Differences between the continuity results of Pier 34 North and Pier 37 North reported by Vector, presented in Chapter 3, and the values listed in Table 5.1 can be attributed to the lead wire used by University of Minnesota personnel to measure resistance.

5.3 Resistivity Probes

To complement the embeddable half-cells, a corrosion monitoring probe was developed to serve as an indicator of areas actively corroding, and if possible to obtain a corrosion rate. Initial efforts at fabricating such an instrument focused on the use of fiber optic cables coated with a thin metal film at the fiber tip, but manufacturing and installation issues prohibited the use of these sensors in the field study.

The instrument chosen in lieu of the fiber optic sensor was a resistivity probe developed at the University of Minnesota. The field durability of this particular instrument was much higher than that of the fiber optic sensor and provided similar information. The resistivity probe was comparable to the electrical resistance probe presented and discussed in Chapter 2, although a

device to compensate for temperature fluctuations was not included [64]. In addition, the resistivity probes used in this investigation were designed as "on/off" corrosion indicators, and were not capable of establishing corrosion rates through changes in cross section, as determined through laboratory experimentation. The probe consisted of a 2.5 cm loop of thin iron wire with ends soldered to lead wire. These soldered connections were coated with a silicone caulk to ensure that the only portion of the probe susceptible to corrosion was the iron wire loop itself. Similar to the fiber optic sensors, iron wire was chosen to replicate the corrosive behavior of the reinforcing steel within the concrete structures. Two diameters of iron wire were used. Theoretically, the diameter of the wire is linearly correlated with the time to corrosion of the probes. This study used probes of either 0.5 mm or 0.25 mm diameter iron wire. The use of 0.05 mm diameter wire was also investigated but the wire lacked the stiffness to be successfully embedded in grout and it was much more difficult to work with when fabricating the probes. Wire thicker than 0.5 mm was not investigated. A schematic of the resistivity probe has been included as Figure 5.3 and a 0.5 mm probe after fabrication is shown in Figure 5.4.

Resistance through the iron wire loop was measured after connecting the lead wire of the probe to the terminals of a standard ohmmeter. Because the wire loop was relatively short and less than 1 mm in diameter, initial resistance measurements were less than 2 Ohms depending on the length of lead wire attached. Once corrosion of the iron wire was severe enough to cause breakthrough of the cross section, either by completely corroding through the metal or creating a corrosion induced stress failure at some point along the loop, resistance was essentially infinite due to the discontinuity in the wire. Two probes were installed at each half-cell location in the columns and pier caps to indicate whether or not those areas were actively corroding. Electrode potentials measured with the embedded Ag/AgCl half-cells, and results of chloride samples previously collected at each instrumentation location, could assist in the analysis of any observed probe failures.

5.4 Humidity Probe

Because 75% of the columns and pier caps in the study were either wrapped or sealed, the issue of retained moisture or water within the concrete was a significant one. By monitoring the relative humidity of the concrete over time, and with respect to the unwrapped columns in similar locations, these concerns could be evaluated. Areas of high relative humidity on wrapped

columns indicated regions with the potential to develop into contained corrosive environments, depending on the permeability of the composite wraps, especially if similar areas on unwrapped columns provided much lower readings.

To monitor the moisture levels of the columns and pier caps in the study, especially the wrapped and sealed structures, a Concrete Master III humidity sensing probe and installed humidity sleeves, manufactured by Protimeter in England, were selected. The humidity sleeves were hollow, plastic cylinders measuring approximately 5 cm long and 1.6 cm in diameter with slits, or vents, located along the shaft. A picture of the sleeve is shown in Figure 5.5. When used in conjunction with the installed humidity sleeves, the relative humidity probe was capable of measuring both ambient temperature and relative humidity (to within +/- 3% RH).

Installation of the sleeve in concrete required a drilled hole of dimensions matching the diameter and length of the sleeve. After drilling the appropriate size hole in the concrete structure to be monitored, the sleeve was pushed in until the lip abutted the concrete surface. Data was collected by removing the cap on the sleeve and inserting the humidity probe of the Concrete Master III. A schematic of the data collection process is shown in Figure 5.6. After allowing the probe 15 minutes to equilibrate, readings of ambient temperature and relative humidity were collected.

5.5 Locations of Field Instrumentation

Because the chloride samples collected in the pre- and post-ECE sampling periods were major tools in analyzing the effectiveness of the ECE process, all corrosion monitoring instrumentation was placed near Mn/DOT chloride sample locations. The placement of instruments at these locations ensured that data obtained from the corrosion sensors could be correlated with the observed chloride concentrations to assist in data analysis. Of the 72 locations where Mn/DOT collected chloride samples in the pre- and post-ECE sampling periods, 50 were selected for instrumentation placement. In placing the 50 embeddable half-cells, priority was given to areas that exhibited a high corrosive potential. However, the need to monitor every column and pier cap as equally as possible, due to the various combinations of ECE and column wrapping/sealing that needed to be analyzed for the purposes of this study, was also considered when instrument locations were selected.

Illustrations of the instrument plan are included in Figures 5.7-5.12, with a legend. As shown in Figure 5.7, a solid black circle identifies each chloride sample location. The corrosion monitoring instruments have been identified in these figures using rectangles, triangles, and open circles, indicating resistivity probes, moisture sleeves, and half-cells, respectively. Patched and painted areas, on the structures are also indicated.

To be identified uniquely, a moniker was given to each instrumentation location. The identification tag format was selected to identify whether the sensors were located in a column or pier cap, as well as the position in the structure relative to other sensors. This was accomplished for the resistivity probes and the half-cells by first identifying all pier sensor locations by PIER and all column sensor locations by column number. Position in the structure was identified from either the bottom of the column to the top, or north to south in the pier caps, using hyphenated numbers starting at 1. Pier cap locations were further identified by the vertical face in which the instruments were placed, either west (W) or east (E). For example, location 34B-1 identifies the instrument location (consisting of two resistivity probes and a half-cell) closest to the ground on Column 34B. Location PIER 40N-W1 identifies the northernmost instrument location (consisting of two resistivity probes and a half-cell) on the west face of the pier cap at Pier 40 North. The locations of the moisture sleeves were identified separately, because the sleeves were not embedded at the same locations as the resistivity probes and half-cells. Column and hyphenated number also identified the humidity sleeves, although the included diagrams simply indicate the number assigned to each sleeve, increasing from bottom to top of the column. Chloride ion sample locations that were not instrumented were identified using the same format as the instrumented locations. The identification tags for the locations that were not instrumented have not been included in Figures 5.8-5.12 to avoid confusion, but were presented in Chapter 3 where all of the chloride sample locations were identified.

An embeddable half-cell and two resistivity probes were installed at each instrumentation location so that data collected from both instrument types could be correlated. Each reference electrode was placed approximately 15 cm away from the chloride sample location to avoid embedment in the grout placed after chloride sampling. The two resistivity probes were placed approximately 10 cm from the half-cell, and 10 cm apart from each other. Locations that reported very high or very low chloride concentrations (over 2000 ppm or less than 1000 ppm) at multiple sample depths, in the post-ECE sampling period, were instrumented with two small

probes. This format was selected to provide sensor redundancy in the event of an expected or unexpected probe failure, in areas of high and low corrosive potential respectively. Locations with moderate to low corrosive potential at the majority of sample depths were instrumented with both a large and a small probe to enable estimation of corrosion rates from the differences in probe diameter and time to corrosion.

The instrument locations on each pier cap were selected on a worst case basis, with respect to corrosion potential, as determined from the results of the pre and post-ECE chloride sampling periods discussed in Chapter 4. Instrumentation was placed at half of the chloride sample locations on each of the pier caps, except for Pier 40 North which had instruments placed at 75% of chloride sample locations, as shown in Figures 5.8-5.12. This constituted two locations on each vertical face of Pier 34 North, Pier 34 South, and Pier 37 North, and one location on each face of Pier 37 South. Pier 40 North was instrumented at three locations on each vertical face because of very high chloride concentrations reported at multiple depths during both the pre and post-ECE sampling periods. Unfortunately, the Ag/AgCl half-cell that was installed at location PIER 34N-W1 was broken at the concrete interface during the instrument wiring procedure. Therefore, only two resistivity probes were operative at that location, shown in Figure 5.8.

As shown in Figure 5.8, every Mn/DOT chloride sample location on Columns 34A-C, located at Pier 34 North which was treated with ECE, had corrosion monitoring instrumentation installed. This was based on the extremely high chloride concentrations reported in these structures prior to ECE, as discussed in Chapter 4. All of these columns were treated with ECE and subsequently sealed in some fashion, creating an excellent set of locations to assist in the evaluation of both the ECE process and the FRP wraps, with respect to corrosion mitigation.

Instrument locations on the untreated columns and pier cap of Pier 34 South are shown in Figure 5.9. Similar to Pier 34 North, all of the column sample locations, except for one, were instrumented because of high chloride concentrations reported at multiple locations and depths, in both sampling periods. This pier was not treated with ECE but portions of the structure were wrapped with FRP wraps. Therefore, the extensive instrumentation of Pier 34 South was to be used to provide data to assist in the analysis of concrete wrapping and its effects on corrosion in untreated structures. The only potential column location not instrumented on Pier 34 South was 34E-3 because of the low chloride concentrations reported at all sample depths, during both

sampling periods. Although location 34E-1 also reported very low chloride levels in both sampling periods, this location was instrumented to monitor any changes in corrosion potential that may be attributable to column wrapping.

In total, only six out of nine potential locations were instrumented on Columns 37A-C of Pier 37 North (treated with ECE), as shown in Figure 5.10, because of the low corrosive potential indicative of the low chloride concentrations reported before and after ECE treatment. The two locations on each column were selected on a worst case basis with respect to post-ECE chloride levels.

Column 37D was the only column of Pier 37 South instrumented. This pier was not treated with ECE. All three chloride sample locations on Column 37D were instrumented, as shown in Figure 5.11. Locations 37D-2 and 37D-3 were instrumented because of the high chloride levels reported in both the pre and post-ECE sampling periods. Although location 37D-1 reported very low chloride levels in both periods, this location was instrumented because Column 37D was a control column not treated with ECE, and not wrapped or sealed. Data collected from instruments at location 37D-1 were to assist in the determination of whether or not column wrapping affects corrosion conditions in areas of initially low corrosive potential. This was to be accomplished by comparing results with location 34E-1, which was also untreated and reported very low chloride levels in both sampling periods, but was wrapped with the GFRP composite. In addition, the effect of ECE and concrete sealers on corrosion conditions in areas of low initial corrosive potential, could be assessed through the comparison of results collected from multiple sensor locations on Columns 37A-C. Those columns were treated with ECE and had a variety of sealant systems (i.e. FRP wraps and concrete sealers) applied.

The instrumentation plan for Pier 40 North, which was not treated with ECE, is shown in Figure 5.12. Because Column 40A was wrapped with the MBrace CFRP, but was not treated with ECE, all three chloride sample locations were instrumented. Only one chloride sample location on Column 40C was instrumented, 40C-1, which reported very high chloride concentrations, at multiple sample depths, during the pre- and post-ECE sampling periods. Because Column 40C was a control column, instrumentation at location 40C-1 was to assist in evaluating the changes in corrosion conditions at an untreated and unwrapped area of high initial corrosive potential. The two other chloride sample locations on Column 40C were not instrumented because of very low chloride concentrations reported during both sampling periods.

A total of 48 humidity sleeves were placed in the twelve columns of the study. Because the desired result was to obtain relative humidity in the concrete structure, and not necessarily at each instrument location, these sleeves were not placed with the half-cells and the resistivity probes. This was desired because moisture levels in the columns were expected to be relatively independent of exact location and would likely only be affected by height from ground level. Data collected from the moisture sleeves was primarily intended to evaluate the moisture retention of sealed columns in comparison to similar unsealed columns. Structures retaining more moisture than others could then be identified as potentially corrosive, particularly those reporting resistivity probe failures or highly negative half-cells. Only the columns were instrumented with humidity sleeves to ease data collection because each sleeve had to be read manually.

To evaluate the variability of relative humidity with respect to height from ground level, three columns were selected to each have seven sleeves installed. The seven sleeves were spaced approximately 46 cm apart in a vertical line. The columns selected were 37A (ECE and MBrace CFRP), 37B (ECE and sealer), and 37D (control). The orientation of the installed sleeves in these structures is illustrated in Figures 5.10 and 5.11. Placement in these columns permitted the analysis of humidity variation as a function of height for treated and untreated columns, in terms of ECE, that were subjected to different types of wraps and concrete sealants, at the same pier location. The other nine columns in the study had three humidity sleeves installed along the height of the column. The locations of all installed moisture sleeves is documented in Figures 5.8-5.12.

5.6 Installation Procedure

Installation of the corrosion monitoring instrumentation took place during the first few weeks of December 1998. Even though most of the laboratory tests of the resistivity probes had not yet been completed, it was determined that the field instruments should be embedded as soon as fabrication was completed.

In order to replicate the concrete used in the columns and pier caps as closely as possible and to prohibit freezing of water in the mixture, a special grout mixture was needed for embedment of the reference electrodes and resistivity probes; the humidity sleeves did not require grout for embedment. The selected mix design was based on the properties and

proportions used in the bridge substructure concrete. To minimize the potential for air voids created by frozen water, and prevent damaging of the instruments, Rapid Set was chosen for the grout mixture. Rapid Set was a non-shrink cement not affected by the cold temperatures. For freeze-thaw durability, an air entrainment admixture was added to the grout mixture. The concrete used in the bridge structure was also air entrained due to element exposure. The water to cement ratio of the grout mixture was selected to be 0.5, the same ratio used in the concrete of the substructure. To avoid cooling of the grout, very small batches were mixed with warm water, as needed, at each instrument installation location. Each prepared batch was composed of 100 ml of water and 200 g of grout. Two drops of air entraining agent were then added with an eyedropper, but the air content of the resultant mix was not measured. A grout mixture containing aggregate would have been more comparable to the concrete in the columns and pier caps but would have required much larger holes to be drilled in order to fit both the mix and the instrument in each hole. This would have greatly increased the size of each intrusion into the concrete, and was deemed undesirable.

A 2.54 cm diameter concrete drill bit was used to drill the holes for installation of the embeddable half-cells. This drill size provided an additional 0.3 cm of diameter around the instrument, facilitating placement of both the grout mixture and the half-cell. The resistivity probe holes were drilled with a 1.59 cm drill bit due to the smaller size of these probes. Both diameters were selected because they were approximately the smallest hole sizes that permitted installation of the instruments, thus minimizing the intrusion at each location.

The installation process began by locating the reinforcing steel at each sensor location with a pachometer. After determining the depth of the steel, two 1.588 cm diameter holes and one 2.54 cm diameter hole were drilled laterally into the concrete at each sensor location to the specified depth of reinforcing steel. The position of the sensor holes relative to each other, and to the location of the Mn/DOT chloride sample, was discussed in the previous section. Drilled hole depth was monitored with a measuring tape.

After the correct hole depth was drilled, concrete dust was cleaned from the hole using compressed air. After cleaning the hole, the specified grout mixture was prepared. The selected mix design resulted in a fairly loose grout and could not be immediately used for embedment because it was not viscous enough to remain in place on all sides of the instrument in the drilled holes. Therefore, the mixture was monitored and stirred slowly for approximately five minutes

until it thickened. After becoming thick enough to facilitate placement, the holes were filled using a 1.25 cm brick pointer. Grout was applied in the back of the hole and around the circumference, before being packed into the center of the hole. The hole was considered filled when it would not accept anymore grout, and the mixture spilled out of the bottom of the hole as more was pushed in. At this point the specified instrument was installed slowly, checking for air pockets during placement. If an air pocket was felt as the instrument was pushed into the grout, the instrument was removed and the hole was filled again. The grout within the instrument hole provided noticeable resistance against instrument insertion, so air pockets were easily recognized when the grout resistance was suddenly, and only temporarily, relieved. The installation process was repeated until proper placement was achieved. Each instrument was placed near the depth of each hole and then grout was used to backfill around the instrument. A picture of a typical sensor location after installation of the three instruments has been included as Figure 5.13.

To ensure continuity of the FRP wrap and concrete sealer systems around each embedded instrument, the same epoxy or sealer used on the structure needed to be applied around and over the top of each sensor to prevent permeation of water and chloride ions through the grout backfill. However, both the MBrace and AMOCO epoxy systems could not be applied at temperatures under 50ºF, as was the case during early December. Therefore, after installing the instruments at each location, and after the grout had cured for 24 hours, each sensor hole that was drilled into a wrapped or sealed structure was covered with bearing grease. Bearing grease was selected as a temporary sealant because it effectively sealed each hole through the winter but was easily removed once temperatures rose during the spring months. Holes drilled into the control columns were not sealed in any way.

During February 1999, wiring from the sensors on each of the columns and pier caps was run to a central data collection point for each pier. The placement of all wire ends at one point on each pier eased the data collection process, and minimized the potential for vandalism. Lead wires from the resistivity probes and the half-cells, at each location, were fed through sections of 2.54 cm diameter PVC conduit. The sections of PVC were then strapped to the columns and pier caps using non-metallic ratchet straps. Using PVC also helped minimize the potential for vandalism and weathering of the wires. The sections of PVC were oriented to run all sensor wiring to the center of each pier cap, where an electrical box was placed. In May 1999, the

sensor wire ends were soldered to binding posts on an electrical board located inside the box, and each board was clearly labeled using the sensor identification tags discussed in Section 5.5.

Lead wire from the half-cells was connected to the positive terminal on each binding post and jumper wires were used to connect the wire attached to the reinforcing steel connection to each negative terminal. Jumper wires were also used to connect every negative terminal of the resistivity probe binding posts to an electrical switch. The switch was also connected to the reinforcing steel, and thus all of the resistivity probes could be electrically connected to the rebar by flipping the switch, and closing the circuit. The decision to interconnect each of the probes and the reinforcing steel was pending laboratory test results of the resistivity probes, so the circuit was initially left open and the probes were not interconnected. Results of the laboratory testing and the reasons for investigating interconnection effects is presented in Chapter 6.

To minimize moisture in the electrical boxes, indicating silica gel desiccant was placed in the bottoms of the boxes in perforated plastic bags. In addition, each of the three wire entry holes drilled into the electrical boxes, in both side panels and in the bottom, were sealed with insulating foam and silicone caulk. A picture of the PVC wiring system and the installed electrical box on Pier 34 North is included in Figure 5.14.

The final portion of the installation procedure was undertaken during May 1999. The bearing grease at each sensor location was removed using a gasoline soaked toothbrush to scrub out the grease, and paper towels to dry the gasoline from the concrete. Once the grease was removed, and after letting the concrete dry for 24 hours, all sensors placed on structures wrapped with the AMOCO system were sealed with the same Tyfo epoxy used to apply the wraps. This mixture was prepared as specified by the manufacturer and was brushed onto the concrete with a paintbrush. The MBrace epoxy and each of the column sealers were not applied around the sensor holes at this time, due to difficulties in obtaining samples. After unsuccessfully trying to obtain a sample of the original MBrace epoxy, an alternative MBrace product that was essentially the same epoxy in a different color, Concressive LPL, was used to seal the MBrace systems in July 1999.

The humidity sleeves were installed during May 1999 after drilling a 1.59 cm diameter hole, approximately 5 cm in depth, at each desired location. These holes were thoroughly cleaned with compressed air before the sleeves were installed with their caps in place. A picture of an installed moisture sleeve has been included in Figure 5.15. The moisture sleeves were not

sealed with epoxy because the diameter of the instrument holes that were drilled was slightly smaller than the actual sleeve diameter. The lip of the moisture sleeve then covered the minimal amount of concrete exposed by drilling through the respective wrap system, so sealing around the sleeve was neither necessary or beneficial. Preliminary results from all of the installed sensors are included and discussed in Chapter 7.6. Overview of Laboratory Study

This chapter summarizes the laboratory experiments conducted to calibrate and evaluate the corrosion monitoring instrumentation, and to determine the diffusion and bond strength properties of the FRP wrap systems. The sensor calibration methods and procedures are presented for each of the three sensor types, and laboratory test results are discussed. The diffusion testing apparatus is explained and the diffusion properties of the three FRP wrap systems are summarized. The final portion of this chapter presents the peel testing apparatus and discusses the results collected during the initial series of peel tests.

6.1 Sensor Calibration and Testing

Prior to installation in the field structures, laboratory experiments were conducted to calibrate and evaluate each of the three sensor types. Calibration of the embeddable Ag/AgCl half-cells was conducted to ensure that the reproducibility of each electrode met the manufacturer's specifications, and to evaluate the effect of temperature on the obtained potential readings. Laboratory experiments were performed to assess the time to corrosion of the resistivity probes, analyzing the effects of several variables. These variables included iron wire diameter, testing medium, chloride concentration, and wire interconnection effects. Finally, relative humidity readings were collected from two moisture sleeves embedded in a laboratory specimen to evaluate the reproducibility of the readings between sleeves, and over time.

6.1.1 Ag/AgCl Half-Cells

To ensure that all of the half-cells were functioning correctly prior to installation in the field structures, and to evaluate the reproducibility between units, calibration tests were conducted in the laboratory. The manufacturer's specifications indicated that the potential readings should be reproducible, between different half-cells against the same reference electrode, to +/- 2.4 mV. To perform this calibration, each half-cell was submerged in 500 ml of de-ionized water, at room temperature, along with a saturated calomel electrode (SCE) which served as the reference electrode. The potential between the two electrodes was measured with a voltmeter.

After evaluating the reproducibility of the units, further testing of the half-cells was conducted to evaluate the temperature response of the obtained potentials. These tests were also conducted relative to an SCE. One half-cell was randomly selected for this experiment, and it was submerged in a beaker containing 250 ml of 1M KCl, along with the SCE reference. The beaker, containing the two electrodes in solution, was then placed in a temperature bath, which was used to control and alter the temperature of the solution as desired. Half-cell potentials were collected at a variety of temperatures to evaluate the sensitivity of the sensor reading with respect to surrounding temperature. Data was recorded after both the temperature of the solution, and the electrode potential, had stabilized, or after approximately one minute.

6.1.1.1 Results and Discussion

The results of the half-cell calibration tests conducted relative to a saturated calomel electrode in de-ionized water have been included in Table 6.1. The temperature of the water was 22 ∀C and was held constant for the duration of the experiment. A total of 50 half-cells were calibrated for future field installation. As evident in this table, the average electrode potential was –38.06 mV with a standard deviation of 1.12 mV. The range of potential observed was +/- 2.05 mV, or as high as –36 mV and as low as –40.1 mV. One half-cell reported a potential of –8 mV relative to the SCE and was thus considered defective. This half-cell was replaced and re-calibrated before installation in the field structures commenced.

The results of the temperature bath calibration have been included in Table 6.2. Only one-half cell was evaluated in this experiment, out of the fifty electrodes to be installed in the field structures. As evident in this table, half-cell potential was dependent on the surrounding temperature and readings became more negative as temperature increased. The temperature range evaluated during the calibration was 20 ∀C to 52 ∀C. The range of expected temperatures during data collection from the embedded half-cells in the field structures was 0 ∀C to 35 ∀C. While field temperatures will fall below 0 ∀C during the winter months, the instrument specifications indicate that potentials collected below freezing are not reliable. Temperatures lower than 20 ∀C were not evaluated in the laboratory because of the limitations of the temperature bath.

In general, changes in potential strictly due to temperature fluctuations can be considered negligible with respect to the field instrumentation because the difference between potentials at the highest and lowest temperatures was only 7.7 mV. In addition, potentials measured in the field were expected to be on the order of hundreds of millivolts as opposed to approximately 40 mV. Because readings with the units have a natural range of +/- 2.4 mV, identifying a change in a field measurement strictly due to temperature would be essentially impossible.

6.1.2 Resistivity Probes

To calibrate and investigate the behavior of the resistivity probes, several laboratory experiments were conducted. Preliminary tests were performed to ensure that the probe was a viable corrosion monitoring instrument for concrete structures because it was not clear whether a

probe failure in grout would be observable through resistance measurements alone. Corrosion of the iron wire in solution, or in air, allowed failure by either an induced stress failure after partial corrosion of the wire diameter or by complete oxidation of the cross section. Visual verification of failure could also be performed. A probe placed in grout could fail only after the cross section was completely oxidized because the iron wire was not free to move once the grout set. It was also not clear whether the iron oxide remaining after corrosion would continue to be conductive, keeping resistance measurements at the same pre-corrosion levels despite probe failure. Because visual inspections of a probe placed in grout were not possible, the probe needed to indicate infinite resistance after failure in order to be useful for this study. In addition, the elevated pH and lower levels of oxygen and moisture present in hardened grout made corrosion of the probes a potentially lengthy phenomenon, even if measurable. All of these concerns were investigated to ensure that the resistivity probe could be used as a corrosion indicator.

To establish approximate corrosion rates and observe the behavior of the resistivity probes when experiencing corrosion, an initial experiment was conducted in solution. This experiment, identified as Test 1, consisted of a total of ten probes, five probes of 0.5 mm diameter wire (large) and five of 0.25 mm wire (small). All ten probes were placed in a large evaporating dish filled with 175 ml of a 0.33M solution of NaCl and de-ionized water at a pH of 6.8. The strength of the salt solution was chosen randomly, although sufficient chlorides needed to be present to corrode all ten probes. A salt solution was used, instead of a strong acid for example, to model the behavior of road salt in concrete in light of planned probe tests in grout. The probes were spaced out evenly, alternating large and small probes, around the circumference of the dish and each probe was completely submerged in the solution. Resistance measurements and visual observations of each probe were recorded once a day for the duration of the experiment.

While the solution test was underway, a similar test was set up with probes placed in grout. This test was identified as Test 2. To encourage corrosion, the grout was seeded at a chloride concentration of 32,000 ppm by weight of cement. This was achieved by mixing 5.5 ml of 0.33M NaCl solution and 2 g of grout in a 10 ml beaker. This mix resulted in a grout plug with a total volume of 23.1 cm^3 at pH 11.2. The chloride concentration was chosen to ensure a high enough concentration to corrode all of the probes in a relatively short time frame. After approximately five minutes, or after the grout was thick enough to support the resistivity probes,

three large and three small probes were placed in the grout plug. The probes were inserted without controlling the depth or position of the probes. Once the grout had cured, approximately 2 ml of 0.33M NaCl solution was continuously ponded on top of the grout plug in the 10 ml beaker. The pH of the shallow ponded solution was 10.2, due to the contact with the grout surface. Resistance measurements were collected daily but visual inspection of the probes could not be performed. While the experiment was underway, a decision was made to crack open the beaker and remove the grout plug, so that it could be submerged in a 0.33 M NaCl solution, permitting chloride permeation from all sides of the plug, not just the upper surface. This grout plug was not wet/dry cycled.

After a preliminarily evaluation of the corrosion rates and behavior of the probes in both solution and grout, several variables were investigated in a more controlled fashion through further laboratory experiments. Because both the solution test and the grout test used relatively high chloride concentrations to quickly corrode the probes, experiments more indicative of field conditions were conducted. The exact effect of solution concentration, or grout seeding concentration, on corrosion rate was also a variable in the further investigation. More precise examinations of the difference in time to corrosion between a probe in grout and one in solution, at the same chloride concentration, were also performed. Finally, tests to examine the interconnection effect of the probes were conducted to evaluate whether an electrical connection between adjacent probes would affect corrosion rate. The results of these tests would also help to establish the difference in the time to corrosion of the small and large probes under identical testing conditions in both grout and solution. To investigate each of these five variables, a test matrix was established and a total of five new experiments, three in grout and two in solution, were conducted. Each experiment used a total of six probes, three large and three small. The complete resistivity probe test matrix has been included as Table 6.3, where the characteristics and objectives of each experiment have been listed.

The objective of Test 3 was to evaluate the reproducibility of the probes in a solution containing chloride levels much lower than used in Test 1. This was achieved by completely submerging and centering each of the six probes in six separate 30 ml beakers. Each beaker was filled with 25 ml of 0.05M solution of NaCl and de-ionized water. The probes were centered so that they were not in contact with the sides of the beaker. The initial solution pH of each test was 6.9. A schematic of this test set-up is shown in Figure 6.1. Similar to the preliminary tests

conducted, resistance measurements and visual observations of the probes were recorded daily until probe failure.

The main objective of the next two tests, Tests 4 and 5, was to evaluate the difference in the time to corrosion for probes placed in grout and solution. The solution test, Test 4, was set up with each probe again isolated, centered, and submerged in a small beaker containing 25 ml of a 0.1M solution of NaCl in de-ionized water. This concentration was chosen to evaluate the effect of solution strength on time to corrosion of the probes by comparing the time to failure of similar sized probes between Tests 3 and 4. These two tests were identical except Test 4 used a solution with twice the chloride concentration of Test 3. Test 5 also used the same 0.1M NaCl solution as Test 4, and probes placed in individual beakers, except this test was set up with the probes embedded in grout. The grout in this experiment was seeded at a chloride concentration of 11,000 ppm by weight of cement, or approximately twice the worst case, pre-ECE field conditions and five and a half times the established threshold for corrosion of 2000 ppm. This value was chosen to evaluate the corrosion behavior of the probes in conditions more similar to those present in the bridge structure than used in Test 2, while still corroding the probes at an accelerated rate for calibration purposes. To obtain this seeded grout mixture, 12.5 g of grout and 7.75 ml of the 0.1M NaCl solution was mixed in each of the six, 30 ml beakers. This mixture was very loose initially and probes could not be placed until the mixture had been allowed to set up for approximately 10 minutes. While the grout was setting, the depth of the grout mixture in each beaker was recorded. This was found to be 25 mm in each case. To draw meaningful comparisons between similar sized probes placed in similarly seeded grout, the position of each probe in each beaker, or grout plug, was identical. This was accomplished by straightening each probe as much as possible and then marking each with a permanent marker, on the attached lead wire, at exactly 20 mm back from the tip of the iron wire loop, while the grout was solidifying. The probes were straightened to ensure that they could be centered in the grout plug as much as possible, eliminating contact with the sides of the beaker. Marking the probes at 20 mm from the tip guaranteed that all probes were placed at the same depth in the grout plug, 5 mm from the bottom of the mixture. After the grout had become viscous enough to facilitate accurate placement, each probe was inserted in the center of the beaker until the 20 mm mark on the lead wire was at the surface of the mixture. Each probe was then slightly moved back and forth to ensure that it was not in contact with the beaker, and to remove any air voids. After allowing

each grout plug 24 hours to set completely, each beaker was cracked apart and all six grout plugs were submerged in a large dish filled with 250 ml of 0.1 M NaCl solution at a pH of 7. The grout plugs were then wet/dry cycled every four days, two days wet followed by two days dry, and resistance measurements were collected daily.

The final two tests, Tests 6 and 7, were conducted to evaluate a potential wire interconnection effect on the corrosion rates of the probes. The change in corrosion rate based on grout seeding levels could also be evaluated, approximately, through comparison to Test 5 results, although Tests 6 and 7 were somewhat different because each plug contained two probes as opposed to only one in Test 5. To investigate the effect of wire interconnection, two probes were paired in each of three grout plugs. For both experiments, 24 g of grout and 15 ml of a 2.5M NaCl solution were mixed together in each of three, 30 ml beakers. This resulting grout mix had a pH of 11.2 and was seeded at a chloride concentration of 55,000 ppm by weight of cement, or five times the level used in Test 5. This mixture was also fairly loose, and needed approximately ten minutes of setting time before probe placement could commence. Similar to Test 5, the depth of each grout plug was recorded, 30 mm, and each probe was straightened and then marked 25 mm from the loop tip. This again ensured placement of all probes at 5 mm from the bottom of the beaker. After the grout had thickened enough to hold the probe positions, probe placement began with two small probes placed in one of the beakers approximately 0.625 cm. apart, two large probes in another, and one of each size in the final beaker. This placement was the same for both Tests 6 and 7. After slightly shaking each probe to ensure they were not in contact with each other, or with the sides of the beaker, the grout was allowed to cure for 24 hours with the probes in place. After 24 hours each beaker from Test 6 was cracked open and the three grout specimens were submerged in a large dish containing 200 ml of 0.5M NaCl solution at pH 6.8. The specimens for Test 7 were also removed from their beakers and placed in an identical, but separate, saltwater bath. The plugs from both tests were wet/dry cycled every four days, two days wet followed by two days dry. The only difference between the tests was that in Test 7, probes located in the same grout plug had one of their lead wires interconnected by a jumper wire. Resistance measurements were again collected daily. One of the grout plugs from Test 6 during a drying cycle is shown in Figure 6.2.

6.1.2.1 Results and Discussion

The results of the resistivity probe experiments have been included in Tables 6.4-6.10.

As evident in Table 6.4, the small resistivity probes of Test 1 failed approximately five times faster than the large probes. The initial pH of the solution was 6.8, but at the end of the test the solution had become much more basic, with a pH of 8.7. The increase in alkalinity of the solution can probably be attributed to the large number of probes placed in the same solution. As corrosion of the large probes proceeded, thick oxides were noticeable on the iron wire loops, and significant amounts of iron oxide had accumulated in the bottom of the solution basin. However, previous research has indicated that corrosion rate of iron or steel is not affected by changing pH, as long as the solution pH remains within the range of 4-10 [69]. The corrosion rate will decrease in solutions of pH higher than ten, and will increase in acidic solutions of pH less than four. Therefore, it can be assumed that the increase in solution pH through the experiment duration did not adversely affect the results. Nonetheless, the proximity of the large and small probes may have affected the experimental corrosion rates although an exact determination of the effect is difficult. The oxides that formed on the probes during the experiment, indicating the anodic region of the iron wire loop, were generally located only at the apex of the loop. This observation indicates that localized corrosion on the iron wire loops probably initiated the probe failures, as opposed to uniform corrosion of the entire loop. In conclusion, the average time to failure for the small and large probes of Test 1 appeared fairly reliable, and were consistent with subsequent tests, indicating the selected test set-up probably did not affect the results.

The results of Test 2 have been included in Table 6.5. The main objective of this test was to determine if a probe failure could be distinguishable in grout. Failure of all six probes was witnessed, indicating the resistivity probe is a viable instrument for corrosion monitoring in concrete structures. The time to corrosion for both size probes was much longer than in Test 1, although the difference can be attributed to the increased alkalinity of the grout, and the restriction on chloride ion and water movement that occurred in the solidified grout. On average, the small probes corroded approximately 2.5 times as fast as the large probes, although the time to failure varied between similar probes. The difference in failure time can be attributed to the test set-up. Because neither position, nor depth, was controlled when the probes were placed in the grout mixture, some probes were undoubtedly closer to the grout surfaces than others. These probes probably corroded faster than the other probes because chloride ions, and water were

more readily available from the saltwater bath. In addition, oxygen from the atmosphere was more available to probes closer to the surfaces of the grout plugs, than to probes deeply embedded within the grout. These results should only be considered qualitative though because the test set-up was changed after the test had begun, as discussed in the previous section.

The results of Test 3 are included in Table 6.6. In this experiment, the small probes corroded approximately 4.5 times as fast as the large probes. This is similar to the results witnessed in Test 1, where the small probes corroded five times faster than the large probes, although Test 1 was less controlled than Test 3, with regards to the initial and final solution pH and the individual testing basins provided for each probe. Thick, localized oxides were witnessed on the apex of the iron wire loop of the large probes of Test 3, in addition to significant oxide accumulation in the bottoms of the beakers containing the large probes. Unlike Test 1 however, the oxides produced did not significantly affect the solution pH of Test 3 because only one probe was submerged in each beaker, as opposed to the ten probes that shared the same solution bath in Test 1. The initial solution pH of Test 3 were measured with a pH meter, but because of difficulties that occurred with the pH meter, universal pH strips were instead used to measure the final solution pH. This procedure was also used to obtain initial and final pH values for Tests 4-7. However, the universal pH strips were only accurate to whole pH values (i.e. 6, 7, 8 etc.), and thus a pH reading of 7 actually corresponded to the pH range of 6.5-7.5. Oxide accumulation was not as noticeable on the small probes of Test 3 as on the large probes, or in the beakers containing the small probes, but the oxides that formed were also typically located only at the apex of the iron wire loop. Therefore, localized corrosion may have initiated the failures of the small and large probes of Test 3, similar to that witnessed in Test 1.

The results of Test 4 were interesting in comparison to Test 3 because they were the same experiment, except Test 4 was run at twice the solution strength of Test 3. These results are included in Table 6.7. The small probes of Test 4 all failed after five days, and oxide accumulation, both on the small probes and in the beakers, was minimal. Therefore, doubling the solution strength decreased the time to corrosion of the small probes by 45%, in comparison with Test 3. The large probes of Test 4 failed after an average of 27.3 days. This corresponds to a decrease of only 30% in the time to failure of the large probes from that witnessed in Test 3, despite a solution of twice the molarity. The effects of increased NaCl concentration on the time to failure of the resistivity probes in Tests 1, 3, and 4 will be analyzed later in this section.

Similar to the previous solution tests, relatively thick and localized oxides were noticeable near the apex of the iron wire loops of the large probes of Test 4. In addition, a significant amount of iron oxide accumulated in the bottom of the beakers containing the large probes. As previously mentioned, significantly less oxide accumulation was witnessed on the iron wire loops of the small probes, although that which formed was generally also located in the region of the loop apex. Only minimal oxide accumulation was witnessed in the beakers containing the small probes of Test 4. These observations correlated with the assumed method of corrosion failure witnessed in the two other solution tests (Tests 1 and 3), or localized as opposed to uniform corrosion of the entire loop. Overall, the small probes in Test 4 corroded approximately 5.5 times as fast as the large probes. However, the small probes of Test 3 corroded approximately 4.5 times as fast as the large probes. Potential explanations for the differences between the ratio of failure times between large and small probes at the same solution strength, as determined through experimental results, will be discussed later in this section.

The results of Test 5 are included in Table 6.8. Test 5 was conducted to evaluate the difference in time to corrosion between probes placed in grout and solution, through comparison with Test 4. The results of this experiment indicated that the small probes of Test 5 failed after an average of approximately 87 days, and the large probes reported failure after an average of approximately 181 days. Therefore, the difference in time to corrosion of the small and large probes of Test 5 was a factor of 2.1.

The results of Test 6 are included in Table 6.9. The times to failure of the large and small probes that were embedded in the same grout plug are outlined together, using a bold line, as shown in Table 6.9. The grout plug with two small probes reported one probe failure after only 27 days, while the other probe lasted 74 days. These results were similar in the plug containing both a large and a small probe, where the small probe failed in 33 days, and the large lasted 98 days. In the grout plug containing two large probes, one probe failed after 99 days, while the other lasted 105 days. Averaging the times to corrosion of all of the small and large probes, the small probes corroded after an average of 45 days and the large probes after 100 days. Therefore, the small probes corroded slightly more than twice as fast as the large probes (2.2 times faster). An initial testing objective was to draw conclusions about the effect of chloride concentration on time to corrosion through comparison of Test 5 and Test 6. The small probes of Test 6 corroded

about two times faster than the small probes of Test 5, and the large probes of Test 6 corroded approximately 1.8 times faster. The grout plugs of Test 6 were seeded at five times the chloride concentration of the grout plugs of Test 5 (55000 ppm vs. 11000 ppm, respectively). However, the evaluation of grout seeding concentration, drawn through comparison of results from Test 5 and Test 6, should only be considered qualitative.

The results of Test 7 are included in Table 6.10. The times to failure of the large and small probes that were embedded in the same grout plug are outlined together, using a bold line, as shown in Table 6.10. In the grout plug containing two small probes, one probe failed after 25 days, while the other failed after 95 days. These results were similar to the results witnessed in Test 6, with regards to the two small probes placed in the same grout plug where it appeared that one probe may have driven the corrosion of the other probe. Averaging these two numbers shows that the small probes in Test 7 failed after an average of 60 days. One of the large probes in the plug containing two large probes failed after 110 days, while the other failed after 132 days. These failure times resulted in an average time to corrosion of 121 days for the large probes. The results of the large and small probes embedded in the same grout plug were not included in the averages because the large probe may have driven corrosion of the smaller probe, because the two were interconnected, affecting the corrosion rate and the overall average time to failure. The small probe in the plug containing a large probe and a small probe failed after 45 days and the large probe failed after 141 days. Because the average time to failure of the small and large probes were fairly similar to the average failure times that were observed in Test 6, wire interconnection apparently did not affect the results. The results of Test 7 indicate that wire interconnection may have slowed corrosion rates, because all of the Test 6 probes failed more rapidly than the probes in Test 7 under identical experimental conditions, aside from the interconnection of one lead wire. However, these differences can probably be attributed to the inhomogenous nature of grout and not the deleterious effects of wire interconnection. The preliminary results of Test 7 indicated that the small probes failed two times faster than the large probes, which was also the ratio of failure times observed in Test 6.

In summary, the average time to failure of the small resistivity probes in solution was approximately five times faster than the large probes. The small probes failed approximately two times faster than the large probes in grout. These experimental results correlate with the theoretical difference in the time to failure of the large and small resistivity probes. Although

having twice the diameter of the small probes means the large probes have four times the cross-sectional area that needs to be oxidized to reach failure, they also have twice the surface area on which corrosion can initiate, resulting in an overall factor of two on time to failure. The experimental failure times of the large and small probes placed in grout differed by approximately a factor of two, as expected using the theoretical relationship. However, the laboratory test in solution indicated that the large probes failed five times slower than the small probes, not twice as slow. The difference that was observed between the experimental and the theoretical failure times of the large and small probes in solution can be explained from test observations.

Inspection of failed small probes in solution indicated that almost all failures occurred at the center of the wire loop, where the stresses from bending the wire during fabrication would be greatest, as shown in Figure 6.3. The small probes also had minimal oxide formation localized at the apex of the wire loop, indicating that most failures were corrosion induced stress failures after some of the cross section had been removed. This is supported further by the observation that the two halves of the iron wire loop were significantly separated after failure of the probe. Corrosion failure of the probe did not simply produce a discontinuity in the wire loop, but it caused the two wire halves to snap apart from each other noticeably. Therefore, after corrosion removed some of the cross section of the small probes, stresses within the wire loop probably failed the probe, and a discontinuity was observed. This can be attributed to the small diameter of the wire and the fabrication process, which likely produced large residual stresses in the wire loop, especially at the apex of the loop. The failed large probes looked very similar to the untested large probes, except a small portion of the wire loop was removed. The two wire portions on a failed large probe were not significantly separated. Therefore, localized corrosion that created corrosion-induced stress failures may have also occurred on the large probes, but these failures were much less obvious.

In light of the failure observations, the difference in time to corrosion between the large and small probes was affected by the selected testing medium, i.e. either grout or solution. In solution, the small probes failed more rapidly than in grout because after partial corrosion of the cross section the wire loop could simply snap. In grout, complete oxidation of the cross section was required before a failure was witnessed, because the probe could not move in the hardened grout. Therefore, the difference in time to corrosion between large and small probes was closer

to the theoretical value in grout than in solution. The theoretical time to corrosion is based on complete oxidation of the cross section.

A plot of the relative corrosion rate of iron in an aerated NaCl solution, with respect to NaCl concentration, is included in Figure 6.4 [69]. This plot presents relative corrosion rates for solutions of various sodium chloride concentrations, as presented in the textbook *Corrosion and Corrosion Control* [69]. As shown in Figure 6.4, a solution containing a NaCl concentration of 0% corresponds to a relative corrosion rate of approximately 1.4. This solution represents distilled water. The relative corrosion rate presented corresponds to only the data included in the graph. As an example, at a NaCl concentration of 26% and a relative corrosion rate of 0.4, corrosion occurs approximately 3.5 times slower than in distilled water, or a 0% NaCl solution where the relative corrosion rate is indicated as 1.4 (i.e. 1.4 / 0.4 = 3.5). As evident in this figure, the relative corrosion rate of iron increases until the concentration of NaCl reaches 3%, at which point the rate decreases linearly. The increasing portion of the curve in dilute sodium chloride solutions corresponds to an increase in the availability of dissolved oxygen to cathodic areas, due to a change in the nature of the native, protective oxide on the iron specimen. The decreasing portion of the curve corresponds to high contents of dissolved salts that decrease the solubility of dissolved oxygen [69]. The three solution concentrations selected for Tests 1,3, and 4, have also been indicated in this figure.

The effect of increasing the NaCl concentration in solution, as determined through comparison of the results of Tests 1, 3, and 4 conducted in the laboratory, is indicated in Table 6.11. The values listed for theoretical increases in corrosion rate, based on the specified increase in solution strength, were interpolated from Figure 6.4. As evident in this table, doubling the sodium chloride concentration from 0.05M to 0.1M should theoretically result in a 10% increase in the corrosion rate. However, comparing Tests 3 and 4 indicates that the doubling the NaCl concentration from 0.05M to 0.1M caused the small resistivity probes to fail 44% faster, and the large probes 30% faster. In addition, an increase in NaCl concentration from 0.1M to 0.33M, between Tests 4 and 1, increased the average failure time of the large probes by 47% and the small probes by 45%. The theoretical increase in the corrosion rate of iron between solutions of 0.1M and 0.33M NaCl concentrations was only approximately 25%, as determined through Figure 6.4. Finally, increasing the NaCl concentration from 0.05M to 0.33M should have resulted in an increase in the relative corrosion rate of approximately 33%. However, comparing

the results of Tests 3 and 1 indicates that the small probes failed 66% faster, while the large probes failed 62% faster.

Although the effects of increased NaCl concentration, as witnessed in the laboratory, do not correlate with the theoretical increases in relative corrosion rate, several considerations can serve to explain the differences. The theoretical effect of NaCl concentration on the relative corrosion rate of iron, as presented in Figure 6.4, corresponds to an unstressed piece of iron subjected to uniform corrosion. Because the fabrication of the resistivity probes used in this investigation required a piece of iron wire bent into a loop, residual stresses in the completed loop may have decreased the time to failure by encouraging a corrosion-induced stress failure. In addition, the process of bending the iron wire may have preferentially fractured the natural oxide on the wire at areas of high bending stresses. A fracture in the protective oxide left areas of the wire immediately exposed to the chloride ions and dissolved oxygen in solution, and thus corrosion, after the probe was submerged. Areas where the native oxide was fractured would have been preferentially corroded over areas on which the native oxide remained. This phenomenon most likely occurred in the region near the apex of the wire, where the bending and residual stresses created during the fabrication process were probably greatest. This assumption also serves to explain why the oxides that formed during corrosion were generally located at only the apex of the iron wire loop on both the small and large probes, as shown in Figure 6.3 and as previously discussed. At this location, the residual stresses were probably greatest and the native oxide of the iron wire was probably already cracked when the probe was submerged, potentially resulting in a very small anodic region in which a corrosion-induced stress failure would be likely. The adjacent portions of the iron wire loop may have even acted as the cathodes, forming a type of pitting corrosion at the apex of the iron wire loop. The combination of localized or pitting corrosion and the probable occurrence of corrosion-induced stress failures (as opposed to uniform corrosion of an unstressed iron element) can probably account for the differences between the theoretical and experimental increases in corrosion rate with increasing NaCl concentration. Because of these differences, the data presented in Figure 6.4 should only be used to verify that the corrosion rate of iron increases with increasing chloride concentration, within the range of NaCl concentrations in which Tests 1, 3, and 4 were conducted. This conclusion corresponds with the experimental data presented in Table 6.11.

An additional testing objective was to determine the effect of grout seeding strength on the time to corrosion of the resistivity probes in the laboratory, in order to predict approximate failure times for the probes embedded in the field structures. These predictions of approximate field failure times were to be determined through comparison of the chloride concentrations witnessed in the post-ECE sampling period with the specific grout seeding levels investigated in the laboratory experiments. The failure times of the laboratory probes would then be extrapolated to predicted field failure times, based on the difference between the laboratory seeding level and the chloride concentration witnessed in the post-ECE sampling period.

However, comparisons between the results of the laboratory tests of probes embedded in grout are approximate at best, because of differences in the test set-up and procedure. Test 2 was different from the other three tests conducted with probes embedded in grout (Tests 5,6, and 7), because three small and three large probes were embedded in the same grout plug, and the position and depth of the probes was not controlled or measured. In contrast, probe position was controlled in Tests 5, 6, and 7, and no more than two probes were placed in each plug (one probe in each plug of Test 5, two in each of Tests 6 and 7). Therefore, comparisons between the results of Test 2 and the three other grout tests, in order to evaluate the effects of grout seeding levels, are somewhat inaccurate. Comparisons between the results of Test 5 and Tests 6 and 7 are slightly more reliable because of the similarity in the method of probe embedment, but Tests 6 and 7 evaluated two probes placed in the same grout plug, as opposed to only one in Test 5. In addition, Test 7 investigated the effects of wire interconnection. Because of dissimilarities in the test set-up between the four laboratory experiments conducted with probes embedded in grout, the effects of chloride seeding level on the time to failure of resistivity probes cannot be determined accurately. Therefore, predictions of a minimum time to failure of the resistivity probes embedded in the field structures, based on the results of laboratory tests conducted at specific chloride concentration, cannot be made. In addition, resistivity probes embedded in the field structures were installed with unseeded grout, while all of the laboratory tests were conducted in seeded grout. This difference further complicated any comparisons of field and laboratory failure times.

In conclusion, the small resistivity probes failed approximately two times faster than the large probes when the probes were embedded in grout, which is the testing medium of interest with respect to the field instrumentation. This ratio of time to failure correlates with the expected

failure ratio between the small and large probes, as determined using the theoretical relationship based on the wire diameter of the probes. Electrically connecting adjacent probes had no effect on corrosion rate, as determined through comparison of Test 6 and 7 results. Finally, increased solution strength, with respect to NaCl concentration, significantly decreased the failure times of the probes. However, the exact nature of the effect of increasing chloride concentrations on increasing the corrosion rates of the probes could not be determined through the experimental results, and could not be determined through the results of previous research. Therefore, extrapolation of the laboratory results to expected failure times for the resistivity probes embedded in the field structures at worst case chloride levels, prior to ECE, cannot be accurately made.

6.1.3 Humidity Probe Testing and Results

In order to evaluate the variability of relative humidity readings collected with the Concrete Master III humidity probe, an experiment was conducted. Two holes were drilled in a concrete beam located in the laboratory, each hole 1.58 cm in diameter and approximately 5 cm deep. The two holes were spaced approximately 10 cm apart. After cleaning the holes with compressed air, a moisture sleeve was installed in each hole until the lip abutted with the concrete surface. The sleeves were installed with their caps in place, and the caps were not removed until immediately before data collection. Conditions within each sleeve were allowed to equilibrate with the concrete substrate for 24 hours before data collection commenced.

The experiment consisted of two phases that were identical, except that the second phase occurred four months after the initial data collection period. Relative humidity and ambient temperature readings were collected from each sleeve at one minute intervals until the readings stabilized. The measured values of temperature and humidity were unimportant because the test variables of interest were the time necessary to obtain stable readings, and the difference between readings obtained from the same concrete substrate. In addition, the difference in readings collected from the same sleeve, in the same concrete substrate, between testing periods was also investigated. The temperature and relative humidity levels in the laboratory were not measured in either phase.

The results from both tests, at both humidity sleeves, indicated that stable readings of relative humidity and ambient temperature were obtained after approximately 16 minutes of

monitoring. Therefore, this time period was established as the minimum required for field data collection. The stabilized humidity readings between adjacent sleeves in the same concrete substrate were almost identical (35.6 and 37.8 in the first phase, 37.2 and 38.9 in the second phase), indicating that readings collected with the humidity probe are reliable and reproducible. In addition, similar humidity values were obtained at each sleeve in each phase. Because the specified accuracy of the probe is +/- 3% relative humidity, these results were considered satisfactory.

6.2 FRP Diffusion Testing

To evaluate the effectiveness of each of the three FRP wrap systems in sealing the concrete columns and pier caps, diffusion testing was conducted to obtain rates of water flow through the cured composite systems. The permeation of chloride ions through the FRP wrap sheets was also an issue for investigation but it was assumed that these ions would only permeate the wraps when in water, as opposed to the ions alone. This was assumed because there was not a charge imbalance at the wrap/concrete interface that would be needed to electrically draw only chloride ions through the composites.

The chosen testing method to obtain diffusion rates of water through the FRP systems was pervaporation. A schematic of this testing procedure is shown in Figure 6.5. As shown in this figure, the test apparatus consisted of a sealed water reservoir attached to a sealed glass chamber. The premise of this type of test is to force water to permeate the desired test specimen using a pressure head, or the difference in elevation between the water level in the reservoir and the diffusion interface. The water reservoir is sealed to minimize water evaporation that may be misinterpreted as diffusion. The glass chamber sitting on top of the test specimen, and the connecting tube to the water reservoir, were filled with water to maximize the pressure head applied at the diffusion interface. A steady airflow across the bottom of the test specimen was also provided so that water that permeated the specimen, and reached the other side, was removed. If water, or moisture, was allowed to accumulate on the underside of the test specimen the diffusion gradient would decrease, slowing diffusion rates.

The laboratory tests were performed on circular composite sections cut from the collected field samples, each measuring approximately 10 cm in diameter. The section of composite was caulked to an O-ring of the glass chamber located above the specimen, to ensure an airtight seal

at the upper diffusion interface. This can be seen in Figure 6.5. After letting the caulk dry for 24 hours, the two glass chambers were placed above and below the specimen and clamped tightly in place. The chamber on top of the composite specimen was filled with water making sure to remove all air bubbles while filling. During the filling process, the testing apparatus was checked for leaks, especially at the diffusion interface and around the O-rings. The location of leaks required that the test set-up be disassembled and re-started until an air and watertight seal was achieved. The tube connecting the upper glass chamber to the water reservoir was inserted into the upper glass chamber and filled with water, while again checking for leaks and removing all air bubbles. After all air bubbles were removed, the tube was connected to the filled water reservoir, which was then opened briefly and resealed so that atmospheric pressure could create continuity of flow between the reservoir and the tube. The final step was to connect the steady airflow, from a continuous compressed air feed, to the bottom glass chamber. While the flow was detectable, determined by touching the air outlet located on the opposite side of the bottom chamber, it was not excessive or audible. The completed set-up of the diffusion testing apparatus is shown in Figures 6.6 and 6.7.

To calculate approximate diffusion rates, a millimeter rule was taped to the side of the water reservoir to measure the height of the water displaced, by diffusion through the specimens over time. Because the cross-sectional area of the reservoir was known, the volume of water that permeated the composite specimen during a set time period was used to establish diffusion rates.

The first system to be tested was the MBrace epoxy. Only the epoxy was tested because it provided an upper bound diffusion rate for the complete FRP system, including the FRP sheet, because diffusion through the solid carbon fibers was assumed to be approximately zero. Wicking of water along the carbon fiber and epoxy interface was not a concern because of the material properties of the carbon fibers, and the diffusion of water into a carbon fiber/epoxy composite has been shown to occur in the epoxy matrix [55]. After completion of the epoxy test, a cured specimen of the GFRP wrap was tested. The final diffusion test was conducted on a cured sample of the AMOCO CFRP. This test warranted further diffusion tests of different AMOCO samples, as will be discussed in the next section.

While experiments were in progress, daily monitoring included recording the height of the water in the reservoir, checking for leaks at the wrap interface and at the tube joints, and evaluating the extent of noticeable evaporation within the reservoir. Tests were either stopped

once an accurate diffusion rate had been determined, or after three months of continuous testing without measurable flow through the specimen. After that time period without any detectable diffusion, it was determined that the specimen should be considered impermeable with respect to this project.

6.2.1 Results and Discussion

The results of all conducted diffusion tests have been included in Table 6.12. The test conducted on the MBrace epoxy specimen, with a thickness of 430 microns, lasted 87 days and did not result in any noticeable diffusion through the specimen. Although the water level in the reservoir decreased from an initial height of 78 mm to 75 mm, this can be attributed to noticeable evaporation on the inside of the reservoir. A correlation between the amount of moisture evaporated on the inside of the reservoir, and the declining water level, was easily distinguishable during periodic checks of the test apparatus. As the water level slowly declined, the number and size of water droplets on the inside of the reservoir increased noticeably. Periodic checks of the underside of the test specimen for water droplets, or moisture accumulation, revealed none, even at the end of the testing period. After the test was stopped, the underside of the specimen was checked for dampness by touch, and by placing the specimen on a dry paper towel. The provided air flow across the underside of the test specimens would have removed water droplets or slight moisture accumulation resulting from diffusion through the specimen, but the specimens were checked from dampness regardless. Neither check revealed any indication of water having reached the underside of the test specimen. Therefore, although some permeation into the epoxy may have occurred, it would have been a minimal amount of water, and diffusion resulting in breakthrough on the other side of the specimen was not observed.

Although it appeared as though the amount of water displaced in the reservoir, 3 mm in height, could be accounted for as evaporation inside the reservoir, a “worst case” diffusion rate was determined assuming that this volume diffused into or through the MBrace epoxy specimen. This corresponded to a diffusion rate of 0.02 mm/day, calculated using the following equation:

$$DiffusionRate \left| \frac{\left(\frac{V_w}{A_s} \right)}{t} \right. \tag{20}$$

where V_w, or the volume of displaced water, was calculated from the 3 mm drop in water elevation in a 7.5 cm diameter reservoir, A_s was the specimen surface area, or 8110 mm^2, and t was the 87 day testing period. However, the actual diffusion rate of water into the MBrace epoxy was assumed to be less than this value because at least a portion of the displaced volume could be accounted for as evaporation within the reservoir, and not diffusion into or through the specimen. Therefore, this value is presented as an upper bound for the diffusion rate of the MBrace epoxy.

A diffusion test was conducted on a GFRP wrap specimen, even though the specimen was also fabricated with the MBrace epoxy. Concerns about the possibility of water 'wicking' along the individual glass fibers and through the test specimen warranted the diffusion test [48]. The 'wicking' effect was not applicable for carbon fibers, and thus the MBrace CFRP wrap, because of material property differences. Therefore, this concern was strictly applicable for the GFRP specimens.

The results of the GFRP diffusion test were very similar to those collected during the MBrace epoxy test. The GFRP specimen had a thickness of 640 microns, or approximately 1½ times the thickness of the epoxy specimen. The GFRP test lasted 81 days and did not result in any noticeable diffusion through the specimen. The water level in the reservoir decreased from 75 mm to 74 mm, but water evaporation within the reservoir was observed, although not to the extent of the MBrace epoxy test, even though both tests were conducted for approximately the same duration. Periodic checks of the specimen underside revealed that no moisture had accumulated and water droplets were not observed in the bottom of the lower glass chamber. After the test was stopped, the specimen was checked for moisture on the specimen underside, again using touch and a dry paper towel, but no indication of diffusion breakthrough was observed. As previously stated, the air flow across the specimen underside would have removed any moisture accumulation, but the test specimen was checked to ensure that result.

The difference in the amount of evaporation witnessed between the MBrace epoxy and GFRP diffusion tests was probably due to conditions within the water reservoir. The amount of suspended evaporation was dependent on the quantity of organics, or particulates, located on the upper surface of the reservoir on which water could adhere. In the first diffusion test, or the MBrace epoxy test, a number of large water droplets were witnessed suspended on the upper surface of the reservoir. After that test was completed, the reservoir was rinsed and the GFRP

test was initiated. Therefore, the material on the upper surface of the reservoir, such as dust, grease, organics, etc., to which water evaporation likely clung during the MBrace epoxy tests was probably removed during the cleaning process. Because less material was present on the upper surfaces of the reservoir during the GFRP test, the amount of noticeable evaporation was much less than in the MBrace epoxy test. Therefore, water that had evaporated during the GFRP test would have trickled back down the sides of the upper surfaces of the reservoir, and back into the standing volume of water. The actual amount of water evaporation during the testing period was probably the same during both the MBrace epoxy and GFRP diffusion tests, but the amount of visible, suspended evaporation was different.

Similar to the MBrace epoxy test, it appeared as through the amount of water displaced in the reservoir, 1 mm in height, could be accounted for as evaporation inside the reservoir. However, by assuming that this volume diffused into or through the GFRP specimen a "worst case" diffusion rate was determined. This assumption corresponded to a diffusion rate of 0.007 mm/day, calculated with Equation (20), from the 1 mm drop in the water elevation of a 7.5 cm diameter reservoir, through a 8110 mm^2 specimen, over the 81 day testing period. However, the actual diffusion rate of water into the GFRP specimen was assumed to be less than this value because at least a portion of the displaced volume, if not all, could be accounted for by the droplets within the reservoir, and not diffusion into or through the specimen. Therefore, this value is presented as an upper bound for the diffusion rate of the GFRP wrap.

A specimen of the MBrace CFRP wrap was not tested for diffusion rates in light of the GFRP and MBrace epoxy test results. This decision was made because the diffusion rate through a carbon fiber should be essentially zero, indicating that the diffusion through an MBrace CFRP specimen would take at least as long as the epoxy specimen alone. The rate of diffusion into the MBrace CFRP was assumed to be very similar to the diffusion rate of the GFRP wrap because it was also fabricated with the MBrace epoxy.

Diffusion tests of the AMOCO CFRP wrap produced different results than those discussed from the previous two tests. The initial test of the AMOCO wrap, using a specimen with a thickness of 920 microns, was not completed because of problems encountered during test set-up. After adhering the O-ring from the upper glass chamber to the AMOCO wrap specimen, on the smoothed surface, the specimen was clamped between the two glass chambers. While filling the upper glass chamber with water, leakage through the composite specimen and into the

lower glass chamber was observed., Inspection revealed that seams, or cracks, in the wrap specimen were the source of the water leakage. Slight openings in the fiber matrix, between carbon fibers where epoxy resin had not settled, allowed water to drip through the wrap specimen and into the lower glass chamber. Multiple seams were visible when the wrap specimen was held to a light source. The length and width of the seams varied, although each was shorter than 2 cm, and no wider than approximately 0.1 mm. The seams, or cracks, were also observable on the other AMOCO laboratory specimens that were created for diffusion testing. Because of the existence of the seams, diffusion rates could not be measured for the AMOCO wrap specimens with the pervaporation testing apparatus. Therefore, the diffusion test was not conducted.

The source of the seams in the AMOCO wrap specimens were initially attributed to the sample fabrication process, and the possibility that the use of mold release on Plexiglas may have adversely affected the permeation of resin into the fiber matrix. Therefore, smaller samples of cured AMOCO wrap were cut from peel test strips that had been removed during the bond strength experiments. These strips were applied to a concrete substrate, removing concerns about the use of mold release on Plexiglas to fabricate specimens. One peel strip was cut into five diffusion samples, each approximately 2.54 cm wide and 2.54 cm long. Because the specimens were too small to place in the pervaporation apparatus, each was caulked onto a sample of the MBrace epoxy with a square hole cut in the middle of it. MBrace epoxy was selected because previous tests had indicated that it was relatively impermeable. This testing set-up is illustrated in Figure 6.8. The MBrace sample, with the AMOCO peel strip caulked behind it and exposed in the middle, was then placed in the pervaporation apparatus following the procedure previously discussed. The surface area of each AMOCO peel specimen that was exposed for diffusion, removing the dimensions that were needed to caulk the sample behind the MBrace specimen, has been included in Table 6.12. The tests of the AMOCO peel samples were each conducted for ten minutes, and the change in elevation in the reservoir was recorded. A testing period of ten minutes was selected because diffusion through the seams in the wrap occurred immediately, and thus if diffusion was not observed after ten minutes, that wrap section was not considered to possess seams or cracks in the resin. Although diffusion may have potentially occurred through the resin matrix, had the test duration approached that used for the other FRP systems or approximately 90 days, the diffusion test was not continued. This was decided because of the

differences in dimensions and preparation between the AMOCO CFRP peel strips, and the MBrace epoxy and GFRP test specimens that were previously tested. The segments of the peel strips were only tested in the diffusion apparatus to evaluate the existence of seams in the AMOCO CFRP wrap when applied to a concrete substrate, to investigate the specific effects of using a Plexiglas substrate in specimen fabrication with respect to that system. Once it was determined that seams could also exist in the AMOCO CFRP wrap when applied to concrete, the tests were terminated.

As evident in Table 6.12, diffusion was witnessed through one of the five specimens in the ten minute testing period. After testing was completed, the sample that did allow water to pass through the wrap was checked visually for seams, by holding the specimen in front of a light source, and one seam was found in the middle of the specimen that was approximately 1 cm long. The diffusion rate for this specimen was calculated at 9907 mm/day, using Equation (20), from a 7 mm drop in the water elevation of a 7.5 cm diameter reservoir, through a 450 mm^2 specimen, over the ten minute testing period. This rate was not indicative of diffusion through the wrap sheet itself, but through the system as applied to a concrete substrate. Diffusion rates for the other four peel specimens were considered approximately zero.

6.2.2 Summary

The results of the diffusion tests indicate that the MBrace epoxy and GFRP wrap systems can be considered impermeable for the purposes of this five-year investigation. Although a rate of diffusion was presented for the MBrace epoxy and GFRP systems, 0.02 mm/day and 0.0007 mm/day, respectively, these rates were clearly upper bounds rates, and much of the displaced water could be accounted for as evaporation that condensed as droplets on the reservoir. It was assumed that the amount of diffusion into each specimen type during the specified test duration was insignificant, and thus each type of system was essentially impermeable. Although the MBrace CFRP wrap was not tested, the system as applied to the field structures can also be considered impermeable because measurable diffusion through the MBrace epoxy was not witnessed during the laboratory testing period. As previously discussed, the addition of carbon fibers to the MBrace epoxy matrix was assumed to slow the diffusion rates because diffusion through the carbon fibers should be zero. Diffusion in a CFRP composite has been shown to occur through cracks and voids in the epoxy matrix, and not through the carbon fibers [55]. In

addition, the results of the GFRP wrap test support the assumption that the combination of MBrace epoxy and carbon fibers would produce a relatively impermeable surface sealant system, because measurable diffusion into or through the GFRP specimen was not witnessed during the test.

These conclusions of field impermeability are reasonable because the wrap specimens tested in the laboratory were placed in an environment where water was continuously ponded on the surface and a driving force, in the form of a pressure head, was provided to encourage diffusion. Because measurable diffusion did not occur within three months in this type of laboratory environment, diffusion rates through the field FRP systems can be considered negligible. Water, or moisture, that is present on the wrapped columns or pier caps would probably not be present for three months continuously, and there will be no driving force pushing the water into and through the wraps. The field wrap systems also contain additional components that were not included on the laboratory specimens that would probably decrease the diffusion rates even further, as discussed in Chapter 3.

In addition, it can be assumed from these results that the diffusion of water out of the wrapped structures, from inside the concrete, can also be considered negligible. Water present within the structures at the time of wrap application, or water that enters the structures, potentially entering the columns through the ground or from the pier caps above, will be retained.

Determining diffusion rates through the AMOCO CFRP wrap was somewhat more complex. Multiple seams were found in the AMOCO wrap specimens prepared for diffusion testing that allowed water to easily permeate the wrap. However, these specimens were created on treated Plexiglas that may have adversely affected the fabrication and curing process of the wrap. The majority of the diffusion specimens cut from a peel strip were basically impermeable, although diffusion testing of peel strip samples revealed one seam that allowed diffusion, at a rate of 9907 mm/day. The peel strip was applied to a primed concrete substrate, like the field FRP systems, but the seam may be a byproduct of damage that occurred during the peel testing procedure. Therefore, it is difficult to draw a precise conclusion on the diffusion properties of the AMOCO CFRP system. While the existence of seams in the field systems is likely, the UV paint coat applied over top of the wrap system could potentially cover them. The diffusion properties of the UV paint coat were not evaluated in the laboratory.

In conclusion, the AMOCO CFRP wrap cannot be considered impermeable because of the existence of seams or cracks in the cured wrap sheets. The potential for diffusion through the AMOCO CFRP system should be considered much greater than that of the two other FRP systems, i.e. MBrace CFRP and GFRP wraps. However, diffusion through the AMOCO CFRP as applied to the field structures could potentially be minimal. This conclusion is based on the severity of the laboratory environment in encouraging diffusion, in comparison to the field environment, and the lower frequency of seams found on the peel sample which was applied to a primed concrete substrate, as opposed to treated Plexiglas.

6.3 FRP Peel Testing

Although each of the three FRP wrap systems exhibited high initial bond strength to the field structures, as discussed in Chapter 4, it was not certain that this strength would be maintained throughout the duration of the study, especially when exposed to winter weather conditions, or freeze/thaw cycling. To periodically evaluate the bond strength between each of the FRP wrap systems and the concrete substrate, a peel test apparatus was constructed and peel tests were performed on the created laboratory specimens.

With the peel samples completed and ready for testing, a peel test apparatus similar to the fixture developed by Karbhari and Engineer, discussed in Chapter 2, was fabricated [57]. Peel testing and this particular type of apparatus were selected to evaluate bond strength because of the advantages they provide over other similar tests, such as the blister test or the pure shear test [58]. The advantages of the modified peel test used by Karbhari and Engineer are that bond strength failure proceeds at a controlled rate, and that peel force is a direct measure of the work of detachment, or the state of stress at the peel front can be considered to be independent of the amount of peeling prior to that instant [58]. A schematic of the peel test is shown in Figure 6.9. As the actuator applies tensile force to the composite strip, the strip peels from the concrete substrate. While the peeling of the strip proceeds, the linear bearing slides the entire apparatus forward, maintaining the desired peel angle and ensuring that the point of peeling remains centered underneath the actuator.

Because only nine peel specimens were created for each type of FRP wrap, and peel testing was planned at multiple time intervals throughout the duration of the project, one peel angle was selected at which to run all peel tests. By maintaining the same peel angle,

comparisons of bond strength could be drawn between the different types of FRP wraps during each testing period, and between testing periods, because the only difference would be the duration of environmental exposure on the project site. Because previous research indicated that a peel angle of 45∀induced a low bending stress in the composite strips while minimizing stretching, all tests were conducted with the specimen plate on the apparatus inclined at 45∀[59]. Actuator speed was also set for all three tests at 5 mm/min, as used by Karbhari and Engineer [57]. Prior to peel testing, slits were cut in the epoxy between adjacent peel strips on the specimen blocks. This was done to avoid damaging multiple strips during the testing process as the epoxy and wrap strip were peeled from the surface of the concrete substrate. A specimen block in the testing apparatus is shown in Figure 6.10. The slits are visible in this figure.

Initial peel testing of the three FRP wrap types was conducted in mid-March 1999, approximately six months after the wraps were installed on the field structures. The initial series of peel tests were the only experiments conducted at the time of this report. Cross-head position and applied load were recorded during each test. These values were used to approximate the load necessary to peel the wrap from the concrete substrate. The most important aspect of each test that was monitored was the type of failure witnessed. Failure could potentially be observed within the concrete substrate, at the wrap/concrete interface, or in the composite strip. Determining the type of failure that occurred during each test permitted a qualitative analysis of each FRP wrap system, with respect to bond strength. In addition, the failure load required to peel the strips from the concrete substrate was an important variable to monitor, to evaluate the effects of environmental exposure on the composite systems. Weathering of the specimens may result in deleterious effects on the bond of the peel strips and on the concrete strength, due to the impermeability of the applied wrap strips, resulting in lower peel loads.

6.3.1 Results and Discussion

The first system to be tested with the peel apparatus was the AMOCO CFRP wrap. The results of these tests are graphed in Figure 6.11. Two tests were conducted on the AMOCO CFRP wrap because this was the initial series of peel tests, and the results of only one test could not give an indication of repeatability. Therefore, two tests were run to obtain baseline values. The graphs of the peel test results consist of a series of peaks and valleys, as evident in Figure 6.11. This was similar for all conducted peel tests. A peak represented the load that initiated

peeling of the strip, and the subsequent valley corresponded to the situation when the peel apparatus slid forward and the load frame picked up the slack in the composite strip. Therefore, load dropped significantly while cross head position increased. As the cross-head position increased, and the strip was put back in tension, load increased accordingly. A lack of sufficient travel on the linear bearing also prompted each peel test to be stopped during the testing period, at which point the specimen was advanced on the testing apparatus, so testing could continue. As previously discussed, the peel test provides a direct measure of the work of detachment. Therefore, stopping the experiments during the middle of peeling did not affect the results of the tests because the state of stress at the peel front can be considered independent of the amount of peeling that had taken place previously. Adjusting the concrete substrate so that testing could continue would not affect the load required to reinitiate peeling over the remainder of the wrap specimen. The load and position where this adjustment was made have been identified for each test, in the peel test result graphs. The recording of load and cross-head position was re-initiated only after the slack had been removed in the peel strip, and the loading rate used was the same as for the initial segment of each peel test, or 5 mm/min. The linear bearing has since been replaced with one of sufficient travel.

The average peeling force for the AMOCO CFRP system was approximately 40 N, as determined through analysis of Figure 6.11. The first peel test, AMOCO 1, attained a peak peeling load of approximately 185 N as the test began, and peeling load steadily declined after that point. The initial peak can be attributed to the rigidity of the cured peel strip on the concrete block. The peak load occurred as the grips of the testing machine began to apply tension on the strip. Because the strip was not flexible, a large peeling force was required to initiate peeling at the lip of the concrete substrate, where epoxy resin had accumulated around and over top of the strip. After separating the strip from the concrete substrate at the lip, peeling proceeded at a lower peel force. This force averaged approximately 40 N, although it reached as high as 60N after attaining the initial peak load, and as low as 30 N near the end of the peel strip.

The results of the second peel test, AMOCO 2, have also been included in Figure 6.11. This test produced results that were very similar to those observed in AMOCO 1, aside from the peak load that was observed at the start of AMOCO 1. Because an excess of epoxy resin at the lip of the concrete block was not present on and around the peel strip for AMOCO 2, peeling proceeded at a relatively steady rate from start to finish and a high initial load was not

required to start peeling of the strip. Similar to AMOCO 1, the average peeling load was approximately 40 N in AMOCO 2, but varied from 60 N at the start of the test, to 30 N at the end.

The results of the two tests were very similar graphically, as well as visually. Failure occurred at the bond interface between the composite strip and the concrete substrate during both tests, in each peeling increment. Separation of each peel strip from the concrete block did not leave any concrete on the backside of the peel strips, or composite material on the concrete blocks.

Results of the MBrace CFRP peel tests are included in Figure 6.12. Similar to the AMOCO CFRP, two tests were conducted to obtain baseline values. Although the graphical results of these two tests do not correlate as well as the results of the AMOCO peel tests, the difference was due to the concrete substrate and not the composite strips. Bond failure occurred in the concrete during both peel tests, at each peeling increment. This can be seen in Figure 6.13, where the composite strip had completely separated from the concrete, removing a significant amount of the concrete surface with it. Therefore, peel force was dependent on the tensile strength of the concrete, and not the bond or component strength of the MBrace CFRP wrap system. This type of failure can be considered maximum peeling strength, because the system bond to the concrete performed as effectively as possible. The average peeling load for the MBrace CFRP strips was approximately 80N, as determined through comparison of tests MBrace 1 and 2 shown in Figure 6.12. The peeling strength varied considerably, from a maximum of 150 N observed during MBrace 1, to a minimum of approximately 45 N observed during MBrace 2. Differences between peeling loads at each peeling increment and between tests can be attributed to the inhomogenous nature of concrete, and concrete tensile strength.

The final system to be tested was the GFRP wrap, and results from this test are included in Figure 6.14. Although results from only one peel test have been included in this figure, three tests of the GFRP system were performed. However, the first two peel tests conducted on the GFRP wrap were considered invalid because of problems encountered during testing that were related to specimen preparation. Because of the nature of the fiber mat, the process of cutting 2.5 cm wide strips resulted in the fraying of composite fibers at the edges of the strips. In addition, an excess of the MBrace epoxy was found at the lip of the concrete specimen block. The interaction of these two fabrication errors produced invalid peel test results. A large peel force

was needed to initially separate each strip from lip of the concrete block, where excess epoxy had accumulated. After the peel strip separated from the concrete surface, damaged fibers at the edges of the strip initiated failure through the epoxy matrix. Peeling proceeded through the damaged peel strip, and not at the bond interface as desired. Therefore, the results from these tests are not included.

As evident in Figure 6.14, peeling loads were higher in the GRFP test than in the MBrace CFRP test. The average peeling load for the GFRP was approximately 130 N, in comparison to approximately 80 N for the MBrace CFRP. However, these two composite systems were applied to the concrete identically, except the wrap sheet was different. Observations of the testing process can serve to explain the differences.

Although some excess epoxy was present at the lip of the concrete block, the strip was effectively peeled up through the epoxy, without damaging the edge fibers. The elevated peeling loads, of approximately 160N, at a cross-head position of between 1-2 cm corresponded to the strip being initially separated from the concrete substrate, through the excess of epoxy at the edge of the block. Failure in the concrete substrate was observed, and the test proceeded very similarly to the MBrace CFRP samples. However, the peeling force for the GFRP system reached a peak value of approximately 200 N, at a cross-head position of 2 cm, and the mode of failure that was observed changed drastically. Peeling failure continued through the concrete substrate, but it also initiated through the epoxy matrix and the transverse fibers of the peel strip (with respect to the length of the concrete block). This continued for the reminder of the peel test until the strip was completely removed from the concrete substrate. Higher peeling forces than those witnessed during the MBrace CFRP test were observed in the GFRP test because the peel force included two components: the tensile strength of the concrete and an added strength component from the epoxy matrix and the transverse fibers. This type of failure was initiated by defects incurred in the specimen preparation procedure.

An illustration of the type of failure that was observed in the GFRP peel strip is included in Figure 6.15. As shown in Figure 6.15, the longitudinal fibers of the GFRP peel strip, for which results were presented in Figure 6.14, were oriented slightly askew, or at an angle, to the length of the concrete substrate. As peeling of the GFRP wrap strip initiated at the lip of the concrete substrate and proceeded in the concrete layer, a defect at the edge of the peel strip, potentially from a damaged or frayed fiber, caused peeling to begin in the epoxy matrix. As the actuator

continued to apply tensile force on the peel strip, failure proceeded diagonally through the concrete, alongside an angled longitudinal fiber in the peel strip. With respect the specimen orientation presented in Figure 6.15, peeling failure occurred in the concrete substrate to the left of the indicated "Line of Failure", and through the transverse fibers and epoxy matrix on the right of the "Line of Failure". The portion of the peel strip located to the right of the "Line of Failure" remained intact on the concrete substrate because these fibers were not engaged by the grips of the load frame. Failure of the slightly angled longitudinal fiber, outside the "Line of Failure", would have allowed peeling to again proceed along the edge of the composite strip, and again in the concrete substrate. However, a much higher load would have been required to fail this longitudinal fiber than that required for shear failure of the transverse fibers and epoxy matrix of the peel strip. Therefore, failure proceeded diagonally through the GFRP peel strip for the remainder of the peel test, and not at the edge of the peel strip as desired. Had the longitudinal fibers of the GFRP peel strip been oriented parallel to the length of the concrete substrate, and the transverse fibers oriented perfectly perpendicular, failure would have occurred in the concrete as witnessed in the MBrace CFRP test, regardless of the presence of damaged edge fibers. Therefore, the peel should not be considered representative of the actual peeling force required of the GFRP system, because of defects incurred in the specimen preparation procedure. The peeling forces and failure behavior of the GFRP wrap system should have been very similar to those witnessed in the MBrace CFRP system, because both systems were applied identically (using the MBrace primer/putty/epoxy application technique). The only difference between the MBrace CFRP and GFRP systems was the type of composite fibers present in the peel strips.

The final method used to analyze the peel test results was to integrate the area underneath each of the peel force graphs, in order to assess bond energy. This was performed for the GFRP test, the MBrace 1 test, and both AMOCO tests, as shown in Table 6.13. The peel force curves were integrated between 2-5 cm of cross-head position travel, so that all four integrations would be over comparable distances. The first 2 cm of cross-head travel were not integrated to avoid including the large peel forces required to initiate peeling, in some peel specimens, at the lip of the concrete block where epoxy had accumulated. The MBrace 2 test was not included in the bond energy tabulation because the test was stopped after the cross-head had traveled slightly over 4 cm, and approximately half of the composite strip was removed. This was decided

because the type of failure witnessed in the MBrace 2 test, i.e. tensile failure in the concrete substrate, matched that observed in the MBrace 1 test, and the peeling loads were comparable although slightly lower.

As evident in Table 6.13, the GFRP peel strip released the highest bond energy, at 3.24 Nm, which can be attributed to the type of failure witnessed during the experiment, through the concrete substrate, transverse glass fibers, and the epoxy. Therefore, this value is not truly indicative of the bond strength of the GFRP wrap system, but instead only correlates to the type of failure that was observed because of a defective test specimen. The MBrace CFRP sample, MBrace 1, reported the next highest bond energy, at 2.62 Nm, over the 2-5cm integration range. A correctly prepared GFRP peel specimen would likely have reported a similar bond strength to that of MBrace 1, or 2.62 Nm instead of 3.24 Nm, over the specified range of integration. Integrating the MBrace 1 and MBrace 2 tests over only the 2-4 cm range, as shown in Figure 6.12, indicated that the MBrace 1 peel sample produced a bond energy of 1.82 Nm while the MBrace 2 specimen reported a bond energy of 1.2 Nm. The difference between the two values can be attributed to differences in the tensile strength of the concrete substrates, because the failure modes for each strip were identical, and failure was observed in the concrete layer. Finally, the AMOCO peel samples exhibited the lowest bond energy of the three tested systems, at 1.02 Nm and 0.77 Nm, or an average of 0.9 Nm, integrated over the 2-5 cm range of cross-head position.

In conclusion, the initial series of peel tests revealed that the MBrace CFRP and GFRP were the most effective sealing systems, with respect to bond strength with the concrete substrate. The GFRP wrap system reported the highest bond energy, but a definitive peel test was not obtained due to problems incurred during specimen fabrication. Failure was controlled by concrete properties for the MBrace CFRP, and thus maximum possible bond strength was achieved. This type of failure, i.e. in the concrete substrate, can also be assumed for the GFRP wrap system. Even though the GFRP wrap possessed transverse and longitudinal fibers and the MBrace CFRP wrap consisted of only longitudinal fibers, because failure occurred in the concrete substrate for the MBrace CFRP wrap, the addition of transverse fibers should not have affected the peeling strength of the GFRP wrap. The peeling strength of both systems should have instead been governed by the tensile strength of the concrete substrate, because both used the MBrace epoxy and putty layer application technique, and not the strength or nature of the

composite wrap applied. The laboratory results correlated well with the pull tests performed in the field on the MBrace CFRP and GFRP wrap systems, discussed in Chapter 4, where failure occurred in either the testing apparatus or the concrete for both wrap types, but not in the composite system. The AMOCO CFRP wrap did not perform as well, and bond failure was witnessed at the interface between the composite peel strip and the concrete surface. The peeling load that caused bond failure in the AMOCO CFRP peel samples, and the bond energy of the system, were both lower than the values witnessed for the other two systems. These preliminary results indicate that composite wraps applied with the AMOCO system do not adhere to the concrete as effectively as those applied with the MBrace system. Further peel testing to evaluate the environmental effects on initial bond strength will be run as desired and as the remaining number of peel specimen dictates.

6.4 Summary of Laboratory Results

Calibration of the embeddable half-cells and the relative humidity probe illustrated that both could be considered relatively accurate and reliable for corrosion monitoring purposes in the field structures.

Laboratory experiments of the resistivity probes demonstrated that the small resistivity probes can be expected to report failure in half the time of the large probes, as theoretically predicted, when embedded in grout. The time to failure of the resistivity probes was not affected by wire interconnection of probes embedded in the same grout plug. However, the effects of chloride concentration on the time to failure of the resistivity probes, in either grout or solution, could not be accurately quantified through the results of the laboratory study.

Diffusion testing of the three FRP wrap systems indicated that the MBrace epoxy and GFRP wraps should be considered relatively impermeable, although upper bound diffusion rates were presented for each system (0.02 mm/day and 0.0007 mm/day for the MBrace epoxy and GFRP systems, respectively). From these results, the MBrace CFRP wrap was also considered essentially impermeable, although it was not tested. The permeation of water through cracks, or seams, in the AMOCO CFRP wrap was observed during diffusion testing performed with specimens prepared on both treated Plexiglas and concrete, indicating the AMOCO system cannot be considered impermeable. The rate of diffusion through these seams was computed at 9907 mm/day.

Finally, the initial series of peel tests indicated that MBrace CFRP and GFRP wraps exhibited a higher peeling load and bond energy than the AMOCO CFRP, as well as a more desirable mode of failure. Peeling failure occurred in the concrete substrate for both the GFRP and MBrace CFRP wraps, applied with the MBrace system of a putty layer and the MBrace epoxy, indicating the maximum possible bond strength was attained. Peeling failure occurred at the composite/concrete interface in the AMOCO CFRP system.

7. Field Instrumentation Data and Preliminary Results

The preliminary data collected from the embedded corrosion monitoring instrumentation installed in the field structures is presented in this chapter. The results of laboratory experiments, and chloride concentrations and half-cell potentials collected in the pre- and post-ECE corrosion condition surveys, are used to evaluate and analyze the preliminary sensor data.

7.1 Preliminary Sensor Readings

The data collected through August 1999 with the embedded Ag/AgCl half-cells is presented in Tables 7.1-7.5. The potentials collected with the installed instruments are identified as Sensor readings, and they are listed alongside half-cell potentials collected in October 1997 by Mn/DOT, prior to the ECE treatment period, and the Vector half-cells where applicable, that were collected in November 1998 following the ECE treatment period. Half-cell potentials from the Mn/DOT site survey completed in October 1997 were determined approximately through comparison of the sensor locations and the contour plots of half-cell potential that were presented in Chapter 4. A similar approximation was made to determine the Vector half-cell potentials listed in the field result tables. Values more negative than –0.254 V, indicating active corrosion potential, are identified with bold font.

The preliminary results collected from the embedded resistivity probes are listed in Tables 7.6-7.10. Probe failure was identified as a resistance measurement greater than 50 Ohms. Probes considered failed are identified with a bolded Y in the Tables 7.6-7.10 and the data box for that probe has been shaded gray. All of the resistivity probes that were installed in the field structures were embedded at the depth of the reinforcing steel. Although the exact depth of embedment varied from sensor location to location, each probe was installed in the depth range of 5-7.5 cm, or within the third or fourth depth ranges with respect to chloride sampling (3.75-6.25 cm or 6.25-8.75 cm, respectively). The typical depth of the reinforcing steel was approximately 6.25 cm, but the exact depth of embedment for each sensor varied, and was not recorded.

Readings from the embedded resistivity probes and Ag/AgCl half-cells were collected once every 1.5 months from early April 1999 to mid-August 1999. More specifically, data was collected in mid-April 1999, late-May 1999, early July 1999, and mid-August 1999.

Preliminary relative humidity readings collected with the relative humidity probe from the installed moisture sleeves are presented in Tables 7.11-7.15. The sleeves are identified by number in these tables, increasing from the bottom to the top of each column. Prior to data collection from the humidity sleeves with the relative humidity probe, location 40A-1 was randomly selected to assess the effects of external relative humidity on the readings of concrete relative humidity. External relative humidity was measured with a sling psychrometer and concrete relative humidity was measured in the embedded sleeve, with the relative humidity probe of the Concrete Master III. At an exterior relative humidity of 84%, the humidity probe measured a concrete relative humidity of 75%. The external relative humidity was high because the reading was obtained in the early morning hours, after an overnight storm. Later on that afternoon after temperatures had elevated, and the air had become considerably less humid, readings were collected again. At an external R.H. of 48%, the concrete humidity decreased to 65%, indicating that concrete humidity decreased as exterior humidity did. This experiment was repeated the following day, and at an external R.H. of 60% in the morning hours, the concrete indicated an R.H. of 73%. Later on in the afternoon, at an external R.H. of 48%, the concrete R.H. was 71%. Therefore, at the same external R.H. (48%), the measured concrete R.H. varied 6% from one day to the next. While it appears that external R.H. may indeed affect the collected measurements slightly, the inherent variability of the probe (+/- 3%) made exact quantification of the effects difficult. Ultimately it is recommended that the external relative humidity is determined whenever readings of concrete R.H. are collected, so that the effects of external R.H. can be considered if anomalies, in terms of concrete R.H., are witnessed.

Following the relative humidity calibration at location 40A-1, readings of relative humidity were collected once in July 1999, and a few selected locations were randomly checked again in August 1999 to determine the variability of the collected readings from month to month. At location 37B-6, the sleeve was unexplainably loose in the instrument hole, and so the collected reading is accompanied with an asterisk, indicating the low level of measured relative humidity was probably due to the poor embedment of the sleeve.

7.1.1 Embedded Ag/AgCl Half-Cell and Resistivity Probe Readings in ECE-Treated Structures

On Pier 34 North, which was treated with ECE, the majority of the initial half-cell readings collected following the ECE procedure with the embedded half-cells indicated a high level of passivity in the structure. Of the twelve installed half-cell locations, eleven indicated a 90% probability of no corrosive activity by reporting a half-cell potential more positive than –0.104 V, 14 months after completion of the ECE process in June 1998, as shown in Table 7.1. The remaining sensor location, at 34C-2, indicated uncertain corrosive potential.

Analyzing the preliminary data on Pier 34 North indicates that half-cell potentials have remained stable in the four months of monitoring, although each has decreased from the potentials collected by Vector in November 1998. This decrease in potential was expected because of the nature of the ECE process and the high levels of passivity in the months immediately following ECE, as discussed in Chapter 2. All of the Vector half-cell potentials were collected only five months after completion of the ECE process, and the potential of the structure was expected to slowly become more negative with time, while still remaining relatively passive. The Vector half-cell potentials may have also been affected by the presence of the concrete sealers on the concrete surface, as discussed in Chapter 4. Slight fluctuations in potential were observed between data collection periods, however this can probably be attributed to the natural variability of the instrument and slight changes due to concrete and exterior temperature. None of the twelve instrumentation locations reported a pre-ECE potential in the active corrosion range, although almost 75% indicated uncertain potential. Post-ECE potentials have remained relatively passive, but five locations indicate potentials very similar to the pre-ECE levels (34A-1, 34B-1, 34B-2, 34C-2, and PIER 34N-W2). However, four of these locations also reported very passive potentials prior to treatment. The remaining location, 34C-2, has indicated uncertain potential before and after treatment.

As evident in Table 7.6, three small resistivity probes embedded in Pier 34 North failed, even though this structure was treated with ECE. One small probe at location 34C-1 reported failure in July 1999, approximately seven months after installation. One small probe at locations 34A-3 and 34C-3 each failed during the subsequent month, in August 1999. All three of these probes had reported resistance values of less than 1 Ohm in each data collection period prior to

that in which failure readings were witnessed. Therefore, the probe at location 34C-1 failed between 170-215 days after installation, and the probes at locations 34A-3 and 34C-3 failed between 215-250 days after installation. While the half-cell potentials collected at these locations by the embedded Ag/AgCl electrodes indicated that the reinforcing steel was passive, chloride concentrations collected in the post-ECE sampling period indicated corrosive potential at all three of these locations, as shown in Chapter 4 and Appendix A. More specifically, at location 34A-3, chloride concentrations still exceeded 2000 ppm in the first three sample depths following ECE. At location 34C-1, a chloride content in excess of 2000 ppm was reported in the first sample depth and at location 34C-3, chloride concentrations exceeded the corrosion threshold in the first four sample depths, following ECE treatment.

Interestingly, of the nine instrumented locations in the columns of Pier 34 North, each location that reported at least one post-ECE chloride concentration in excess of 2000 ppm had reported a resistivity probe failure through the August 1999 data collection period. However, locations on the pier cap that reported post-ECE chloride concentrations in excess of 2000 ppm had not reported any resistivity probe failures through August 1999.

As shown in Table 7.3, the effectiveness of the ECE treatment was not as evident on Pier 37 North in terms of increased passivity. Of the ten instrumented locations, only five, or 50%, were more positive than –0.104 V, although one potential, at location PIER 37N-W2, was very passive and has indicated increasing passivity in each data collection period. The potential at that location was more positive than +0.3 V, 14 months after completion of the ECE process. Four of the locations, or 40%, indicated an uncertain corrosive potential, and one location, 37C-1, indicated a 90% probability of corrosive activity in each data collection period following installation of the corrosion monitoring instrumentation.

On Pier 37 North, most half-cell potentials have remained stable, although the readings at PIER 37N-W2, and 37C-1 have fluctuated considerably between data collection periods, and this variability is somewhat unexplainable. Coincidentally, these two locations reported the most passive and active readings on that pier, respectively, and location 37C-1 reported a 90% probability of corrosion following instrumentation. These results were unexpected and unexplainable in light of the high levels of passivity indicated after the half-cell potential mapping conducted by Vector in November 1998, and the pre-ECE potentials at that location which indicated uncertain corrosive potential. However, the Vector and pre-ECE potentials listed

in Table 7.3 were approximations, and column 37C had reported the largest areas of active and uncertain corrosive potential in the pre-ECE potential mapping period. Therefore, the collected readings are unexpected, but not unrealistic. Prior to ECE treatment, two locations on the pier cap of Pier 37 North, PIER 37N-W2 and PIER 37N-E1, indicated an active corrosion potential. Both of these locations were in the very large region of active potential witnessed on the pier cap of Pier 37 North, as discussed in Chapter 4. However, location PIER 37N-W2 reported the most passive potential in the months following ECE, of all of the instrumented locations in the entire study indicating effective treatment and increased passivation at that location. The potential at location PIER 37N-E1 also decreased significantly, although uncertain corrosive potential was reported in each data collection period following treatment. Similar to Pier 34 North, data collected with the embedded sensors indicated that each potential had increased significantly from that reported by Vector five months after the completion of the ECE treatment procedure. This was expected for reasons previously discussed.

On Pier 37 North, one small resistivity probe at location 37A-1 reported failure in the July 1999 data collection period, as shown in Table 7.8. Failure at this location occurred approximately seven months after embedment, or between 170-215 days after the probe was installed. The failure at this location was somewhat more unexpected in light of both the passive half-cell potentials collected with the embedded electrodes and the low post-ECE chloride concentrations reported at that location. However, as evident in Appendix A, a chloride sample collected at that location between 2.5-3.75 cm reported a chloride concentration of 1973 ppm, almost exceeding the corrosion threshold. Therefore, failure of the probe was not unreasonable.

7.1.2 Embedded Ag/AgCl Half-Cell and Resistivity Probe Readings in Untreated Structures

Half-cell potentials collected with the Ag/AgCl electrodes embedded in the untreated structures (Pier 34 South, Pier 37 South, and Pier 40 North), correlated fairly well with approximate values determined in the October 1997 site survey, and remained relatively stable between data collection periods.

As shown in Table 7.2, eleven of the twelve instrumented locations on Pier 34 South indicated a passive potential in October 1997, and one location, 34F-3, reported uncertain

corrosive potential. Fourteen months later, ten of twelve locations reported passive potentials and two indicated uncertain corrosive potential. Although many of the locations that reported passive potentials in October 1997 still reported a passive corrosion potential over a year later, most of the potentials had increased slightly. The location that reported an uncertain potential in October 1997, 34F-3, still reported an uncertain potential in August 1999, although the actual potential reading had decreased slightly. Location PIER 34S-E2 increased from a passive corrosion potential into the range of uncertain corrosion potential between the October 1997 and April 1998 data collection periods. In general, potential readings collected with the embeddable Ag/AgCl electrodes from Pier 34 South through August 1999 remained fairly stable between each data collection period, and correlated fairly well with the values collected in October 1997.

The correlation between October 1997 approximations and instrumentation data was not as evident on Pier 37 South, especially on Column 37D, as shown in Table 7.4. In October 1997, three of five locations on Pier 37 South, one on column 37D and both locations on the pier cap, indicated a passive potential, and two indicated uncertain corrosion potential, both on Column 37D. In April 1999, half-cell potentials increased dramatically at each location in Column 37D, and data collected with the embedded electrodes indicated an active corrosion potential, or greater than a 90% probability of ongoing corrosion, in each data collection period. Potentials collected with the half-cells installed on the pier cap remained passive at both locations. Because Column 37D is a control column, the large increases in potential were unexpected and unexplainable because the column was not treated or sealed in any way. Potentials collected from locations 37D-2 and 37D-3 were fairly reasonable because potentials collected in October 1997 indicated uncertain corrosive potential, and these potentials may have increased in the 18 months between the October 1997 mapping period and the first series of embedded instrument data collection in April 1999. However, location 37D-1 indicated a passive potential in October 1997 but a highly negative potential in April 1999. The potential recorded at this location was very unstable and it increased significantly, or became less negative, between each data collection period. In light of the low chloride concentrations reported at each depth at this location, as shown in Chapter 4, and the variability of the potentials collected from month to month, it is reasonable to assume that the instrument at this location may be damaged or defective. This can be assumed because the potential results collected through August 1999 do not correlate with any of the previously collected data at that location (half-cell potentials or

chloride contents), and the readings have not been stable. Potential readings at the four other locations on Pier 37 South remained relatively stable between collection periods.

In October 1997, only two of the ten instrumented locations on Pier 40 North indicated a passive corrosion potential, as shown in Table 7.5. Seven of the ten locations reported uncertain potential, and one location, 40A-3, indicated an active corrosion potential. Potentials collected with the embedded Ag/AgCl electrodes correlated fairly well with each of these October 1997 values, in each data collection period from April 1999 to August 1999. Location 40C-1 indicated a passive potential in October 1997 and still reported passivity in August 1999, although the exact potential decreased. The other location that indicated a passive pre-ECE potential, 40A-1, reported an uncertain corrosion potential in each data collection period. Similar to the October 1997 results, seven of ten instrumented locations reported an uncertain potential in August 1999. Location PIER 40N-W1 indicated an active corrosion potential in each data collection period with the embedded half-cells after reporting an uncertain potential in October 1997. Therefore, potential decreased at that location between October 1997 and April 1999. However, this decrease in potential is reasonable because, as shown in Figure 4.6, multiple depths at that location reported chloride concentrations in excess of the established corrosion threshold of 2000 ppm, in both the October 1997 and April 1999 chloride sampling periods. The location that reported an active corrosion potential in October 1997, 40A-3, reported an uncertain corrosion potential in each data collection from April 1999 to August 1999, indicating a decrease in corrosive activity. However, the listed October 1997 potential was approximated, and the sensor location at 40A-3 was on the edge of an uncertain corrosion potential region reported in October 1997, at the top of Column 40A. This can be determined upon comparison of the contour plot of October 1997 half-cell potential and the instrument location illustration for Column 40A, in Figures 4.11 and 5.12, respectively. Therefore, the potentials collected with the embedded half-cells from April 1999 to August 1999 were considered to be reasonable and the differences between the initial and embedded instrument potentials may be attributed to inaccuracies in obtaining the approximate October 1997 half-cell potential value for comparison. The embedded instrument readings correlate very well with October 1997 potentials that were collected a few feet away in every direction, into the region of uncertain corrosive potential. In general, embedded instrument readings were stable on this pier and values correlated with pre-ECE approximations as expected.

Three resistivity probe failures were observed through August 1999 on two of the three untreated structures, Pier 34 South and Pier 40 North, although two of these failures were questionable. At locations PIER 34S-W2 and PIER 40N-W2, two of the large resistivity probes reported failure in July 1999, or between 170-215 days after installation, as evident in Tables 7.7 and 7.10, respectively. However, the small probes also embedded at these two locations had not reported failure as of August 1999. Although chloride concentrations were reported in excess of 2000 ppm in multiple sample depths at both locations, in the post-ECE sampling period, the large probes should not have failed before the small probes because of the increased cross section, as verified in Chapter 6. However, the large probes were not embedded in the exact same position as the small probes at these locations, and the environments in terms of chloride concentrations in which the large and small probes were placed may have be different. Nonetheless, laboratory experiments of large probes embedded in grout that was seeded at a chloride concentration of 5500 ppm had not failed by the time of this report in August 1999, or after approximately 140 days of monitoring. Chloride concentration samples collected in April 1998, following the ECE treatment period, indicated chloride concentrations at these locations, at the depth of probe embedment, of approximately 2000 ppm. Therefore, failures of these two probes were probably initiated by defects in the iron wire loops of the probes, incurred either during manufacturing or installation, and not due solely to corrosion failure. However, each of the large probes that reported failure at locations PIER 34S-W2 and PIER 40N-W2 had not indicated failure in the data collection periods previous to July 1999. Therefore, it is also plausible that rapid corrosion failure of the probes, not initiated by a defect in the iron wire loop, occurred instead. Corrosion of the large probes could have been driven by the reinforcing steel bar that was in close proximity of the embedded probe, in some form of a corrosion cell. The small resistivity probe, embedded at essentially the same location as the large probe, may not have been included in that corrosion cell. While this may potentially explain how the large probes could have failed before the small probes, when both were placed at approximately the same location, reasons for why the small probe would not also be included in the corrosion cell are undetermined.

A small resistivity probe reported failure at location 40A-3 in July 1999, or between 170-215 days after installation. Chloride concentrations collected in the post-ECE sampling period at this location were in excess of the established corrosion threshold in the first three sample

depths, and were similar to those witnessed at the failure locations on Pier 34 North, as can be determined through data comparison in Appendix A. The resistivity probe at location 40A-3 was embedded between the third and fourth chloride sample ranges, as previously discussed. Half-cell potentials at this location collected with the embedded half-cells were in the uncertain range in each data collection period but October 1997 potentials indicated an active corrosion potential in the surrounding area, as discussed in Section 7.1.1.2. Therefore, corrosion failure of a small probe at this location was considered reasonable. Probe failures were not observed through August 1999 on Pier 37 South, despite the highly negative half-cell potentials reported at each column instrumentation location, and very high chloride concentrations at locations 37D-2 and 37D-3. Considering the probe failures at the locations of high chloride concentrations in the columns of Pier 34 North, this inactivity was unexpected.

7.1.3 Relative Humidity Probe Readings

As evident in Tables 7.11-7.15, concrete relative humidity levels appeared to depend on both the position within the site and the type of sealant system used. In general, the highest humidity level in each column was witnessed near grade level and readings fluctuated with height from the ground. Relative humidity levels in Column 37A and 40A (wrapped in MBrace CFRP), located on the north end of the bridge, were much higher on average than the other columns included in the investigation, at approximately 70% R.H. Relative humidity levels in Columns 34B and 34D were fairly different, averaging 62% and 50% respectively, even though each was wrapped with the GFRP wrap and located on the interior of a pier cap. Humidity levels averaged approximately 60% on Pier 34 North, and were as high as 70%, in Column 34A on the north end of Pier 34 but only approximately 54% in Column 34F at the south end of Pier 34. Each column was sealed with the AMOCO CFRP wrap. Two of the control columns, Columns 34D and 37D, reported similar humidity levels, at approximately 50%, although a third control column, Column 40C, indicated much higher humidity, at approximately 67%. Finally, each of the three sealed columns, 34C, 37B, and 37C, indicated an average humidity of approximately 55%, although the average was slightly higher on Column 37B.

In summary, although only a few moisture readings were obtained on each column of the study at the time of this report, preliminary results indicate that humidity is dependent on position and the type of exterior sealant used. The three columns on the northern exterior of the

site, 34A, 37A, and 40A, reported the highest humidity levels of all twelve columns in the study through August 1999. It appeared that the columns sealed with the MBrace CFRP may retain more moisture than the other two wrap systems, or concrete sealers. These initial field results partially correlate with the laboratory results presented in Chapter 6. The results of the laboratory tests of the diffusion properties of the three wrap systems indicated that both the GFRP and MBrace CFRP field systems could be considered impermeable. Water or moisture present within the columns sealed with either of these systems, either at the time of wrapping or that entered the columns through the ground or from the pier cap above following wrapping, would be trapped inside. However, relative humidity levels within the GFRP wrapped columns were not as high as in the columns wrapped with the MBrace CFRP. Therefore, more data is needed to verify this assumption because both of the columns wrapped with the MBrace CFRP were also located on the northern side of the bridge, where humidity levels appeared highest. Relative humidity appeared to vary somewhat with height from grade level, although an exact determination of the effects cannot be made at the time of this report.

8. Preliminary Conclusions and Recommendations

This chapter preliminarily addresses the main objective of this investigation. This objective was to evaluate the effectiveness of ECE, in conjunction with concrete wrapping/sealing, in reducing corrosion rates and rehabilitating structures that have experienced moderate corrosion damage. Preliminary conclusions are presented, and recommendations for future research projects applying or investigating ECE are discussed.

8.1 Effectiveness of ECE and FRP Wraps for Corrosion Mitigation

As discussed in Chapter 4, initial chloride concentrations in Pier 34 North and Pier 37 North were reduced significantly, at the selected sample locations, through ECE treatment. Average reductions in chloride concentration were approximately 50% at each sample depth in each structure, although the effectiveness varied somewhat from location to location, and depth to depth. Treatment was most effective near the concrete surface, and overall effectiveness appeared to hinge on both the pre-ECE chloride content, with locations containing high initial chloride concentrations being treated more effectively, and the likely proximity of the sample location to reinforcing steel. However, multiple locations with chloride concentrations in excess of the established threshold for corrosion, of 2000 ppm by weight of cement, at multiple sample depths were still reported in the treated structures following ECE treatment. Preliminary half-cell potential readings collected with the Ag/AgCl electrodes embedded in the two treated structures, Pier 34 North and Pier 37 North, indicated that the majority of the structures had a greater than 90% probability of corrosive inactivity in the 14 months following completion of ECE process. However, one potential, at location 37C-1 on Pier 37 North reported an active corrosion potential in each data collection period following ECE treatment, and a few locations indicated uncertain corrosion potential. Three small resistivity probes embedded in Pier 34 North, at areas of high chloride concentrations (i.e. in excess of 2000 ppm at multiple sample depths), and one small probe embedded in Pier 37 North, at an area with one relatively high post-ECE chloride concentration (1973 ppm), failed by the time of this report in August 1999. Therefore, while the majority of the treated structures can be considered passive, with respect to corrosion, the failure of embedded corrosion sensors at areas of high chloride concentrations cannot be ignored, and corrosion within the treated structures can still occur.

While the failure of some of the small resistivity probes embedded in the treated structures, Pier 34 North and Pier 37 North, is a cause for concern, precautions need to be taken when using these results to draw conclusions on the effectiveness of the ECE process in corrosion mitigation. Although the probe failures should not be ignored, the occurrence of corrosion failure in the probes, and corrosion rates obtained from their times to failure, may not correlate with the corrosion conditions at the reinforcing steel, within the treated structures.

Because the resistivity probes were embedded approximately six months after completion of the ECE treatment process, the individual probes, or more specifically the iron wire components of each probe, were not treated with ECE. The ECE process probably re-passified the steel through the generation of hydroxyl ions, as discussed in Chapter 2 and supported by the preliminary half-cell data collected from the treated structures, but the probes themselves were not treated. The resistivity probes were embedded in clean, unseeded grout, and the alkalinity of the environment surrounding the probes was probably similar to that surrounding the reinforcing steel, although pH measurements were not obtained from either environment. Laboratory experiments conducted in this investigation of a somewhat similar grout indicated that initial pH values were around 11.2, as shown in Chapter 6. The pH of uncontaminated concrete has been reported through previous research to be in the range of 13-14, although pH levels following chloride contamination and subsequent ECE treatment have not been reported [32]. Although the probes were embedded at the level of reinforcing steel, the effects of increased alkalinity and passivation in the grout used to install the probes was probably not the same as in the treated concrete, although an exact determination is difficult. Therefore, it is likely that the resistivity probes were not embedded with an identical, initial state of passivity as the treated reinforcing steel**.** The majority of the reinforcing steel reported a passive corrosion potential following ECE treatment, and may again possess the thin, oxide film that acts to protect the steel from corrosion. Because the resistivity probes consisted of much less iron that the reinforcing steel, a protective oxide film of the same nature and thickness as that present at the reinforcing steel was not likely.

In addition, the time to failure of the small resistivity probes embedded in the field structures may have been affected by the environment in which the probes were placed. Because two probes were embedded in close proximity to each other and the reinforcing steel, some form of a corrosion cell between these three components may have potentially accelerated the corrosion rates of the small probes, with respect to the laboratory predictions of time to failure. It

is possible that the largest component of the cell, the reinforcing steel bar, may have driven the corrosion of the small resistivity probes.

In summary, corrosion failure of probes that were installed in areas of high chloride concentrations would be more likely to occur than corrosion of the reinforcing steel, because of the lower degrees of passivity that were probably present in the probes**.** The conditions in which the probes were embedded, and the conditions of the probes themselves, can be assumed to be less ideal than at the reinforcing steel level, due to the effects of ECE treatment. Therefore, the corrosion failure of several resistivity probes in the ECE treated structures indicates that corrosion can potentially reoccur once chloride ions migrate back to the reinforcing steel level, decreasing the concrete alkalinity and destroying the passivity of the reinforcing steel. The time to corrosion of the small resistivity probes embedded in the field structures may have also been affected by the existence of a corrosion cell, between the probes and the reinforcing steel, that could have potentially accelerated corrosion rates.

The long-term effectiveness of the ECE treatment will probably depend on the time necessary for chloride ions to migrate back to the reinforcing steel level. Because several areas reported chloride concentrations in excess of 2000 ppm following treatment, chloride levels sufficient to reinitiate corrosion remain in each treated structure, as illustrated by the resistivity probe failures. Continued monitoring of the resistivity probes and additional probe failures may provide more specific conclusions on the corrosion conditions and corrosion rates within the treated structures, especially in areas of low post-ECE chloride concentrations.

At the time of this publication, it was not possible to make a conclusion regarding the effectiveness of the FRP wrap and concrete sealer systems in corrosion mitigation. Although failures of small resistivity probes were reported (two within Column 34C sealed with Hydrozol Enviroseal, one within Column 34A wrapped with AMOCO CFRP, and one within Columns 37A and 40A wrapped with MBrace CFRP), these failures appeared related to post-ECE chloride concentrations, and not necessarily the type of sealant system used. Long-term monitoring of the embedded corrosion sensors will yield more specific conclusions on the effectiveness of each system in preventing, or slowing, the corrosion process. Data regarding the moisture retention or concrete relative humidity of each type of system is also premature, although the preliminary data indicates the MBrace CFRP wrap system may confine more moisture in the columns than

the other sealant systems. Continued monitoring of the humidity sleeves will provide a more precise evaluation of each system.

8.2 Summary and Recommendations

In conclusion, the preliminary effectiveness of the ECE treatment in this investigation, as determined through chloride concentration sampling and half-cell potential mapping, correlated well with results published from other similar studies [30,31,32,33,34]. While large reductions in pre-ECE chloride concentration were witnessed in this study (50% average reduction), several areas containing chloride contents in excess of the established threshold for corrosion were reported following ECE treatment. The majority of post-ECE half-cell potentials collected from Pier 34 North indicated that the structure was passive following treatment, 92% of instrumented locations had a 90% probability of corrosive inactivity. The increased passivity was not as extensive on Pier 37 North, and only 40% of instrumented locations indicated the structure became more passive as a result of ECE treatment, while 50% of instrumented locations indicated areas of uncertain corrosive potential. Multiple studies have identified similar increases in passivity of the treated structures, in the months immediately following ECE treatment [31,32,33,34]. The duration of the increased passivity as a result of ECE treatment has not yet been determined in this investigation, although previous research has suggested that increases in passivity are long-term [30,32].

To evaluate the long-term effectiveness of ECE and column wrapping/sealing as a corrosion mitigation technique in the state of Minnesota, and to determine the most effective treatment combination, continued monitoring of the installed instrumentation is needed. Additional chloride sampling, at the instrument locations, would be useful to evaluate the migration of chloride ions since August 1998, especially in the treated structures. Results of this sampling could be used in conjunction with the results of the post-ECE chloride sampling period, and data collected from the corrosion sensors, to assist in the evaluation of site corrosion conditions.

For future corrosion rehabilitation projects, the use of concrete sealers, as opposed to FRP wraps, to prevent the ingress of new chloride ions in ECE treated structures is recommended. As discussed in Chapter 2, concrete sealers have been proven in previous studies to be more effective barriers against chloride intrusion than water- or solvent-based epoxies,

especially on structures in which traffic wear is not a concern, and they do not obscure the concrete surface [7]. Visual inspection of the concrete can enable engineers to clearly identify any symptoms of corrosion (such as staining, spalling, cracking, or delaminations), whereas wrapping the treated structures obscures the concrete surface, prohibiting visual inspection. Therefore, sealing a treated structure with a concrete sealer, such as Silane, provides an additional tool to assess corrosion conditions that cannot be used on wrapped structures, while effectively preventing, or minimizing future chloride ingression [7]. The only advantage an FRP wrap appears to provide, that a concrete sealer cannot, is added confinement and shear strength. Unless corrosion has significantly deteriorated the design strength of a structure, the use of FRP wraps to seal concrete following ECE is not required and not recommended, although significant strength degradation may warrant replacement, and not rehabilitation, of the structure.

Recommendations for future studies to evaluate the effectiveness of ECE and concrete wrapping/sealing as a corrosion rehabilitation alternative are as follows:

- Use larger-scale embeddable corrosion monitoring probes that can more closely model the corrosion rates of the reinforcing steel, such as the “3LP” or “polarization resistance” techniques, in unwrapped structures, or a galvanic corrosion cell containing an embedded anode and cathode, for wrapped structures.
- Extensively monitor one or two treated structures that report high initial chloride concentrations and large areas of active corrosion potential. By collecting chloride samples and installing corrosion monitoring instruments at several locations, more specific conclusions on the effectiveness of the treatment on the entire structure could be drawn (i.e. 10-15 sample and instrument locations per column, or more, as opposed to three).

References

1. **Jones, Denny A.,** *Principles and Prevention of Corrosion*, Second Edition, Prentice Hall, Upper Saddle River, NJ, 1996.
2. **Fontana, M.G.,** *Corrosion Engineering*, McGraw-Hill Inc., New York, NY, 1986.
3. **Lorentz, T.L.,** French, C.W., Leon, R.T., "Corrosion of Coated and Uncoated Reinforcing Steel in Concrete", Structural Engineering Report 92-03, Department of Civil and Mineral Engineering, University of Minnesota, May 1992.
4. *Handbook of Chemistry and Physics*, 71st Edition, CRC Press, 1991.
5. **Jeon, M.G., Leon, R.T.,** "Effect of Reinforcing Bar Chemical Composition on Corrosion Resistance", Mn/DOT Report 95-04, Minnesota Department of Transportation, St. Paul, MN, October 1994.
6. **Locke, C.E.,** "Mechanism of Corrosion of Steel in Concrete", *Solving Rebar Corrosion Problems in Concrete*, National Association of Corrosion Engineers, Houston, TX, 1983.
7. **Zemajtis, J., Weyers, R.E.,** "Concrete Bridge Service Life Extension Using Sealers in Chloride-Laden Environments*", Transportation Research Record*, n. 1561, Nov. 1996, pp. 1-5.
8. **Locke, C.E.,** "Corrosion of Steel in Portland Cement Concrete: Fundamental Studies", *Corrosion Effect of Stray Currents and the Techniques for Evaluating Corrosion of Rebars in Concrete*, ASTM STP 906, V. Chaker, Ed., American Society for Testing and Materials, Philadelphia, 1986.
9. **Chin, D.,** "A Calcium Nitrate-Based, Non-Corrosive, Non-Chloride Accelerator", *Corrosion, Concrete, and Chlorides, Steel Corrosion in Concrete: Causes and Restraints,* ACI SP-102, Frances W. Gibson, ed., American Concrete Institute, Detroit, MI, 1987.
10. **Smith, P.,** "Effects of Two Non-Chloride Accelerating Agents on Setting Characteristics of Portland Cement Mortars", *Corrosion, Concrete, and Chlorides, Steel Corrosion in Concrete: Causes and Restraints,* ACI SP-102, Frances W. Gibson, ed., American Concrete Institute, Detroit, MI, 1987.
11. **Bennett, J.,** "Corrosion of Reinforcing Steel in Concrete and Its Prevention by Cathodic Protection", *Anti-Corrosion Methods and Materials*, v. 33, No. 11, Oct. 1986.
12. **Berkeley, K.G.L., Pathmanaben, S.,** *Cathodic Protection of Reinforcement Steel in Concrete*, Butterworth & Co., London, 1990.

13. **Slater, J.E.,** *Corrosion of Metals in Association with Concrete*, ASTM STP 818, American Society for Testing and Materials, Philadelphia, PA, 1983.
14. **Mindess, S., Young, J.F.,** *Concrete*, Prentice-Hall, Englewood Cliffs, New Jersey, 1981.
15. **Hinatsu, J.T., Graydon, W.F., Foulkes, F.R.,** "Voltammetric Behavior of Iron in Cement. I. Development of a Standard Procedure for Measuring Voltammograms", *Journal of Applied Electrochemistry*, v. 19, 1989, pp. 868-876.
16. **Clear, K.C., et al.,** *Time-to-Corrosion of Reinforcing Steel in Concrete Slabs*, Vol. I. FHWA-RD: 73/32, Federal Highway Administration, Washington D.C., 1973.
17. **Clear, K.C., et al.,** *Time-to-Corrosion of Reinforcing Steel in Concrete Slabs*, Vol. III. FHWA-RD: 76/70, Federal Highway Administration, Washington D.C., 1976.
18. **Clear, K.C., et al.,** *Time-to-Corrosion of Reinforcing Steel in Concrete Slabs*, Vol. V. FHWA-RD: 83/012, Federal Highway Administration, Washington D.C., 1979.
19. **Pfiefer, D.W.,** *Protective Systems for New Prestressed and Substructure Concrete*, FHWA-RD: 86/193, Federal Highway Administration, Washington D.C., 1980.
20. **Clear, K.C., et al.,** *Time-to-Corrosion of Reinforcing Steel in Concrete Slabs*, Vol. II. FHWA-RD: 73/33, Federal Highway Administration, Washington D.C., 1973.
21. **Clear, K.C., et al.,** *Time-to-Corrosion of Reinforcing Steel in Concrete Slabs*, Vol. IV. FHWA-RD: 82/028, Federal Highway Administration, Washington D.C., 1978.
22. **Coggins, F., French, K.,** "Material Properties of a Twenty-Year-Old Prestressed Bridge Girder Obtained by Nondestructive Testing", Structural Engineering Report No. 89-03, Department of Civil and Mineral Engineering, University of Minnesota, July 1989.
23. **Hope, B.B., Ip, A.K.,** "Chloride Corrosion Threshold in Concrete", *ACI Materials Journal*, v. 84, No. 4, 1987.
24. ASTM C 876-87. "Standard Test Method for Half-Cell Potentials of Uncoated Reinforcing Steel in Concrete", *ASTM Book of Annual Standards 1990*.
25. *Field Evaluation of a New Aluminum Alloy for Sacrificial Cathodic Protection of steel Embedded in Concrete*, Final Report, FHWA-RD-98-058, U.S. Department of Transportation, April 1998.
26. **Bennett, J., Schue, T.J.,** *Chloride Removal Implementation Guide*, SHRP-S-347, National Research Council, Washington D.C., 1993.

27. **Morrison, G.L., Virmani, Y.P., Stratton, F.W., Gilliland, W.J.,** *Chloride Removal and Monomer Impregnation of Bridge Deck Concrete by Electro-Osmosis*, FHWA-KS-RD-74-1, Kansas Department of Transportation, 1976.

28. **Jayaprakash, G.P., Bukovatz, J.E., Ramamurti, K., Gilliland, W.J.,** *Electro-Osmotic Techniques for Removal of Chloride from Concrete and for Emplacement of Concrete Sealants*, FHWA-KS-82-2, Kansas Department of Transportation, 1982.

29. **Slater, J.E., Lankard, D.R., Moreland, P.J.,** "Electrochemical Removal of Chlorides from Concrete Bridge Decks", *Transportation Research Record*, n. 604, 1976, pg. 6.

30. **Clemena, G.G., Jackson, D.R.,** "Pilot Applications of Electrochemical Chloride Extraction on Concrete Bridge Decks in Virginia", VTRC 96-IR3, Virginia Transportation Research Council, May 1996.

31. **Bennett, J., Schue, T.J.,** *Evaluation of NORCURE Process for Electrochemical Chloride Removal from Steel-Reinforced Concrete Bridge Components*, SHRP-C-620, National Research Council, Washington D.C., 1993.

32. **Velivasakis, E.E., Henriksen, S.K., Whitmore, D.W.,** "Halting Corrosion by Chloride Extraction and Realkalization", *Concrete International,* v. 19, n. 12, Dec. 1997, pp. 39-45.

33. **Bennett, J.E, Thomas, T.J., Clear, K.C., Lankard, D.L., Hartt, W.H., Swiat, W.J.,** *Electrochemical Chloride Removal and Protection of Concrete Bridge Components: Laboratory Studies*, SHRP-S-657, National Research Council, Washington D.C., 1993.

34. **Bennett, J.E, Fong, K.F., Schue, T.J.,** *Electrochemical Chloride Removal and Protection of Concrete Bridge Components: Field Trials*, SHRP-S-669, National Research Council, Washington D.C., 1993.

35. **Manning, D.G., Pianca, F.,** *Electrochemical Removal of Chloride Ions from Reinforced Concrete: Initial Evaluation of the Pier S19 Field Trial*, MAT-90-14, Ontario Ministry of Transportation, Ontario, Canada, 1990.

36. **Castellote, M., Andrade, C., Alonso, C.,** "Electrochemical Chloride Extraction: Influence of Testing Conditions and Mathematical Modeling", *Advances in Cement Research*, v. 11, no. 2, April 1999, pp. 63-80.

37. **Hansson, I.H.L., Hansson C.M.,** "Electrochemical Extraction of Chlorides from Concrete. Part Y- A Qualitative Model of the Process*", Cement and Concrete Research*, v. 23, 1993, pp. 1141-1152.

38. **Priestley, M.N., Seible, F.,** *Repair of Shear Column Using Fiber Glass/Epoxy Jacket and Epoxy Injection*, Report #93-04, SEQAD Consulting Engineers, July 1993.

39. **Saadatmanesh, M., Ehsani, M., Li, M.,** "Strength and Ductility of Concrete Columns Externally Reinforced with Fiber Composite Straps*", ACI Structural Journal*, v. 91, n. 4, July-August 1994, pp.443-446.

40. **Xiao, Y.,** "Shear Retrofit of Reinforced Concrete Bridge Piers Using Prefabricated Composites*", Second International Conference on Composites in Infrastructure*, Tucson, AZ, 1998, pp. 221-233.

41. **Chaallal, O., Nollet, M.J., Saleh, K.,** "Use of CFRP Strips for Flexure and Shear Strengthening of RC Members", *Second International Conference on Composites in Infrastructure*, Tucson, AZ, 1998, pp. 249-259.

42. **Hutchinson, R., Abdelrahman, A., Rizkalla, S.,** "Shear Strengthening Using CFRP Sheets for Prestressed Concrete Bridge Girders in Manitoba, Canada", *Second International Conference on Composites in Infrastructure*, Tucson, AZ, 1998, pp. 261-275.

43. **Taljsten, Bjorn,** "Strengthening of Concrete Structures for Shear With Bonded CFRP-Fabrics", *Recent Advances in Bridge Engineering*, July 1997, pp. 57-64.

44. **Lemming, M.B., Peshkam, L.G.,** "Robust Solution to Strengthening Bridges", *Proceedings of the Sixth International Conference, Structural Faults and Repair,* v. 1, 1995, pp. 161-164.

45. **Emmons, P.H., Vaysburd, A.M., Thomas, J.,** "Strengthening Concrete Structures, Part II", *Concrete International*, v. 20, n.4, April 1998, pp. 56-60.

46. **Labossiere, P., Neale, K.W., Martel, S.,** "Strengthening of Existing Structures With Composite Materials: Practical Applications in Quebec*", Recent Advances in Bridge Engineering*, July 1997pp.89-97.

47. **Zemajtis, J., Weyers, R.E.,** "Service Life Evaluation of Concrete Surface Coatings", *Transportation Research Record*, n. 1490, July 1995, pp. 67-74.

48. **Lekatou, A., Faidi, S.E., Ghidaoui, D., Lyon, S.B., Newman, R.C.,** "Effect of Water and its Activity on Transport Properties of Glass/Epoxy Particulate Composites", *Composites Part A*, v. 28A, 1997, pp. 223-236.

49. **Howell, B.F.,** "Investigation of Water Permeation into Epoxy Composites by Transmission Electron Microscopy", *Proceedings of the ACS Division of Polymeric Materials Science and Engineering*, v. 60, Washington D.C., pp. 797-799.

50. **Soudki, K.A., Green, M.F.,** "Freeze-Thaw Response of CFRP Wrapped Concrete", *Concrete International*, v. 19, n.8, August 1997, pp. 64-67.

51. **Green, M.F., Soudki, K.A.,** "FRP Strengthened Concrete Structures in Cold Regions", *Recent Advances in Bridge Engineering*, July 1997, pp. 219-226.

52. **Tysl, S.R., Imbrogno, M., Miller, B.D,** "Effect of Surface Delamination on the Freeze/Thaw Durability of CFRP-Reinforced Concrete Beams*", First International Conference on Durability of Fiber Reinforced Polymer (FRP) for Construction*, Quebec, Canada, August 1998, pp. 317-324.

53. **Karbhari, V.M., Engineer, M.,** "Effect of Environmental Exposure on the External Strengthening of Concrete with Composites- Short Term Bond Durability", *Journal of Reinforced Plastics and Composites*, v. 15, Dec. 1996, pp. 1194-1216.

54. **Walter, E., Ashbee, K.H.G.,** "Osmosis in Composite Materials", *Composites*, 1982, pp. 365-368.

55. **Boll, D.J., Bascom, W.D., Motiee, B.,** "Moisture Absorption by Structural Epoxy-Matrix Carbon-Fiber Composites", *Composites Science and Technology*, v. 24, n. 4, 1985, pp. 253-273.

56. **Dutta, P.K.,** "A Micromechanical Study of the Freeze-Thaw Behavior of Polymer Composites", *Proceedings of the Seventh International Offshore and Polar Engineering Conference*, May 1997, pp. 672-676.

57. **Karbhari, V.M., Engineer, M.,** "On the Durability of Composite Rehabilitation Schemes for Concrete: Use of a Peel Test", *Journal of Materials Science*, v. 32, 1997, pp. 147-156.

58. **Karbhari, V.M., Engineer, M.,** "Assessment of Interfacial Fracture Energy Between Concrete and Glass Reinforced Composites", *Journal of Materials Science Letters*, v. 14, 1995, pp. 1210-1213.

59. **Engineer, M.P.,** "Use of Composites for Rehabilitation of Concrete Beams: Processing, Performance, and Durability", University of Delaware, Fall 1994, pp. 39-41, 110-112.
60. **Clear, K.C.,** "Measuring Rate of Corrosion of Steel in Field Concrete Structures", *Kenneth Clear Inc.,* Virginia, January 1989.
61. **Schiessl, P., Ruapach, M.,** "Monitoring System for the Corrosion Risk of Steel in Concrete Structures", *Concrete International,* v. 14, n. 7, July 1992, pp.52-55.
62. **Hansson, C.M., Marcotte, T.D.,** "West River East Side Road High Performance Concrete Structure: Installation and Preliminary Testing of Corrosion Monitoring Probes", University of Waterloo, Office of Research, September 1998.
63. **Climent-Llorca, M.A., Viqueria-Perez, E., Lopez-Atalaya M.,** "Embeddable Ag/AgCl Sensors for In-Situ Monitoring Chloride Contents in Concrete*", Cement and Concrete Research*, v. 26, n. 8, 1996, pp. 1157-1161.
64. **Dean, S.W.,** *ASTM STP 908*, American Society for Testing and Materials, Philadelphia, PA, 1996, p.197.
65. ASTM D4580-86. "Standard Practice for Measuring Delaminations in Concrete Bridge Decks by Sounding", *ASTM Book of Annual Standards 1997*.
66. **Turley, M.,** "Final Report: Minnesota Department of Transportation Fiber Reinforced Wrap Project for Substructure Rehabilitation Bridge #27831, I-394 Over Dunwoody Ave., Minneapolis", Vector Construction, September 1998.
67. ASTM C1152-90. "Standard Test Method for Acid-Soluble Chloride in Mortar and Concrete", *ASTM Book of Annual Standards 1990*.
68. **Karbhari, V.M.,** Personal communication.
69. **Uhlig, R.H.,** *Corrosion and Corrosion Control*, New York, 1963, pp. 98-113.

Tables

Table 2.1: Relevant standard electromotive force potentials at 25∀C (reduction) [4]

Reaction	Standard Potential (vs. SHE)
$Fe^{3+} + e^{-} = Fe^{2+}$	+0.771
$Cu^{+} + e^{-} = Cu$	+0.521
$Cu^{2+} + 2e- = Cu$	+0.337
$2H^{+} + 2e^{-} = H_2$	0.000
$Fe^{2+} + 2e^{-} = Fe$	-0.440

Table 2.2: Standard potentials for common reference electrodes [1]

Electrode System	Half-Cell Reaction	Potental V vs. SHE
Mercury - Mercurous Sulfate	$HgSO_4 + 2e^{-} = 2Hg + SO_4^{2-}$	+0.615
Copper-Copper Sulfate	$CuSO_4 + 2e^{-} = Cu + SO_4^{2-}$	+0.318
Saturated Calomel	$Hg_2Cl_2 + 2e^{-} = 2Hg + 2Cl^{-}$	+0.241
Silver-Silver Chloride	$AgCl + e^{-} = Ag + Cl^{-}$	+0.222
Standard Hydrogen	$2H^{+} + 2e^{-} = H_2$	+0.000

Table 2.3: Chloride ion concentrations after 830 daily saltings (mean values in ppm) [17]

Sample Group	W/C Ratio		Sample Location Depth, cm			
		0.71	2.54	5.08	7.62	10.16
1	0.4	5108	404	BL	BL	BL
2	0.5	5644	2912	450	140	BL
3	0.6	7126	3499	983	197	135

Table 2.4: Interpretation of $Cu/CuSo_4$ Hal-Cell Readings as per ASTM C-876 [24]

Half-Cell Reading (Volts)	Interpretation
> -0.20	90% probability of no corrosion activity
-0.20 to -0.35	Uncertain
< -0.35	90% probability of corrosion activity

Table 2.5: Percentage of chloride samples exceeding the corrosion threshold [30]

HALF-SPAN	4N	5N	4S	5S
BEFORE ECE	100	100	100	100
AFTER ECE	20	33	25	20

Table 2.6: Corrosion potential measurements, Burlington Skyway [32]
(mV vs. Cu-$CuSO_4$)

	NORTH FACE			WEST FACE			SOUTH FACE			EAST FACE		
Before and	-200 to			-200 to			-200 to			-200 to		
After Treatment	<-200	-350	>-350	<-200	-350	>-350	<-200	-350	>-350	<-200	-350	>-350
Before	0	85	15	0	96	4	0	96	4	0	84	16
1 year after	41	59	0	98	2	0	100	0	0	100	0	0
2 years after	41	59	0	100	0	0	100	0	0	98	2	0
3 years after	26	74	0	96	4	0	100	0	0	96	4	0
4 years after	26	70	4	98	2	0	100	0	0	96	4	0
5 years after	19	74	7	96	4	0	96	4	0	96	4	0
6 years after	26	59	15	96	4	0	93	7	0	93	7	0
7 years after	30	63	7	96	4	0	96	4	0	91	9	0

Table 2.7: Corrosion potential measurements, Highways 11 & 16 [32]
(mV vs. Cu-$CuSO_4$)

	Col. Line 1			Col. Line 2			Col. Line 3			Col. Line 4		
Before and	-200 to			-200 to			-200 to			-200 to		
After Treatment	<-200	-350	>-350	<-200	-350	>-350	<-200	-350	>-350	<-200	-350	>-350
Before	42	33	25	76	16	8	46	29	25	43	21	36
1 year after	98	2	0	100	0	0	100	0	0	95	5	0
2 years after	100	0	0	100	0	0	98	2	0	95	5	0

Table 2.8: Average increase in chloride concentration from baseline values at 13 mm depth (in kg/m^3) and corresponding std.deviation [7]

		Number of One-Week Exposure Cycles					
		10		20		30	
Exposure	Sealer	Cl^- gain	ω	Cl^- gain	ω	Cl^- gain	ω
Wall	Control	2.05	0.784	3.52	0.629	4.54	0.429
	WBE	0.36	0.112	0.55	0.182	1.11	0.393
	SBE	0.39	0.193	0.77	0.208	1.61	0.736
	SIL	0.2	0.072	0.25	0.1	0.18	0.108
	SLX	0.15	0.085	0.27	0.12	0.37	0.353
Slab	Control	1.22	0.388	2.27	0.531	4.18	0.862
	WBE	0.8	0.247	1.74	0.249	3.86	0.562
	SBE	1.1	0.215	2.18	0.753	4.14	0.619
	SIL	0.17	0.085	0.13	0.025	0.13	0.042

Table 2.9: Estimated service lives based on diffusion characteristics [7]

	Estimated Service Life (years)					
	VA		PA		NY	
Surface Treatment	Horiz.	Vert.	Horiz.	Vert.	Horiz.	Vert.
Control	35.5	35.5	21.2	21.2	13.5	13.5
WBE	75	39.2	64	23.2	30.9	14.5
SBE	75	36.1	48.4	21.5	25.1	13.7
SIL	75	75	75	75	63.2	61.7
SLX	75	75	75	75	53.3	64.4

Table 3.1: Resistance between rebar connections on Pier 34 North (in Ohms) [66]

	Col A	Col B	Col C	Pier Cap 1	Pier Cap 2	Pier Cap 3	Pier Cap 4
Col A	-	0.2	0.1	0.2	0.1	0.2	0.2
Col B	-	-	0.2	0.1	0.1	0.1	0.2
Col C	-	-	-	0.2	0.2	0.1	0.1
Pier Cap 1	-	-	-	-	0.2	0	0.2
Pier Cap 2	-	-	-	-	-	0.1	0.1
Pier Cap 3	-	-	-	-	-	-	0.2
Pier Cap 4	-	-	-	-	-	-	-

Table 3.2: Resistance between rebar connections on Pier 37 North (in Ohms) [66]

	Col A	Col B	Col C	Pier Cap 1	Pier Cap 2	Pier Cap 3	Pier Cap 4
Col A	-	0.2	0.2	0.3	0.2	0.1	0.2
Col B	-	-	0.1	0.2	0.1	0.2	0.2
Col C	-	-	-	0.1	0.3	0.2	0.2
Pier Cap 1	-	-	-	-	0.2	0.1	0.2
Pier Cap 2	-	-	-	-	-	0.2	0.2
Pier Cap 3	-	-	-	-	-	-	0.2
Pier Cap 4	-	-	-	-	-	-	-

Table 3.3: Chloride concentrations in Pier 37 North (collected by Vector) [66]

LOCATION	SAMPLE DEPTH (cm)	INITIAL CHLORIDE LEVEL	FINAL CHLORIDE LEVEL	% CHANGE
	0 - 2.5	1128	680	-39.49
Column 37A	2.5 - 5	795	420	-47.4
	5 - 7.5	203	160	-22.1
	0 - 2.5	300	120	-61.43
Column 37B	2.5 - 5	121	90	-21
	5 - 7.5	100	90	-10.4
	0 - 2.5	1569	130	-91.7
Column 37C	2.5 - 5	1169	90	-92.58
	5 - 7.5	395	100	-74
Pier 37 North	0 - 2.5	1133	690	-39.2
East Face	2.5 - 5	241	150	-35.7
	5 - 7.5	118	60	-48.3
Pier 37 North	0 - 2.5	3823	1560	-58.9
East Face	2.5 - 5	1426	1140	-19.8
	5 - 7.5	226	280	23.93
Pier 37 North	0 - 2.5	4067	1320	-67
West Face	2.5 - 5	3059	880	-71.2
	5 - 7.5	1118	780	-30.1
Pier 37 North	0 - 2.5	2359	900	-61.6
West Face	2.5 - 5	1290	720	-44
	5 - 7.5	482	290	-39.22

Table 3.4: Average chloride concentrations in ECE structures (collected by Vector) [66]

SAMPLE	**AVERAGE CHLORIDE CONCENTRATIONS (PPM)**				**% CHANGE IN**	
DEPTH	PIER 34 NORTH		PIER 37 NORTH		**CHLORIDE CONTENT**	
(cm)	BEFORE ECE	AFTER ECE	BEFORE ECE	AFTER ECE	PIER 34	PIER 37
0 - 2.5	2280	1230	2040	770	-46.3	-68.97
2.5 - 5	1700	970	1150	500	-42.92	-56.82
5 - 7.5	770	440	380	250	-43.29	-32.68

Table 3.5: Results of the pull-off tests on field FRP systems [66]

Location	Wrap Type	Pull Load (N)	Dolly Area (cm^2)	Bond Strength (MPa)	Failure Location
Column 40A	MBrace CFRP	5785	14.52	4.0	Dolly Paste
Pier 40 North	MBrace CFRP	4895	14.52	3.4	Dolly Paste
Column 37A	MBrace CFRP	5785	14.52	4.0	Dolly Paste
Pier 37 North	MBrace CFRP	5785	14.52	4.0	Dolly Paste
Column 34A	AMOCO CFRP	4005	14.52	2.8	Concrete
Pier 34 North	AMOCO CFRP	4227.5	14.52	2.9	Concrete
Column 34B	GFRP	5429	14.52	3.7	Concrete
Pier 34 North	GFRP	4939.5	14.52	3.4	Concrete
Column 34E	GFRP	5607	14.52	3.9	Concrete
Pier 34 South	GFRP	5028.5	14.52	3.5	Concrete
Column 34F	AMOCO CFRP	4450	14.52	3.1	Concrete
Pier 34 South	AMOCO CFRP	2447.5	14.52	1.7	Dolly Paste

Table 4.1: Percentages of pre and post-ECE chloride samples over 2000 ppm

Sample Location	PRE-ECE SAMPLING PERIOD		POST-ECE SAMPLING PERIOD	
	Number of Chloride Samples Above 2000 ppm	Percentage of Chloride Samples Above 2000 ppm	Number of Chloride Samples Above 2000 ppm	Percentage of Chloride Samples Above 2000 ppm
PIER 34 NORTH (ECE)	49 / 77	63.6	17 / 85	20.0
PIER 34 SOUTH	30 / 89	33.7	20 / 85	23.5
PIER 37 NORTH (ECE)	23 / 91	25.3	4 / 85	4.7
PIER 37 SOUTH	12 / 38	31.6	4 / 35	11.4
PIER 40 NORTH	18 / 69	26.1	24 / 70	34.3
TOTALS	132 / 364	36.3	69 / 360	19.2
ECE STRUCTURES	72 / 168	42.9	21 / 170	12.4
NON-ECE STRUCTURES	60 / 196	30.6	48 / 190	25.3

Table 4.2: Pre-ECE average chloride levels in each structure at each sample depth

Location	0 - 1.25	1.25 - 2.5	2.5 - 3.75	3.75 - 6.25	6.25 - 8.75	Average
34A	4207	4004	3932	2381	1440	*3193*
34B	2425	2639	1908	1230	814	*1803*
34C	2960	4371	2877	2292	1318	*2764*
PIER CAP 34N	3028	3066	2427	1719	1273	*2303*
34D	2588	2349	2022	407	308	*1535*
34E	888	1058	757	175	107	*597*
34F	3347	3490	1790	927	808	*2072*
PIER CAP 34S	2352	1744	1370	863	742	*1414*
37A	677	512	408	313	199	*422*
37B	604	772	804	875	518	*715*
37C	772	566	449	153	154	*419*
PIER CAP 37N	2323	2245	1957	1780	1493	*1960*
37D	1532	1824	2233	1577	975	*1628*
PIER CAP 37S	2981	1599	1025	825	414	*1369*
40A	2085	1406	947	483	187	*1022*
40C	2104	1403	785	691	530	*1103*
PIER CAP 40 N	2422	2177	1971	1236	690	*1699*

Table 4.3: Pre-ECE chloride concentration averages in each sample depth range

Sample Depth (cm)		0 - 1.25	1.25 - 2.5	2.5 - 3.75	3.75 - 6.25	6.25 - 8.75
PRE-ECE	ECE Structures	2245	2293	1919	1428	1055
	Non-ECE Structures	2288	1904	1486	910	596
	OVERALL	2269	2075	1677	1152	812

Table 4.4: Post-ECE average chloride levels in each structure at each sample depth

Location	0 - 1.25	1.25 - 2.5	2.5 - 3.75	3.75 - 6.25	6.25 - 8.75	Average
34A	1826	1900	1287	1087	565	*1333*
34B	653	922	845	655	264	*668*
34C	1687	2038	1418	1103	372	*1324*
PIER CAP 34N	1822	1728	1414	899	672	*1307*
34D	1606	1708	907	258	313	*958*
34E	1548	1165	539	292	204	*750*
34F	3090	2041	1989	1144	319	*1717*
PIER CAP 34S	2114	1907	1188	754	287	*1250*
37A	485	632	1017	296	232	*532*
37B	314	791	711	482	271	*514*
37C	175	941	633	293	193	*447*
PIER CAP 37N	1334	1658	1121	748	418	*1056*
37D	1497	1958	1584	947	457	*1289*
PIER CAP 37S	1339	809	434	258	252	*618*
40A	2241	1910	1356	813	340	*1332*
40C	1509	1286	270	1329	796	*1038*
PIER CAP 40 N	2015	2328	1930	1076	754	*1621*

Table 4.5: Percent change in pre- and post-ECE average chloride levels

Location	0 - 1.25	1.25 - 2.5	2.5 - 3.75	3.75 - 6.25	6.25 - 8.75	Average
34A	-56.6	-52.6	-67.3	-54.3	-60.7	*-58*
34B	-73.1	-65.1	-55.7	-46.7	-67.6	*-62*
34C	-43	-53.4	-50.7	-51.9	-71.8	*-54*
PIER CAP 34N	-39.8	-43.6	-41.7	-47.7	-47.1	*-44*
34D	-37.9	-27.3	-55.5	-36.7	1.6	*-31*
34E	74.3	10	-28.8	67.3	90.3	*43*
34F	-7.7	-41.5	11.1	23.5	-60.5	*-15*
PIER CAP 34S	-10.1	9.3	-13.4	-12.5	-61.3	*-18*
37A	-28.3	23.5	149.1	5.3	16.6	*33*
37B	-48	2.5	-11.6	-44.9	-47.7	*-30*
37C	-77.4	66.3	41.1	91.3	25.5	*29*
PIER CAP 37N	-42.6	-26.2	-42.7	-58	-72	*-48*
37D	-2.3	7.3	-29.1	-40	-53.2	*-23*
PIER CAP 37S	-55	-49.4	-57.6	-68.7	-39.1	*-54*
40A	7.5	35.9	43.2	68.5	81.8	*47*
40C	-28.3	-8.4	-65.6	92.3	50.3	*8*
PIER CAP 40 N	-16.8	6.9	-7.1	-12.9	9.3	*-4*

Table 4.6: Pre- and post-ECE chloride ion averages in each sample depth range

Sample Depth (cm)		**0 - 1.25**	**1.25 - 2.5**	**2.5 - 3.75**	**3.75 - 6.25**	**6.25 - 8.75**
PRE-ECE	ECE Structures	2245	2293	1919	1428	1055
	Non-ECE Structures	2288	1904	1486	910	596
	OVERALL	2269	2075	1677	1152	812
POST-ECE	ECE Structures	1196 **(-46.7)**	1434 **(-37.5)**	1118 **(-42)**	733 **(-48.7)**	424 **(-59.8)**
	Non-ECE Structures	1917 **(-17)**	1772 **(-6.9)**	1226 **(-17.9)**	790 **(-13.2)**	437 **(-26.7)**
	OVERALL	1442 **(-31)**	1522 **(-26.7)**	1103 **(-34.2)**	712 **(-38.2)**	376 **(-53.7)**

Table 5.1: Measured resistance between rebar connections for field instrumentation

GENERAL LOCATION	CONNECTION 1	CONNECTION 2	RESISTIVITY (in Ohms)
Pier 34 North	Pier Cap 1	**Column A**	1.0
Pier 34 South	**Column D**	Column E	0.7
Pier 37 North	**Pier Cap 2**	Column A	1.0
Pier 37 South	**Column E**	Column F	1.3
Pier 40 North	Column B	**Column C**	1.5

Bold Font: Indicates reinforcing steel connection used for all embedded instrumentation on that pier

Table 6.1: Calibration of half-cells

STATISTIC	RESULT
AVERAGE	-38.05
HIGHEST	-40.1
LOWEST	-36 **
RANGE (+/-)	2.05
ST. DEVIATION	1.121

** - A lower potential of –8 mV was measured was from a defective/replaced half-cell

Table 6.2: Temperature effects on potential of an Ag/AgCl electrode vs. SCE

TEMPERATURE (Celsisus)	POTENTIAL (mV)
Room Temp	-41.2
20	-41.8
25	-43.1
30	-43.3
35	-45.5
40	-46.6
52	-48.9
Room Temp	-42.7

Table 6.3: Resistivity probe test matrix

TEST	PROBES	TESTING MEDIUM	TEST OBJECTIVE	TEST PROCEDURE
1	5 Small 5 Large	0.33 M Solution: NaCl and Deionized Water	Determine if probes are viable corrosion monitoring instrument and evaluate difference in time to corrosion of different diameter probes	All probes in same 0.33 M solution. Probes not in contact with each other. Probes placed around circumference alternating large and small
2	3 Small 3 Large	Grout Seeded at 32,000 ppm Cl^- in 0.33M NaCl Bath	To determine if corrosion of probes in grout can be detected and evaluate difference between failure times in grout and solution	All 6 probes placed in same grout plug and neither depth of probe or position was controlled. Test started in small beaker then moved plug to saltwater bath at 0.33M
3	3 Small 3 Large	0.05 M Solution: NaCl and Deionized Water	Establish corosion rate of probes in conditions more indicative of field conditions than Test 1	Each probe isolated in 30 ml beaker containing 25 ml of 0.05 M NaCl solution. Probes centered and completely submerged
4	3 Small 3 Large	0.10 M Solution: NaCl and Deionized Water	Determine effect of solution concentration on corrosion rate through comparison with Test 3	Each probe isolated in 30 ml beaker containing 25 ml of 0.1 M NaCl solution. Probes centered and completely submerged
5	3 Small 3 Large	Grout Seeded at 11,000 ppm Cl^- in 0.1M NaCl Bath	Evaluate time to corrosion of probes in grout and solution at same chloride concentration through comparison with Test 4. Cycled 2 days wet and 2 days dry	Probes isolated in 30 ml beaker filled with 12.5g grout, 7.75 ml 0.5M NaCl solution. Probes centered at 5mm from bottom of grout plug. All grout plugs in same 0.1M saltwater bath
6	3 Small 3 Large	Grout Seeded at 55,000 ppm Cl^- in 0.5M NaCl Bath	Approximately evaluate effect of grout seeding level and saltwater bath on corrosion rates through comparison with Test 5. Cycled 2 days wet and 2 days dry	Two probes in each of 3, 30 ml beakers filled with 24g grout, 15 ml 2.5M NaCl solution. Probes centered 0.625 cm apart at 5mm from bottom of grout plug. All grout plugs in same 0.5M saltwater bath.
7	3 Small 3 Large	Grout Seeded at 55,000 ppm Cl^- in 0.5M NaCl Bath	Evaluate wire interconnection effect through comparison with test 6. Cycled 2 days wet and 2 days dry	Two probes in each of 3, 30 ml beakers filled with 24g grout, 15 ml 2.5M NaCl solution. Probes centered 0.625 cm apart at 5mm from bottom of grout plug. All grout plugs in same 0.5M saltwater bath. Probes in same plug interconnected.

Table 6.4: Days to failure of resistivity probes in Test 1

PROBE	1	2	3	4	5	AVG.	INITIAL pH	FINAL pH
SMALL	2.5	2.5	3	2.5	3	**2.7**	6.8	8.6
LARGE	9	15	14	16	19	**14.6**		

Table 6.5: Days to failure of resistivity probes Test 2

PROBE	1	2	3	AVG.	INITIAL pH	FINAL pH
SMALL	41	73	76	**63.3**	11.2 (grout)	N/A (grout)
LARGE	98	154	179	**143.7**	10.2 (ponded water)	6.8 (saltwater bath)

Table 6.6: Days to failure of resistivity probes in Test 3

PROBE	1	2	3	AVG.	INITIAL pH	FINAL pH
SMALL	9	9	9	**9**	6.8	7
LARGE	36	38	41	**38.3**		

Table 6.7: Days to failure of resistivity probes in Test 4

PROBE	1	2	3	AVG.	INITIAL pH	FINAL pH
SMALL	5	5	5	**5**	6.8	7
LARGE	28	27	27	**27.3**		

Table 6.8: Days to failure of resistivity probes in Test 5

PROBE	1	2	3	AVG.	INITIAL pH	FINAL pH
SMALL	85	76	101	**87.3**	11	10 (saltwater bath)
LARGE	164	184	196	**181.3**		

Table 6.9: Days to failure of resistivity probes in Test 6

PROBE	1	2	3	AVG.	INITIAL pH	FINAL pH
SMALL	27	74	33	**45**	11.2	10 (saltwater bath)
LARGE	99	105	98	**100**		

Table 6.10: Days to failure of resistivity probes in Test 7

PROBE	1	2	3	AVG.	INITIAL pH	FINAL pH
SMALL	25	95	45	**60 ***	11.2	10 (saltwater bath)
LARGE	110	132	141	**121***		

* - Indicates that the results of the small and large probes embedded in the same grout plug were not included in the average time to failure

Table 6.11: Change in resistivity probe failure time vs. NaCl concentration

Experiment Comparison	Increase in NaCl Concentration	Theoretical Increase in Time to Failure	Increase in Time to Failure of Small Probes	Increase in Time to Failure of Large Probes
Test 3 vs. Test 4	x 2	10%	44%	30%
Test 4 vs. Test 1	x 3.33	33%	66%	62%
Test 3 vs. Test 1	x 6.66	25%	45%	47%

Table 6.12: Results of diffusion tests on FRP wraps

Test Number	Specimen	Sample Area (cm^ 2)	Test Started	Test Ended	Total Time	Initial Water Level (mm)	Final Water Level (mm)	Evap.?	Leaks?
1	MBrace Epoxy	81.1	10/13/98	1/8/99	87 days	78	75	Y	N
2	AMOCO CFRP Wrap	81.1	1/10/99	1/10/99	0	N/A	N/A	N/A	Y
3	GFRP Wrap	81.1	1/11/99	4/2/99	81 days	75	74	Y	N
4	AMOCO Peel Sample #1	4.5	4/2/99	4/2/99	10 min.	96	89	N	N
5	AMOCO Peel Sample #2	10.5	4/7/99	4/7/99	10 min.	94	94	N	N
6	AMOCO Peel Sample #3	3.9	4/7/99	4/7/99	10 min.	90	90	N	N
7	AMOCO Peel Sample #4	4.6	4/7/99	4/7/99	10 min.	91	91	N	N
8	AMOCO Peel Sample #5	4.1	4/7/99	4/7/99	10 min.	97	97	N	N

Table 6.13: Bond energy of FRP systems

WRAP TYPE	MBRACE 1	MBRACE 2	AMOCO 1	AMOCO 2	GFRP
ENERGY (N-m)	2.62	1.86	1.02	0.77	3.24

Table 7.1: Half-cell potentials vs. Ag/AgCl electrode on Pier 34 North (ECE)

LOCATION	SENSOR	Mn/DOT	Vector	Sensor	Sensor	Sensor	Sensor
		(Oct. '97)	(Nov. '98)	(Apr. '99)	(May '99)	(Jul. '99)	(Aug. '99)
	1	-0.067	N/A	-0.072	-0.064	-0.078	-0.069
34A	2	-0.183	N/A	-0.086	-0.088	-0.093	-0.085
	3	-0.223	N/A	-0.089	-0.083	-0.075	-0.072
	1	0.028	N/A	-0.065	-0.067	-0.078	-0.072
34B	2	-0.062	N/A	-0.067	-0.069	-0.073	-0.069
		-0.12	N/A	-0.077	-0.079	-0.083	-0.076
	1	-0.136	-0.009	-0.054	-0.055	-0.073	-0.07
34C	2	-0.163	0.031	-0.196	-0.196	-0.194	-0.174
	3	-0.168	0.02	-0.085	-0.088	-0.101	-0.096
PIER 34N	W2	-0.051	N/A	-0.066	-0.072	-0.076	-0.071
	E1	-0.128	-0.021	-0.085	-0.077	-0.077	-0.07
	E2	-0.033	-0.033	-0.11	-0.111	-0.103	-0.096

Table 7.2: Half-cell potentials vs. Ag/AgCl electrode on Pier 34 South (NON-ECE)

LOCATION	SENSOR	Mn/DOT (Oct. '97)	Sensor (Apr. '99)	Sensor (May '99)	Sensor (Jul. '99)	Sensor (Aug. '99)
	1	-0.011	-0.069	-0.074	-0.085	-0.083
34D	2	0.024	-0.059	-0.061	-0.057	-0.053
	3	0.085	-0.072	-0.072	-0.072	-0.06
34E	1	0.102	-0.032	-0.035	-0.049	-0.043
	2	0.036	-0.045	-0.046	-0.057	-0.043
	1	0.081	-0.051	-0.055	-0.059	-0.055
34F	2	-0.096	-0.048	-0.057	-0.057	-0.063
	3	-0.202	-0.111	-0.117	-0.134	-0.119
	W1	-0.007	-0.033	-0.038	-0.027	-0.019
PIER 34S	W2	-0.05	-0.075	-0.088	-0.101	-0.097
	E1	-0.007	-0.039	-0.044	-0.036	-0.027
	E2	-0.079	-0.107	-0.122	-0.115	-0.116

Table 7.3: Half-cell potentials vs. Ag/AgCl electrode on Pier 37 North (ECE)

LOCATION	SENSOR	Mn/DOT	Vector	Sensor	Sensor	Sensor	Sensor
		(Oct. '97)	(Nov. '98)	(Apr. '99)	(May '99)	(Jul. '99)	(Aug. '99)
37A	1	0.032	N/A	-0.102	-0.103	-0.107	-0.101
	2	-0.177	N/A	-0.166	-0.167	-0.149	-0.143
37B	1	0.081	0.127	-0.073	-0.076	-0.093	-0.089
	2	0.109	0.023	-0.185	-0.179	-0.175	-0.178
37C	1	-0.136	0.061	**-0.297**	**-0.264**	**-0.303**	**-0.294**
	2	-0.249	0.072	-0.081	-0.08	-0.089	-0.081
	W1	-0.012	0.033	-0.112	-0.132	-0.156	-0.152
PIER 37N	W2	**-0.348**	-0.029	0.228	0.246	0.331	0.342
	E1	**-0.318**	0.002	-0.114	-0.118	-0.123	-0.116
	E2	-0.107	0.078	-0.086	-0.084	-0.098	-0.089

Table 7.4: Half-cell potentials vs. Ag/AgCl electrode on Pier 37 South (NON-ECE)

LOCATION	SENSOR	Mn/DOT	Sensor	Sensor	Sensor	Sensor
		(Oct. '97)	(Apr. '99)	(May '99)	(Jul. '99)	(Aug. '99)
37D	1	0.086	**-0.545**	**-0.525**	**-0.414**	**-0.402**
	2	-0.2	**-0.36**	**-0.365**	**-0.379**	**-0.382**
	3	-0.206	**-0.368**	**-0.37**	**-0.382**	**-0.378**
PIER 37S	W1	-0.074	-0.082	-0.078	-0.083	-0.089
	E1	-0.078	-0.097	-0.094	-0.07	-0.074

Table 7.5: Half-cell potentials vs. Ag/AgCl electrode on Pier 40 North (NON-ECE)

LOCATION	SENSOR	Mn/DOT (Oct. '97)	Sensor (Apr. '99)	Sensor (May '99)	Sensor (Jul. '99)	Sensor (Jul. '99)
	1	-0.062	-0.131	-0.143	-0.139	-0.137
40A	2	-0.123	-0.095	-0.1	-0.108	-0.11
	3	**-0.309**	-0.169	-0.17	-0.173	-0.176
40C	1	0.049	-0.094	-0.097	-0.1	-0.092
	W1	-0.168	**-0.332**	**-0.34**	**-0.359**	**-0.345**
	W2	-0.132	-0.184	-0.189	-0.188	-0.178
PIER 40N	W3	-0.164	-0.134	-0.133	-0.147	-0.15
	E1	-0.109	-0.154	-0.165	-0.183	-0.187
	E2	-0.182	-0.191	-0.194	-0.187	-0.191
	E3	-0.104	-0.095	-0.101	-0.101	-0.095

Table 7.6: Resistivity probe results on Pier 34 North (ECE)

LOCATION	SENSOR	PROBE SIZE	FAILURE? (Apr. '99)	FAILURE? (May '99)	FAILURE? (Jul. '99)	FAILURE? (Aug. '99)
	1	S	N	N	N	N
		S	N	N	N	N
34A	2	L	N	N	N	N
		S	N	N	N	N
	3	S	N	N	N	**Y**
		S	N	N	N	N
	1	L	N	N	N	N
		S	N	N	N	N
34B	2	S	N	N	N	N
		S	N	N	N	N
	3	L	N	N	N	N
		S	N	N	N	N
	1	S	N	N	**Y**	**Y**
		S	N	N	N	N
34C	2	S	N	N	N	N
		S	N	N	N	N
	3	S	N	N	N	**Y**
		S	N	N	N	N
	W1	S	N	N	N	N
		S	N	N	N	N
	W2	S	N	N	N	N
PIER 34N		S	N	N	N	N
	E1	L	N	N	N	N
		S	N	N	N	N
	E2	L	N	N	N	N
		S	N	N	N	N

Table 7.7: Resistivity probe results on Pier 34 South (NON-ECE)

LOCATION	SENSOR	PROBE SIZE	FAILURE? (Apr. '99)	FAILURE? (May '99)	FAILURE? (Jul. '99)	FAILURE? (Aug. '99)
	1	S	N	N	N	N
		S	N	N	N	N
34D	2	S	N	N	N	N
		S	N	N	N	N
	3	S	N	N	N	N
		S	N	N	N	N
	1	S	N	N	N	N
34E		S	N	N	N	N
	2	L	N	N	N	N
		S	N	N	N	N
	1	L	N	N	N	N
		S	N	N	N	N
34F	2	L	N	N	N	N
		S	N	N	N	N
	3	L	N	N	N	N
		S	N	N	N	N
	W1	L	N	N	N	N
		S	N	N	N	N
	W2	L	N	N	**Y**	**Y**
PIER 34S		S	N	N	N	N
	E1	L	N	N	N	N
		S	N	N	N	N
	E2	L	N	N	N	N
		S	N	N	N	N

Table 7.8: Resistivity probe results on Pier 37 North (ECE)

LOCATION	SENSOR	PROBE SIZE	FAILURE? (Apr. '99)	FAILURE? (May '99)	FAILURE? (Jul. '99)	FAILURE? (Aug. '99)
	1	S	N	N	N	N
37A		S	N	N	**Y**	**Y**
	2	S	N	N	N	N
		S	N	N	N	N
	1	S	N	N	N	N
37B		S	N	N	N	N
	2	S	N	N	N	N
		S	N	N	N	N
	1	S	N	N	N	N
37C		S	N	N	N	N
	2	S	N	N	N	N
		S	N	N	N	N
	W1	L	N	N	N	N
		S	N	N	N	N
	W2	L	N	N	N	N
PIER 37N		S	N	N	N	N
	E1	L	N	N	N	N
		S	N	N	N	N
	E2	L	N	N	N	N
		S	N	N	N	N

Table 7.9: Resistivity probe results on Pier 37 South (NON-ECE)

LOCATION	SENSOR	PROBE SIZE	FAILURE? (Apr. '99)	FAILURE? (May '99)	FAILURE? (Jul. '99)	FAILURE? (Aug. '99)
	1	L	N	N	N	N
		S	N	N	N	N
37D	2	S	N	N	N	N
		S	N	N	N	N
	3	S	N	N	N	N
		S	N	N	N	N
	W1	L	N	N	N	N
PIER 37S		S	N	N	N	N
	E1	L	N	N	N	N
		S	N	N	N	N

Table 7.10: Resistivity probe results on Pier 40 North (NON-ECE)

LOCATION	SENSOR	PROBE SIZE	FAILURE? (Apr. '99)	FAILURE? (May '99)	FAILURE? (Jul. '99)	FAILURE? (Aug. '99)
	1	L	N	N	N	N
		S	N	N	N	N
40A	2	L	N	N	N	N
		S	N	N	N	N
	3	L	N	N	N	N
		S	N	N	**Y**	**Y**
40C	1	L	N	N	N	N
		S	N	N	N	N
	W1	L	N	N	N	N
		S	N	N	N	N
	W2	L	N	N	**Y**	**Y**
		S	N	N	N	N
	W3	L	N	N	N	N
PIER 40N		S	N	N	N	N
	E1	L	N	N	N	N
		S	N	N	N	N
	E2	L	N	N	N	N
		S	N	N	N	N
	E3	L	N	N	N	N
		S	N	N	N	N

Table 7.11: Relative Humidity of Pier 34 North (ECE)

LOCATION	COLUMN SEALANT	SENSOR	% R.H. (Jul. '99)	% R.H. (Aug. '99)
		1 (Lowest)*	65	70
34A	AMOCO CFRP	2	54	58
		3 (Highest)	59	
		1 (Lowest)	59	66
34B	GFRP	2	60	67
		3 (Highest)	55	
		1 (Lowest)	57	
34C	ENVIROSEAL	2	51	
		3 (Highest)	56	

(Lowest)* - Represents the lowest moisture sleeve position on each column

Table 7.12: Relative Humidity of Pier 34 South (NON-ECE)

LOCATION	COLUMN SEALANT	SENSOR	% R.H. (Jul. '99)	% R.H. (Aug. '99)
		1 (Lowest)	53	
34D	CONTROL	2	49	
		3 (Highest)	54	
		1 (Lowest)	50	55
34E	GFRP	2	45	
		3 (Highest)	48	
		1 (Lowest)	51	48
34F	AMOCO CFRP	2	56	54
		3 (Highest)	56	

Table 7.13: Relative Humidity of Pier 37 North (ECE)

LOCATION	COLUMN SEALANT	SENSOR	% R.H. (Jul. '99)	% R.H. (Aug. '99)
		1 (Lowest)	70	69
		2	77	80
		3	71	
37A	MBRACE CFRP	4	64	
		5	68	
		6	68	
		7 (Highest)	70	
		1 (Lowest)	63	60
		2	56	
		3	57	
37B	SILANE 40	4	63	
		5	67	
		6	41*	
		7 (Highest)	60	
		1 (Lowest)	59	
37C	NICOTOTE FOSROC	2	52	
		3 (Highest)	53	

Table 7.14: Relative Humidity of Pier 37 South (NON-ECE)

LOCATION	COLUMN SEALANT	SENSOR	% R.H. (Jul. '99)
		1 (Lowest)	54
		2	49
		3	51
37D	CONTROL	4	53
		5	51
		6	56
		7 (Highest)	54

Table 7.15: Relative Humidity of Pier 40 North (NON-ECE)

LOCATION	COLUMN SEALANT	SENSOR	% R.H. (Jul. '99)	% R.H. (Aug. '99)
		1 (Lowest)	71	72
40A	MBRACE CFRP	2	68	64
		3 (Highest)	65	
		1 (Lowest)	72	65
40C	CONTROL	2	66	
		3 (Highest)	68	

Figures

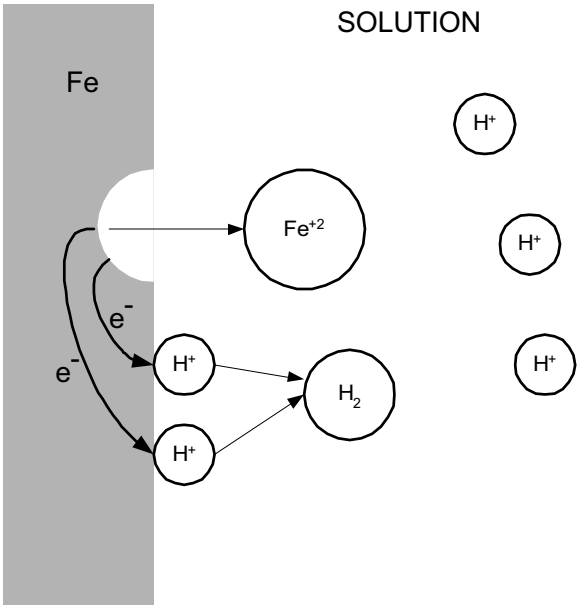

Figure 2.1: Schematic of nickel dissolution in sulfuric acid [1]

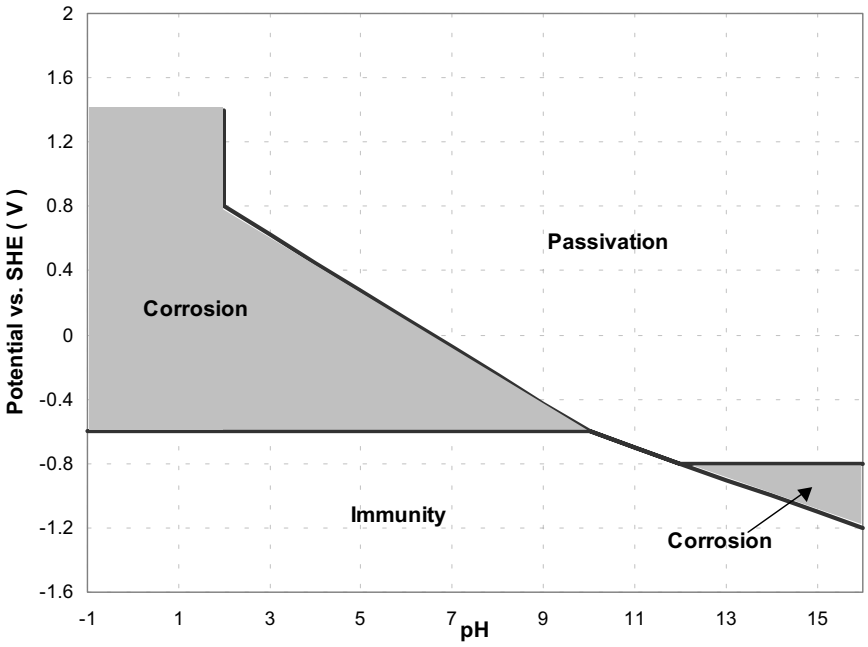

Figure 2.2: Pourbaix diagram for iron and water [1]

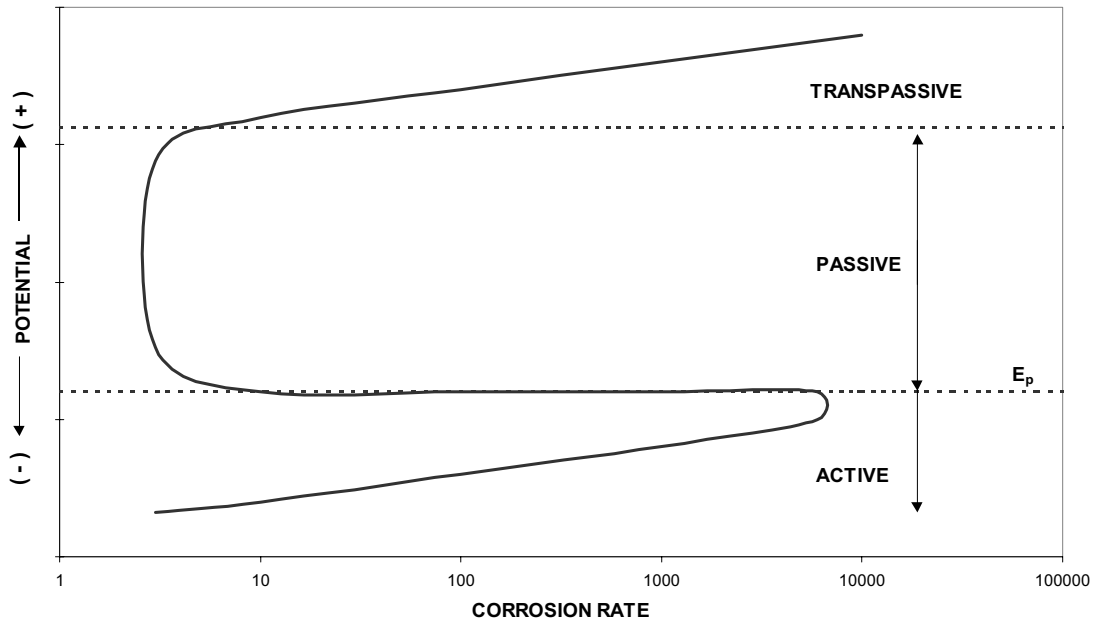

Figure 2.3: Typical corrosive response of a metal with passive tendencies [1]

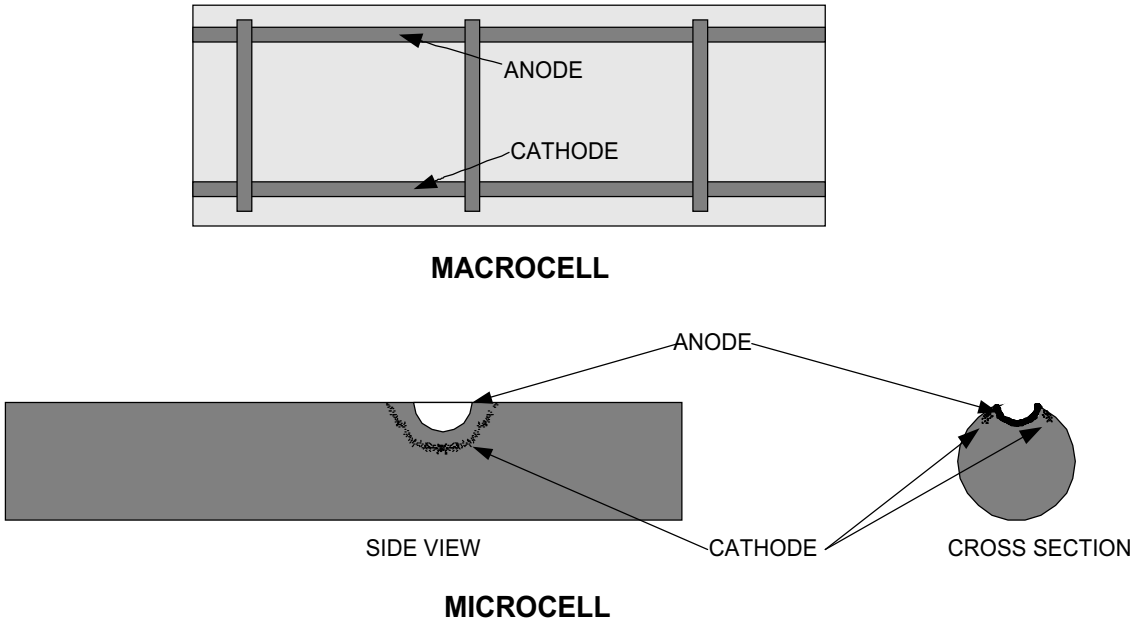

Figure 2.4: Types of corrosion cells [5]

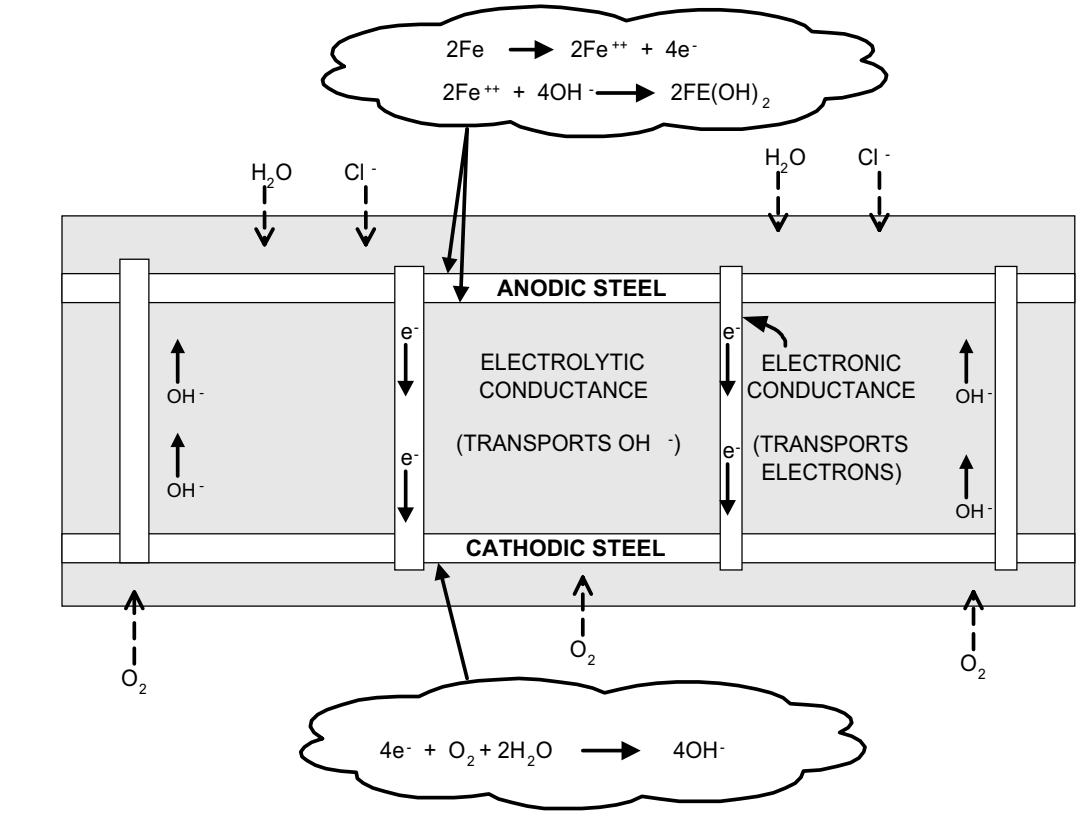

Figure 2.5: The corrosion process in a macrocell [5]

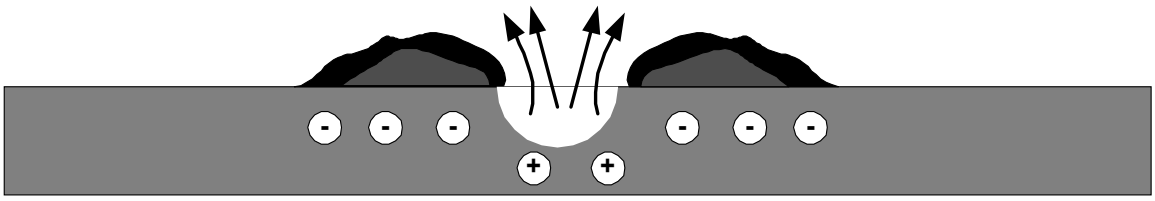

Figure 2.6: An example of microcell corrosion in the form of pitting corrosion [3]

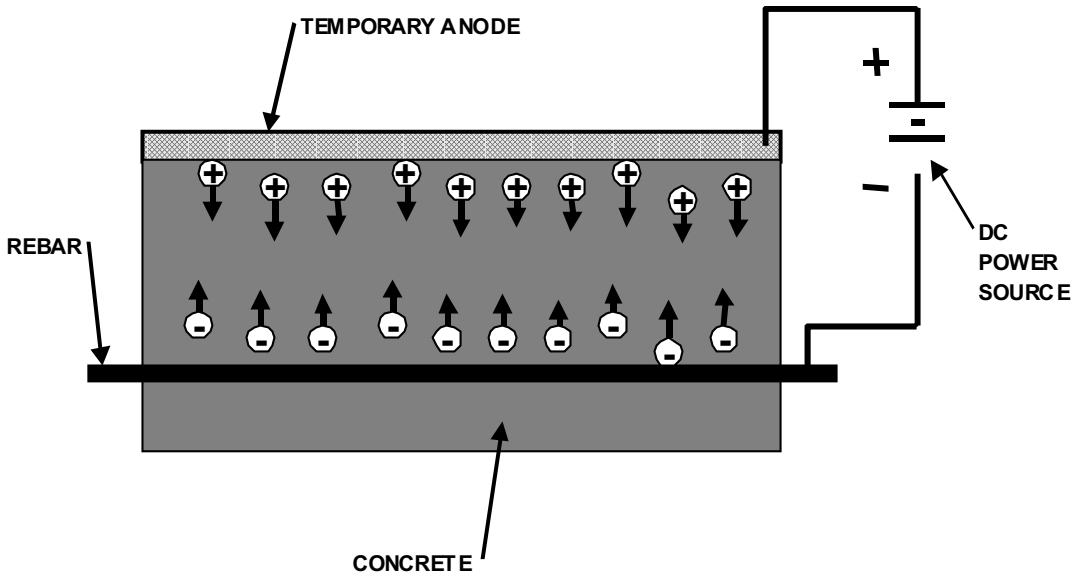

Figure 2.7: Electromigration of anions and cations during ECE [27]

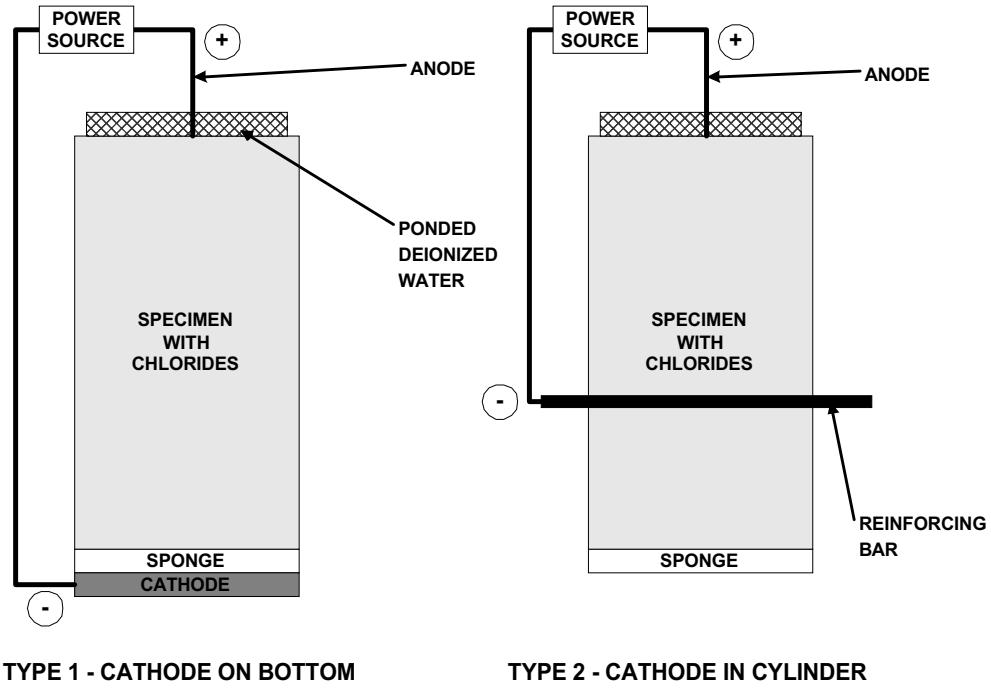

Figure 2.8: Arrangement for ECE experiments conducted by Castellote, et al. [36]

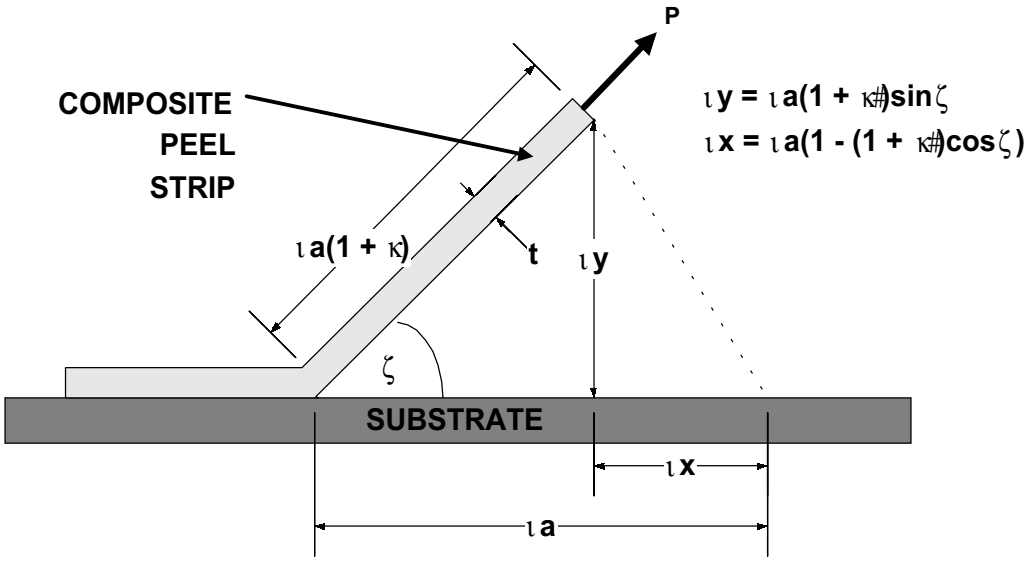

Figure 2.9: Schematic of the mechanics of the peel test set-up [57]

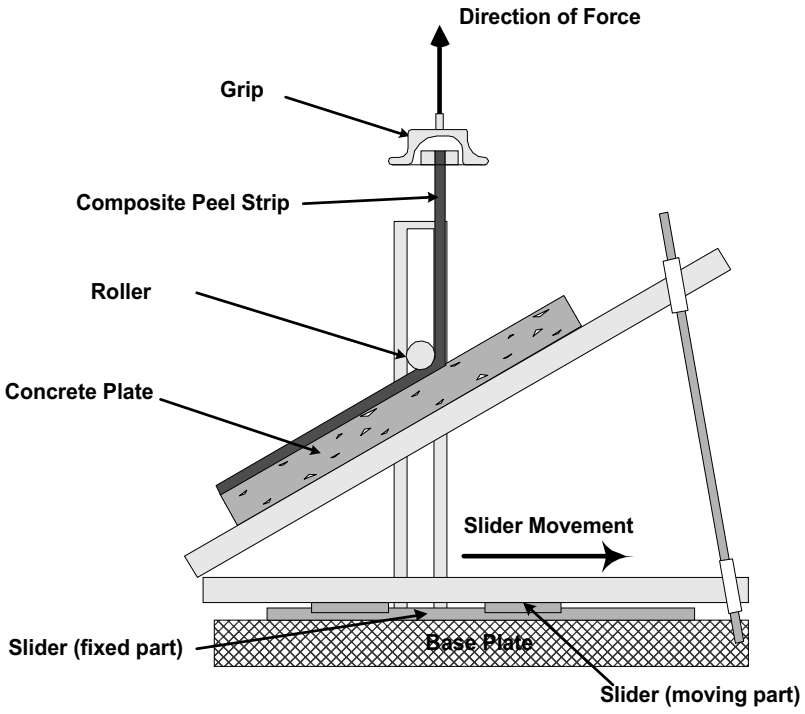

Figure 2.10: Details of peel apparatus [57]

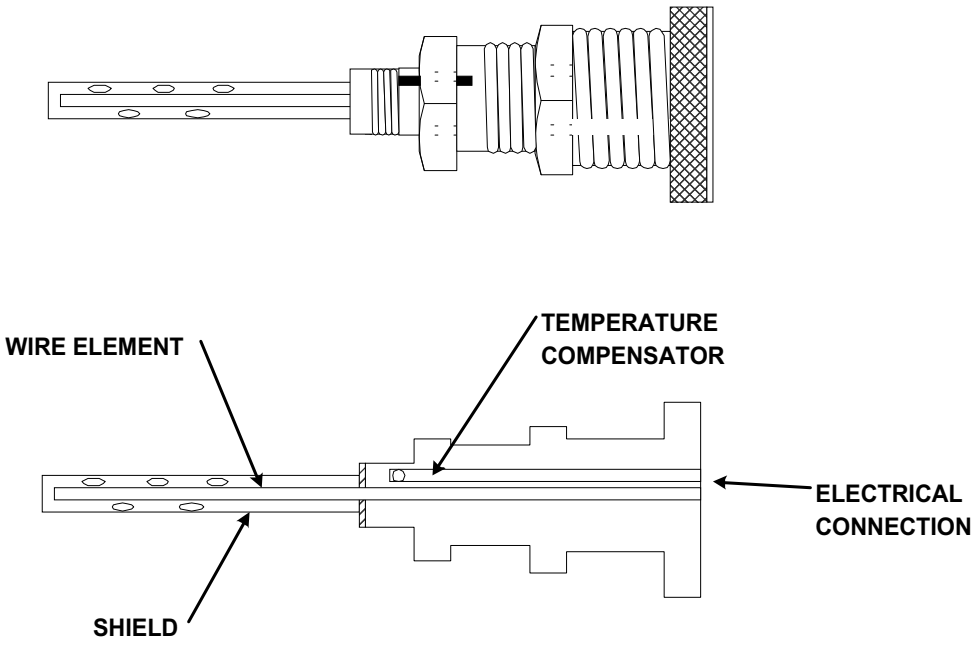

Figure 2.11: Electrical resistance probe for corrosion monitoring [64]

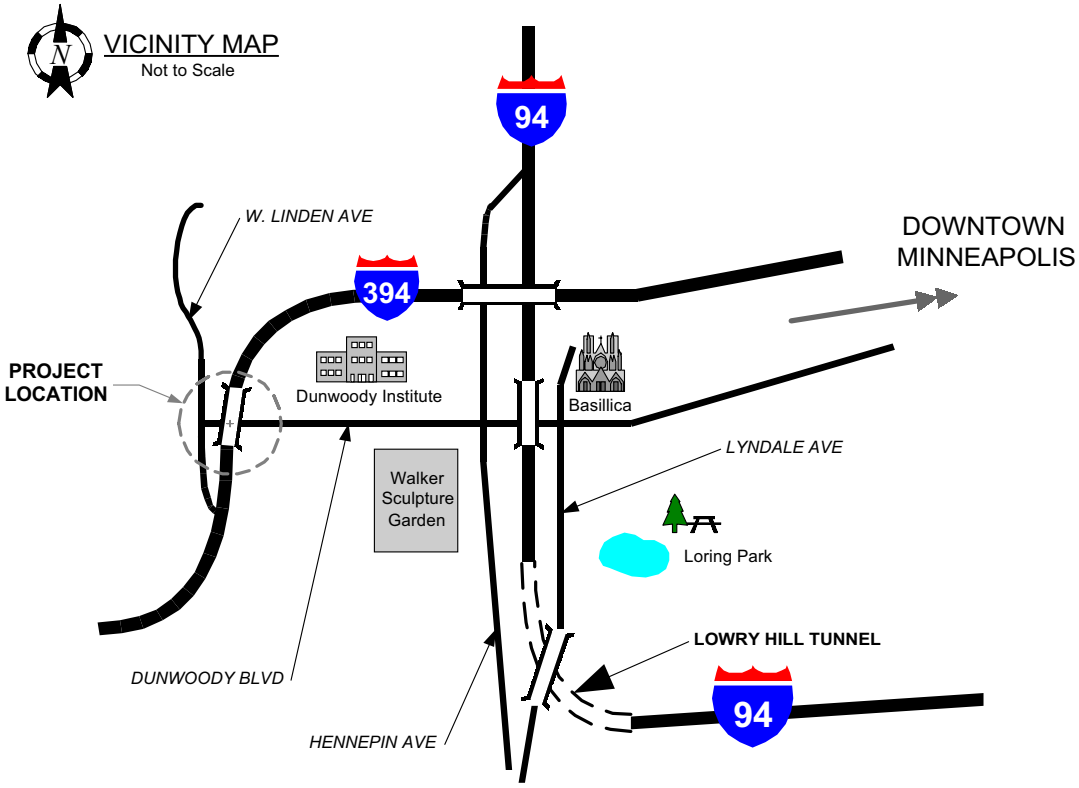

Figure 3.1: Location of Bridge #27831 in Minneapolis, MN

Figure 3.2: Intersection of Dunwoody Blvd. and Linden Ave. facing project site

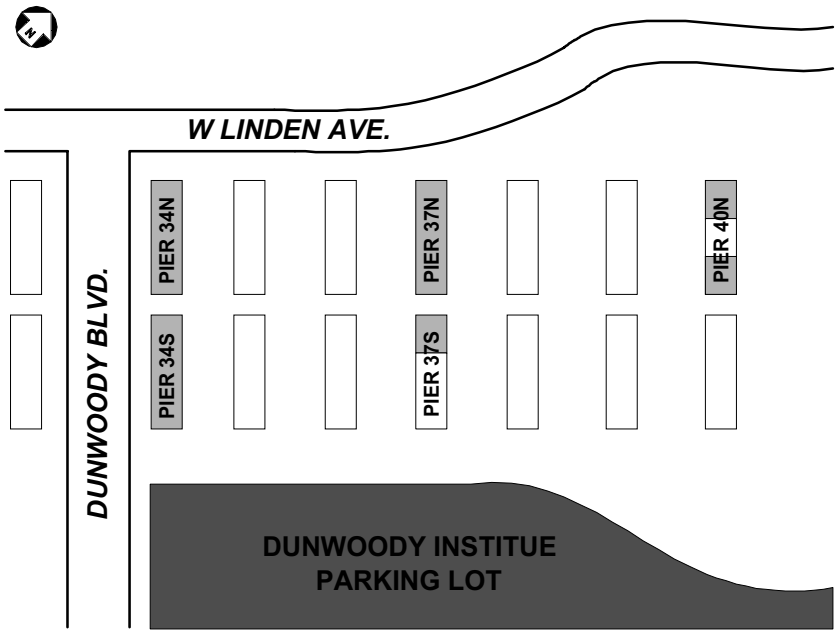

Figure 3.3: Location of columns and piers included in the investigation

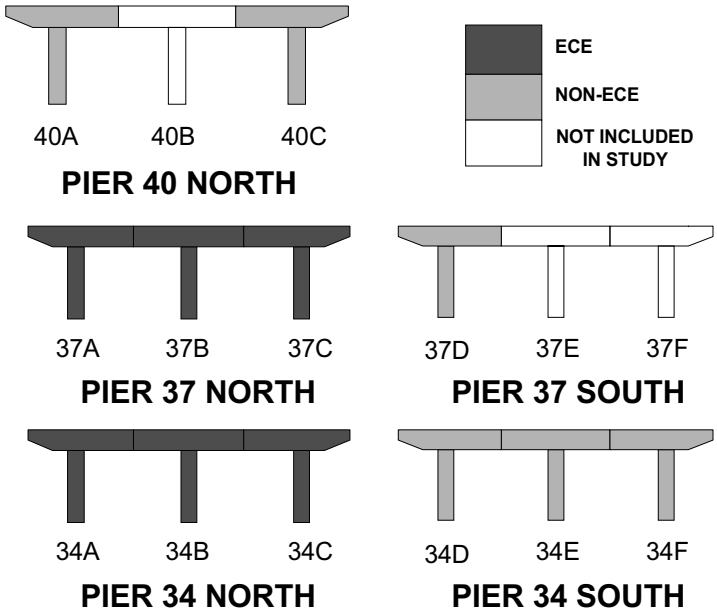

Figure 3.4: Elevation view of east face of structures included in investigation

Figure 3.5: Repair on Pier 34 North between columns 34B and 34C [66]

Figure 3.6: Close-up of column 34C after removal of damaged concrete [66]

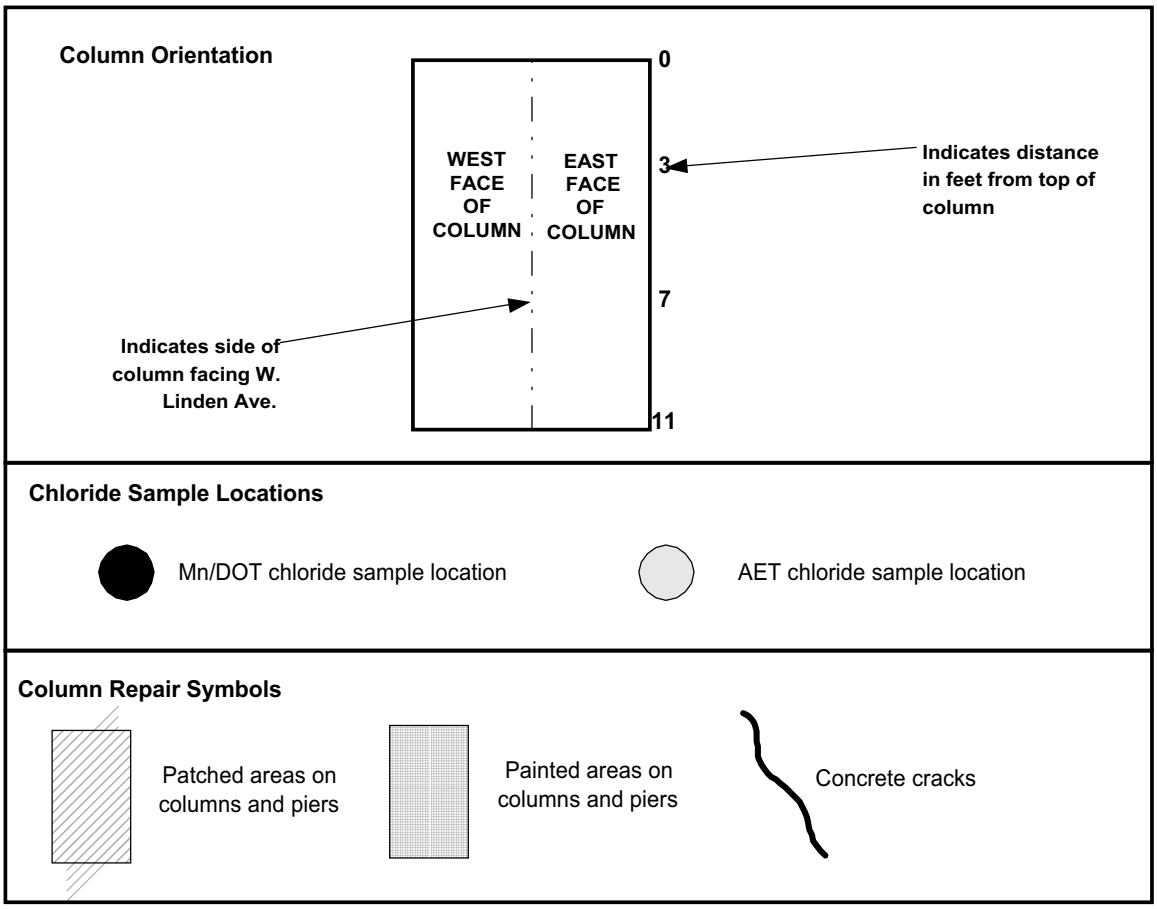

Figure 3.7: Legend for concrete repair and chloride sample location illustrations

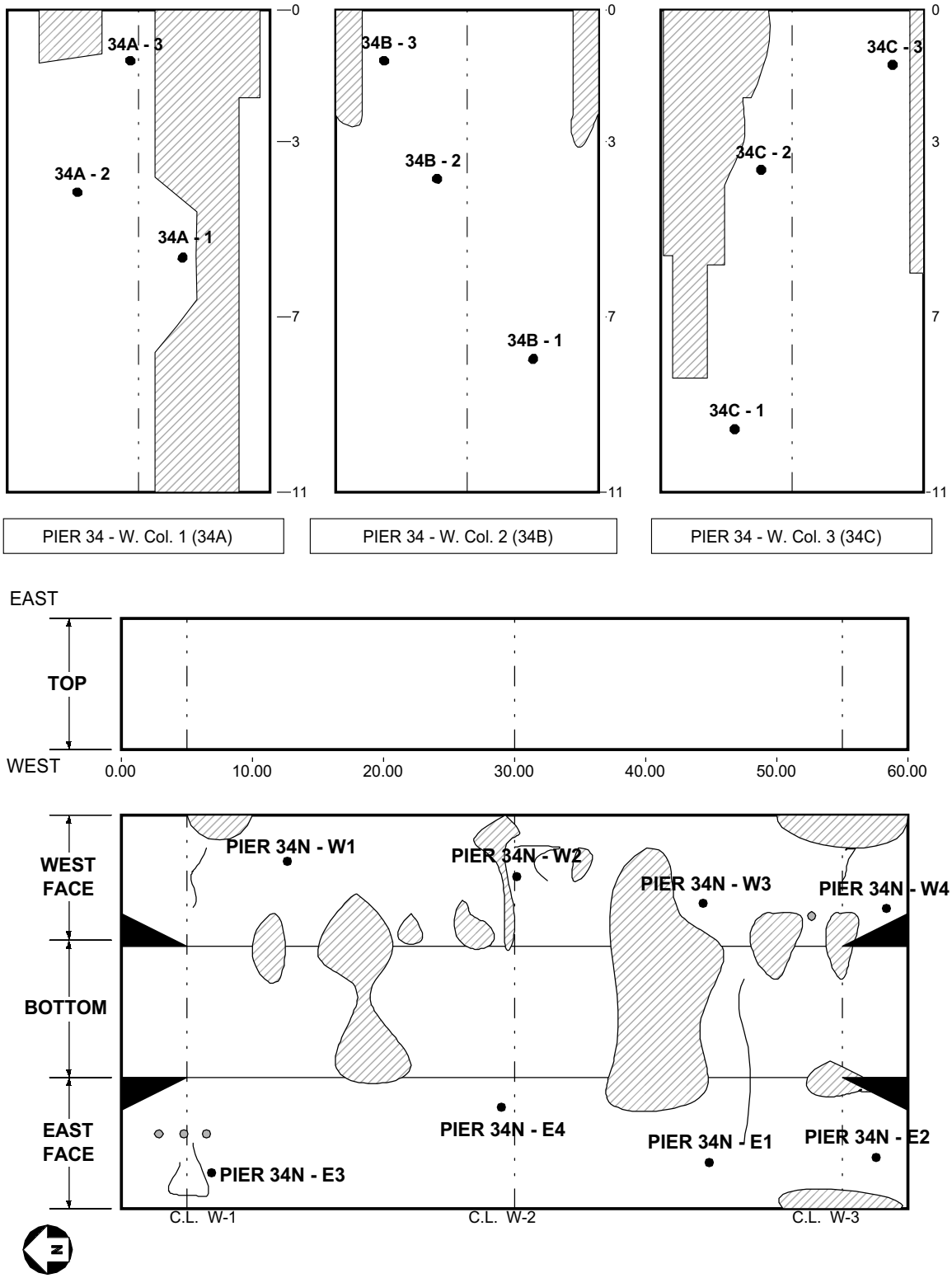

Figure 3.8: Chloride sample locations on Pier 34 North

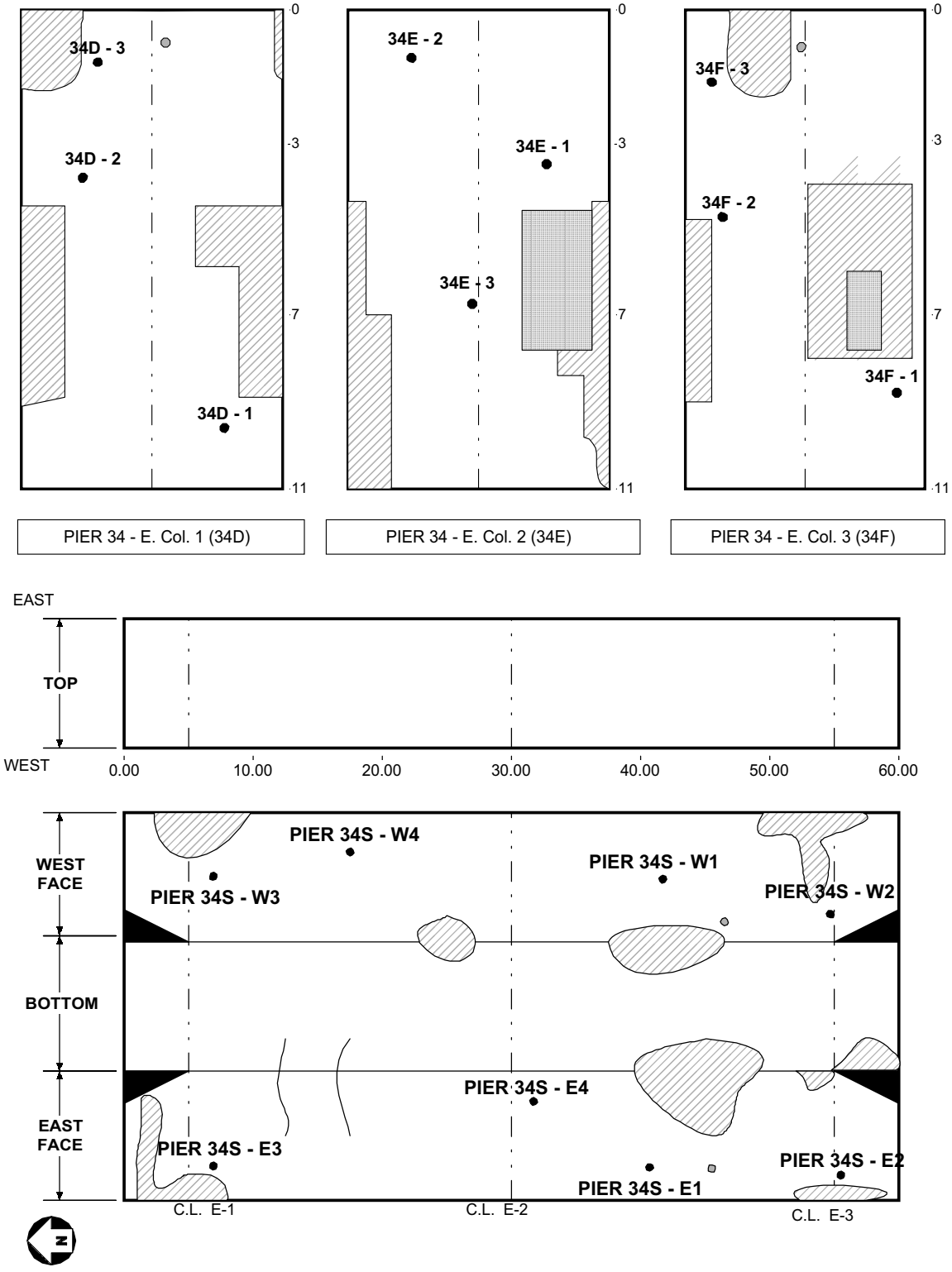

Figure 3.9: Chloride sample locations on Pier 34 South

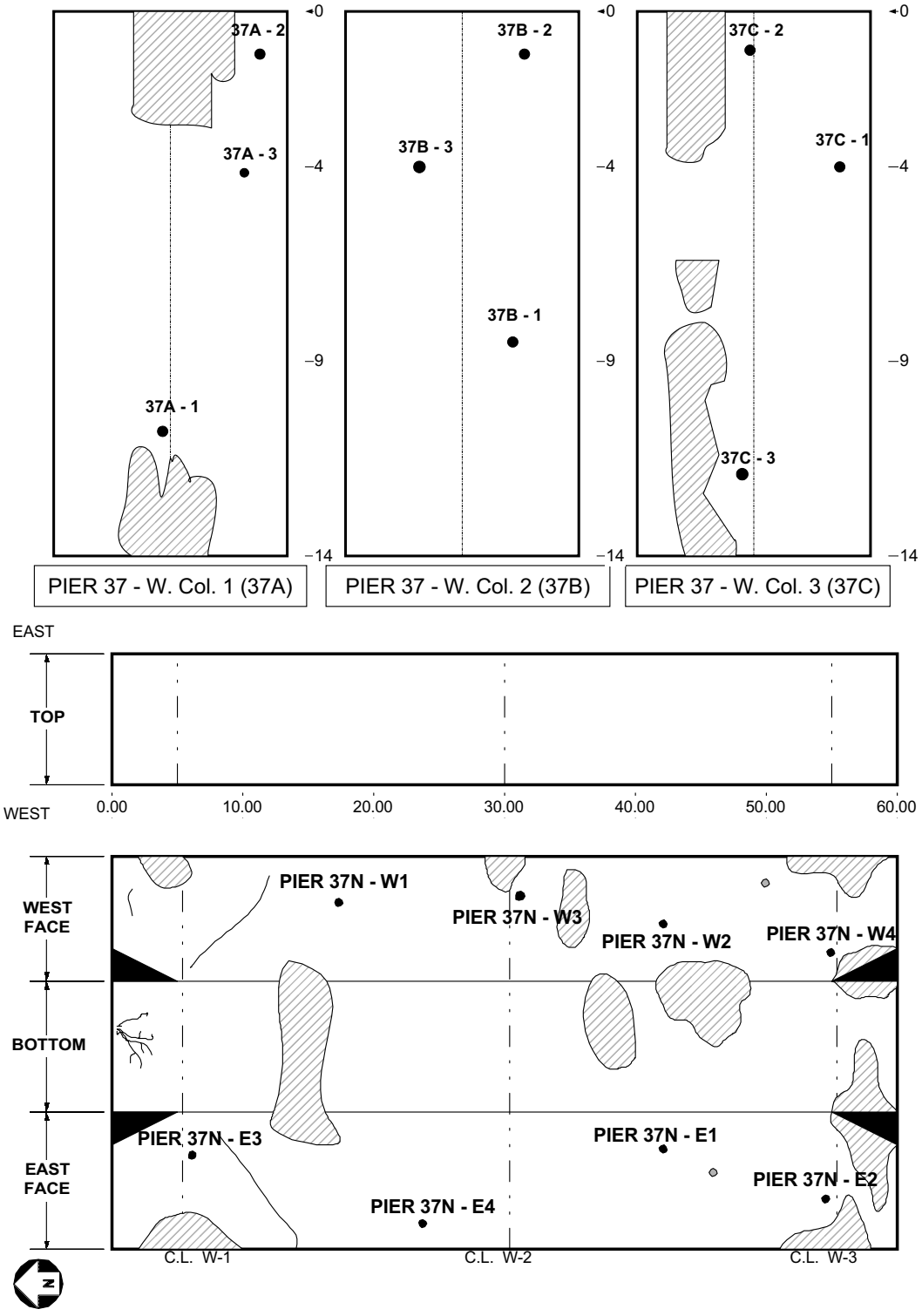

Figure 3.10: Chloride sample locations on Pier 37 North

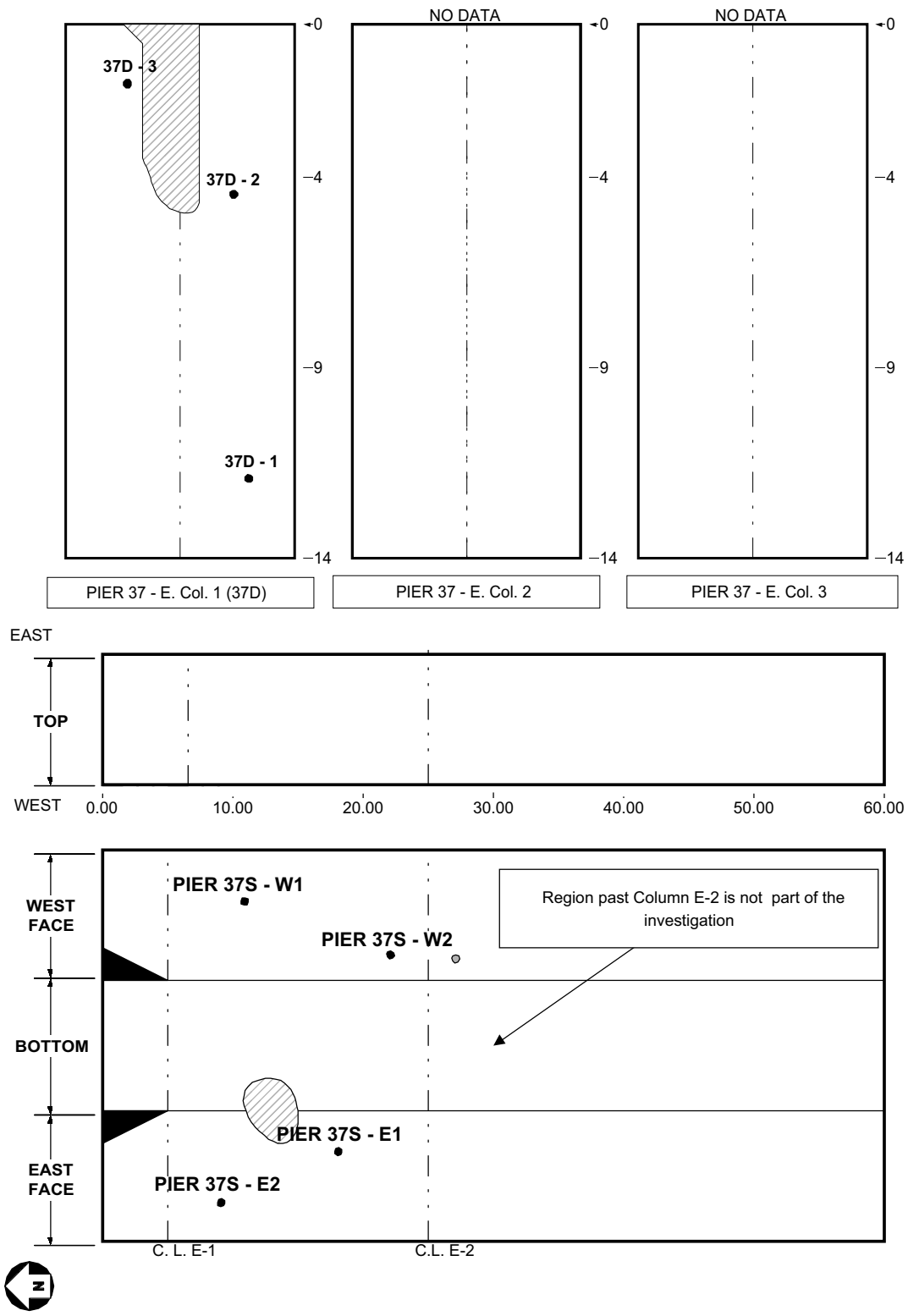

Figure 3.11: Chloride sample locations on Pier 37 South

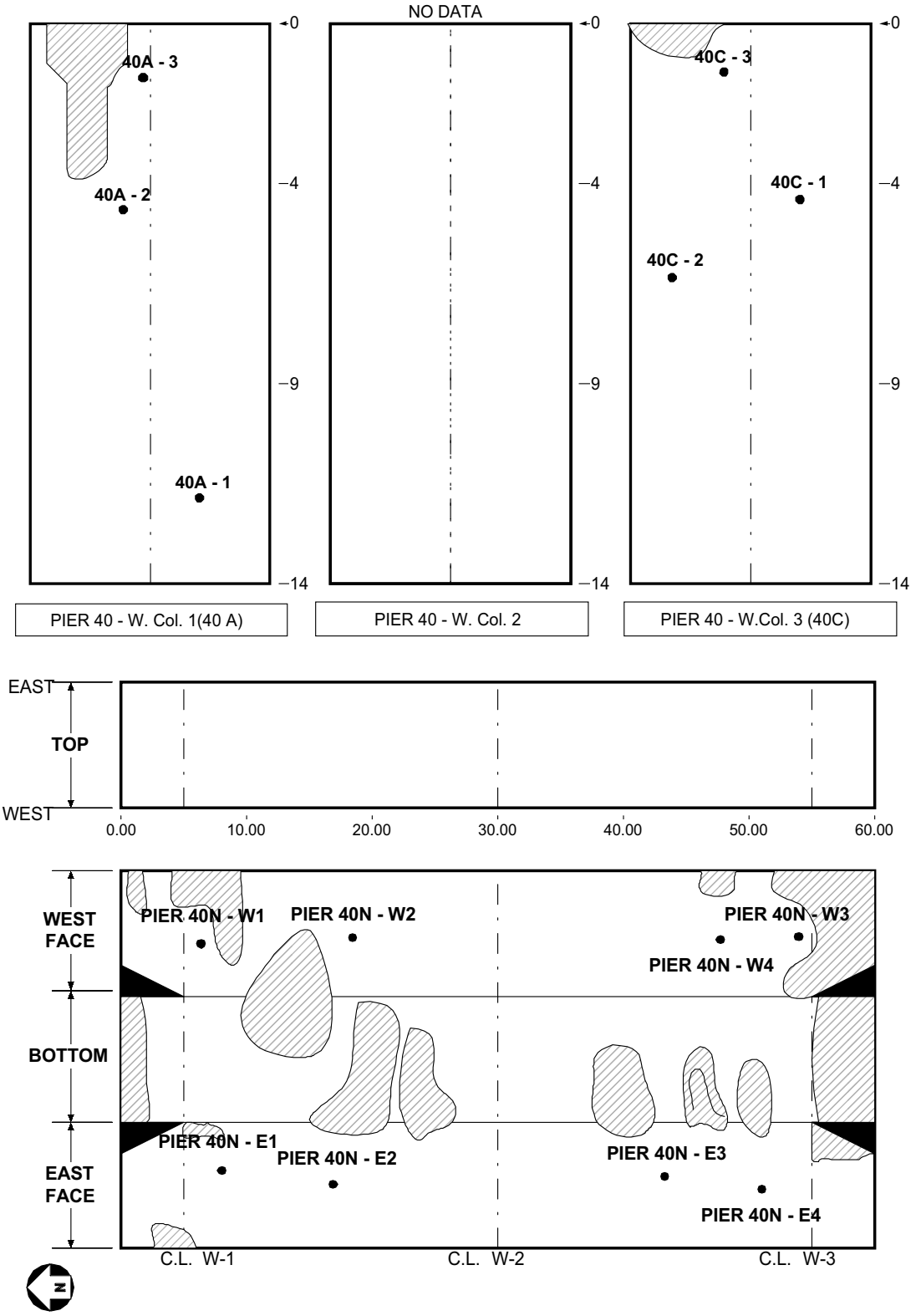

Figure 3.12: Chloride sample locations on Pier 40 North

Figure 3.13: Cellulose fiber application on a column in Regina, SK, Canada

Figure 3.14: ECE system in place on Pier 34 North

Figure 3.15: ECE system in place on Pier 37 North

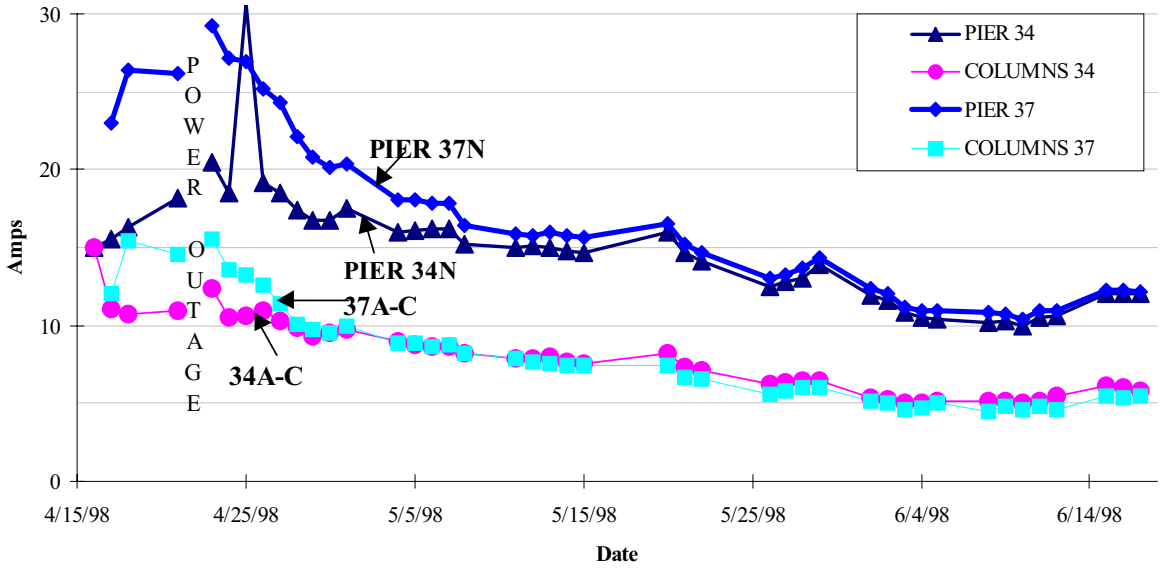

Figure 3.16: Current through treated structures during ECE process

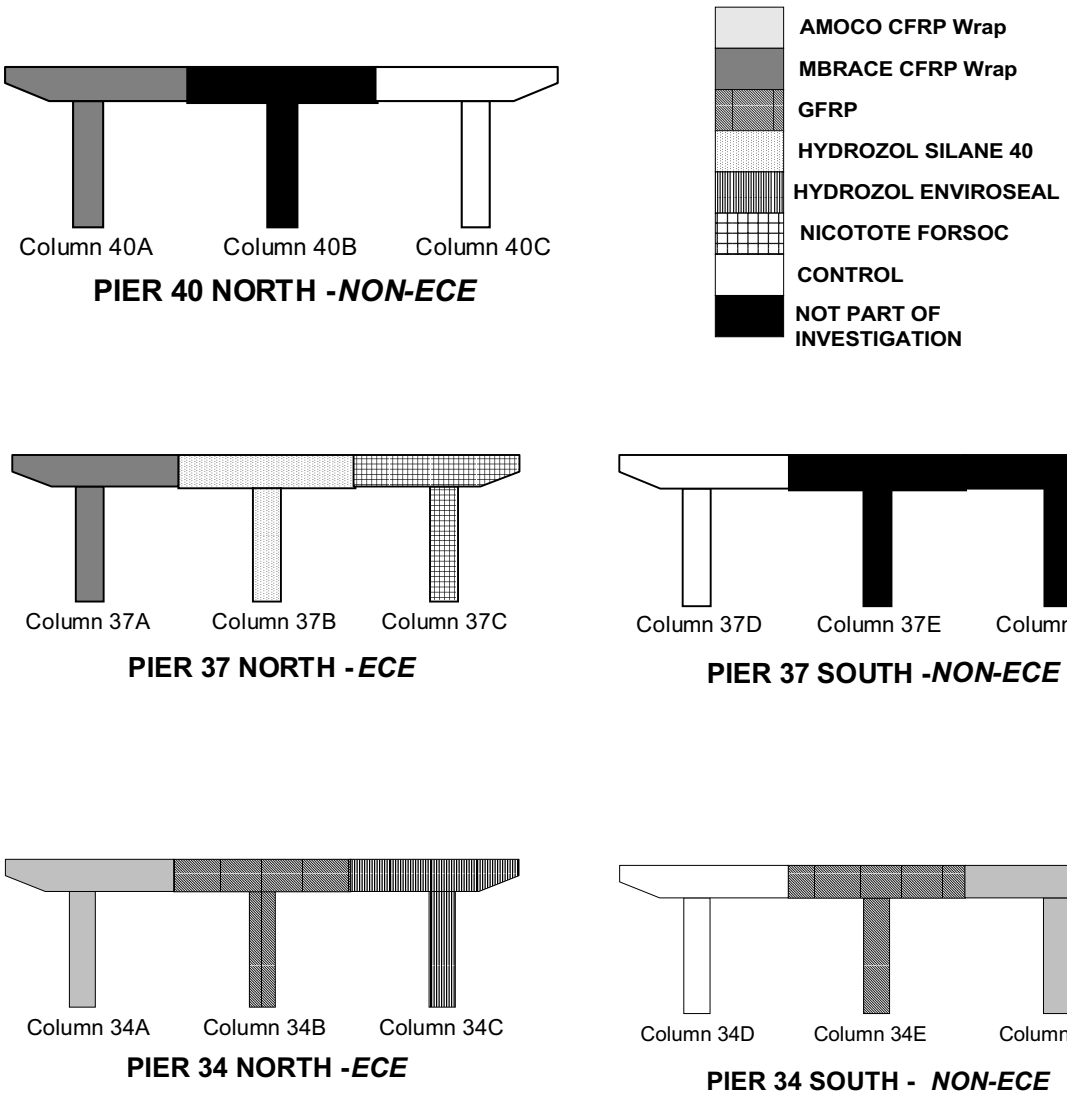

Figure 3.17: Elevation view of column and pier treatment schedule

Figure 3.18: MBrace CFRP in place on Column 40A

Figure 3.19: Installation of AMOCO CFRP in progress above Column 34F

Figure 3.20: Caulk seam at top of column and drip ledge along wrap overlap

Figure 3.21: Fabrication of diffusion test specimens of MBrace CFRP composite

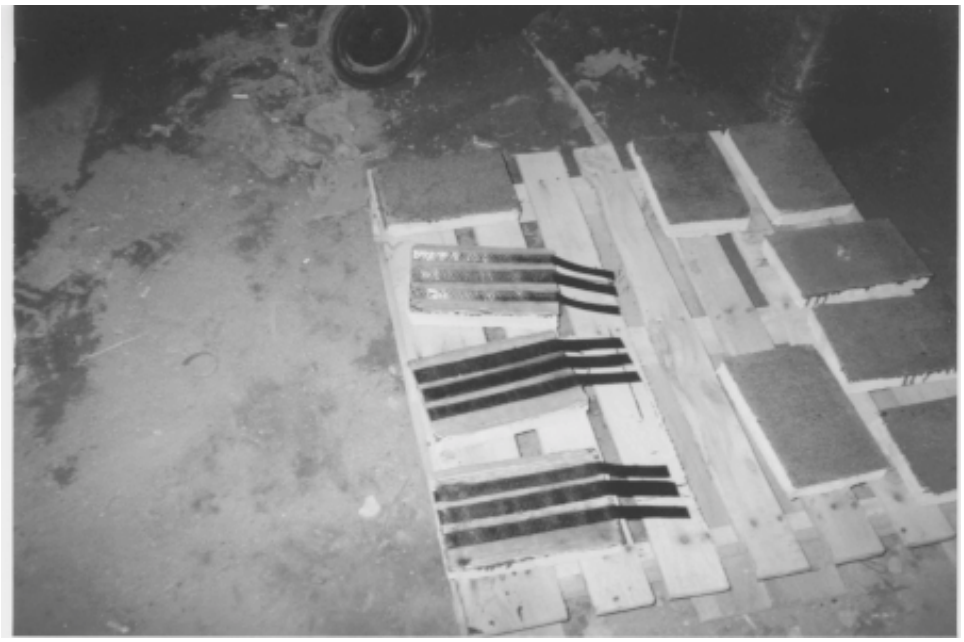

Figure 3.22: Peel test specimens for the MBrace CFRP system

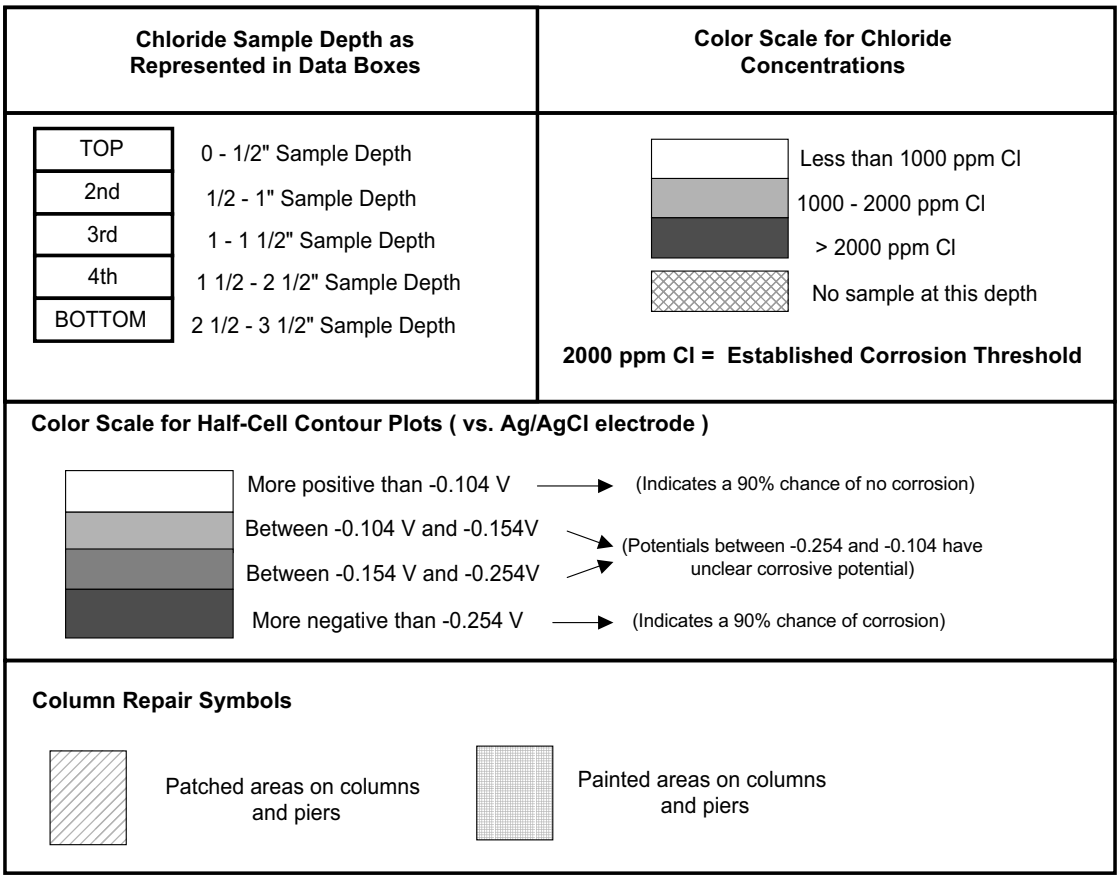

Figure 4.1: Legend for site condition illustrations

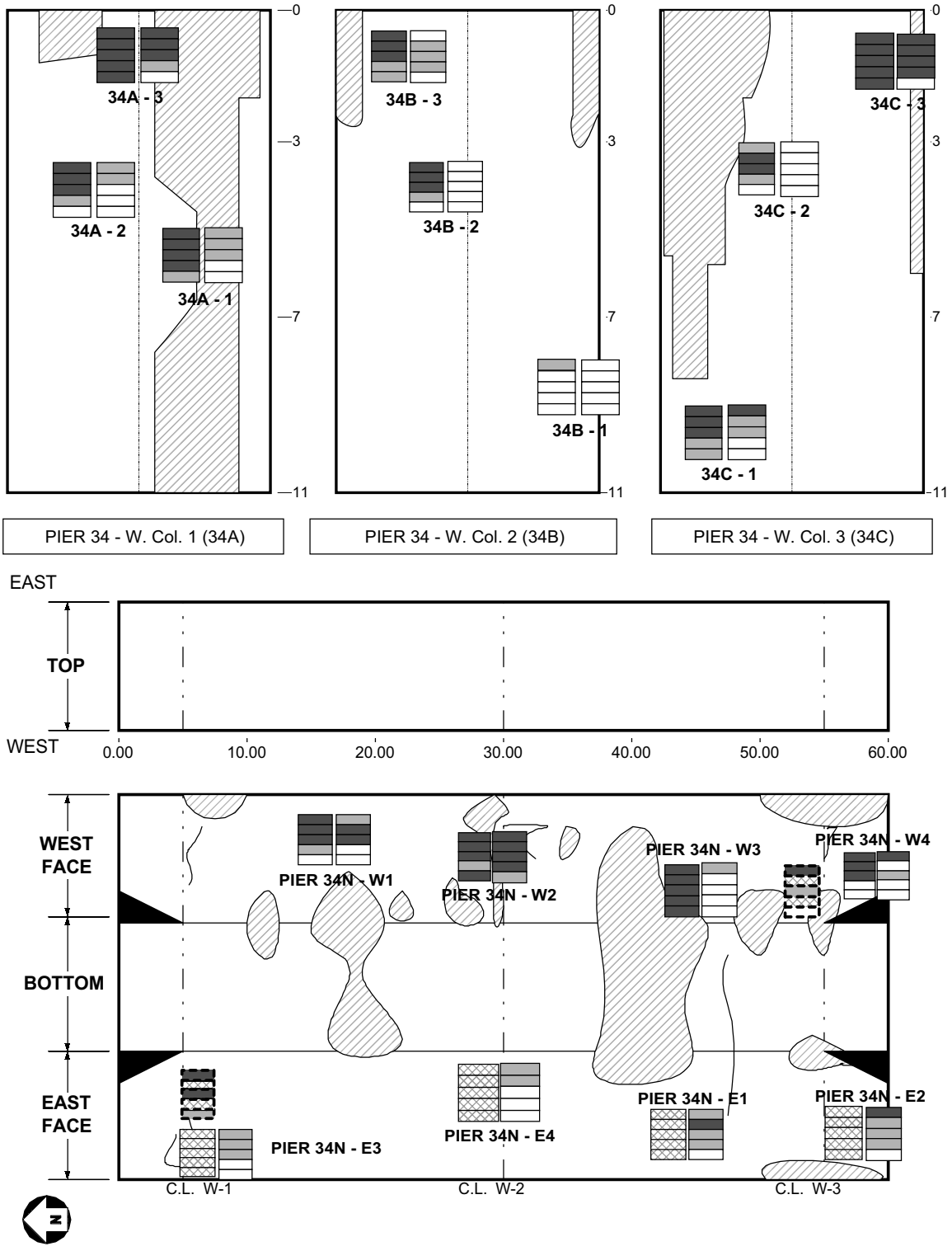

Figure 4.2: Pre and post ECE chloride concentrations on Pier 34 North (ECE)

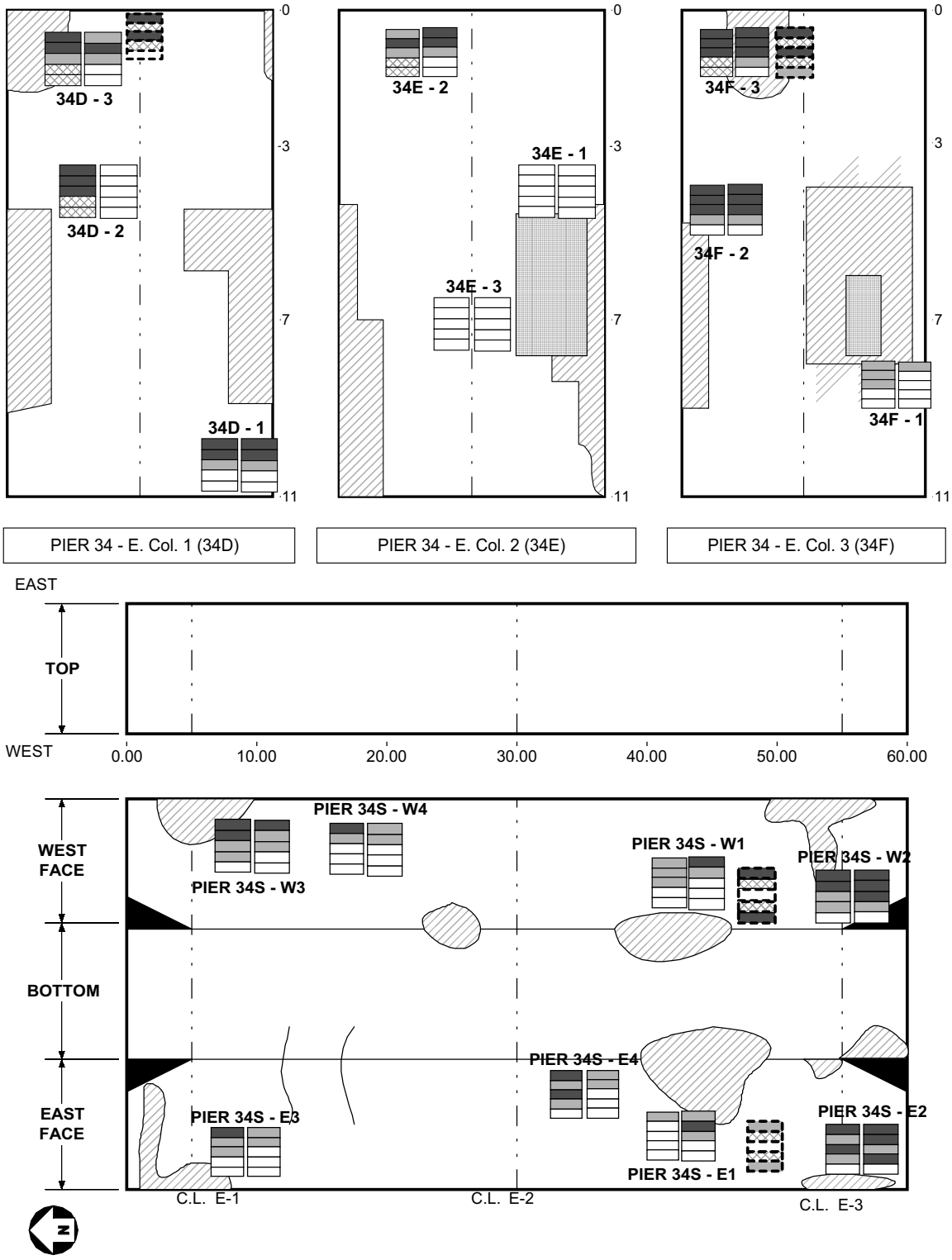

Figure 4.3: Pre and post ECE chloride concentrations on Pier 34 South (non-ECE)

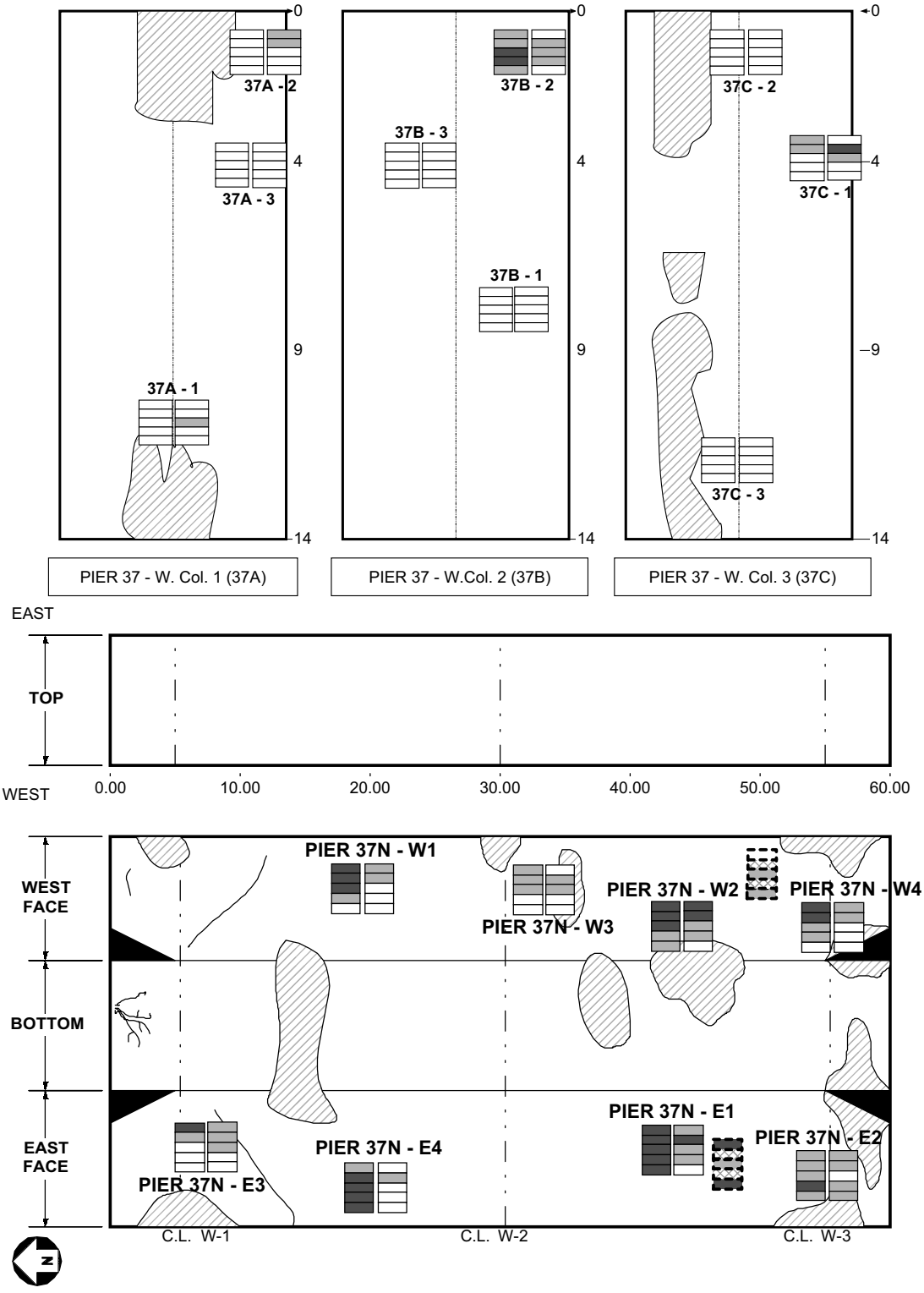

Figure 4.4: Pre and post ECE chloride concentrations on Pier 37 North (ECE)

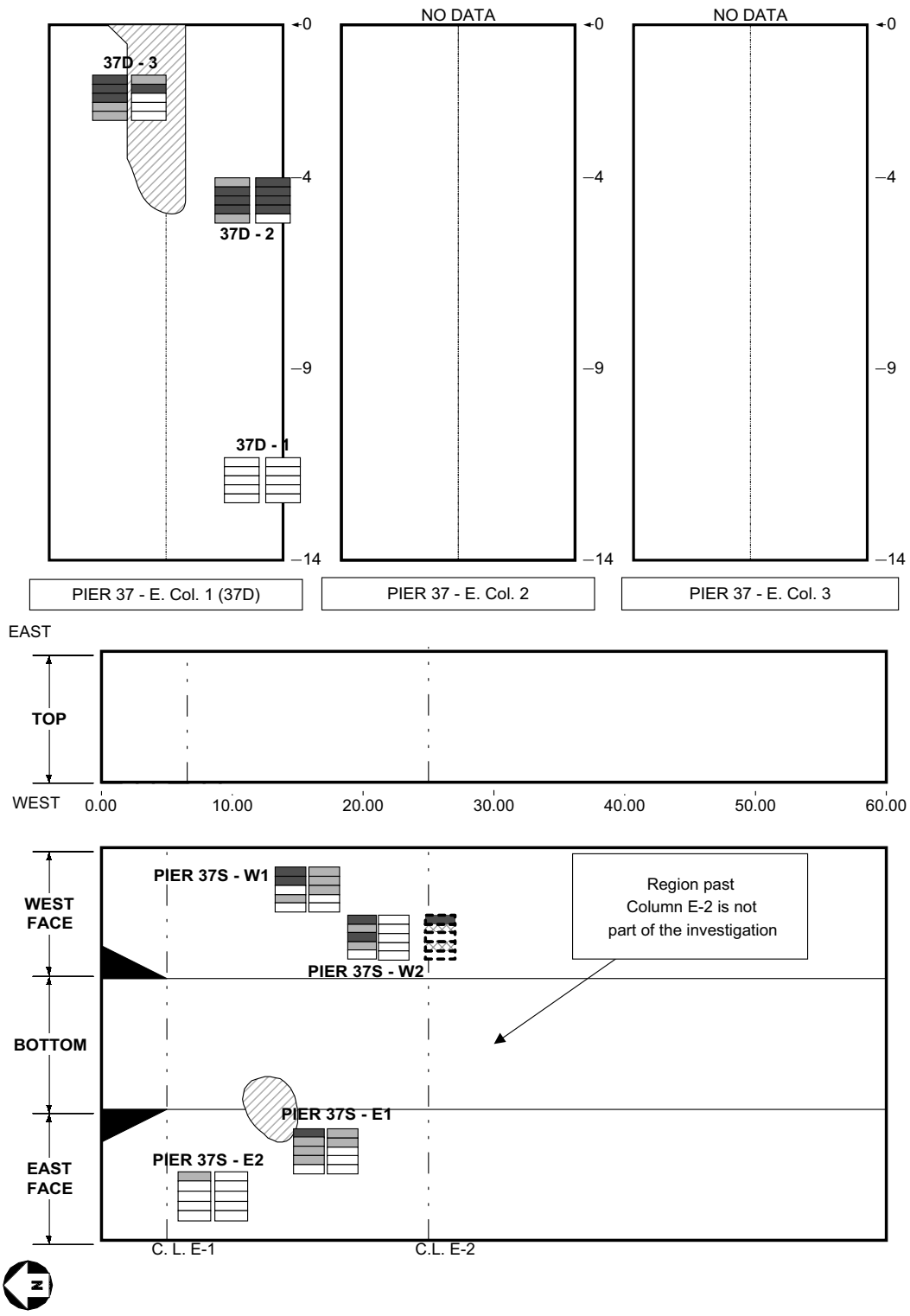

Figure 4.5: Pre and post ECE chloride concentrations on Pier 37 South (non-ECE)

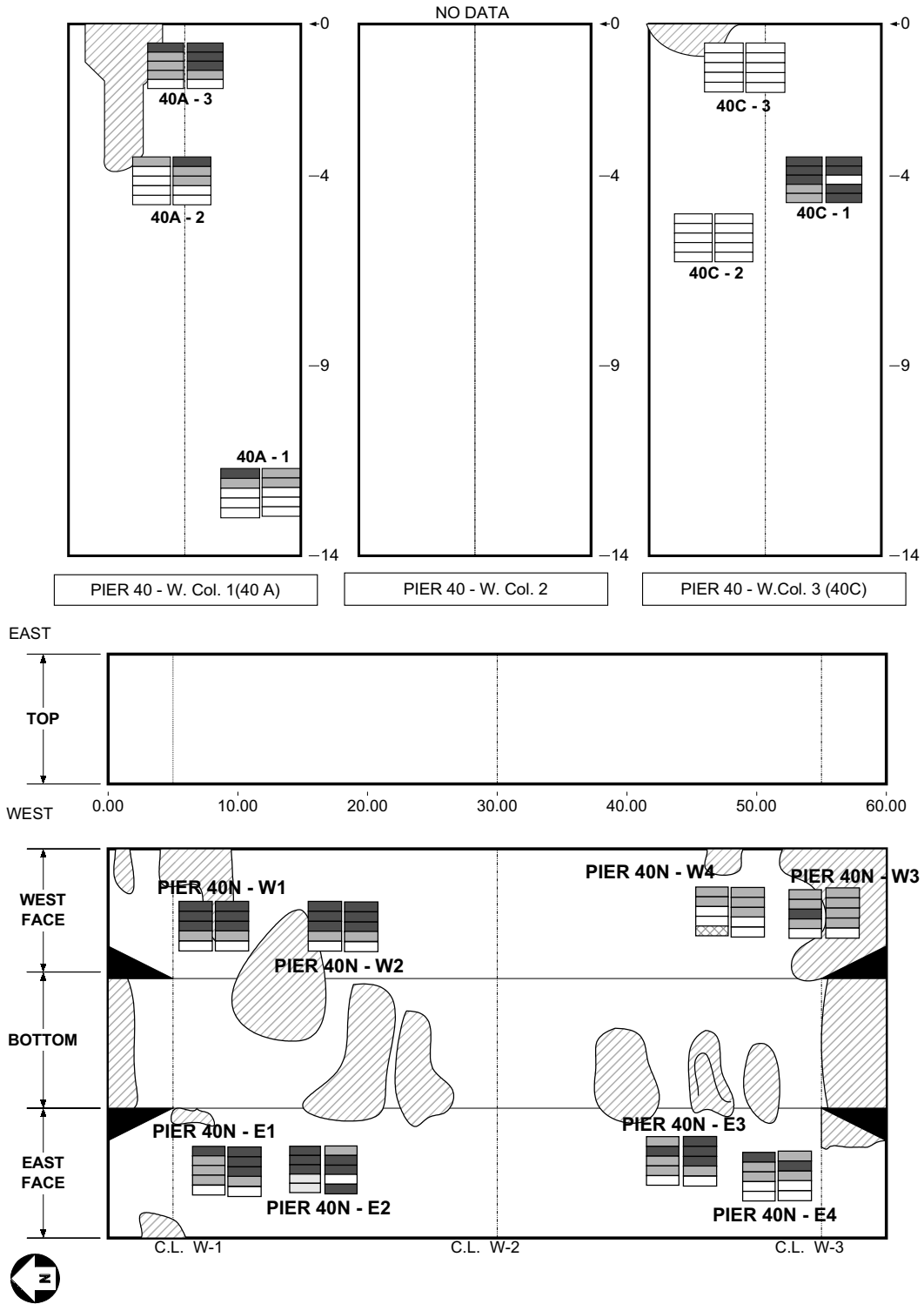

Figure 4.6: Pre and post ECE chloride concentrations on Pier 40 North (non-ECE)

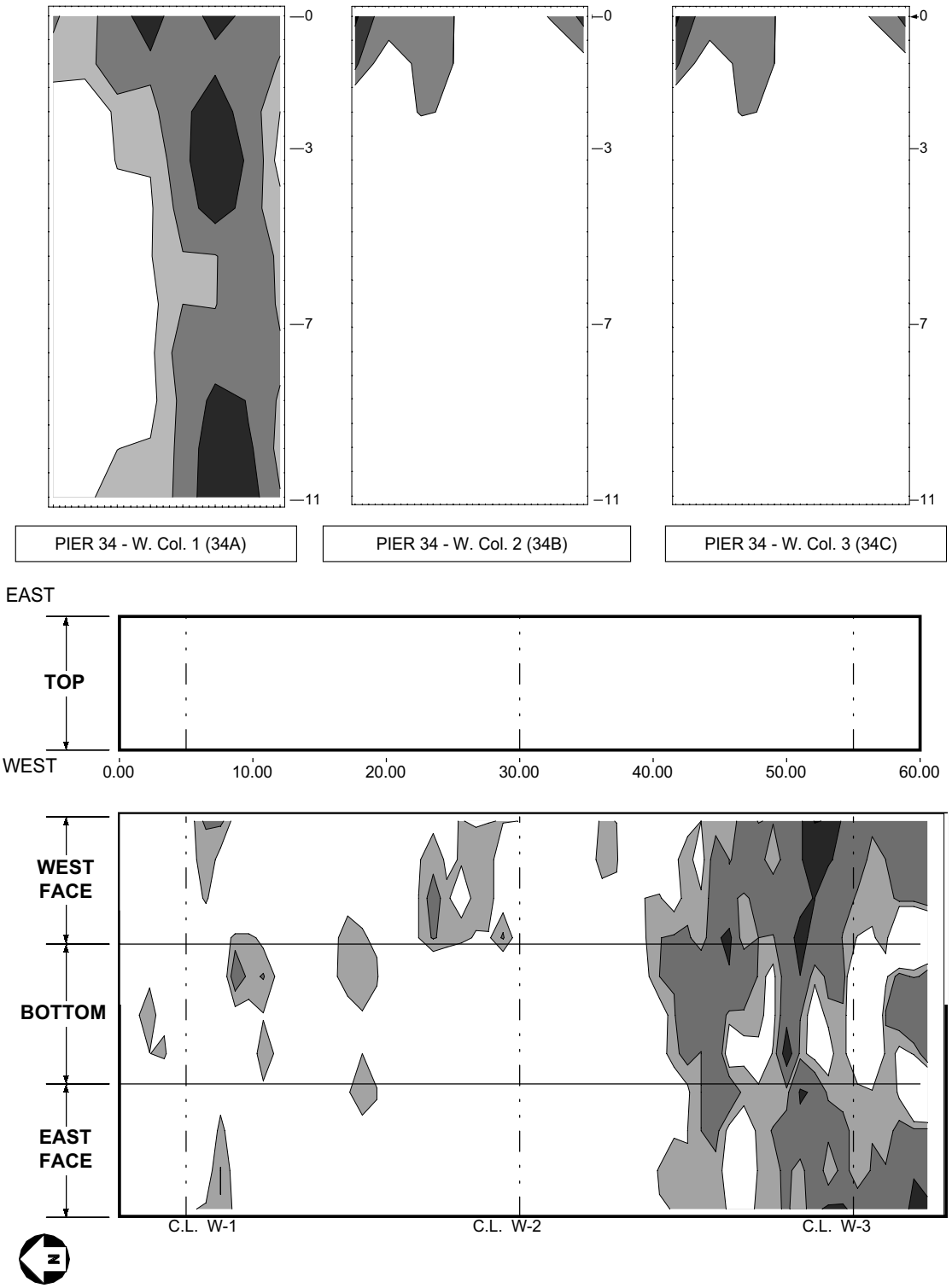

Figure 4.7: Contour plots of half-cell potential on Pier 34 North

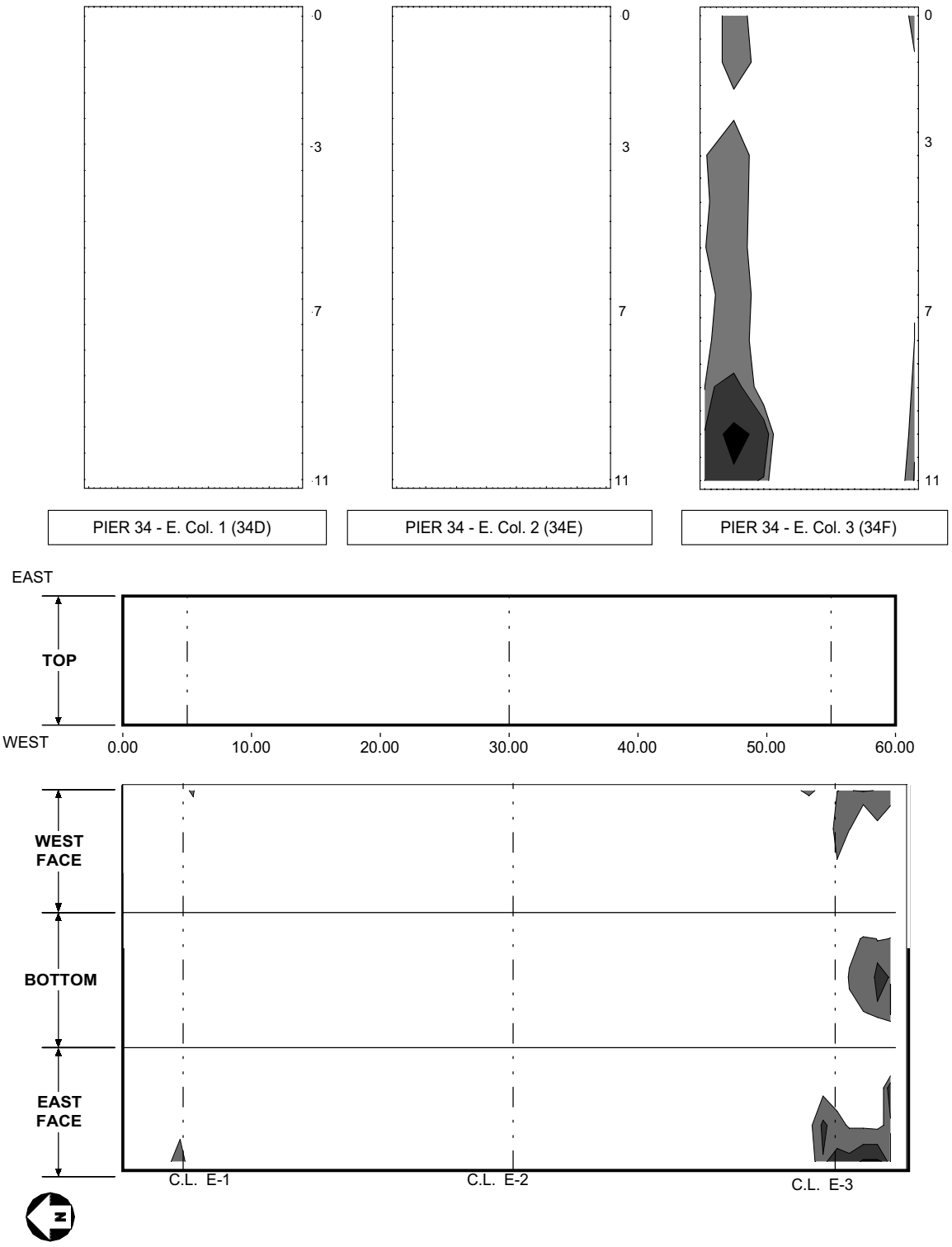

Figure 4.8: Contour plots of half-cell potential on Pier 34 South

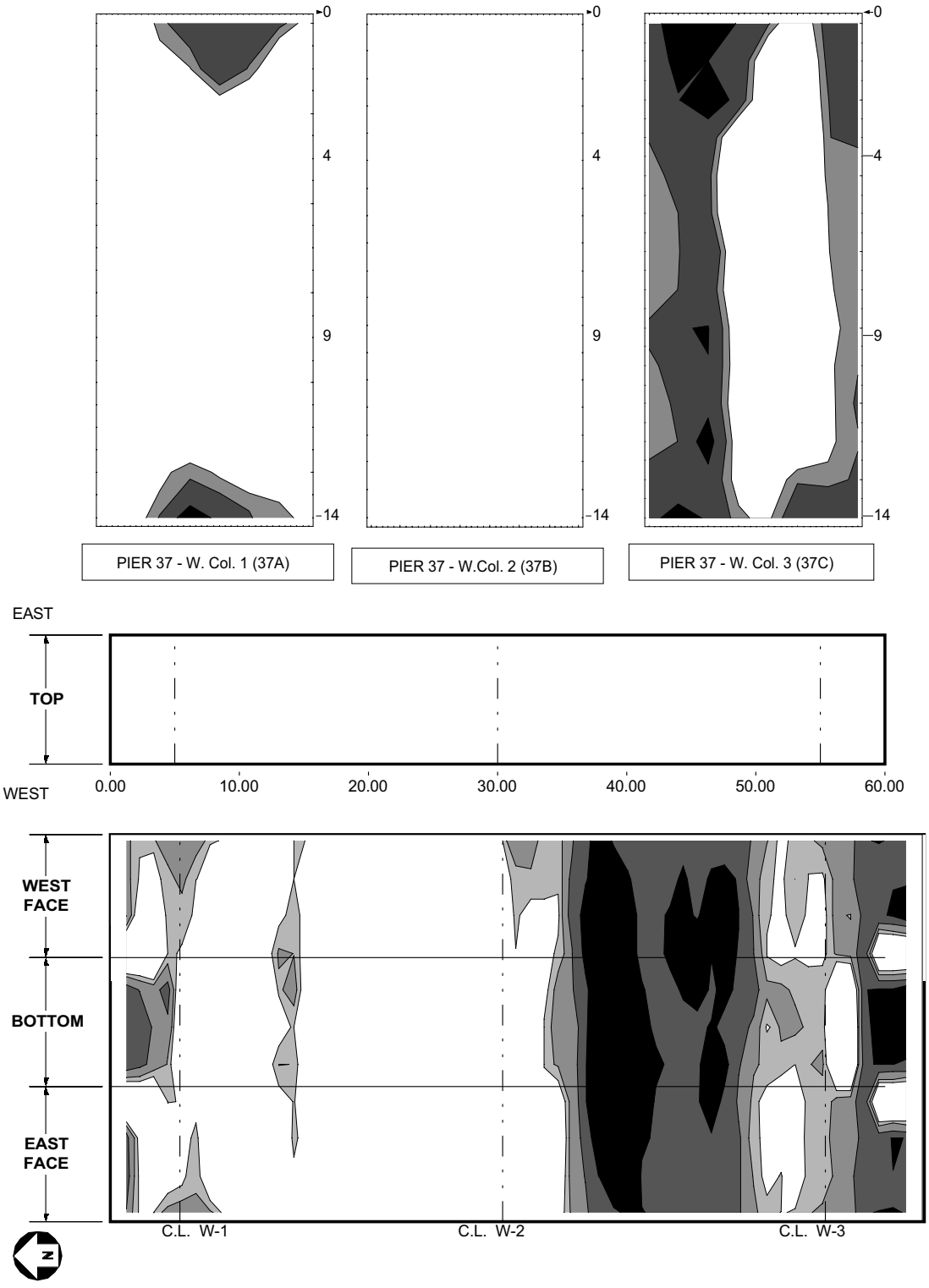

Figure 4.9: Contour plots of half-cell potential on Pier 37 North

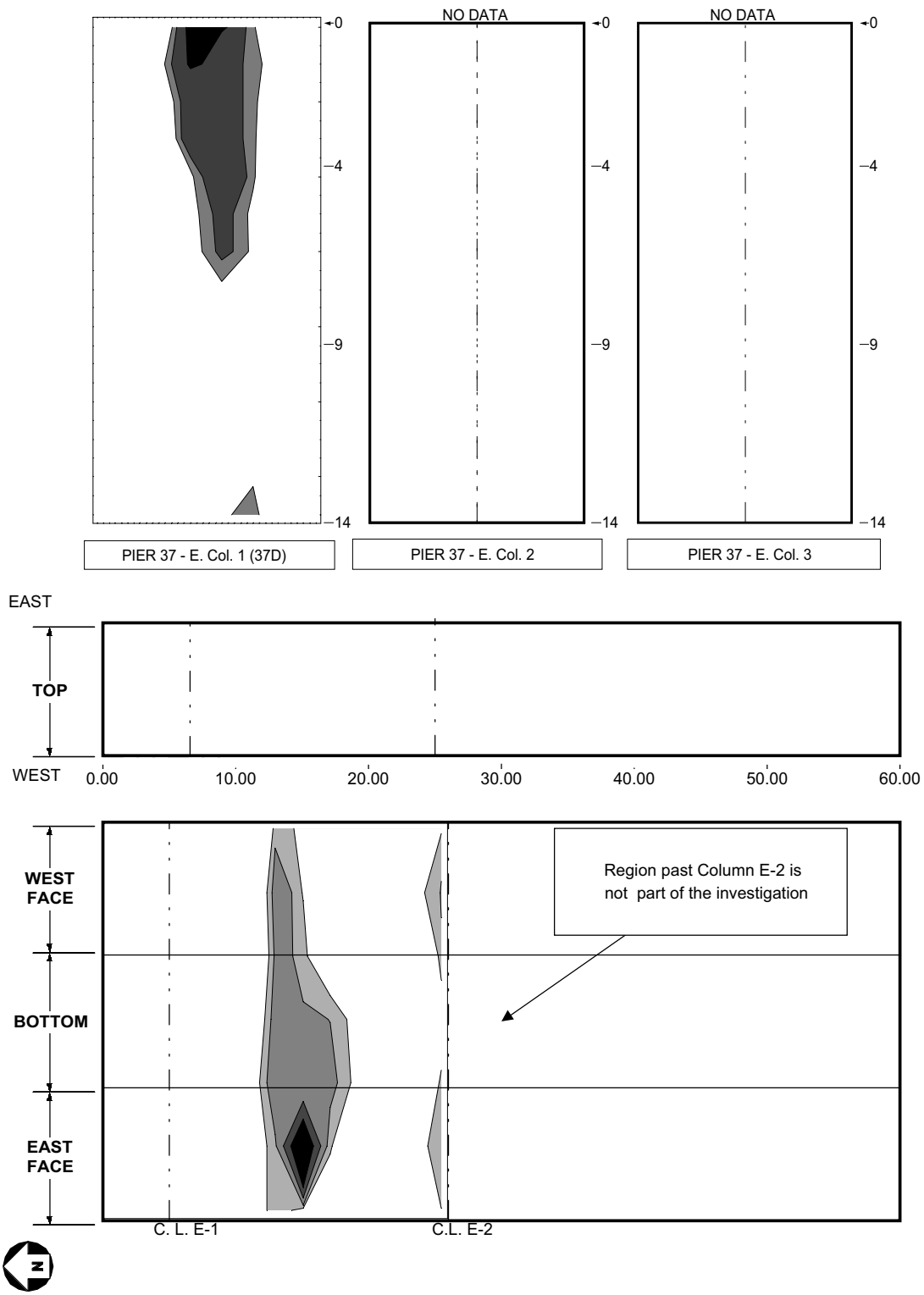

Figure 4.10: Contour plots of half-cell potential on Pier 37 South

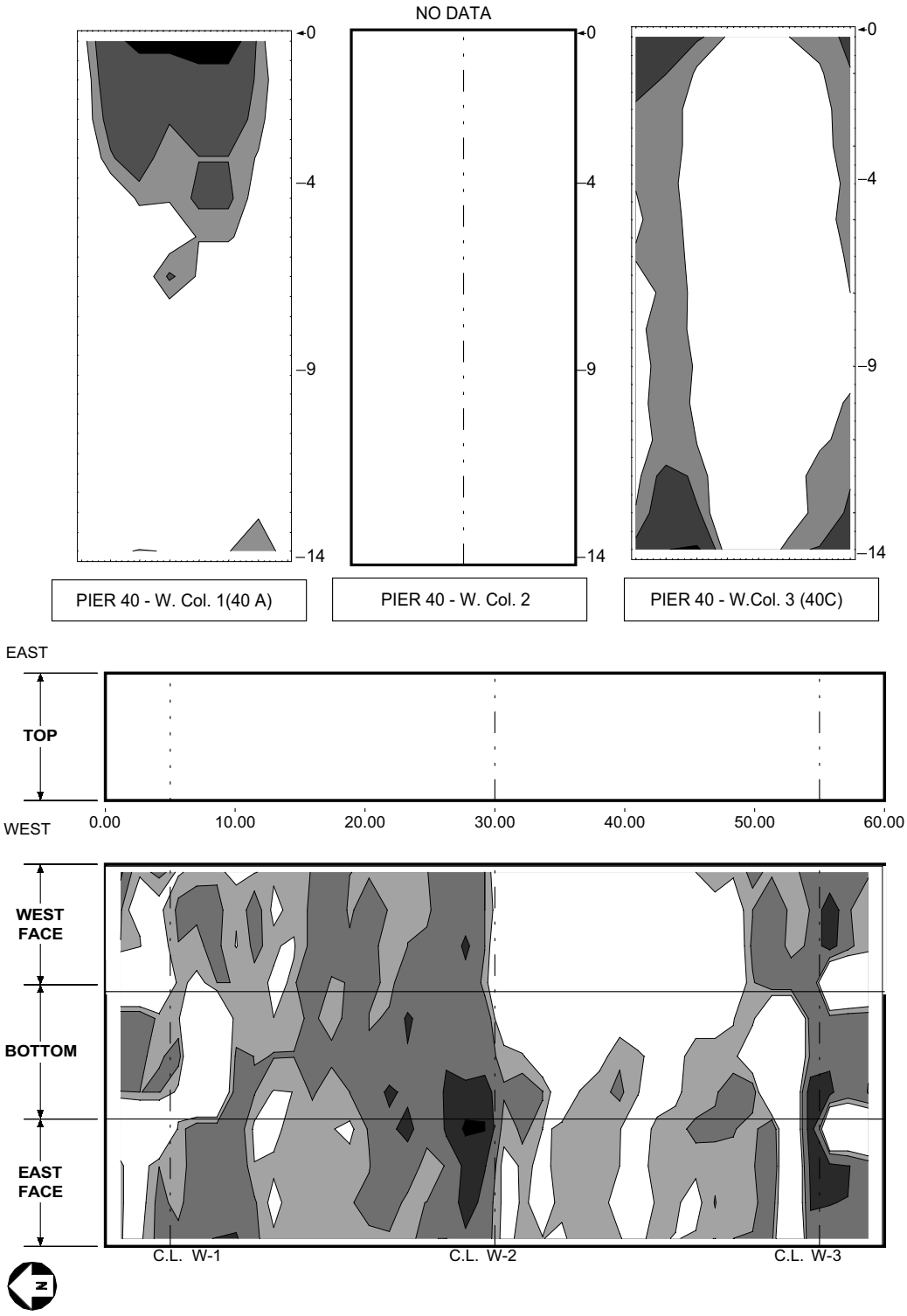

Figure 4.11: Contour plots of half-cell potentials on Pier 40 North

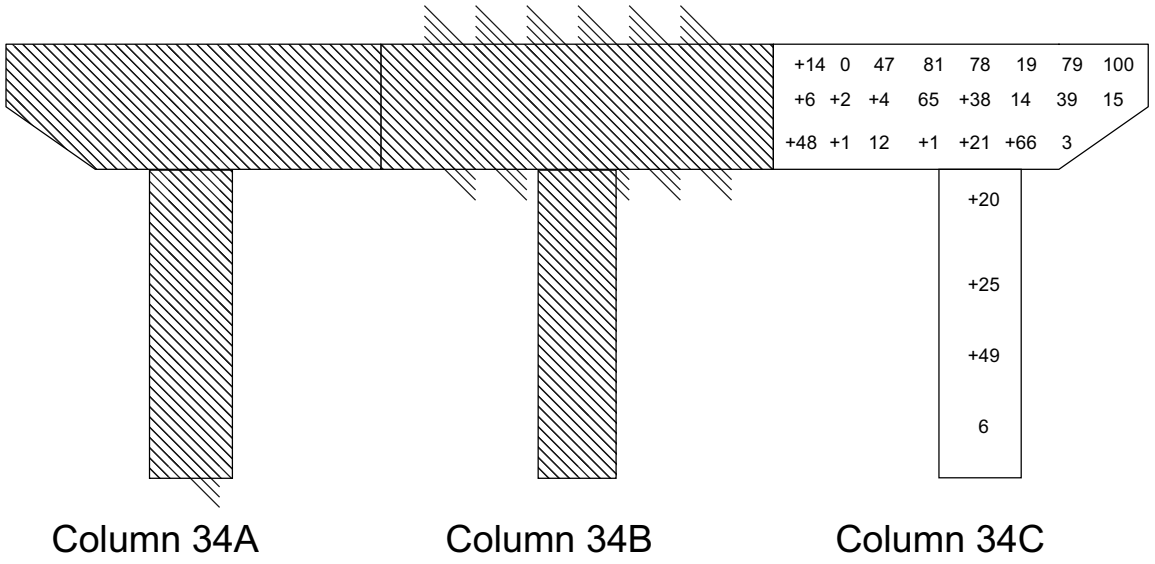

PIER 34 NORTH - WEST FACE

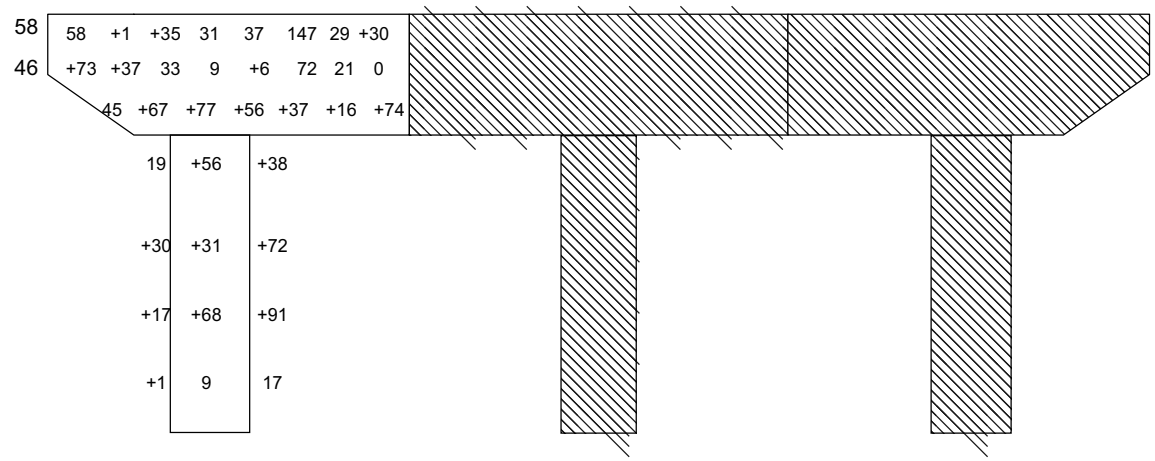

PIER 34 NORTH - EAST FACE

FRP WRAPPING

Figure 4.12: Post-ECE half-cell potentials, in millivolts, on Pier 34 North [66]

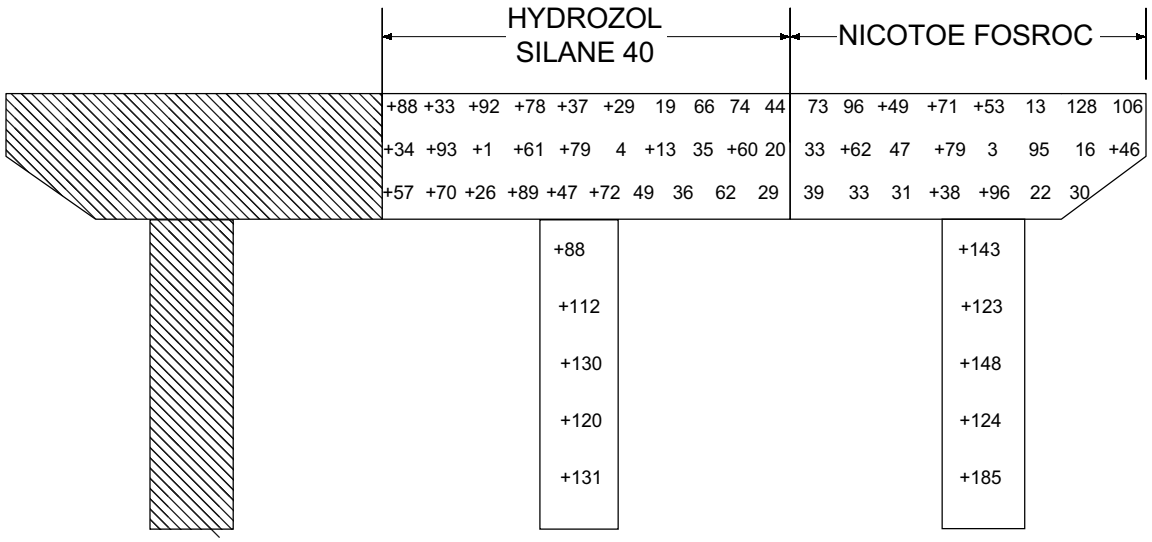

Column 37A Column 37B Column 37C

PIER 37 NORTH - WEST FACE

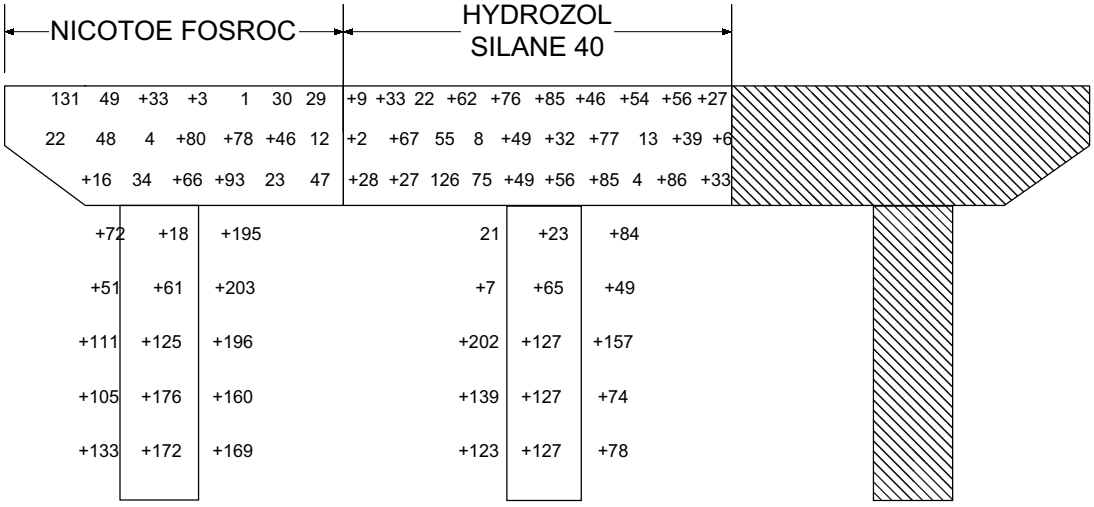

Column 37C Column 37B Column 37A

PIER 37 NORTH - EAST FACE

FRP WRAPPING

Figure 4.13: Post-ECE half-cell potentials, in millivolts, on Pier 37 North [66]

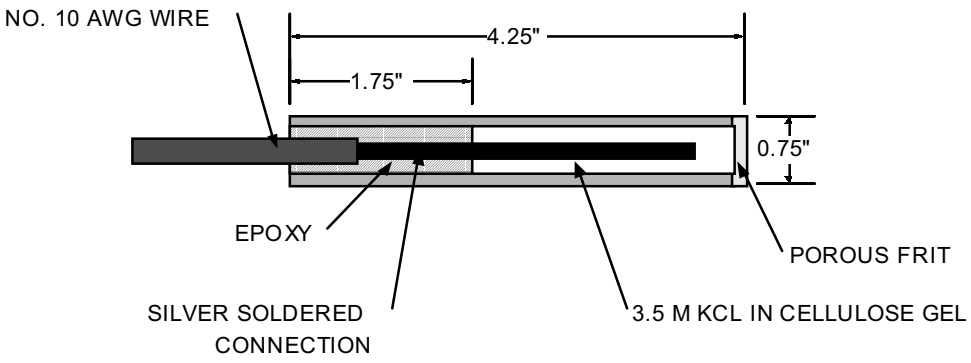

Figure 5.1: Schematic of Ag/AgCl reference electrode

Figure 5.2: Picture of an embeddable half-cell

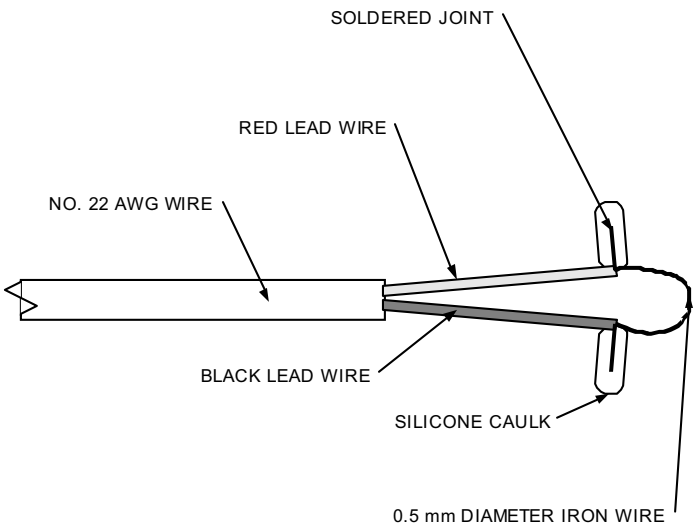

Figure 5.3: Schematic of large resistivity probe

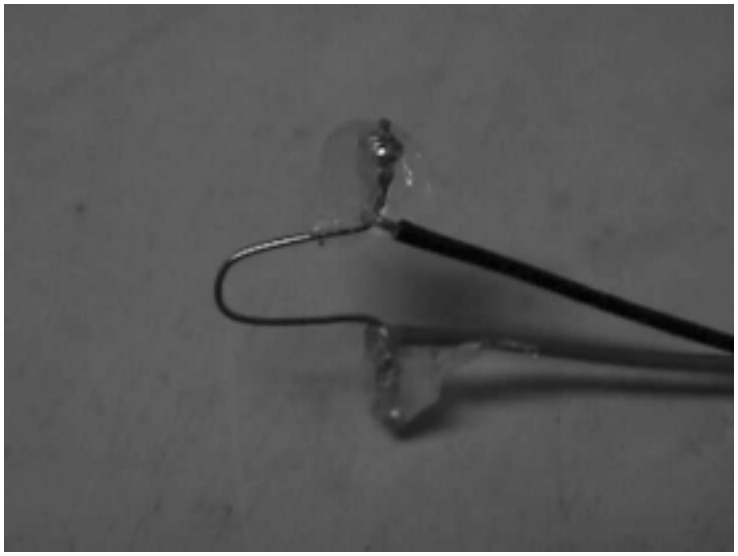

Figure 5.4: Picture of large resistivity probe

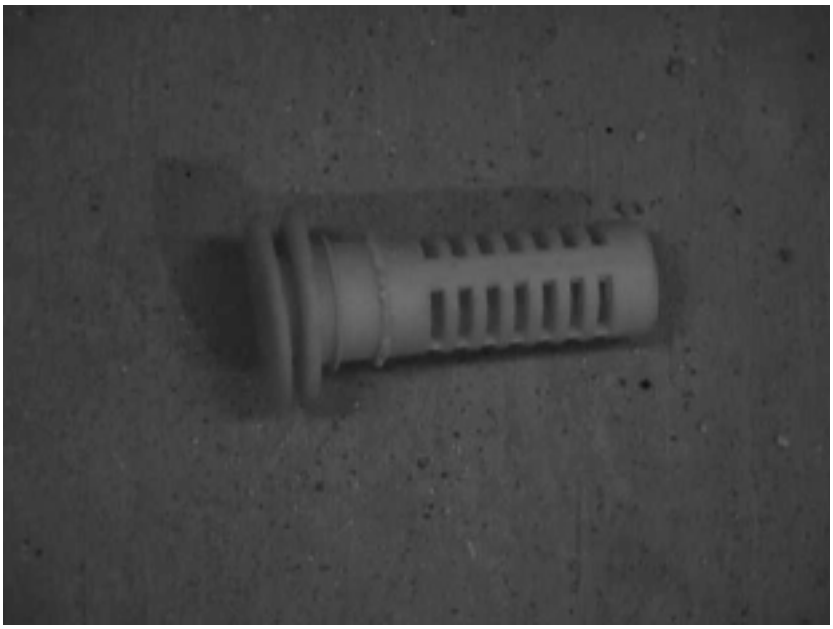

Figure 5.5: Picture of moisture sleeve

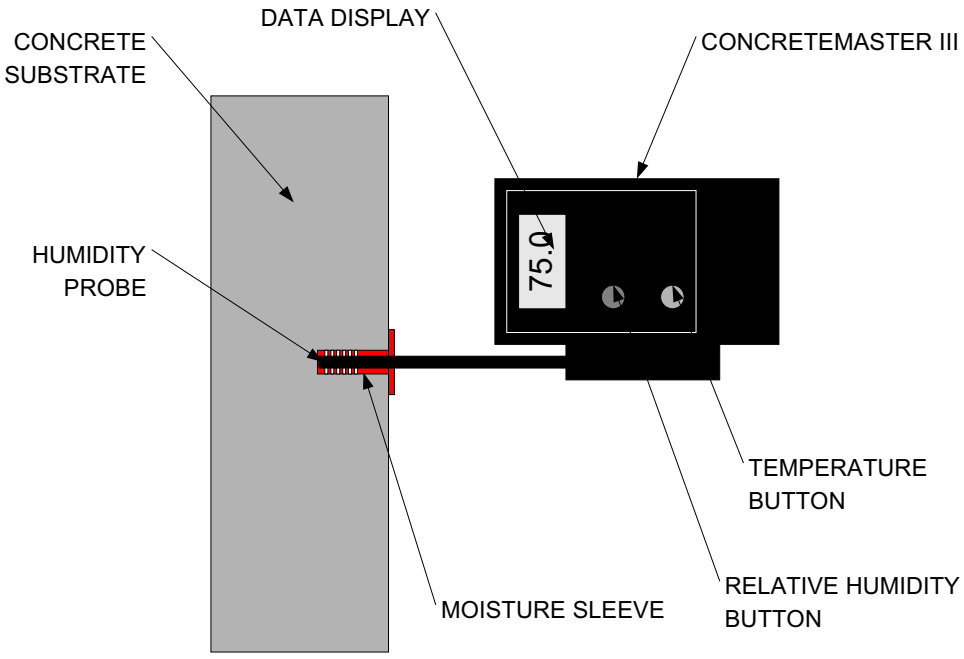

Figure 5.6: Schematic of relative humidity data collection

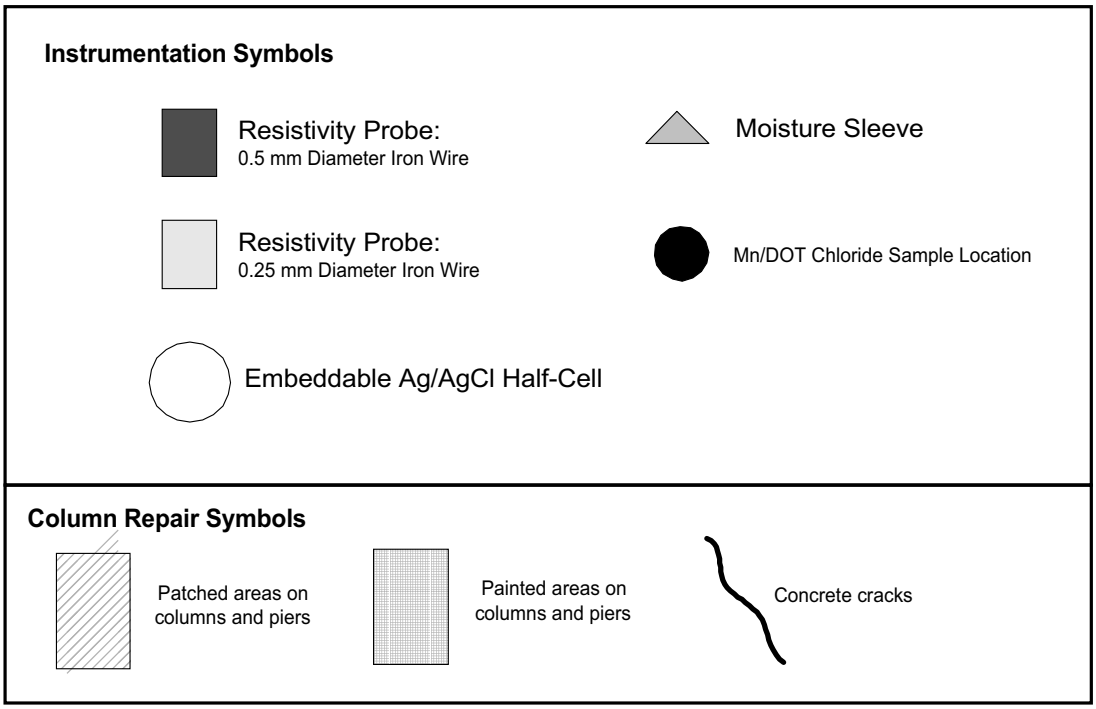

Figure 5.7: Legend for instrumentation location figures

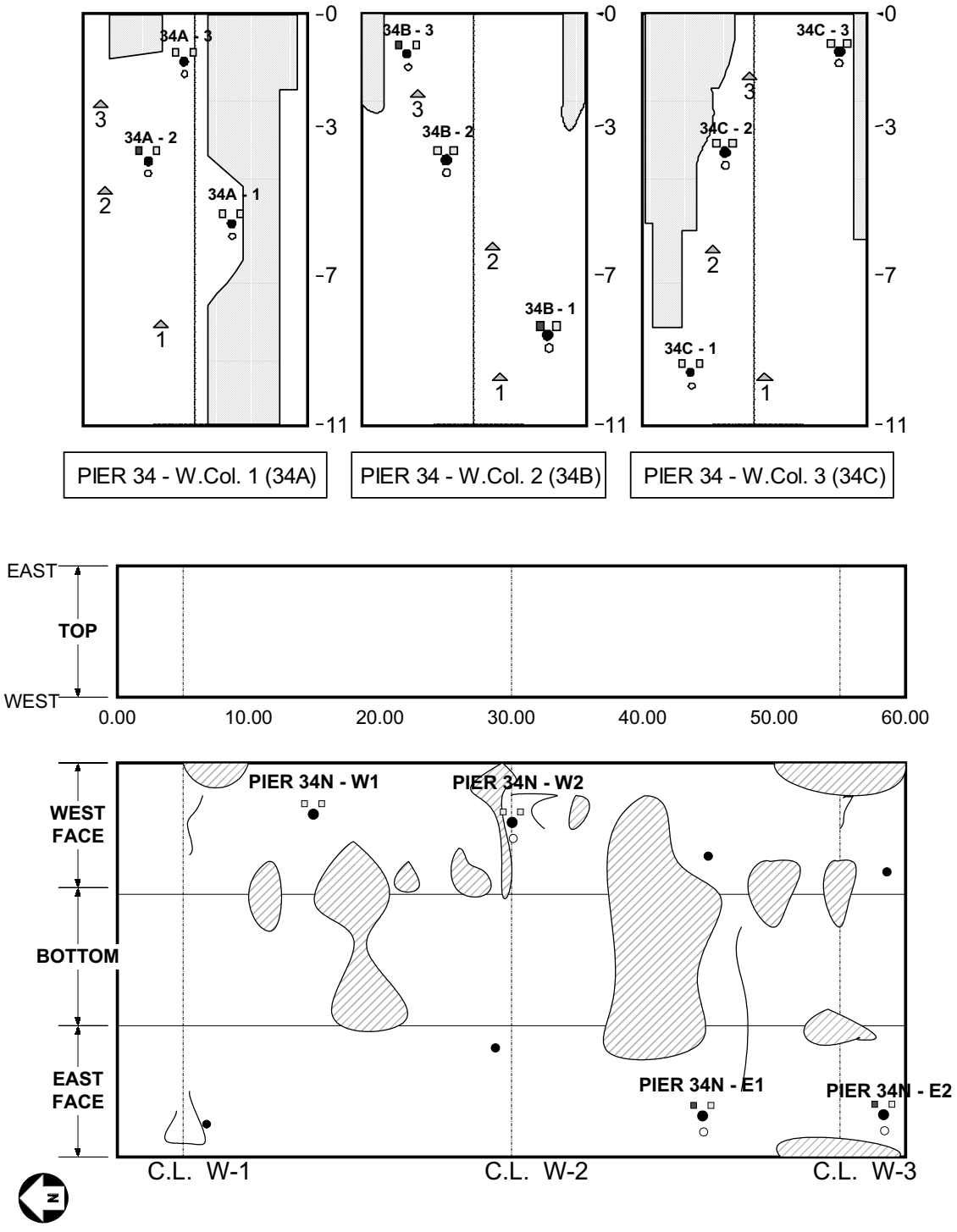

Figure 5.8: Instrumentation on Pier 34 North

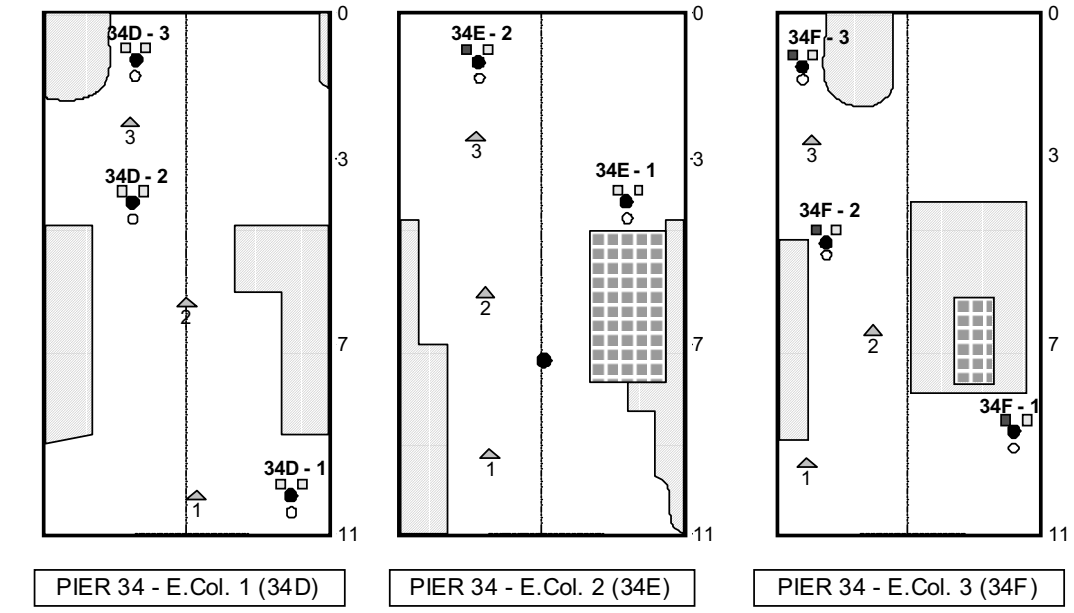

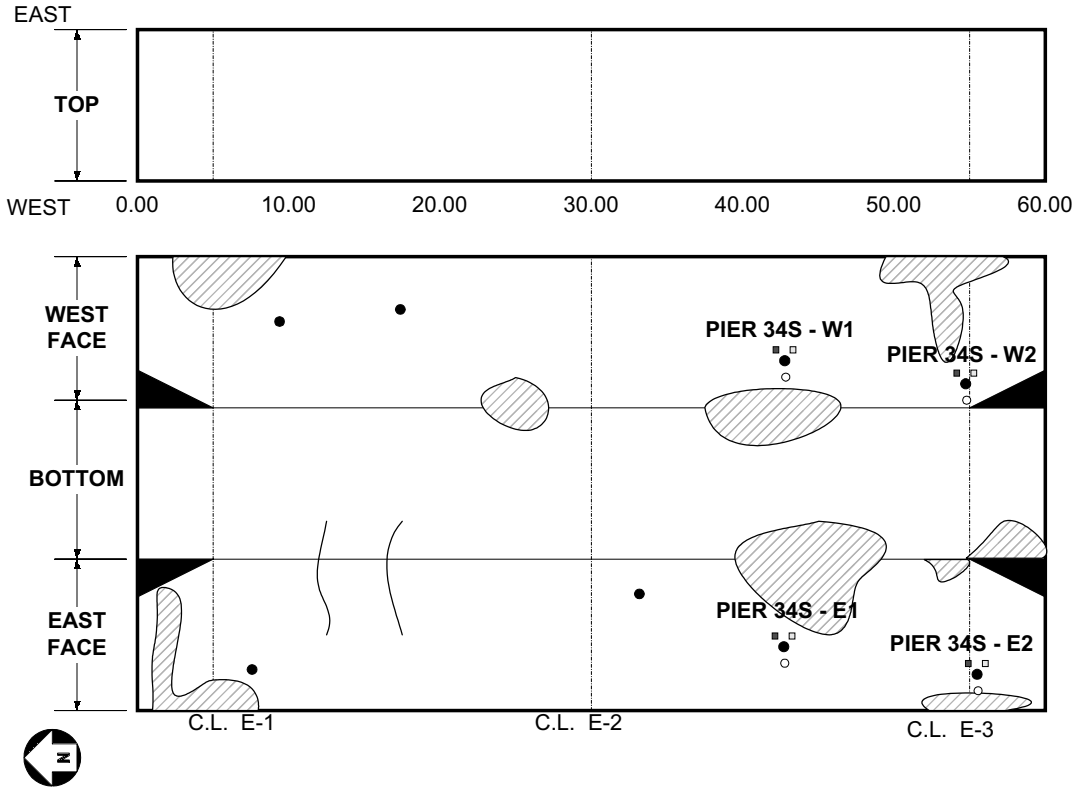

Figure 5.9: Instrumentation on Pier 34 South

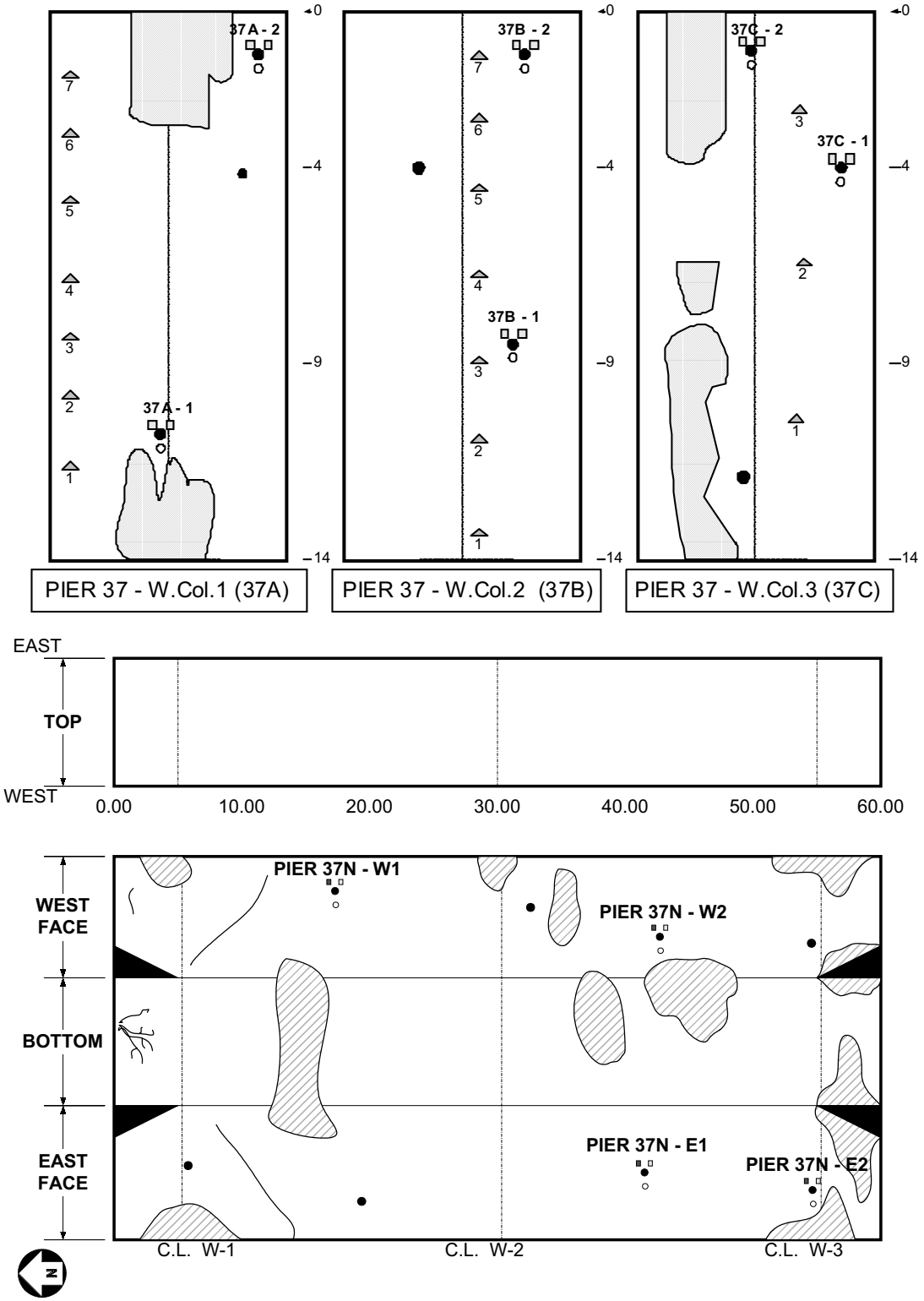

Figure 5.10: Instrumentation on Pier 37 North

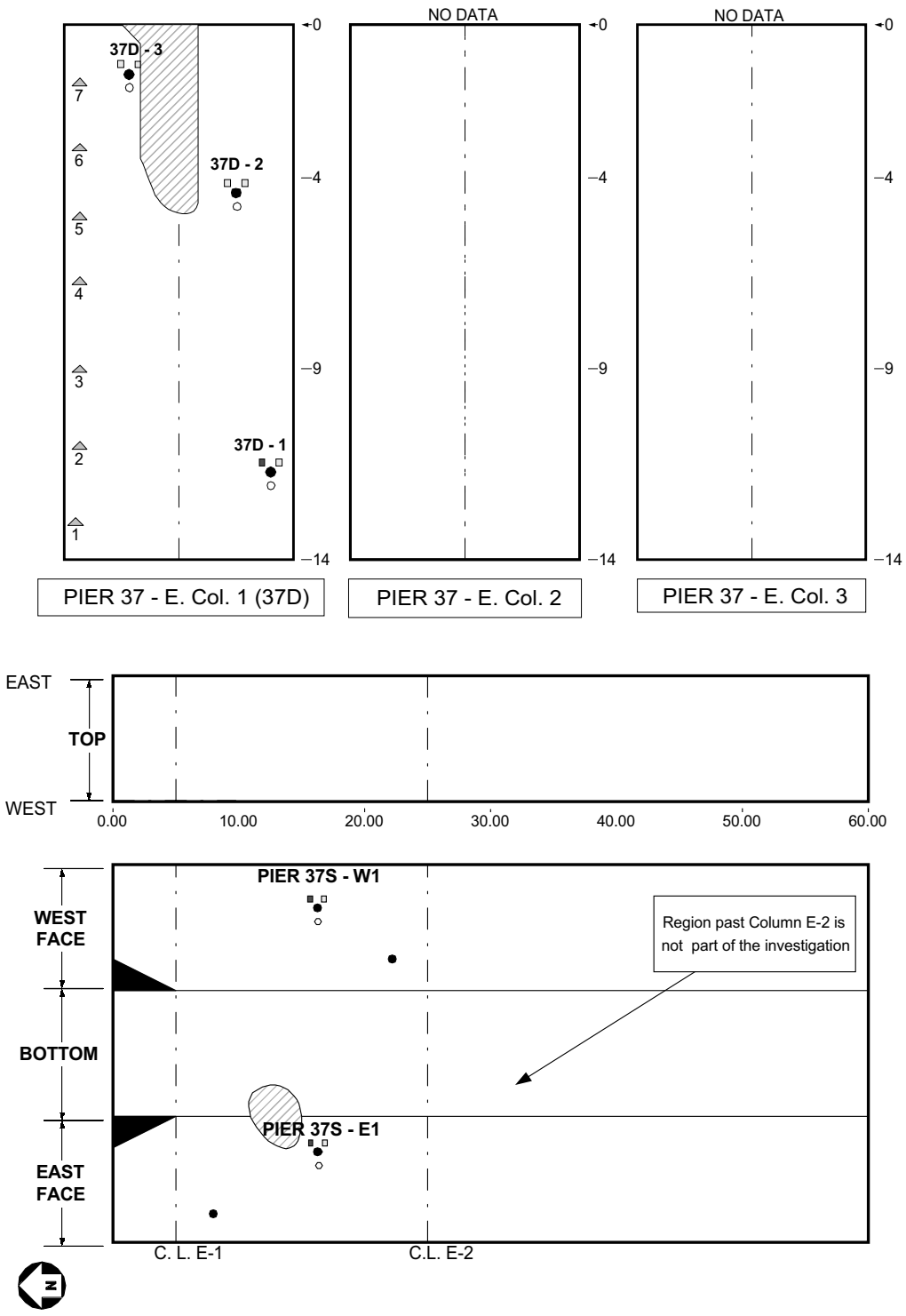

Figure 5.11: Instrumentation locations on Pier 37 South

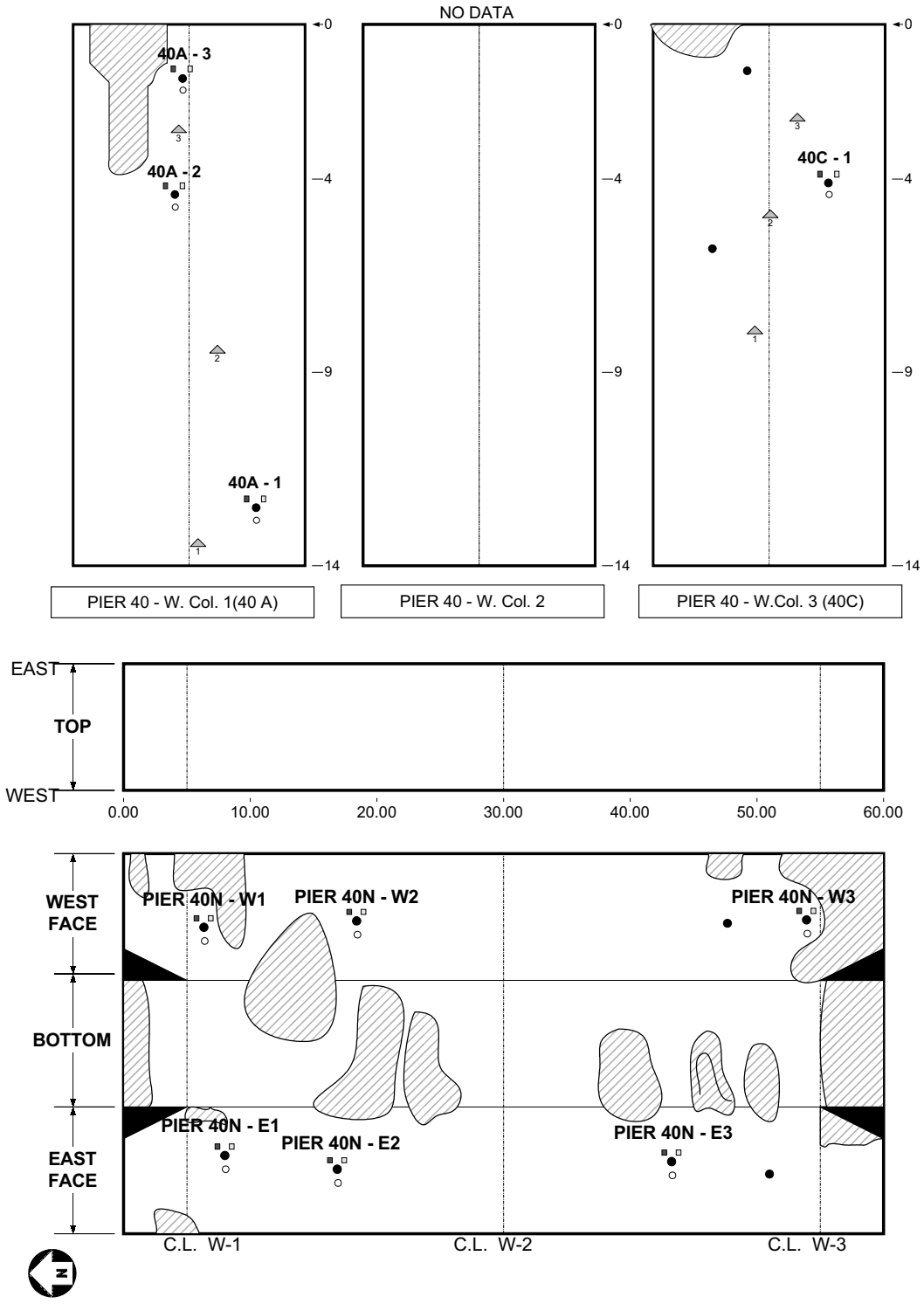

Figure 5.12: Instrumentation locations on Pier 40 North

Figure 5.13: Installed and sealed corrosion monitoring instrumentation

Figure 5.14: Instrumentation wiring system on Pier 34 North

Figure 5.15: Installed moisture sleeve

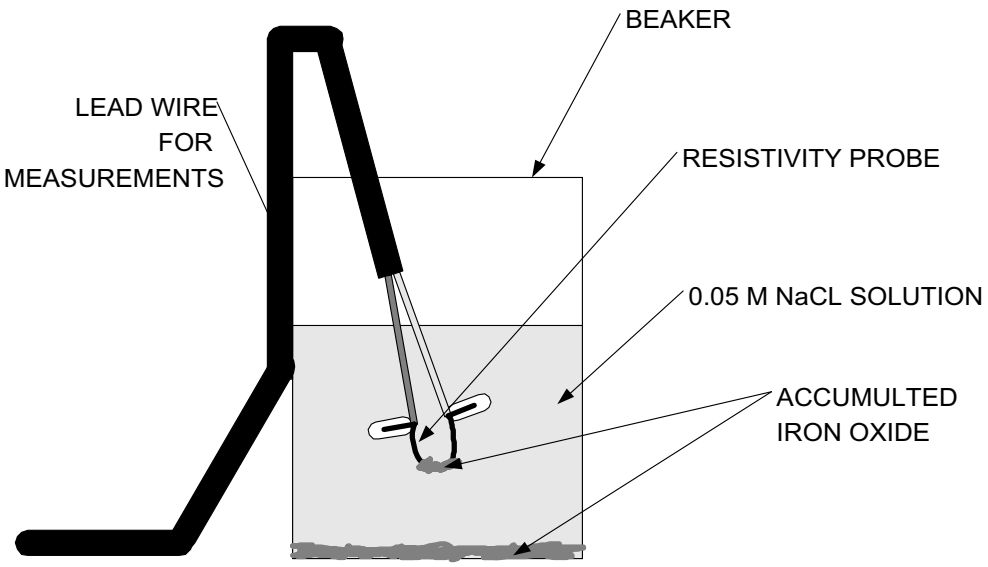

Figure 6.1: Schematic of resistivity probe Test 3 in solution

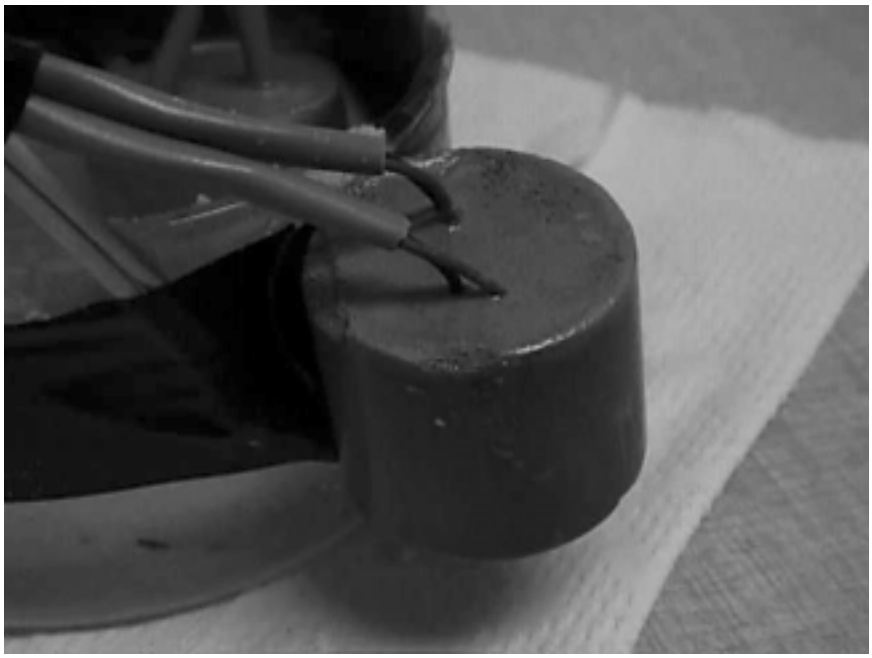

Figure 6.2: Grout plug from Test 6 during drying cycle

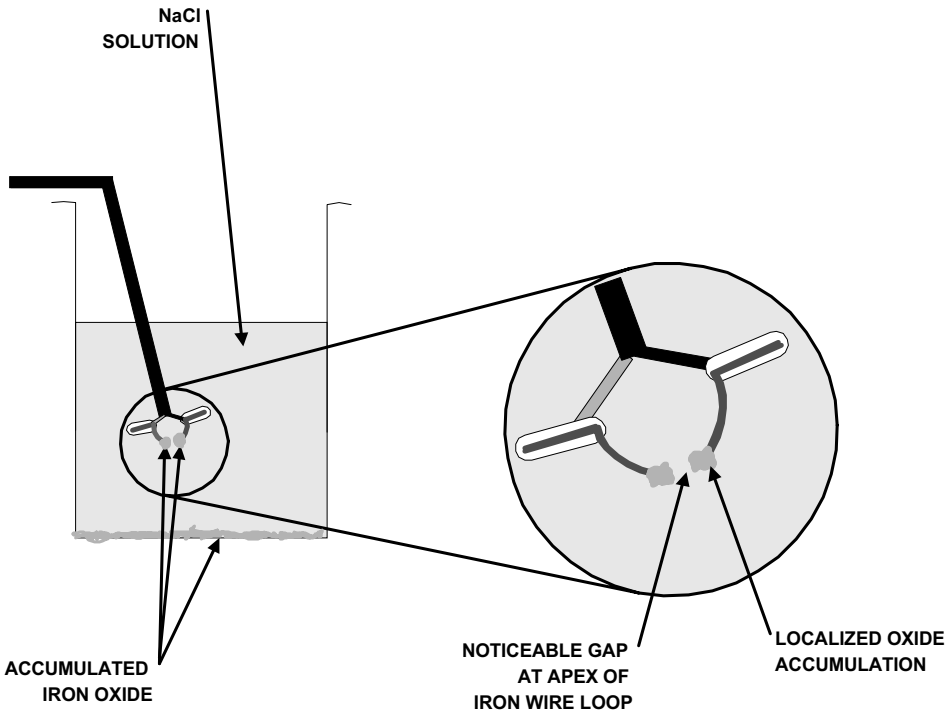

Figure 6.3: Schematic of a typical small resistivity probe failure

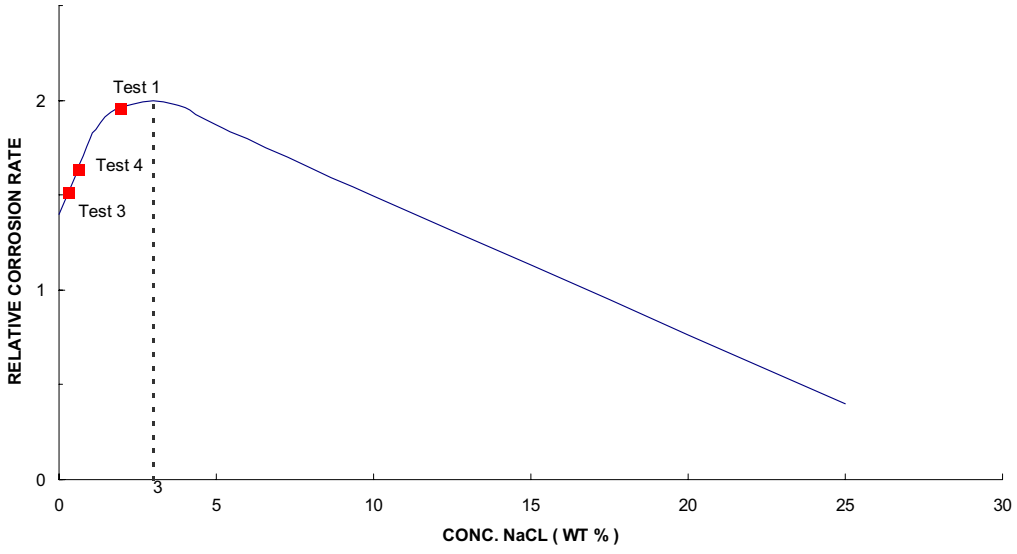

Figure 6.4: Effect of NaCl concentration on corrosion of iron [69]

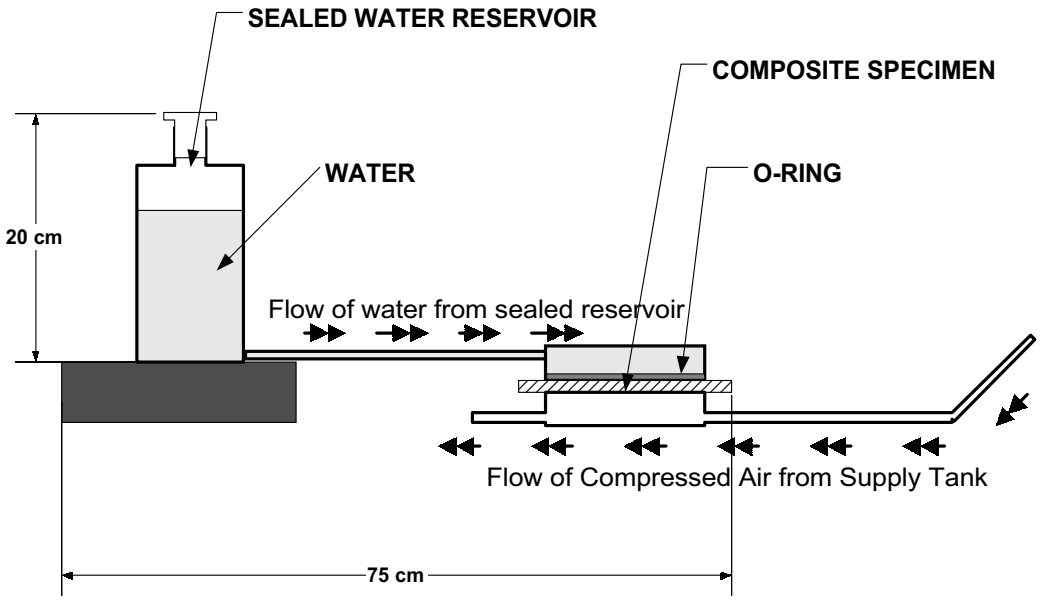

Figure 6.5: Illustration of diffusion test apparatus (not to scale)

Figure 6.6: Diffusion test in progress on MBrace epoxy specimen

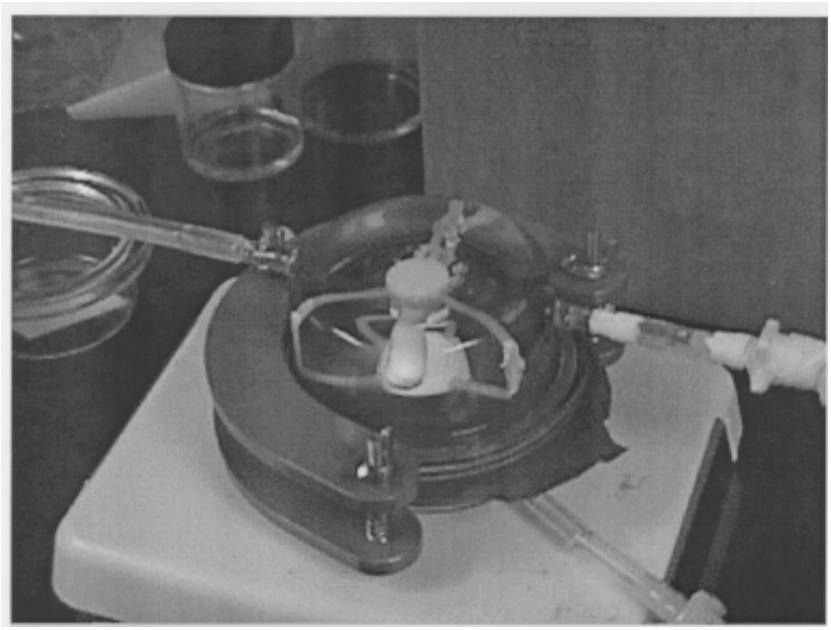

Figure 6.7: Close up of pervaporation chamber

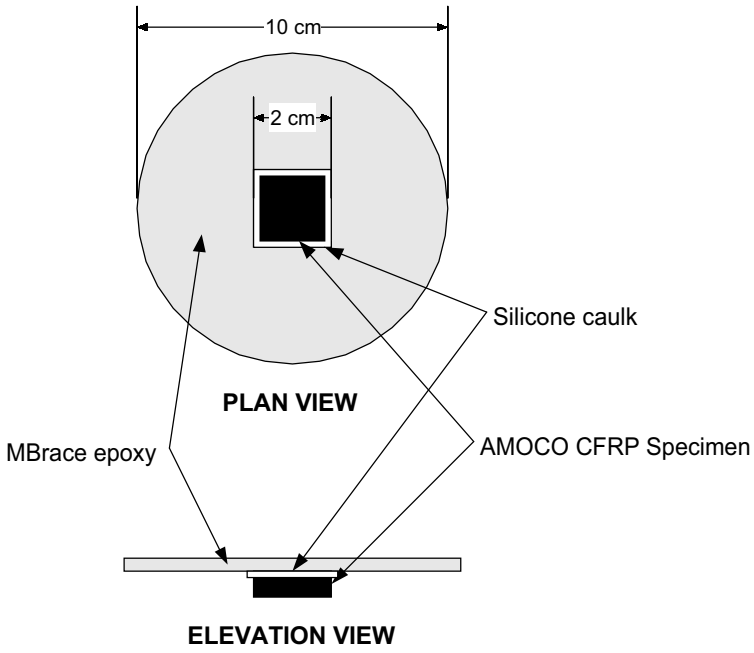

Figure 6.8: AMOCO peel sample in MBrace epoxy for diffusion testing

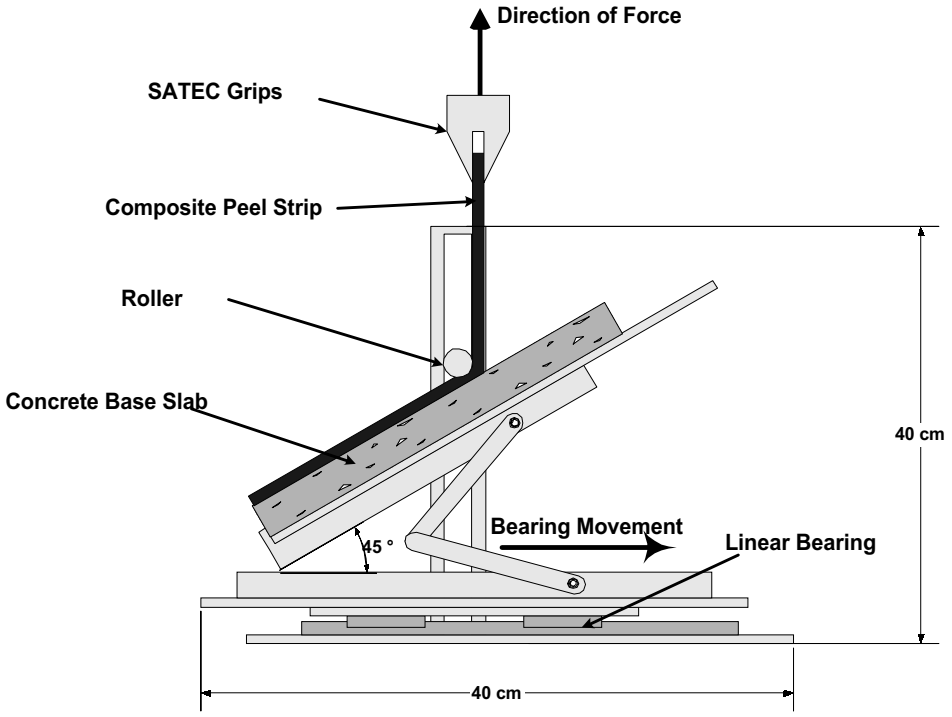

Figure 6.9: Illustration of the peel test apparatus

Figure 6.10: Peel test of MBrace composite in progress on SATEC load frame

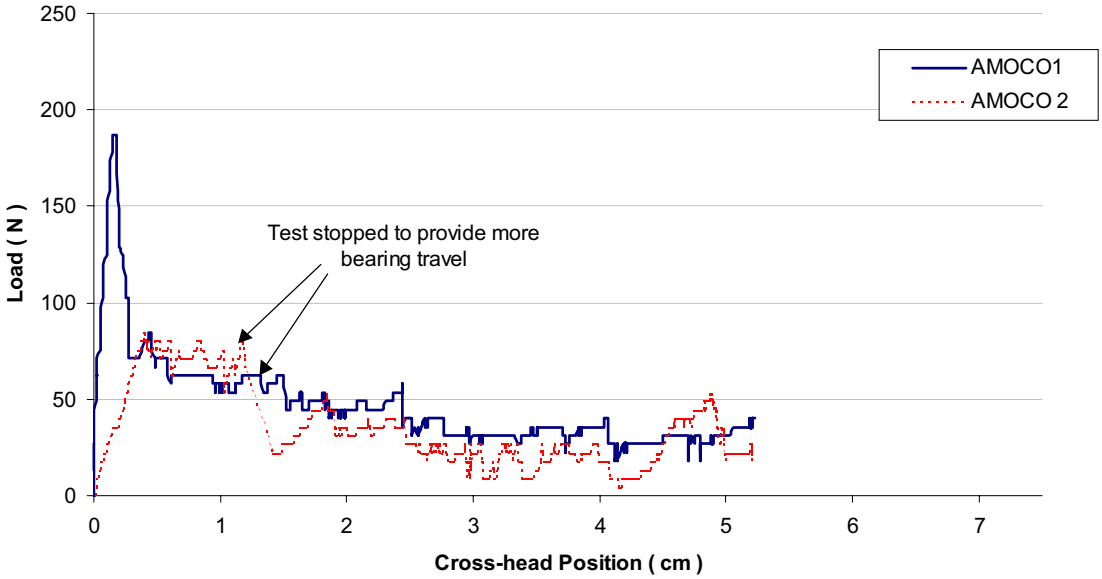

Figure 6.11: Peel test results of AMOCO CFRP wrap

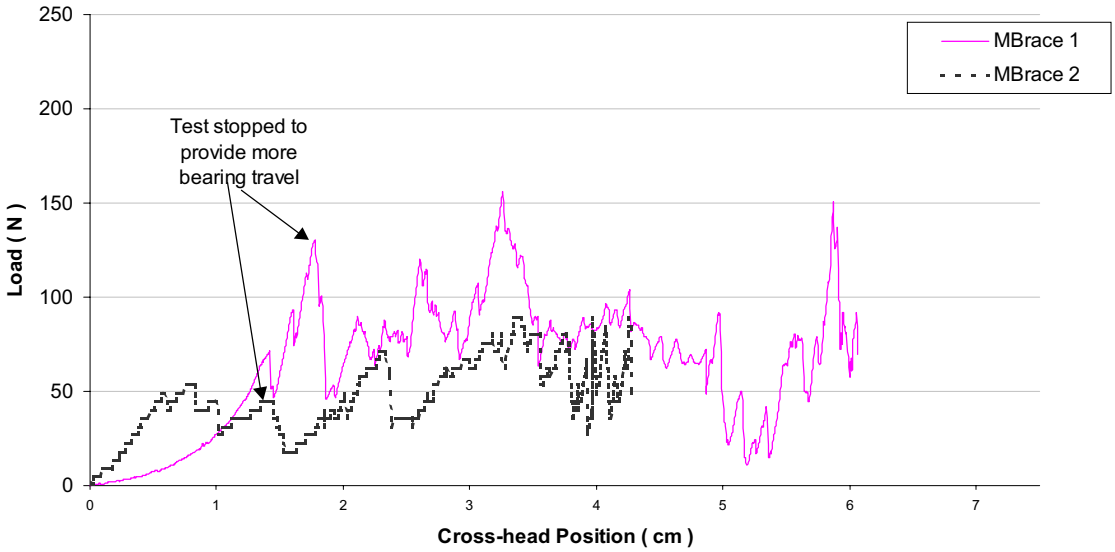

Figure 6.12: Peel test results of MBrace CFRP wrap

Figure 6.13: Peel test of MBrace CFRP wrap

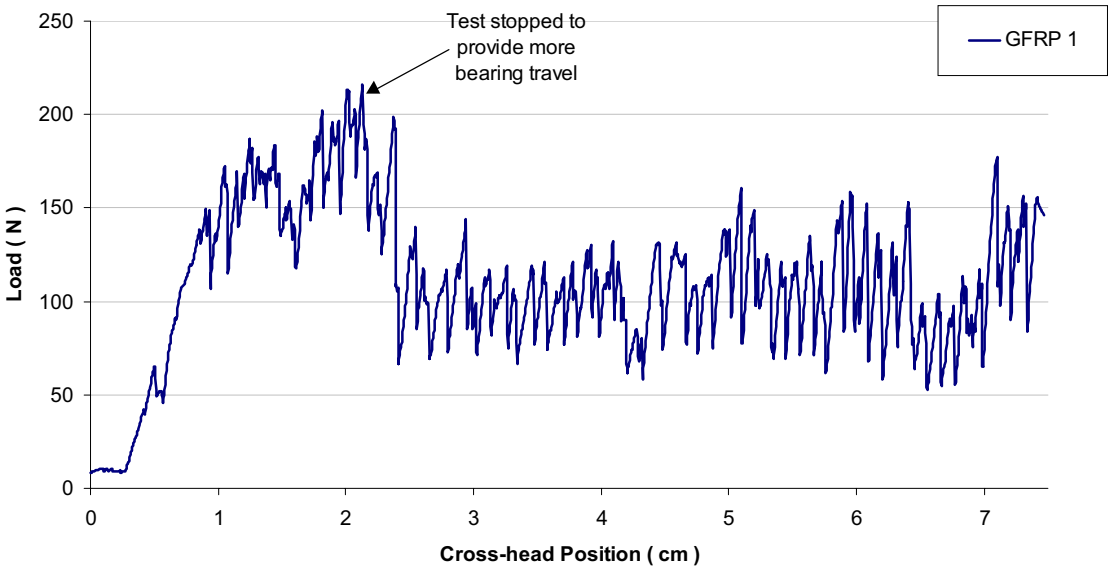

Figure 6.14: Peel test results of GFRP wrap

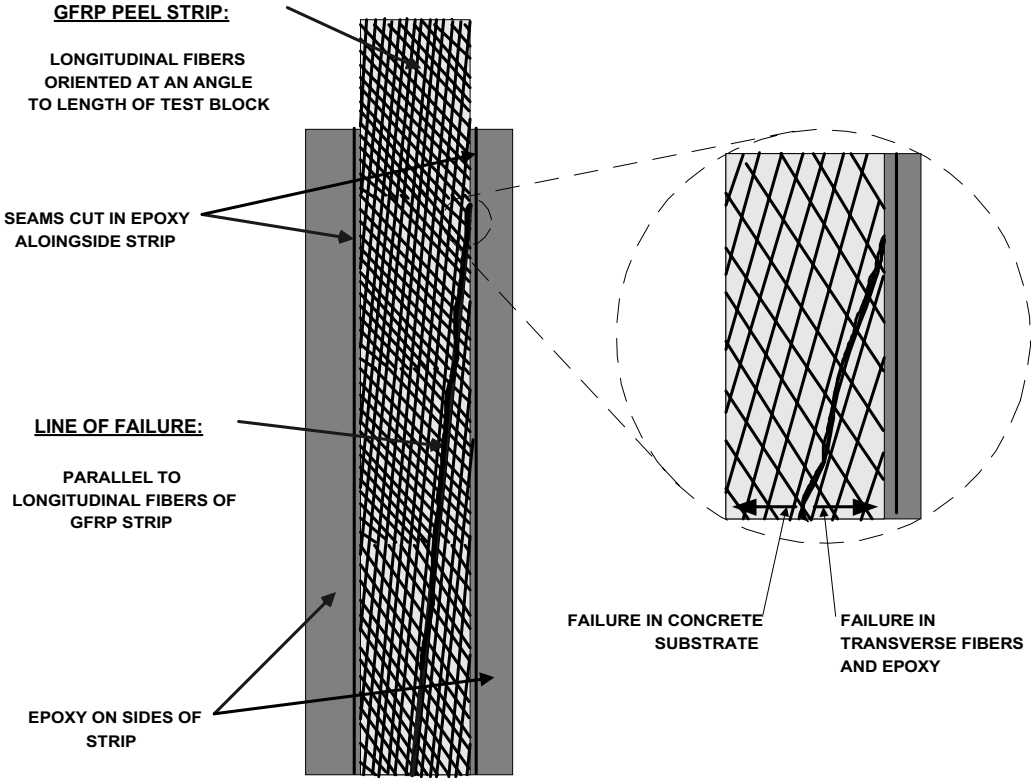

Figure 6.15: Failure observed in GFRP peel test specimen

Appendix A

Chloride Concentration Results from Pre- and Post-ECE Sampling Periods

This appendix presents the results collected during the pre- and post-ECE chloride concentration sampling periods. Each sample location has been identified by its assigned location moniker in the result tables. Results from the chloride samples collected by AET prior to the ECE treatment period are also included in these tables. Because location identifiers were not assigned to the location of AET samples, their chloride concentration results are italicized in parentheses alongside the results of the closest Mn/DOT chloride sample, at the appropriate sample depth. The three adjacent AET chloride samples collected from the east face of Pier 34 North were averaged because of their similarity, in terms of both chloride concentration and location, and listed alongside the results of Mn/DOT sample PIER 34N-E3. Chloride concentrations in excess of the established threshold for corrosion, 2000 ppm by weight of cement, are indicated with a bold font. The change in chloride concentration between sampling periods is also indicated in these tables at each sample location, for each sample depth. Concentration changes at each sample location were computed using the results of the Mn/DOT chloride samples collected during the pre- and post-ECE sampling periods, except for location PIER 34N-E3. The change in concentration at that location was computed using the averaged pre-ECE sample collected by AET because the results of the Mn/DOT sample collected from that location were not reported.

Column 34A (ECE)

Location I.D.	Sample Depth	Chloride Level		
		Pre-ECE	Post-ECE	% Change
34A -1	0 - 1.25 cm.	**3719**	1873	-49.6
	1.25 - 2.5 cm.	**3733**	1355	-63.7
	2.5 - 3.75 cm.	**3918**	1034	-73.6
	3.75 - 6.25 cm.	**2250**	800	-64.4
	6.25 - 8.75 cm.	1426	599	-58.0
34A -2	0 - 1.25 cm.	**4495**	1308	-70.9
	1.25 - 2.5 cm.	**3352**	1620	-51.7
	2.5 - 3.75 cm.	**2446**	803	-67.2
	3.75 - 6.25 cm.	1445	949	-34.3
	6.25 - 8.75 cm.	854	212	-75.2
34A -3	0 - 1.25 cm.	**4406**	**2298**	-47.8
	1.25 - 2.5 cm.	**4927**	**2724**	-44.7
	2.5 - 3.75 cm.	**5432**	**2025**	-62.7
	3.75 - 6.25 cm.	**3447**	1512	-56.1
	6.25 - 8.75 cm.	**2039**	885	-56.6

Column 34B (ECE)

Location I.D.	Sample Depth	Chloride Level		
		Pre-ECE	Post-ECE	% Change
34B -1	0 - 1.25 cm.	1630	539	-66.9
	1.25 - 2.5 cm.	593	374	-36.9
	2.5 - 3.75 cm.	427	355	-16.9
	3.75 - 6.25 cm.	242	333	37.6
	6.25 - 8.75 cm.	229	202	-11.8
34B -2	0 - 1.25 cm.	**2598**	428	-83.5
	1.25 - 2.5 cm.	**3737**	903	-75.8
	2.5 - 3.75 cm.	**2127**	554	-74.0
	3.75 - 6.25 cm.	1584	178	-88.8
	6.25 - 8.75 cm.	731	134	-81.7
34B -3	0 - 1.25 cm.	**3047**	993	-67.4
	1.25 - 2.5 cm.	**3587**	1489	-58.5
	2.5 - 3.75 cm.	**3169**	1625	-48.7
	3.75 - 6.25 cm.	1865	1455	-22.0
	6.25 - 8.75 cm.	1482	456	-69.2

Column 34C (ECE)

Location I.D.	Sample Depth	Chloride Level		
		Pre-ECE	Post-ECE	% Change
34C -1	0 - 1.25 cm.	**3438**	**2383**	-30.7
	1.25 - 2.5 cm.	**4224**	1872	-55.7
	2.5 - 3.75 cm.	**2952**	1121	-62.0
	3.75 - 6.25 cm.	1888	813	-56.9
	6.25 - 8.75 cm.	1190	246	-79.3
34C -2	0 - 1.25 cm.	1987	407	-79.5
	1.25 - 2.5 cm.	**4113**	688	-83.3
	2.5 - 3.75 cm.	**2058**	299	-85.5
	3.75 - 6.25 cm.	1901	234	-87.7
	6.25 - 8.75 cm.	683	154	-77.5
34C -3	0 - 1.25 cm.	**3456**	**2272**	-34.3
	1.25 - 2.5 cm.	**4775**	**3553**	-25.6
	2.5 - 3.75 cm.	**3622**	**2834**	-21.8
	3.75 - 6.25 cm.	**3086**	**2262**	-26.7
	6.25 - 8.75 cm.	**2082**	716	-65.6

Column 34D (non-ECE)

Location I.D.	Sample Depth	Chloride Level		
		Pre-ECE	Post-ECE	% Change
34D -1	0 - 1.25 cm.	**2581**	**2103**	-18.5
	1.25 - 2.5 cm.	**2199**	**2430**	10.5
	2.5 - 3.75 cm.	1284	1028	-19.9
	3.75 - 6.25 cm.	407	146	-64.1
	6.25 - 8.75 cm.	166	282	69.9
34D -2	0 - 1.25 cm.	**3575**	725	-79.7
	1.25 - 2.5 cm.	**2466**	264	-89.3
	2.5 - 3.75 cm.	**2066**	251	-87.9
	3.75 - 6.25 cm.	N/A	169	N/A
	6.25 - 8.75 cm.	N/A	287	N/A
34D -3	0 - 1.25 cm.	**2117** ***(2077)***	1990	-6.0
	1.25 - 2.5 cm.	**2383**	**2431**	2.0
	2.5 - 3.75 cm.	1808 ***(2931)***	1441	-20.3
	3.75 - 6.25 cm.	N/A	458	N/A
	6.25 - 8.75 cm.	N/A *(449)*	371	N/A

Column 34E (non-ECE)

Location I.D.	Sample Depth	Chloride Level		
		Pre-ECE	Post-ECE	% Change
34E -1	0 - 1.25 cm.	297	551	85.5
	1.25 - 2.5 cm.	366	310	-15.3
	2.5 - 3.75 cm.	314	185	-41.1
	3.75 - 6.25 cm.	196	230	17.3
	6.25 - 8.75 cm.	142	242	70.4
34E -2	0 - 1.25 cm.	1888	**3124**	65.5
	1.25 - 2.5 cm.	**2669**	**2935**	10.0
	2.5 - 3.75 cm.	1880	1214	-35.4
	3.75 - 6.25 cm.	N/A	450	N/A
	6.25 - 8.75 cm.	N/A	185	N/A
34E -3	0 - 1.25 cm.	479	969	102.3
	1.25 - 2.5 cm.	140	249	77.9
	2.5 - 3.75 cm.	76	217	185.5
	3.75 - 6.25 cm.	153	196	28.1
	6.25 - 8.75 cm.	72	184	155.6

Column 34F (non-ECE)

Location I.D.	Sample Depth	Chloride Level		
		Pre-ECE	Post-ECE	% Change
34F -1	0 - 1.25 cm.	1759	1724	-2.0
	1.25 - 2.5 cm.	1416	807	-43.0
	2.5 - 3.75 cm.	1374	759	-44.8
	3.75 - 6.25 cm.	294	224	-23.8
	6.25 - 8.75 cm.	181	155	-14.4
34F -2	0 - 1.25 cm.	**4046**	**3873**	-4.3
	1.25 - 2.5 cm.	**3953**	**2919**	-26.2
	2.5 - 3.75 cm.	**2721**	**3162**	16.2
	3.75 - 6.25 cm.	1559	1934	24.1
	6.25 - 8.75 cm.	870	374	-57.0
34F -3	0 - 1.25 cm.	**4364** ***(3220)***	**3672**	-15.9
	1.25 - 2.5 cm.	**5100**	**2396**	-53.0
	2.5 - 3.75 cm.	**3429** ***(2635)***	**2046**	-40.3
	3.75 - 6.25 cm.	N/A	1275	N/A
	6.25 - 8.75 cm.	N/A *(1373)*	427	N/A

Pier 34 North (ECE)

Location I.D.	Sample Depth	Chloride Level		
		Pre-ECE	Post-ECE	% Change
	0 - 1.25 cm.	**3190**	1467	-54.0
	1.25 - 2.5 cm.	**2960**	**2356**	-20.4
PIER 34N - W1	2.5 - 3.75 cm.	**2608**	**2075**	-20.4
	3.75 - 6.25 cm.	1172	709	-39.5
	6.25 - 8.75 cm.	902	411	-54.4
	0 - 1.25 cm.	**3783**	**2142**	-43.4
	1.25 - 2.5 cm.	**2688**	**2546**	-5.3
PIER 34N - W2	2.5 - 3.75 cm.	**2270**	**2635**	16.1
	3.75 - 6.25 cm.	1984	**2302**	16.0
	6.25 - 8.75 cm.	**2458**	1911	-22.3
	0 - 1.25 cm.	**2696**	1508	-44.1
	1.25 - 2.5 cm.	**4198**	961	-77.1
PIER 34N - W3	2.5 - 3.75 cm.	**2832**	490	-82.7
	3.75 - 6.25 cm.	**3087**	110	-96.4
	6.25 - 8.75 cm.	**2016**	86	-95.7
	0 - 1.25 cm.	**3128** ***(2697)***	**2083**	-33.4
	1.25 - 2.5 cm.	**2418**	372	-84.6
PIER 34N - W4	2.5 - 3.75 cm.	***2225 (2820)***	1382	-37.9
	3.75 - 6.25 cm.	634	578	-8.8
	6.25 - 8.75 cm.	*267 (1155)*	951	256.2
	0 - 1.25 cm.	N/A	1477	N/A
	1.25 - 2.5 cm.	N/A	**2509**	N/A
PIER 34N - E1	2.5 - 3.75 cm.	N/A	1345	N/A
	3.75 - 6.25 cm.	N/A	702	N/A
	6.25 - 8.75 cm.	N/A	410	N/A
	0 - 1.25 cm.	N/A	**2997**	N/A
	1.25 - 2.5 cm.	N/A	1693	N/A
PIER 34N - E2	2.5 - 3.75 cm.	N/A	1901	N/A
	3.75 - 6.25 cm.	N/A	1542	N/A
	6.25 - 8.75 cm.	N/A	645	N/A
	0 - 1.25 cm.	N/A ***(2675)***	1819	-32.0
	1.25 - 2.5 cm.	N/A	1786	N/A
PIER 34N - E3	2.5 - 3.75 cm.	N/A ***(2820)***	1117	-60.4
	3.75 - 6.25 cm.	N/A	828	N/A
	6.25 - 8.75 cm.	N/A *(1155)*	658	-43.0
	0 - 1.25 cm.	N/A	1077	N/A
	1.25 - 2.5 cm.	N/A	1598	N/A
PIER 34N - E4	2.5 - 3.75 cm.	N/A	366	N/A
	3.75 - 6.25 cm.	N/A	418	N/A
	6.25 - 8.75 cm.	N/A	307	N/A

Pier 34 South (non-ECE)

Location I.D.	Sample Depth	Chloride Level		
		Pre-ECE	Post-ECE	% Change
PIER 34S - W1	0 - 1.25 cm.	1774 ***(2076)***	**2167**	22.2
	1.25 - 2.5 cm.	1385	1798	29.8
	2.5 - 3.75 cm.	1922 *(916)*	790	-58.9
	3.75 - 6.25 cm.	428	352	-17.8
	6.25 - 8.75 cm.	233 ***(2304)***	208	-10.7
PIER 34S - W2	0 - 1.25 cm.	**3950**	**2960**	-25.1
	1.25 - 2.5 cm.	**2972**	**3102**	4.4
	2.5 - 3.75 cm.	1660	**2545**	53.3
	3.75 - 6.25 cm.	1548	1372	-11.4
	6.25 - 8.75 cm.	351	543	54.7
PIER 34S - W3	0 - 1.25 cm.	**2734**	**2191**	-19.9
	1.25 - 2.5 cm.	**2338**	1606	-31.3
	2.5 - 3.75 cm.	1747	1105	-36.7
	3.75 - 6.25 cm.	1142	713	-37.6
	6.25 - 8.75 cm.	699	215	-69.2
PIER 34S - W4	0 - 1.25 cm.	**2325**	1999	-14.0
	1.25 - 2.5 cm.	1493	1197	-19.8
	2.5 - 3.75 cm.	921	510	-44.6
	3.75 - 6.25 cm.	412	243	-41.0
	6.25 - 8.75 cm.	304	170	-44.1
PIER 34S - E1	0 - 1.25 cm.	1631 *(1684)*	1864	14.3
	1.25 - 2.5 cm.	892	**2351**	163.6
	2.5 - 3.75 cm.	760 *(551)*	1061	39.6
	3.75 - 6.25 cm.	219	470	114.6
	6.25 - 8.75 cm.	201 *(1540)*	138	-31.3
PIER 34S - E2	0 - 1.25 cm.	**2854**	**2627**	-8.0
	1.25 - 2.5 cm.	1675	**2439**	45.6
	2.5 - 3.75 cm.	**2064**	1841	-10.8
	3.75 - 6.25 cm.	1103	**2128**	92.9
	6.25 - 8.75 cm.	820	559	-31.8
PIER 34S - E3	0 - 1.25 cm.	**2481**	1249	-49.7
	1.25 - 2.5 cm.	1749	1373	-21.5
	2.5 - 3.75 cm.	1110	832	-25.0
	3.75 - 6.25 cm.	963	479	-50.3
	6.25 - 8.75 cm.	605	264	-56.4
PIER 34S - E4	0 - 1.25 cm.	**2014**	1851	-8.1
	1.25 - 2.5 cm.	1450	1388	-4.3
	2.5 - 3.75 cm.	**2045**	817	-60.0
	3.75 - 6.25 cm.	1086	278	-74.4
	6.25 - 8.75 cm.	367	199	-45.8

Column 37A (ECE)

Location I.D.	Sample Depth	Chloride Level		
		Pre-ECE	Post-ECE	% Change
37A -1	0 - 1.25 cm.	464	130	-72.0
	1.25 - 2.5 cm.	223	143	-35.9
	2.5 - 3.75 cm.	226	1973	773.0
	3.75 - 6.25 cm.	124	271	118.5
	6.25 - 8.75 cm.	102	299	193.1
37A -2	0 - 1.25 cm.	946	1055	11.5
	1.25 - 2.5 cm.	614	1292	110.4
	2.5 - 3.75 cm.	411	823	100.2
	3.75 - 6.25 cm.	328	477	45.4
	6.25 - 8.75 cm.	124	227	83.1
37A -3	0 - 1.25 cm.	622	271	-56.4
	1.25 - 2.5 cm.	699	462	-33.9
	2.5 - 3.75 cm.	588	256	-56.5
	3.75 - 6.25 cm.	487	141	-71.0
	6.25 - 8.75 cm.	371	170	-54.2

Column 37B (ECE)

Location I.D.	Sample Depth	Chloride Level		
		Pre-ECE	Post-ECE	% Change
37B -1	0 - 1.25 cm.	411	142	-65.5
	1.25 - 2.5 cm.	294	234	-20.4
	2.5 - 3.75 cm.	124	134	8.1
	3.75 - 6.25 cm.	123	297	141.5
	6.25 - 8.75 cm.	151	97	-35.8
37B -2	0 - 1.25 cm.	1079	667	-38.2
	1.25 - 2.5 cm.	1620	1873	15.6
	2.5 - 3.75 cm.	**2027**	1753	-13.5
	3.75 - 6.25 cm.	**2418**	1042	-56.9
	6.25 - 8.75 cm.	1329	615	-53.7
37B -3	0 - 1.25 cm.	321	133	-58.6
	1.25 - 2.5 cm.	401	266	-33.7
	2.5 - 3.75 cm.	260	245	-5.8
	3.75 - 6.25 cm.	85	107	25.9
	6.25 - 8.75 cm.	74	101	36.5

Column 37C (ECE)

Location I.D.	Sample Depth	Chloride Level		
		Pre-ECE	Post-ECE	% Change
37C -1	0 - 1.25 cm.	1661	104	-93.7
	1.25 - 2.5 cm.	1232	**2238**	81.7
	2.5 - 3.75 cm.	965	1487	54.1
	3.75 - 6.25 cm.	280	626	123.6
	6.25 - 8.75 cm.	242	247	2.1
37C -2	0 - 1.25 cm.	254	228	-10.2
	1.25 - 2.5 cm.	139	226	62.6
	2.5 - 3.75 cm.	85	216	154.1
	3.75 - 6.25 cm.	79	178	125.3
	6.25 - 8.75 cm.	107	182	70.1
37C -3	0 - 1.25 cm.	402	192	-52.2
	1.25 - 2.5 cm.	326	358	9.8
	2.5 - 3.75 cm.	297	197	-33.7
	3.75 - 6.25 cm.	101	76	-24.8
	6.25 - 8.75 cm.	113	151	33.6

Column 37D (non-ECE)

Location I.D.	Sample Depth	Chloride Level		
		Pre-ECE	Post-ECE	% Change
37D -1	0 - 1.25 cm.	610	600	-1.6
	1.25 - 2.5 cm.	219	328	49.8
	2.5 - 3.75 cm.	135	224	65.9
	3.75 - 6.25 cm.	152	135	-11.2
	6.25 - 8.75 cm.	170	236	38.8
37D -2	0 - 1.25 cm.	1475	**2306**	56.3
	1.25 - 2.5 cm.	**3105**	**3507**	12.9
	2.5 - 3.75 cm.	**4068**	**3625**	-10.9
	3.75 - 6.25 cm.	**2650**	**2184**	-17.6
	6.25 - 8.75 cm.	1407	964	-31.5
37D -3	0 - 1.25 cm.	**2511**	1585	-36.9
	1.25 - 2.5 cm.	**2149**	**2039**	-5.1
	2.5 - 3.75 cm.	**2495**	902	-63.8
	3.75 - 6.25 cm.	1928	521	-73.0
	6.25 - 8.75 cm.	1349	170	-87.4

Pier 37 North (ECE)

Location I.D.	Sample Depth	Chloride Level		
		Pre-Ece	Post-ECE	% Change
	0 - 1.25 cm.	**2445**	1075	-56.0
	1.25 - 2.5 cm.	**2335**	1557	-33.3
PIER 37N - W1	2.5 - 3.75 cm.	**2016**	768	-61.9
	3.75 - 6.25 cm.	1474	390	-73.5
	6.25 - 8.75 cm.	546	224	-59.0
	0 - 1.25 cm.	**2657**	**2750**	3.5
	1.25 - 2.5 cm.	**3010**	**2545**	-15.4
PIER 37N - W2	2.5 - 3.75 cm.	**2155**	1668	-22.6
	3.75 - 6.25 cm.	1647	1720	4.4
	6.25 - 8.75 cm.	1234	947	-23.3
	0 - 1.25 cm.	1195	973	-18.6
	1.25 - 2.5 cm.	1434	1427	-0.5
PIER 37N - W3	2.5 - 3.75 cm.	1101	1218	10.6
	3.75 - 6.25 cm.	428	583	36.2
	6.25 - 8.75 cm.	258	193	-25.2
	0 - 1.25 cm.	**2234** *(455)*	1076	-51.8
	1.25 - 2.5 cm.	**2214**	1173	-47.0
PIER 37N - W4	2.5 - 3.75 cm.	1940 *(1957)*	921	-52.5
	3.75 - 6.25 cm.	1283	456	-64.5
	6.25 - 8.75 cm.	715 *(1901)*	179	-75.0
	0 - 1.25 cm.	**5583** ***(4105)***	1175	-79.0
	1.25 - 2.5 cm.	**3025**	**2175**	-28.1
PIER 37N - E1	2.5 - 3.75 cm.	**3027** *(1861)*	1855	-38.7
	3.75 - 6.25 cm.	**2807**	1079	-61.6
	6.25 - 8.75 cm.	**2205** ***(2908)***	213	-90.3
	0 - 1.25 cm.	1217	1817	49.3
	1.25 - 2.5 cm.	1936	1936	0.0
PIER 37N - E2	2.5 - 3.75 cm.	1754	504	-71.3
	3.75 - 6.25 cm.	**2818**	1002	-64.4
	6.25 - 8.75 cm.	1988	1186	-40.3
	0 - 1.25 cm.	**2229**	1088	-51.2
	1.25 - 2.5 cm.	1184	1278	7.9
PIER 37N - E3	2.5 - 3.75 cm.	896	1253	39.8
	3.75 - 6.25 cm.	739	522	-29.4
	6.25 - 8.75 cm.	571	232	-59.4
	0 - 1.25 cm.	1107	714	-35.5
	1.25 - 2.5 cm.	**2822**	1172	-58.5
PIER 37N - E4	2.5 - 3.75 cm.	**2866**	781	-72.7
	3.75 - 6.25 cm.	**3042**	232	-92.4
	6.25 - 8.75 cm.	**2602**	167	-93.6

Pier 37 South (non-ECE)

Location I.D.	Sample Depth	Chloride Level		
		Pre-ECE	Post-ECE	% Change
PIER 37S - W1	0 - 1.25 cm.	**2708**	1840	-32.1
	1.25 - 2.5 cm.	**2105**	1394	-33.8
	2.5 - 3.75 cm.	948	1033	9.0
	3.75 - 6.25 cm.	1013	404	-60.1
	6.25 - 8.75 cm.	401	385	-4.0
PIER 37S - W2	0 - 1.25 cm.	**2854** ***(2904)***	966	-66.2
	1.25 - 2.5 cm.	1675	432	-74.2
	2.5 - 3.75 cm.	**2064** *(435)*	196	-90.5
	3.75 - 6.25 cm.	1103	178	-83.9
	6.25 - 8.75 cm.	820 *(306)*	174	-78.8
PIER 37S - E1	0 - 1.25 cm.	**2348**	1697	-27.7
	1.25 - 2.5 cm.	1857	1086	-41.5
	2.5 - 3.75 cm.	1305	323	-75.2
	3.75 - 6.25 cm.	1005	267	-73.4
	6.25 - 8.75 cm.	379	248	-34.6
PIER 37S - E2	0 - 1.25 cm.	1111	851	-23.4
	1.25 - 2.5 cm.	760	325	-57.2
	2.5 - 3.75 cm.	375	183	-51.2
	3.75 - 6.25 cm.	180	183	1.7
	6.25 - 8.75 cm.	164	199	21.3

Column 40A (non-ECE)

Location I.D.	Sample Depth	Chloride Level		
		Pre-ECE	Post-ECE	% Change
40A -1	0 - 1.25 cm.	**2569**	1930	-24.9
	1.25 - 2.5 cm.	1651	1480	-10.4
	2.5 - 3.75 cm.	847	894	5.5
	3.75 - 6.25 cm.	199	540	171.4
	6.25 - 8.75 cm.	197	537	172.6
40A -2	0 - 1.25 cm.	1237	**2089**	68.9
	1.25 - 2.5 cm.	745	1845	147.7
	2.5 - 3.75 cm.	395	1156	192.7
	3.75 - 6.25 cm.	179	575	221.2
	6.25 - 8.75 cm.	44	155	252.3
40A -3	0 - 1.25 cm.	**2448**	**2704**	10.5
	1.25 - 2.5 cm.	1821	**2406**	32.1
	2.5 - 3.75 cm.	1598	**2018**	26.3
	3.75 - 6.25 cm.	1070	1325	23.8
	6.25 - 8.75 cm.	320	328	2.5

Column 40C (non-ECE)

Location I.D.	Sample Depth	Chloride Level		
		Pre-ECE	Post-ECE	% Change
40C -1	0 - 1.25 cm.	**5204**	**3249**	-37.6
	1.25 - 2.5 cm.	**3647**	**3340**	-8.4
	2.5 - 3.75 cm.	**2049**	415	-79.7
	3.75 - 6.25 cm.	1830	**3361**	83.7
	6.25 - 8.75 cm.	1323	**2040**	54.2
40C -2	0 - 1.25 cm.	902	857	-5.0
	1.25 - 2.5 cm.	438	370	-15.5
	2.5 - 3.75 cm.	194	187	-3.6
	3.75 - 6.25 cm.	108	426	294.4
	6.25 - 8.75 cm.	134	195	45.5
40C -3	0 - 1.25 cm.	207	422	103.9
	1.25 - 2.5 cm.	125	148	18.4
	2.5 - 3.75 cm.	112	207	84.8
	3.75 - 6.25 cm.	135	200	48.1
	6.25 - 8.75 cm.	133	154	15.8

Pier 40 North (non-ECE)

Location I.D.	Sample Depth	Chloride Level		
		Pre-ECE	Post-ECE	% Change
	0 - 1.25 cm.	**3152**	**2345**	-25.6
	1.25 - 2.5 cm.	**2671**	**2975**	11.4
PIER 40N - W1	2.5 - 3.75 cm.	**2604**	**2110**	-19.0
	3.75 - 6.25 cm.	1377	1418	3.0
	6.25 - 8.75 cm.	773	615	-20.4
	0 - 1.25 cm.	**3040**	**2585**	-15.0
	1.25 - 2.5 cm.	**2869**	**2394**	-16.6
PIER 40N - W2	2.5 - 3.75 cm.	**2255**	**2087**	-7.5
	3.75 - 6.25 cm.	1176	1450	23.3
	6.25 - 8.75 cm.	598	433	-27.6
	0 - 1.25 cm.	1183	1418	19.9
	1.25 - 2.5 cm.	1453	1637	12.7
PIER 40N - W3	2.5 - 3.75 cm.	**2462**	1509	-38.7
	3.75 - 6.25 cm.	1491	935	-37.3
	6.25 - 8.75 cm.	725	240	-66.9
	0 - 1.25 cm.	1584	1588	0.3
	1.25 - 2.5 cm.	1176	1612	37.1
PIER 40N - W4	2.5 - 3.75 cm.	910	1259	38.4
	3.75 - 6.25 cm.	919	257	-72.0
	6.25 - 8.75 cm.	N/A	483	N/A
	0 - 1.25 cm.	**2866**	**2840**	-0.9
	1.25 - 2.5 cm.	1909	**3032**	58.8
PIER 40N - E1	2.5 - 3.75 cm.	1918	**2176**	13.5
	3.75 - 6.25 cm.	1205	1305	8.3
	6.25 - 8.75 cm.	863	441	-48.9
	0 - 1.25 cm.	**3540**	1920	-45.8
	1.25 - 2.5 cm.	**3099**	**2324**	-25.0
PIER 40N - E2	2.5 - 3.75 cm.	**3161**	**2293**	-27.5
	3.75 - 6.25 cm.	1639	995	-39.3
	6.25 - 8.75 cm.	1186	**2632**	121.9
	0 - 1.25 cm.	1706	**2143**	25.6
	1.25 - 2.5 cm.	**2406**	**2357**	-2.0
PIER 40N - E3	2.5 - 3.75 cm.	1376	**2201**	60.0
	3.75 - 6.25 cm.	1415	1644	16.2
	6.25 - 8.75 cm.	385	764	98.4
	0 - 1.25 cm.	**2288**	1278	-44.1
	1.25 - 2.5 cm.	1836	**2293**	24.9
PIER 40N - E4	2.5 - 3.75 cm.	1080	1803	66.9
	3.75 - 6.25 cm.	667	605	-9.3
	6.25 - 8.75 cm.	297	421	41.8